University of Alberta

Variable Speed Limit Control to Mitigate Freeway Congestion

by

Md. Hadiuzzaman

A thesis submitted to the Faculty of Graduate Studies and Research
in partial fulfillment of the requirements for the degree of

Doctor of Philosophy
in
Transportation Engineering

Department of Civil and Environmental Engineering

Spring 2014
Edmonton, Alberta

This thesis is dedicated to the memory of my father,

Engr. Abdul Gafur (1944 – 1994),

the first person who inspired my fascination in Engineering

Abstract

Over the past few decades, several active traffic control methods have been developed and implemented to mitigate freeway congestion. Among them, Variable Speed Limit (VSL) is considered the most efficient control method. In addition, the latest advances in Intelligent Transportation Systems (ITS) have made it feasible to implement predictive freeway control. The successful implementation of such control requires an accurate macroscopic traffic flow model that can predict all the important traffic dynamics.

To avoid violation of the equilibrium traffic state assumption and to improve traffic state prediction accuracy in the VSL control situation, this research proposes a 2^{nd} order model, DynaTAM-VSL, which drops parameterization of the METANET's FD; instead, it includes speed limit-dependent parameters in the speed and density dynamics. The validation results with the 20-s loop detector data confirmed that, compared to the existing models, the proposed model better simulates traffic flow. With the validated model, this research investigates the impact of control parameters and demand levels on total travel time and throughput under the coordinated VSL control and determined a range of the demand / bottleneck capacity ratio, when VSL simultaneously improves both of the mobility parameters, which resolved the existing paradoxical results.

This research also proposes an isolated VSL control strategy that aims at avoiding capacity drop at recurrent freeway bottlenecks. To evaluate the effectiveness of the control strategy, a base model of the 11-km test site: Whitemud Drive (WMD), Edmonton is calibrated within a microscopic traffic flow simulator to reproduce real-world traffic conditions, while the control strategy is implemented to evaluate its impact.

The sensitivity analysis of the control strategy on safety constraints and VSL update frequencies demonstrates promising results to support practical implementation.

Considering its flexible use in macroscopic simulation, a 1st order traffic flow model, CTM-VSL, is proposed. Unlike the 2nd order models, it is parsimonious: it only includes parameters that can be estimated using routinely available point detector data. However, the model is valid only for the condition of perfect compliance by drivers to VSL control, since it shares same properties of the CTM model. To update the storage capacity of an upstream segment of a VSL sign, a real-time queue estimation model is proposed. Despite the simple structure of the CTM-VSL model, the VSL control shows comparable results with the DynaTAM-VSL in terms of improving mobility parameters.

Finally, this research distinguishes the relative contributions of driver compliance levels (CLs) and a predictive VSL control with different CLs to improve traffic flows. Several CL-to-VSL strategies are modeled with a fixed co-efficient of variance of speeds obtained from static speed limit on WMD. The CLs include speed distributions for aggressive, compliant, and defensive drivers. It is proven that the mobility benefits from the VSL control are not at the expense of increased collision probability and vice-versa.

Acknowledgements

I would like to take this opportunity to thank my supervisor Dr. Zhi-Jun (Tony) Qiu for his invaluable guidance, encouragement and continuous support throughout the entire journey of my PhD. He was with me though any situation during my stay at the University of Alberta. I am grateful to have had such a wonderful supervisor who helped me to gain confidence, think critically and achieve a profound academic background. I very much enjoyed working with him and I am hoping to work with him in future.

I would like to thank the members of my PhD defense committee: Dr. Karim El-Basouny, Dr. Amy Kim, Dr. Jinfeng Liu, Dr. Yongsheng Chen, and Dr. Ming Zhong for their valuable suggestions and time.

I would like to give thanks to Iris Ye, Ken Karunaratne, Wai Cheung, Daniel Kabaroff, Matthew Knezevich, and Craig Walbaum from the traffic operation group in the City of Edmonton for providing me the necessary data to conduct this research.

I would like to acknowledge for the financial support I got from the FS Chia PhD Scholarship, the Alberta Innovates Graduate Student Scholarship, and the Natural Sciences and Engineering Research Council (NSERC) of Canada research fund.

I am indebted to my mother and parents in law for their support and encouragements. Special thanks to my beautiful wife Tamanna and to my son Tausif. Their endless supports, constant inspiration and understanding helped me to stay focused.

Above all, I am thankful to the Almighty Allah for His unbounding blessings in my life.

Table of Contents

List of Tables

List of Figures

List of Abbreviations

Acronym	Definition
API	Application Programming Interface
ATM	Active Traffic Management
ATDM	Active Traffic and Demand Management
CTM	Cell Transmission Model
CD	Capacity Drop
CL	Compliance Level
COM	Component Object Model
COV	Coefficient of Variance
CP	Collision Probability
CPM	Collision Prediction Model
DynaTAM	Dynamic network analysis Tool for Active Traffic and Demand Management
FD	Fundamental Diagram
FOT	Field Operation Test
GHG	Greenhouse Gas Emissions
GUI	Graphical User Interface
ITS	Intelligent Transportation Systems
kph	kilometer per hour
MAE	Mean Absolute Error
MOE	Measure of Effectiveness

MPC	Model Predictive Control
O-D	Origin-Destination
PRT	Perception-Reaction Time
RG	Route Guidance
RM	Ramp Metering
RMRSE	Root Mean Relative Square Error
RSB	Relative Safety Benefit
SL	Speed Limit
SQP	Sequential Quadratic Programming
STD	Standard Deviations
TMC	Traffic Management Center
TTT	Total Travel Time
TTS	Total Time Spent
TTD	Total Travel Distance
VSL	Variable Speed Limit
vphpl	vehicle per hour per lane
vpkpl	vehicle per kilometer per lane
WMD	Whitemud Drive

List of Notations

Symbols related to the CTM-VSL and DynaTAM-VSL model parameters:

Symbol	Definition	Unit
L_i	length of cell/link i	km [kilometer]
λ_i	number of lanes in cell/link i	—
$Q_{max,i}$	capacity of cell/link i	vphpl
Q_b	bottleneck capacity	vphpl
Q'_b	dropped capacity	vphpl
θ	fraction of capacity drop	—
v_{free}	free-flow speed	kph
w	congestion wave speed	kph
ρ_{jam}	jam density	vpkpl
ρ_c	critical density	vpkpl
τ	reaction time parameter when the speed limits in the current link and the downstream links are equal	hr [hour]
τ_{low}	reaction time parameter when the downstream speed limit is lower than the current link	hr
τ_{high}	reaction time parameter when the downstream speed limit is higher than the current link	hr
υ	global anticipation parameter	km^2/hr
κ	positive constant that prevents the anticipation term from becoming too large at low densities	vpkpl
ϕ_i	ratio of s_i and the total flow leaving from link i	—
α	parameter of the fundamental diagram	—

Symbols related to the CTM-VSL and DynaTAM-VSL model variables:

Symbol	Definition	Unit
$\rho_i, \rho_{i+1}, \rho_{i+2}$	estimated/predicted density at the cells/links	vpkpl
v_i, v_{i+1}, v_{i+2}	measured/predicted mean speed at the cells/links	kph
q_i, q_{i+1}, q_{i+2}	estimated/predicted outflow from different cells/links	vphpl
$Q_i(k)$	measured/predicted average flow rate in cell/link i at current time index k	vphpl
$r_i(k)$	measured/predicted on-ramp flow at current time index k	vph
$s_i(k)$	measured/predicted off-ramp flow at current time index k	vph
u_i	variable speed limit in cell/link i	kph
$V_i(\rho(k))$	equilibrium speed for mean traffic density ρ in cell/link i at current time index k	kph
ω	queue length	veh [vehicles]
L_{queue}	queue length	m [meter]

Symbols related to model predictive control (MPC):

Symbol	Definition	Unit
k	simulation time index	—
k_C	control sampling time index	—
T	simulation time step length	hr
T_C	control sampling time step	hr
N_P	number of prediction steps	—

N_C	number of control steps ($N_c \le N_P$)	—
$\boldsymbol{z}(k)$	measured traffic state at time step k	—
$\hat{\boldsymbol{z}}(k)$	predicted traffic states based on the knowledge at k	—
$\boldsymbol{D}(k)$	demand vector at current time step k	—
$\hat{\boldsymbol{D}}(k)$	predicted traffic demand vector	—
$f(z(k),u(k))$	traffic flow model with control variable	—
$\boldsymbol{u}(k)$	initial guessed variable speed limit vector	—
$\boldsymbol{u}^*(k)$	optimal variable speed limit vector	—
V_{min}	minimum allowable speed limit	kph
V_{max}	maximum allowable speed limit	kph
$V_{max,diff}$	maximum decrease in speed limits in between two consecutive VSL signs	kph
$J(\boldsymbol{u}(k))$	objective function	—
$\Phi(\boldsymbol{u}(k))$	equality constraint function	—
$\xi(\boldsymbol{u}(k))$	inequality constraint function	—

Chapter 1

Introduction and research objectives

1.1 Introduction

Traffic congestion is a major transportation issue, particularly in and around large metropolitan areas. Congestion forms during peak hours when too many vehicles use a common roadway with a fixed capacity. According to the 2012 UTTF (Urban Transportation Task Force), there is a high cost of congestion in Canadian cities, approximately 4.6 billion dollars annually due to the consumption of extra time and fuel, and the emission of greenhouse gases (GHG) (COMT 2012). Furthermore, congestion jeopardizes roadway safety due to unstable traffic flow.

Urban freeways suffer the most from congestion. The most widely used strategy to mitigate these problems is to increase roadway capacity by constructing new lanes (sometimes transportation practitioners call this a “brute-force approach”). However, budget constraints, lack of space, and environmental concern have made it difficult for transportation agencies to increase roadway capacity in major metropolitan areas. From a transportation economics point of view, freeway infrastructure and resources are tapped by a rapid increase in travel demand. Thus, growing demand issues cannot be mitigated by the brute-force approach; rather, mitigating traffic congestion calls for innovative control strategies that maximize the efficiency of transportation infrastructure and resources.

Active Traffic Management (ATM), a major component of Intelligent Transportation Systems (ITS), can dynamically manage recurrent and non-recurrent freeway congestion. Variable speed limits (VSL), ramp metering (RM), and route guidance (RG) are the most widely used ATM methods. ATM involves a continuous process: (1) obtaining, conditioning, and analyzing online traffic data from a variety of data sources (loop detectors, probe vehicles, video cameras, etc.); (2) simulating various future traffic conditions considering dynamic control methods (either in an isolated or coordinated mode) and quantifying expected mobility and safety benefits, and (3) implementing the optimal control method in the traffic system. ATM has been practiced for decades to mitigate traffic congestion and improve safety; however, until now, it was not clear how to achieve the maximum benefits of ATM methods. Thus, there is a tremendous need to understand the effects of different control methods on daily freeway operation, and find the most cost-effective control methods.

Although RM is the most widely practiced ATM method, it has gradually been recognized that RM can only control the average density immediately downstream of the controlled on-ramp. RM control aims at limiting vehicle access to freeway mainstream so as to achieve and maintain capacity flow and avoid or mitigate congestion near the on-ramp. However, when vehicles are in the mainstream, RM has no control. When traffic demand is high at the bottlenecks located on a freeway mainline, RM control has very limited impact. However, congestion does not happen only in the merging section of freeway mainlines and on-ramps. Several empirical studies (Chung et al. 2007; Persaud et al. 1998; Şahin and Altun 2008) found the flow breakdown phenomenon at weaving sections, lane drop locations, and at geometric bends on freeways. These locations could be far from the merging section or independent of merging influence near the on-ramp. Hence, using RM alone to control freeway traffic has limited performance when demands from both on-ramp and mainline upstream are high. Furthermore, limited ramp storage space can also hamper the positive impact of RM (Papamichail et al. 2010). RG is most helpful in cases of non-recurrent congestion (due to an incident or collision), which makes the traffic conditions unpredictable (Wang et al. 2006). Once the traffic demand is elevated, RG control is needed to divide traffic flows to alternative routes with sufficient capacity reserves.

By contrast, VSL adjusts freeway speed limits when congestion is imminent due to capacity drops from high traffic demand, collisions, and inclement weather. A suitably operated and enforced VSL control, either as a standalone measure or in combination with RM and/or RG, could avoid the constraints as mentioned above. Given the enormous cost of congestion to society and the urgent need for solutions, this research investigates a solution by exploring VSL effectiveness since its primary advantage is that it can control collective driver behavior on the freeway mainline. In addition, VSL can be implemented with existing transportation infrastructure and limited new investments.

Previously, VSL control performances were reported in European countries, such as the U.K., France, Germany and the Netherlands (e.g., Bertini et al. 2006; Hoogen and Smulders 1994) and North American countries (e.g., Abdel-Aty et al. 2006a; Abdel-Aty et al. 2006b; Lee et al. 2006; Lee et al. 2004; Lee et al. 2003; Piao and McDonald 2008) to homogenize the traffic and improve safety rather than mobility. In addition, numerous VSL control strategies were limited to respond only to inclement weather conditions or work zone management (see, Fudala and Fontaine 2010; Kang and Chang 2006; Kang et al. 2004; Lin et al. 2004; Long et al. 2008b; Stidger 2003; Rämä 1999). Those VSL control strategies did not show significant mobility benefits. To improve freeway mobility, an exclusive VSL strategy is required that proactively addresses important mobility factors: capacity drop and shockwave formation, while not compromising safety. Since driver safety is the most important aspect of traffic management, the developed VSL control strategy must have the capability to consider alternatives for experiments in extreme traffic flow regimes (e.g. large speed differences between upstream and downstream segments or large speed differences between two time steps at the same location), which may lead to potentially unsafe situations.

This research proposes a VSL control algorithm that changes freeway speed limits based on predicted traffic conditions. To solve the dynamic traffic control problem, the algorithm adopts a model predictive control (MPC) framework (Camacho and Bodons 1995; García et al. 1989). In contrast to a traditional optimal control strategy, MPC has several attractive features: (1) ***feedback***: feeding measured data into the control process at regular intervals can reduce the negative impacts of a mismatch between model prediction and actual system dynamics; (2) ***modularity***: independent traffic flow models, control parameters, and objective functions (including optimization method); and (3) ***adaptivity***: changing prediction model, control parameters, and objective function evenly at each control sampling time. These features make the MPC suitable for this research. The main concepts behind an MPC approach are the use of a traffic flow model to obtain the trajectories of future traffic states, the online optimization of an objective function to determine the best sequence of VSL control variable values, and the application of the rolling horizon procedure, so that from the best sequence of control variable values, only the first component is applied to the system over a control horizon. For the next control sampling time, the optimal speed limits that were calculated at the previous sampling time (but were not implemented) are used as initial guessed values for the VSL optimization process. With recent ITS developments, technologized freeways could provide a large amount of real-time traffic data. Using this data, it is feasible to perform real-time, reproducible and cost-effective experiments within an MPC framework.

1.2 Statement of the problem and opportunities

1.2.1 *Violation of the equilibrium traffic state assumption*

The main component of MPC is a macroscopic traffic flow model that is used for short-term traffic state prediction. To represent driver's desired speed in VSL-control situations, previous studies modified fundamental diagram (FD) in speed dynamics of the second-order METANET model (Papageorgiou et al. 1990), which was utilized within an MPC-based VSL control. Unfortunately, as discussed in Chapter 2, this modeling approach violates the equilibrium traffic state assumption, which results in failure to reproduce rapid transition in traffic states. Although several studies (Kotsialos et al. 2002a; Messmer and Papageorgiou 1990; Sanwal et al. 1996) have shown that traffic states with homogeneous speed limits can be reproduced with high accuracy using the METANET, no analysis can be found that investigates whether the existing FD modifications could represent traffic flow sufficiently in the VSL control situation, specifically, as it related to the congested equilibrium region of the FD. This research investigates the speed-density and flow-density curves resulting in different VSL control modeling approaches that adopt the FD modifications. To avoid violation of the equilibrium traffic state assumption and to improve traffic state prediction, this research attempts to derive a second-order model that avoids modifications of the METANET's FD.

1.2.2 *Balanced model accuracy and computational efficiency*

Since the MPC-based VSL control needs to provide traffic state prediction and optimization online, the traffic flow model should be as simple as possible without losing accuracy. Previously, all the MPC-based VSL studies considered a METANET-based traffic flow model as the prediction model within MPC. Although macroscopic simulations of the VSL evaluation have shown travel time improvements in a range of 20-30%, these solutions are more expensive to execute on field traffic (in terms of computational demand) and require more advanced calibration methods, which requires more effort and may limit field deployment. However, the MPC is independent of the traffic flow model, so the VSL control algorithm can be applied using other traffic models, if those models are capable of considering the impact of VSL on traffic flow.

Another class of macroscopic model that has received remarkable research attention is the first-order Cell Transmission Model (CTM) (Daganzo 1994), which is essentially a density dynamics. To predict traffic variables in real-time with the CTM requires very low computational effort (Gomes et al. 2008). This research found that for a prediction horizon of 5 minutes (min), typically 13 seconds (sec) and 16 sec are required on an Intel® Core™ i5 CPU to obtain optimal VSL trajectories associated with two VSL signs for utilizing a CTM-based and METANET-based prediction model within MPC. With a 1 min or longer control sampling time, both the traffic flow models satisfy the online optimization requirements. However, in real-life applications, the overall optimization process consumes more time due to access to the online traffic database at the traffic management center (TMC), data filtering, data conditioning, number of VSL signs and control parameters, etc. Therefore, if the proposed MPC-based VSL control shows comparable results with the METANET-based and CTM-based traffic flow models, the latter model can also be considered as a candidate model for real-life implementation.

However, due to sharing same property of the Lighthill-Whitham-Richards (LWR) model (Lighthill and Whitham 1955; Richards 1956), the implementation of a CTM-based model within MPC must be coupled with strict speed limit enforcements. Furthermore, comparisons of VSL control performance with different classes of traffic flow models could give some insight regarding the long controversy on prediction accuracy by the first-order and second-order models.

1.2.3 *Model calibration in no-VSL situation*

To accurately predict traffic states, the adopted macroscopic traffic flow model within the MPC framework must be well calibrated and validated. Unfortunately, in the past, all the METANET-based traffic flow model parameters for the network were determined based on the validation of the simulated network traffic flow model against field data in an uncontrolled situation. For example, an extended version of the METANET was implemented for modeling freeway traffic flow control involving VSL and RM (Carlson et al. 2010). In that research, the values of the METANET parameters were adopted from Kotsialos et al. (2002b). However, the calibration data used in that research was obtained from an uncontrolled scenario. Hegyi et al. (2005b) proposed another modification of the METANET model with the VSL control variable, which was implemented within a MPC framework to resolve shockwaves. That research also adopted the same values of the METANET parameters from Kotsialos et al. (2002b). It was assumed that with or without the VSL control variable, the parameters in the METANET-based traffic flow models were the same. Yet, obviously, the presence of the VSL control variable in the model would result in different parameter values, thereby altering the model's performance. As a consequence, those models have low predictive power. Therefore, this research proposes a systematic calibration method of the proposed METANET-based traffic flow model in a VSL control situation.

1.2.4 *Improper objective function selection*

To obtain optimal mobility benefits from the MPC-based VSL control, it is important to select proper objective functions. To the author’s best knowledge, none of the previous studies addressed this issue explicitly for the MPC-based VSL control design. The most frequently used objective function is to minimize only the total travel time (TTT) on mainline or total time spent (TTS) for all vehicles in the network. For example, an MPC-based VSL control by Hegyi (2004) used TTS as an objective function to find the optimal VSL control variable values. TTT and TTS are directly related to vehicular densities on segments. Minimizing that objective function keeps freeway density at a low value (by reducing inflow from upstream) on the mainline, which does not guarantee maximum utilization of freeway capacities. Indeed, it could reduce throughput from the freeway. Unfortunately, very few studies quantified throughput improvement with a VSL control. And most of the studies found no improvement in terms of this mobility parameter.

Alternatively, total travel distance (TTD), which is a surrogate measure of throughput, can be used as an objective function within MPC. However, only maximizing TTD increases flow (maintaining higher density), possibly driving traffic flow near bottleneck capacity, which might cause instability with a consequence of congestion. Therefore, this research investigates the impact of different objective functions on both of the defined mobility parameters: total travel time and link throughput. This research also analyzes the sensitivity of weight parameters in multi-objective optimization. In addition to objective functions, the achievable mobility benefits with the MPC-based VSL control also depend on the deployed control strategy (e.g. frequency and traffic conditions under which speed limits are increased and decreased). Therefore, this research attempts to investigate the impact of MPC parameters: control horizon and prediction horizon as well as VSL update frequencies and constraints on VSL values. With these analyzes, a major question will be addressed: when and how MPC-based VSL control can simultaneously improve total travel time and link throughput.

1.2.5 *Optimization accuracy and efficiency*

The discrete characteristics and safety constraints on the VSL values necessary for field application are usually underestimated in the literature. All the previous MPC-based macroscopic/microscopic VSL simulation studies implemented a gradient-based optimization method (e.g., sequential quadratic programming [SQP]) to find the optimal VSL values. However, solving the real-world dynamic traffic problem with SQP is complex and difficult to implement. Therefore, this research proposes an optimization method to obtain practical VSL values (near optimal) within a limited computation time. The main advantage of this method compared to SQP is that the gradient of the objective function does not need to be computed. In addition, by imposing temporal constraints on VSL values it is possible to limit the number of function evaluations at each control sampling time. Specifically, this research found that with the proposed optimization method (i.e., decision tree), the computation time for optimizing the same number of VSL control variables is reduced by approximately 60.0% compared to the SQP.

1.2.6 *Ideal compliance rate assumption*

Due to insufficient evidence in reliably predicting driver response to VSL, existing macroscopic MPC-based VSL studies (Hegyi et al. 2005b; Hegyi et al. 2007; Hegyi et al. 2005a; Long et al. 2008a; Zegeye et al. 2011) assumed that 100% of drivers follow the advised speed limits; this does not represent the real-world situation and the assumption could overestimate the mobility benefits. In contrast, some recent studies have shown that, regardless of compliance level (CL), an MPC-based VSL control provides similar mobility benefits; however, no evidence was found to indicate which CL is most achievable in practice, nor was a description found for the distribution of speed of a given

VSL. Surprisingly, a number of heuristic VSL control strategies have shown that VSL with increased CLs can increase travel time. However, it is yet to be analyzed whether or not that outcome is due to the control strategy design or the CL. There is a tremendous need to develop a method to model different CLs to VSL and quantify the relative contribution that CLs with an MPC-based VSL control have on improving mobility. Thus, this research attempts to model several CL-to-VSL strategies after real-world driver behavior. The research answers a major research question: whether the MPC-based VSL mobility benefits (with the increased CL) are at the expense of increased collision probability and vice-versa.

1.3 Research objectives and scope of work

Considering the observations in the preceding section and the mixed results from the MPC-based VSL simulation studies reported in literature, it can be concluded that the expected overall mobility benefit of applying the VSL control is still unclear. Therefore, this research is devoted to the development of a VSL control algorithm that will address the research problems as mentioned in Section 1.2. The research will propose a method to find the optimal VSL values based on measured and predicted traffic states. The research scope will be restricted to freeways. The test site will be approximately 11-kilometres (km) long in between east of 122 Street and west of 159 Street on Whitemud Drive (WMD), Edmonton, Alberta, Canada (Figure 1.1). This test section has a static speed limit of 80 kilometres per hour (kph) and experiences a directional average annual daily traffic (AADT) of about 100,000 vehicles. The freeway is outfitted with 8 loop detector stations on the mainline, each consisting of dual-loop detector groups in each travel lane. Each of the on-ramp and off-ramps are equipped with loop detectors. In addition to those mainline and ramp detectors, virtual detectors will be coded in the microscopic WMD base model to obtain measured traffic data (flow and mean speed) and feedback to MPC-based VSL control consequently. Furthermore, there are 7 traffic cameras along the mainline, which will be used for observing driver behavior, including lane-changing aggressiveness in different freeway segments, time of congestion formation and congestion duration, and replicating these observations in the base simulation model. Due to the existence of several bottlenecks, the test site experiences recurrent heavy congestions from 7:00 AM to 9:00 AM and 4:00 PM to 6:00 PM. The loop detector collected data showed that in the congestion periods, the average travel speed on the test site can drop from 80 kph to 50 kph, resulting in an increase of travel time by approximately 60.0%. This research will mainly focus on improving mobility in the recurrent congestion scenario. However, the test site is a collision-prone location on which 268 collisions occurred in 2011 and 2012; 144 collisions were during peak hours and 124 occurred in off-peaks. Once a collision blocks travel lanes, a large capacity drop is observed at the non-recurrent bottleneck locations, causing severe congestion. Therefore, if the designed VSL control can improve freeway safety, it can also mitigate non-recurrent congestion in addition to recurrent congestion.

Given the above scopes, this research proposes both first-order and second-order traffic flow models that consider the impact of VSL control variable on traffic flow. The models will be calibrated and validated with 20-sec loop detector data collected from a WMD base model. As demand prediction is out of scope of this research, it will be assumed that the traffic demand on the mainline and ramps are known. However, rather than assuming a particular demand scenario, the MPC-based VSL effectiveness will be explored under different demand scenarios. Moreover, it will be assumed that demand is independent of the VSL control. In other words, implementation of VSL control will not change the traffic demand in the network. The main ingredients for the successful implementation of the VSL control require traffic state prediction and coordination (which is equivalent to optimizing multiple VSL control inputs simultaneously). The MPC-based VSL control algorithm can encapsulate these two ingredients by using traffic dynamics and optimizing an objective function that includes predicted traffic states with the VSL control variables for the entire network. To assess the performance of the VSL control with the known demand inputs, the MPC approach will be implemented within both macroscopic and microscopic simulations. To perform the macroscopic simulation, a simulation tool within MATLAB software will be developed, and the SQP method (Boggs and Tolle 1995) will be used to solve the optimization problem. For the microscopic simulation evaluation of the MPC-based VSL control, a base model will be coded within the state-of-art VISSIM software. VISSIM is advantageous over other types of microscopic traffic simulation models, as it allows precise speed distribution modeling with VSL as a function of CL. To perform the microscopic simulation, a special purpose software module will be developed in C++ through the use of the component object model (COM) application interface (API). For the traffic flow optimization, SQP will be used. However, considering real-world applicability, an efficient optimization method will be proposed that does not require computing the gradient of the objective function; the control performance will be compared for adopting the SQP. Furthermore, driver compliance to VSL will be modeled within the WMD base model considering real-world driver behavior. Finally, this research will explicitly quantify the relative contribution of CL and the MPC-based VSL control in improving freeway mobility. There are several research objectives:

(1) Propose a METANET-based traffic flow model with the VSL control variable that can avoid violation of equilibrium traffic state assumption and can capture all the important traffic dynamics in the VSL control situation.

(2) Propose a CTM-based traffic flow model with the VSL control variable that is flexible to use in macro-simulation and requires minimal effort in finding model's parameters using routinely available point detector data.

(3) Design a robust VSL control strategy that aims at improving freeway traffic mobility considering traffic characteristics at recurrent bottlenecks, and update the speed limit based on real-time traffic measurements and predictions.

(4) Introduce traffic shockwave theory in the VSL control strategy, and develop real-time queue estimation models to assess how the queue control can improve VSL performance when demand is very high.

(5) Perform both macroscopic and microscopic simulation of the proposed MPC-based VSL control algorithm to identify when and how VSL control can simultaneously improve the defined mobility parameters: travel time and throughput.

(6) Model various compliance levels to VSL after real-world driver behaviour to investigate whether the designed MPC-based VSL mobility benefits are at the expense of increased collision probability and vice-versa.

1.4 Research contribution

Through this research, the contributions are listed as below:

(1) Chapter 2 summarizes the impact of previous FD modifications of the METANET's speed dynamics, and proposes a new model that avoids violation of the equilibrium traffic state assumption and improves traffic prediction accuracy.

(2) Chapter 2 proposes a systematic calibration method of the METANET-based traffic flow model that could capture drivers' dynamic responses to VSL.

(3) Chapter 3 summarizes the impact of typical objective functions under coordinated VSL control and proposes a heuristic rule to tune a weight parameter in multi-objective optimization to simultaneously improve TTT and throughput.

(4) Chapter 4 summarizes the impact of recurrent bottleneck on traffic flows and develops an isolated VSL control strategy that reduces inject flow into bottleneck in order to avoid bottleneck activation or reduce its severity.

(5) Chapter 4 proposes a non-gradient-based optimization method to find discrete speed limit values taking into consideration of constraints that ensure the safe operation of speed limits, as well as traffic efficiency.

(6) Chapter 5 introduces cell-dependent piece-wise linear FDs in the CTM to model dynamic capacity at active bottleneck and cells with variable free-flow speeds.

(7) Chapter 5 develops a time-space discrete queue estimation model by utilizing the classical shockwave theory along with the capacity drop phenomenon.

(8) Chapter 6 proposes a statistical framework to model drivers' desired speed distributions within a VSL control scenario at different CLs.

1.5 Organization of the thesis

Figure 1.2 shows the flow-chart for the research. The thesis is organized into sections: Chapter 2 reviews the previous field studies that investigate the impact of VSL control on the FD, as well as, the pros and cons of existing VSL control modeling approaches that use METANET as a base model, and proposes a new second-order model DynaTAM-

VSL (Dynamic Analysis Tool for Active Traffic Management-Variable Speed Limit), which is formulated based on the physical and empirical traffic flow considerations in the VSL control situation. This chapter also presents the method to calibrate model parameters in the VSL control situation. Chapter 3 presents the impact of the objective functions, and the MPC parameters, control horizon and prediction horizon, and demand levels on the VSL control performances to see when and how the VSL control can simultaneously improve travel time and throughput. Chapter 4 presents an efficient optimization method to find the optimal discrete VSL values and evaluates the effectiveness of the proposed VSL control strategy considering DynaTAM-VSL as the prediction model. This chapter also performs sensitivity analysis of mobility and safety parameters due to VSL update frequencies and different values of the safety constraint. Chapter 5 derives a first-order traffic flow model through FD modification of the density dynamics of the CTM and develops time-space discrete queue estimation models that could be applied to update freeway storage capacity in real-time. Modeling of different compliance levels to VSL is discussed in Chapter 6, while the statistical framework to find the lower and upper bound values of desired speed for each VSL is also presented. The research summary, further traffic flow model improvements, and field deployment requirements are presented in Chapter 7.

1.6 References

Abdel-Aty, M., Dilmore, J., and Dhindsa, A. (2006a). "Evaluation of variable speed limits for real-time freeway safety improvement." *Accident Analysis and Prevention,* 38(2), 335-345.

Abdel-Aty, M., Dilmore, J., and Hsia, L. (2006b). "Applying variable speed limits and the potential for crash migration." *Transportation Research Record,* (1953), 21-30.

Bertini, R. L., Boice, S., and Bogenberger, K. (2006). "Dynamics of variable speed limit system surrounding bottleneck on German autobahn." *Transportation Research Record,* (1978), 149-159.

Boggs, P.T., and Tolle, J.W. (1995)." Sequential Quadratic Programming." *Acta Numerica,* 4 1-51.

Camacho, E.F., and Bodons, C. (1995)."Model Predictive Control in the Process Industry." *Springer-Verlag, Berlin, Germany*.

Carlson, R. C., Papamichail, I., Papageorgiou, M., and Messmer, A. (2010). "Optimal motorway traffic flow control involving variable speed limits and ramp metering." *Transportation Science,* 44(2), 238-253.

Chung, K., Rudjanakanoknad, J., and Cassidy, M. J. (2007). "Relation between traffic density and capacity drop at three freeway bottlenecks." *Transportation Research Part B: Methodological,* 41(1), 82-95.

COMT - Council of Ministers Responsible for Transportation and Highway Safety. "The High Cost of Congestion in Canadian Cities". *Report Published by the Urban Transportation Task Force*, Ottawa, ON, 2012.

Daganzo, C. F. (1994). "The cell transmission model: A dynamic representation of highway traffic consistent with the hydrodynamic theory." *Transportation Research Part B,* 28(4), 269-287.

Fudala, N. J., and Fontaine, M. D. (2010). "Interaction between system design and operations of variable speed limit systems in work zones." *Transportation Research Record*, (2169), 1-10.

García, C. E., Prett, D. M., and Morari, M. (1989). "Model predictive control: Theory and practice-A survey." *Automatica*, 25(3), 335-348.

Gomes, G., Horowitz, R., Kurzhanskiy, A. A., Varaiya, P., and Kwon, J. (2008). "Behavior of the cell transmission model and effectiveness of ramp metering." *Transportation Research Part C: Emerging Technologies*, 16(4), 485-513.

Hegyi, A., Burger, M., Schutter, B. D., Hellendoorn, J., and Van den Boom, T. J. J. (2007). "Towards a Practical Application of Model Predictive Control to Suppress Shockwaves on Freeways." *Proceedings of the European Control Conference 2007 (ECC'07), Kos, Greece,* 1764–1771.

Hegyi, A. (2004). "Model Predictive Control for Integrating Traffic Control Measures." *PhD Thesis, Delft University of Technology, Delft, the Netherlands, TRAILThesis Series T2004/2*.

Hegyi, A., De Schutter, B., and Hellendoorn, H. (2005a). "Model predictive control for optimal coordination of ramp metering and variable speed limits." *Transportation Research Part C: Emerging Technologies*, 13(3), 185-209.

Hegyi, A., De Schutter, B., and Hellendoorn, J. (2005b). "Optimal coordination of variable speed limits to suppress shock waves." *IEEE Transactions on Intelligent Transportation Systems*, 6(1), 102-112.

Hoogen, V. E., and Smulders, S. (1994). "Control by variable speed sign: results of the Dutch experiment " *In Proc. of 7th Int.. Conference on Traffic Monitoring and Control, London, England, April 26-28, no. 391,* 145-149.

Kang, K. -., and Chang, G. -. (2006). "A robust model for optimal time-of-day speed control at highway work zones." *IEEE Transactions on Intelligent Transportation Systems*, 7(1), 115-123.

Kang, K. -., Chang, G. -., and Zou, N. (2004). "Optimal dynamic speed-limit control for highway work zone operations." Transportation Research Record, (1877), 77-84.

Kotsialos, A., Papageorgiou, M., Diakaki, C., Pavlis, Y., and Middelham, F. (2002a). "Traffic Flow Modeling of Large-Scale Motorway Networks Using the Macroscopic Modeling Tool METANET." *IEEE Transactions on Intelligent Transportation Systems*, 3(4), 282-292.

Kotsialos, A., Papageorgiou, M., Mangeas, M., and Haj-Salem, H. (2002b). "Coordinated and integrated control of motorway networks via non-linear optimal control." *Transportation Research Part C: Emerging Technologies*, 10(1), 65-84.

Lee, C., Hellinga, B., and Saccomanno, F. (2006). "Evaluation of variable speed limits to improve traffic safety." *Transportation Research Part C: Emerging Technologies*, 14(3), 213-228.

Lee, C., Hellinga, B., and Saccomanno, F. (2004). "Assessing safety benefits of variable speed limits." *Transportation Research Record*, (1897), 183-190.

Lee, C., Hellinga, B., and Saccomanno, F. (2003). "Proactive freeway crash prevention using real-time traffic control." *Canadian Journal of Civil Engineering*, 30(6), 1034-1041.

Lighthill, M. J., and Whitham, J. B. (1955.). "On kinematic waves. I. Flow movement in long rivers. II. A theory of traffic flow on long crowded roads." *In Proc. R. Soc. London: Ser. A*, 229(1178), 281-345.

Lin, P. -., Kang, K. -., and Chang, G. -. (2004). "Exploring the effectiveness of variable speed limit controls on highway work-zone operations." Journal of *Intelligent Transportation Systems: Technology, Planning, and Operations*, 8(3), 155-168.

Long, K., Yun, M., Zheng, J., and Yang, X. (2008a). "Model predictive control for variable speed limit in freeway work zone." *Proceedings of the 27th Chinese Control Conference, CCC,* 488-493.

Messmer, A., and Papageorgiou, M. (1990). "METANET: a macroscopic simulation program for motorway networks." *Traffic Engineering & Control,* 31(8-9), 466-470.

Papageorgiou, M., Blosseville, J. -., and Hadj-Salem, H. (1990). "Modelling and real-time control of traffic flow on the southern part of Boulevard Peripherique in Paris: Part I: Modelling." *Transportation Research Part A: General,* 24(5), 345-359.

Papamichail, I., Kotsialos, A., Margonis, I., and Papageorgiou, M. (2010). "Coordinated ramp metering for freeway networks - A model-predictive hierarchical control approach." *Transportation Research Part C: Emerging Technologies,* 18(3), 311-331.

Persaud, B., Yagar, S., and Brownlee, R. (1998). "Exploration of the breakdown phenomenon in freeway traffic." *Transportation Research Record,* (1634), 64-69.

Piao, J., and McDonald, M. (2008). "Safety impacts of variable speed limits - A simulation research." *IEEE Conference on Intelligent Transportation Systems, Proceedings, ITSC,* 833-837.

Rämä, P. (1999). "Effects of weather-controlled variable speed limits and warning signs on driver behavior." *Transp.Res.Rec.,* (1689), 53-59.

Richards, P. I. (1956). "Shockwaves on the highway." *Operation Research,* 4(1), 42-51.

Şahin, I., and Altun, I. (2008). "Empirical research of behavioral theory of traffic flow: Analysis of recurrent bottleneck." *Transportation Research Record,* (2088), 109-116.

Sanwal, K. K., Petty, K., Walrand, J., and Fawaz, Y. (1996). "An extended macroscopic model for traffic flow." *Transportation Research Part B: Methodological*, 30(1), 1-9.

Stidger, R. W. (2003). "Safer Roads and Road Work Zones." *Better Roads*, 73(11), 73.

Wang, Y., Papageorgiou, M., Sarros, G., and Knibbe, W. J. (2006). "Feedback route guidance applied to a large-scale express ring road." *Transportation Research Record*, (1965), 79-88.

Zegeye, S. K., De Schutter, B., Hellendoorn, J., and Breunesse, E. A. (2011). "Variable speed limits for green mobility." *IEEE Conference on Intelligent Transportation Systems, Proceedings, ITSC*, 2174-2179.

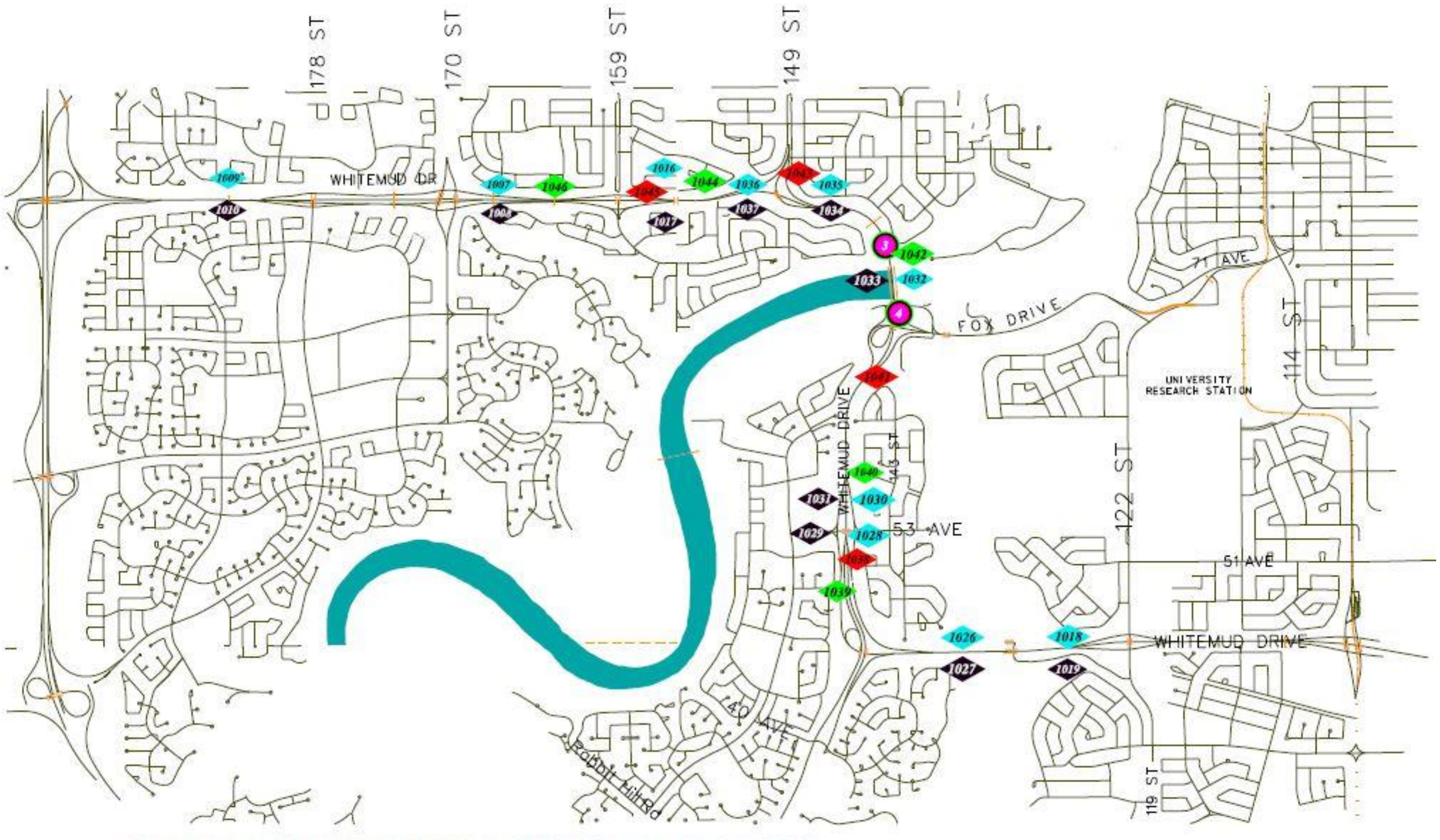

Figure 1.1 The 11-km test site between east of 122 Street and west of 159 Street (Courtesy: City of Edmonton).

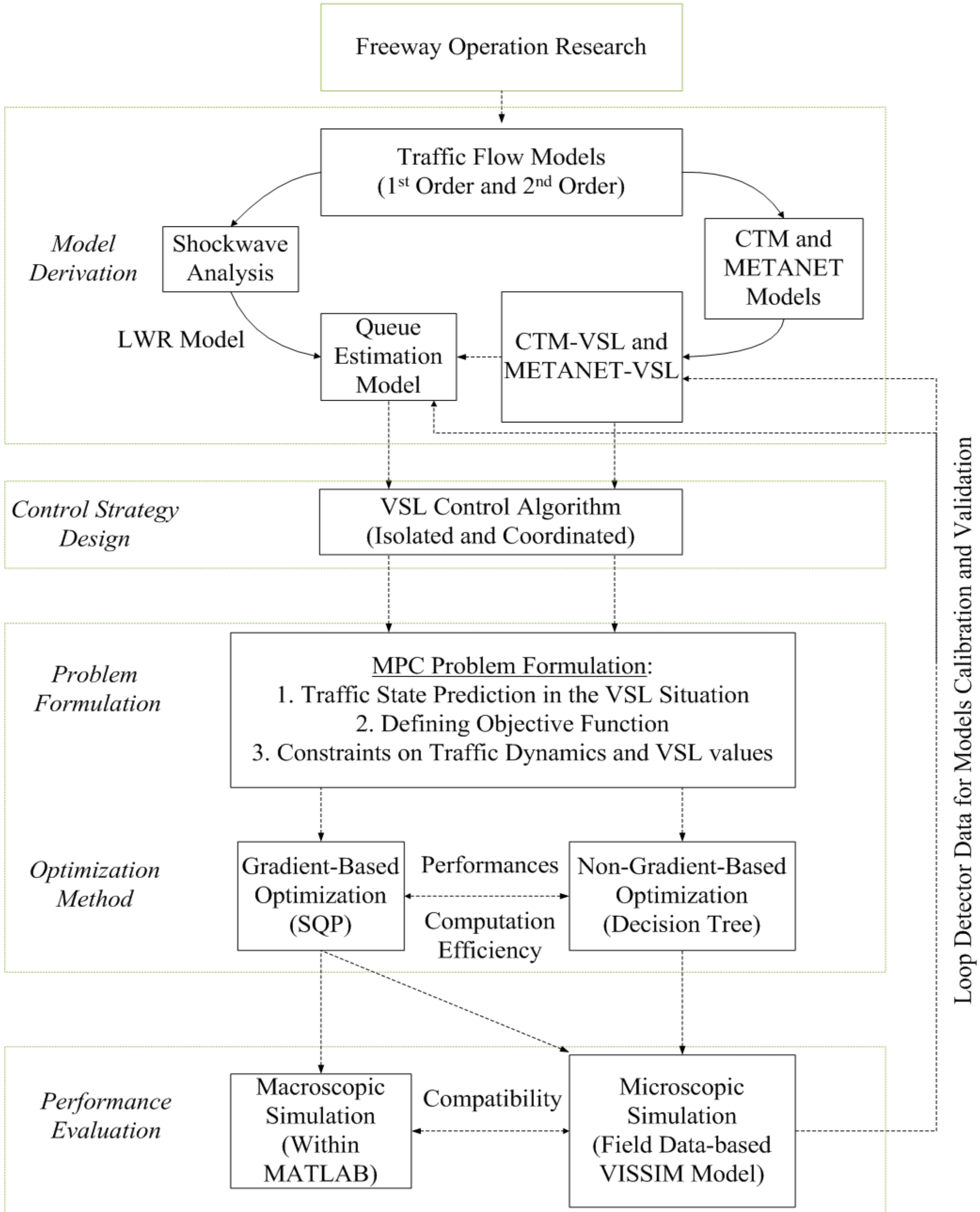

Figure 1.2 The flowchart of the dissertation research.

Chapter 2

Developing METANET-based dynamic model for VSL control situation by investigating accuracy of altered FD*

2.1 Introduction

Macroscopic traffic flow models play an important role in model predictive control (MPC)-based VSL control design and evaluation. Consequently, the underlying traffic flow model that is used as a prediction model within the MPC framework must capture all the relevant traffic dynamics, including free-flow and congestion states, and the transition between them. Macroscopic traffic flow models simulate traffic density, flow, and mean speed over space and time by a system of equations. According to the nature of independent variables, those models can be classified into deterministic or stochastic. Deterministic models assume exact relationships without randomized model components, while stochastic models use random variables. As the deterministic models are derived from well-established traffic flow principles, those models are widely used for traffic flow analysis and control. In addition, oftentimes it is argued that although traffic phenomena may appear to be stochastic in nature from the viewpoint of an individual driver, in a macroscopic treatment where traffic dynamics are represented by aggregate

* *This chapter is a modified version of an earlier manuscript submitted to Transportation Research Part C.* **Hadiuzzaman, M.**, Fang, J., and Qiu, T. Z. "Investigating impact of modified FD on short-term traffic flow prediction by METANET model in control situation."

variables, traffic flow turns out to be a reproducible, i.e., deterministic, process. Consequently, this research derives a second-order deterministic traffic flow model that is applicable for the VSL control situation and operates in discrete space (i.e., it breaks road sections into small links) and discrete time, considering METANET (Papageorgiou et al. 1990) as the base dynamic model.

Previously, several studies (Kotsialos et al. 2002; Messmer and Papageorgiou 1990; Sanwal et al. 1996) showed that traffic states with a homogeneous speed limit on the freeway links can be reproduced with high accuracy using the METANET model. The METANET, which is deduced based on the equilibrium traffic state assumption, is also a candidate model for VSL design since it is coupled with both speed and density dynamics. The equilibrium traffic state assumption in the METANET illustrates that for a given traffic density, the mean speed converges (with a lag time) to the fundamental diagram (FD). Thus, on the speed-density curve, i.e., FD, all the drivers have the same desired speed, and the corresponding point will not move unless the density on that freeway link changes. In the METANET, speed dynamics are not intended to be independent. It generates a reference speed based on a non-linear static speed-density relationship, i.e., the fundamental diagram (FD), and went back to a loop to affect density dynamics through coupling (Lu et al. 2011). Since the FD in the speed dynamics is basically the speed control parameter, in the literature, several approaches can be found to modify or replace the FD to include the impact of the VSL control variable on traffic flow. Thus, (1) the desired speed of the speed dynamics is based on the lesser value of either the static FD or the displayed speed limit (Hegyi et al. 2005; Hegyi et al. 2007); (2) the VSL rates (which are equal to the VSL-induced free-flow speeds divided by the non-VSL free-flow speed) are included by rendering the link-specific parameters of a static FD with the use of some affine functions (Carlson et al. 2010a; Carlson et al. 2010b); and

(3) the parameterization of the speed control variable is dropped and the linear VSL control variable is adopted directly (Hadiuzzaman et al. 2013; Lu et al. 2011).

Hegyi et al. (2005) mentioned that the first approach abated VSL control modeling issues as presented in Lenz et al. (1999) and Alessandri et al. (1999), where the effect of the speed limit downscales the entire speed-density diagram. The above VSL control modeling influences traffic with a speed that is lower than the speed limit, which is unrealistic. Although there is very limited empirical evidence on the impact of VSL on the FD, the second approach resulted in a flow-density relation that better matches the field observations, as reported in Papageorgiou et al. (2008). However, the VSL control modeling approach cannot simulate the influence of VSL on the congested equilibrium region of the FD very well, which is also proved in this research. For the second approach, the purpose of the parameterization of the non-VSL FD with the VSL rate was to make the speed and density follow the desired FD pattern up to a moderate traffic density. Nevertheless, given the possibility of a mismatch between the model simulation and the real-world dynamics, it should not be assumed that the traffic flow model can predict all probable situations, and, therefore, always avoid congestion formations.

In another research, Lu et al. (2011) reported that considering the FD in the METANET-based traffic flow model has several disadvantages: (1) FD calibration often leads to large errors in the congested equilibrium region, which may lead to a significant model mismatch; (2) as the FD is intrinsically a static relationship, the model may not be able to capture rapid transitions between free-flow and congestion states in the VSL control situation; and (3) the control variable appears highly nonlinear in the dynamic model, and, thus, causes problems for the online numerical optimization process.

In the third scenario, the speed control variable appears linearly. This feature could simplify the online numerical optimization process. Furthermore, model mismatches caused by discrepancies between field data and the modified FD curve could be avoided. However, no previous analysis can be found that supports the above arguments. Thus, it is essential to analyze and find the VSL control modeling approach that results in the least number of errors in traffic flow simulation in the control situation, because the ability to demonstrate the mobility improvements made by the VSL control largely depends on the accuracy of the underlying traffic flow model. Moreover, for practical reasons, the VSL experiments with different traffic flow models cannot be performed in a real traffic system; thus, in this research, the micro-simulation model is considered as a substitute for the real world. The micro-simulation model was also considered to assess the effectiveness of a number of VSL control strategies in several studies, including Hegyi et al. (2007), Lee et al. (2006), and Hellinga and Mandelzys (2011).

Furthermore, to accurately simulate the traffic system, the model must be well calibrated and validated before it can be incorporated into the predictive control framework. In the past, all of the METANET-based traffic flow model parameters for the network were determined based on the validation of the simulated network traffic flow model against real field data in the uncontrolled situation. It was assumed that with or without the control variable, the parameters in the METANET-based traffic flow models were the same. However, the presence of the control variable in the METANET model results in different parameter values, thereby altering the model's performance. To this end, this chapter proposes a systematic calibration method of the proposed model, DynaTAM-VSL, in the control situation. This chapter then investigates to what extent the performance of the model is sensitive to the calibrated data set and the extent to which the performance of the model is degraded after small changes in the optimal global parameter values (e.g., ±10%). To validate the DynaTAM-VSL, the underlying traffic network is simulated with different demand scenarios. The objective is to see whether the adopted VSL control modeling approach can accurately simulate traffic flow and quickly catch the rapid traffic state transition during the VSL control.

2.2 Background concept

2.2.1 *The FD*

Since most of the existing VSL control modeling approaches modify the static FD (v - ρ relationship or, equivalently, q - ρ relationship) to model the impact of VSL control variable on the traffic flow, this section briefly describes the parameters related to the FD. Under the assumption that traffic conditions do not change substantially in space and time, FD could be used to approximate the roadway traffic states. Considering an exponential model for a v - ρ relationship as is in Equation 2.7, Figure 2.1 shows the relationships between: (a) speed-density; (b) flow-density of a freeway link. Notably, by joining the origin and any point on the q - ρ diagram, the slope of the line will present the mean speed (v). Thus, any point on the FD can represent the traffic state (v, q, ρ).

The VSL control could have a significant impact on the following FD parameters: critical density (ρ_c) at which a zero slope on the q - ρ curve is attained; capacity (Q_{max}), which corresponds to the zero slope on the q - ρ curve obtained at ρ_c; free-flow speed (v_{free}), which is the speed obtained when the traffic density is very low and the flow is close to zero; critical speed (v_c), which is the speed that corresponds to the Q_{max} and the ρ_c. By contrast, jam density (ρ_{jam}) refers to the maximum number of vehicles associated with a completely stopped traffic flow, usually in the range of 100–200 vpkpl.

2.2.2 *VSL impact on FD*

There are very limited field studies that investigate the impact of VSL control on the parameters related to the FD. Zackor (1991) analyzed the traffic data with and without VSL control collected from a two-lane German motorway. The two major findings were: (1) at a lower traffic density (ρ), VSL control lowers the mean speed (v); and (2) at higher ρ, VSL control increases the v. The author reported a 5% to 10% increase in Q_{max} due to the preceding impact. But, the author did not comment on the possible impact on ρ_c under the influence of VSL control.

Papageorgiou et al. (2008) also investigated the impact of VSL control on FD in a more precise way. Similar to Zackor (1991), the research confirms that the average impact of VSL on the FD (q - ρ curve) at undercritical densities is a visible slope decrease, the intensity of which increases with decreasing VSL. Yet, that research is ultimately inconclusive regarding the potential increase of the flow capacity due to VSL: while some of the FDs corresponding to VSL indicate the potential of a slight increase in capacity, others do not. In addition, the authors found that, beyond the critical density (ρ_c), there are cross points between the curves without and with VSL for some speed limits. The authors found that the ρ_c corresponds to no-VSL shifts to higher values under the VSL impact.

2.3 The METANET model

The following assumptions are used while describing the basic METANET model and the METANET-based traffic flow models that are used for traffic state prediction in the VSL control situation: a freeway section is divided into *i*= (1, 2,…. ….M) links as in Figure 2.2 (the length of each link must be longer than the free-flow travel distance i.e.,

$v_{free}T \leq L_i$ to satisfy the *step size modeling constraint*[1]); a link contains exactly one on-ramp; a link may have multiple off-ramps; each link contains at least one loop detector; and a speed limit sign is located at the beginning of each link that affects the whole link.

In METANET, the density evolution of a link equals the previous density, plus, the inflow from the upstream link and on-ramp, minus the outflow of the link itself and off-ramp (flow conservation law).

$$\rho_i(k+1)=\rho_i(k)+\frac{T}{L_i\lambda_i}\left[\lambda_{i-1}q_{i-1}(k)-\lambda_i q_i(k)+r_i(k)-s_i(k)\right] \tag{2.1}$$

The outflow (q_i) is equal to the link density multiplied by the space mean speed.

$$q_i(k)=\rho_i(k)v_i(k) \tag{2.2}$$

The on-ramp flow (r_i) takes the value of the minimum of three quantities, as in Equation 2.3: (1) the available traffic on the ramp; (2) the maximal flow allowed by the ramp; and (3) the admissible flow due to the mainline traffic conditions. The similar model is also used to compute the inflow (q_0) into the first link.

$$r_i(k)=min\left[D_{ramp}(k)+\frac{\omega_{ramp}(k)}{T}, Q_{max,ramp}, Q_{max,ramp}\left(\frac{\rho_{jam,i}-\rho_i(k)}{\rho_{jam,i}-\rho_{c,i}(k)}\right)\right] \tag{2.3}$$

$$\omega_{ramp}(k)=\omega_{ramp}(k-1)+T\left(D_{ramp}(k-1)-r_i(k-1)\right) \tag{2.4}$$

---

[1] The relations of the (maximum) model time step, the maximum traffic speed and the minimum link length, in order to ensure that traffic doesn't travel more than one link during one time step.

In the above equation, $Q_{max,ramp}$ (vphpl), ρ_i (vpkpl), and $\rho_{jam,i}$ (vpkpl) represent, respectively, the capacity of the ramp, the density on the link *i* connected to the on-ramp, and the jam density of a link *i* connected to the given on-ramp. Here Equation (2.3) is written considering an unmetered on-ramp.

The exit flow (s_i) from link *i* to the off-ramp is calculated using Equation (2.5):

$$s_i(k) = \frac{\phi_i(k)}{1-\phi_i(k)} q_i(k) \tag{2.5}$$

The speed dynamics in METANET equals the summation of the previous speed, a relaxation term (the 2nd term), a convection term (the 3rd term), and an anticipation term (the 4th term) as in Equation (2.6). A brief illustration of these terms is presented below:

$$v_i(k+1)=v_i(k)+\frac{T}{\tau}\left[V[\rho_i(k)]-v_i(k)\right]+\frac{T}{L_i}v_i(k)\left[v_{i-1}(k)-v_i(k)\right]-\frac{1}{\tau}\left[\frac{T\upsilon}{L_i}\frac{\rho_{i+1}(k)-\rho_i(k)}{\rho_i(k)+\kappa}\right] \tag{2.6}$$

Relaxation describes that, with a lag time τ, the mean speed v of the link gets relaxed to the FD without any control or to the variable speed limit u during VSL control.

Convection describes that vehicles entering from upstream link *i*-1 to current link *i* adapt their speed gradually rather than instantaneously.

Anticipation describes that drivers are looking ahead. If a driver sees high traffic density in the downstream link *i*+1, they will slow down, and vice-versa.

In Equation (2.6), the reaction time parameter- τ (hr), anticipation parameter-υ (km^2/hr), and the positive constant-κ (vpkpl) are the model's global parameters, i.e., all the links have the same value. Those parameters must be calibrated using the measured data. In METANET, the above speed dynamics has been derived from Payne's model (Payne 1971). However, the 4th term has been modified relative to Payne's model. Specifically, κ is added to avoid the singularity of the term when modeling low traffic density and υ is added to capture sensitivity of traffic speeds to the downstream traffic density.

The FD—$V[\rho_i(k)]$ (kph) in Equation (2.6) is represented by Equation (2.7):

$$V[\rho_i(k)] = v_{free,i} \exp\left[-\frac{1}{\alpha_i}\left(\frac{\rho_i(k)}{\rho_{c,i}}\right)^{\alpha_i}\right] \tag{2.7}$$

2.4 Model advancement

The speed dynamics (Equation 2.6) does not explicitly describe the effect of VSL control on traffic flow. Since the FD is basically the speed control parameter to be designed, it could be parameterized with the VSL control variable (u) or even without parameterization at all. This research investigates the accuracy of different VSL control modeling approaches that adopt Equation (2.6) as the base model and replace the FD (Equation 2.7) with a modified FD, i.e., the desired speed in the VSL control situation.

2.4.1 *VSL control modeling approaches*

2.4.1.1 Without parameterization

In this approach, the desired speed of the METANET's speed dynamics is based on the lesser value of either the static FD, i.e., $V[\rho_i(k)]$, or the displayed speed limit, i.e., u_i as presented in Equation (2.8).

$$V[\rho_i(k)] = min\left(v_{free,i} \exp\left[-\frac{1}{\alpha_i}\left(\frac{\rho_i(k)}{\rho_{c,i}}\right)^{\alpha_i}\right], u_i(k)\right) \tag{2.8}$$

Figure 2.3 shows the simulation results (v - ρ and q - ρ curves) of Equation (2.8). It can be seen that, after a certain point in density, the desired speed equaling the FD corresponds to a situation without any VSL control. In other words, beyond that point, the displayed speed limit is not achievable by the driver, and they adopt speeds based on the surrounding traffic conditions. Certainly, this result questions the effectiveness of VSL control, since the displayed VSL and the adopted speed by the driver could be significantly different. Moreover, from Figure 2.3(b), it can be seen that beyond a point of ρ_c=40 vpkpl corresponds to v_{free}=80 kph, there is a consistent increase in ρ_c and a consistent decrease in Q_{max} due to the reduction in speed limits. Nevertheless, ρ_c and Q_{max} do not change below that point. Such phenomenon was not observed by Papageorgiou et al. (2008) and Zackor (1991) in real data collected during a VSL control situation. More importantly, the model simulation does not generate any cross point between the q - ρ curves, whereas the fitted curve in real data by Papageorgiou et al. (2008) and Zackor (1991) showed clear cross points.

Figure 2.3 shows that, for any speed limit, it is possible that traffic comes to a complete stop, i.e., to ρ_{jam}, which is logical. Since, VSL does not change the length of vehicles and the length of road sections. In addition, this parameter is not sensitive to the VSL control and will equal the ρ_{jam} obtained in the no-VSL situation.

2.4.1.2 With parameterization

In this approach, all the parameters related to the FD, i.e., $V[\rho_i(k)]$, in the speed dynamics (Equation 2.6) are parameterized by the VSL control variable using some affine functions as can be seen in Equation (2.9).

$$V[\rho_i(k), b_i(k)] = v_{free,i} b_i(k) \exp\left[-\frac{1}{\alpha_i [E_i - (E_i - 1) b_i(k)]} \left(\frac{\rho_i(k)}{\rho_{c,i} \left\{ 1 + A_i \left[1 - b_i(k) \right] \right\}} \right)^{\alpha_i [E_i - (E_i - 1) b_i(k)]} \right] \tag{2.9}$$

Where, b_i =VSL rates. A_i and E_i are constant parameters to be estimated based on real/simulated data. Figure 2.4 shows the simulation results of Equation (2.9). From Figure 2.4(a), it can be seen that the parameterization of the FD by the speed control variable causes the same issues as can be found in Lenz et al. (1999) and Alessandri et al. (1999). Specifically, in the low density region, the modification results in desired speeds that are considerably lower than the displayed VSL and the speed that the driver would assume without VSL, which violates the equilibrium traffic state assumption. As can be seen from the figure, for a density of 20 vpkpl and a speed limit of 40 kph, the desired speed is 32 kph (point B). However, without VSL control, the speed would be around 73 kph (point A) at this density. It is unrealistic to assume that drivers would drive 41 kph slower (from 73 kph to 32 kph) than recommended speed when they would feel safe driving closer to 80 kph in a situation that lacked VSL. Furthermore, in the current VSL control modeling approach, the static v - ρ and q - ρ curves are scaled by the affine functions for the entire range of traffic density. Therefore, within the congested region, the densities in the situation without VSL resulted in speeds that are already lower than the speed limit are still affected. From Figure 2.4(a), it can be seen that a speed limit of 40 kph will lead to a reduction in the speed for a density of 50 vpkpl from 38 kph to 22 kph (from point C to point D). This phenomenon overstates the driver's behavior. Consequently, the parameterized speed dynamics would have low predictive power.

Moreover, in contrast to the desired speed in Equation (2.8), Equation (2.9) shows that ρ_c is not very sensitive to speed limit reduction. From Figure 2.4(b), it can be seen that there is a consistent decrease in Q_{max} due to a reduction of speed limits. By contrast, in real data, Papageorgiou et al. (2008) and Zackor (1991) observed capacity improvements for some speed limits. Interestingly, this VSL control modeling approach could generate cross points between the q - ρ curves (see Figure 2.4b); however, such crossing for all the VSL did not present by Papageorgiou et al. (2008). Moreover, the figure shows that the traffic flow does not come to a complete stop even when segment density reaches jam density, which is not logical. By contrast, simulating Equation (2.8) shows that, with the different speed limits, flow can reach to zero at jam density. Carlson et al. (2010a) and Carlson et al. (2010b) present the simulated q - ρ curve appearing in Equation (2.9) up to a density of 60 vpkpl. Moreover, the authors do not present how the VSL control modeling approach affects the static v - ρ curve. Comparing the simulation results from Equation (2.8) and Equation (2.9), it can be concluded that the current VSL control modeling approach would introduce higher errors in traffic flow simulation.

2.4.1.3 Replacing FD

From the above analysis, it can be concluded that both with and without parameterization of the FD, the desired speed cannot represent the real-world situation very well, specifically in the overcritical region (right-side) of the FD. Nevertheless, there is no reason to assume that VSL control could always keep the traffic flow below a critical density. Thus accurate simulation in the congestion condition as well as non-congested condition is a key to successful implementation of MPC-based VSL control.

An alternative approach[2] could be removing unnecessary and inappropriate FD assumptions from the speed dynamics (Equation 2.6) and to directly adopt the linear control variable (u), where u is equal to the speed limit value indicated on a VSL sign installed on roads. However, in doing so, the underlying assumption is that drivers can achieve the speed limit. Thus it is critical to display appropriate speed limit based on prevailing traffic conditions. This VSL control modeling approach has several advantages over other approaches: (1) the speed control variable appears linearly, which simplifies the problem of finding the optimal values for the control variable in online control, and (2) model mismatches caused by discrepancies between the field data and the modeled FD curve as presented in Section 2.4.1.1 and Section 2.4.1.2 could be avoided. Most importantly, in Equation (2.8) and Equation (2.9), the desired speed has been derived from the FD, which is intrinsically a static relationship. Thus, the model may not be able to capture the inherently rapid transition phases of traffic dynamics very well.

2.4.2 *The DynaTAM-VSL model*

This section derives a 2nd order traffic flow model utilizing the VSL control modeling approach as presented in Section 2.4.1.3. Furthermore, to improve the accuracy in traffic flow simulation, several modifications have been introduced: (1) speed-limit-dependant link-specific parameters in the boundary constraints while calculating the link outflow in which the link-specific parameters are estimated using multiple triangular-shaped FDs calibrated with the 20-s measured traffic data; (2) a new convection term in the speed dynamics that considers whether the immediate downstream link is congested and/or the current link is saturated with the VSL control; (3) a speed-limit-dependant reaction time

[2]*One of the advantages of this VSL modeling approach has provided an opportunity to successfully designing integrated freeway control that has been presented in a journal paper*. Fang, J., **Hadiuzzaman, M.,** Yin, E., and Qiu, T.Z. “DynaTAM: an Online Algorithm with Simultaneously Optimized Pro-Active Traffic Control for Freeway.” (*under-review*)

parameter considering whether a driver has a lower reaction time during the deceleration process when a lower speed limit is displayed in the downstream link and vice-versa; and (4) several simplified constraints to properly address the system dynamics and traffic characteristics during the VSL control. Further details are as follows:

(1) The first modification is related to density dynamics. In METANET, the link-specific parameters, i.e., $Q_{max}, v_{free}\ \rho_c, \rho_{Jam}$ have been appropriately considered through the $v-\rho$ curve, i.e., the FD. The presence of that FD avoids any unrealistic traffic flow evolution through the model simulation. Thus, if the VSL control modeling approach as in Section 2.4.1.3 is adopted (i.e., replacing FD with the control variable), then the link-specific parameters must be introduced to the traffic dynamics. Moreover, the link-specific parameters should not assume fixed values in the VSL control situation. As can be seen, when two consecutive links are operated with different VSL signs, without the speed-limit dependant link-specific parameters, for some freeway links, the errors in traffic flow simulation are higher than the other VSL control modeling approaches. Thus a set of physical constraints with the on-ramp and off-ramp impacts is considered to estimate the transition flow among successive links, as in Equation (2.10). In the equation, at any time index k, the outflow from link *i* to *i* +1 i.e., $q_i(k)$, depends on the average link flow at *i* (as in Equation 2.2), the capacity of the downstream link *i* +1, and the supply from link *i* +1.

$$q_i(k) = \ min\left\{v_i(k)\rho_i(k)+r_{i+1}(k)\text{-}s_{i+1}(k), Q_{max,i+1,u_{i+1}}, w_{i+1,u_{i+1}}\left(\rho_{Jam,i+1}-\rho_{i+1}(k)\right)\right\} \tag{2.10}$$

In the above equation, the parameters—capacity (Q_{max,i,u_i}) and congestion wave speed (w_{i,u_i})—vary for different links (i) with different speed limits (u_i). Those speed-limit-dependant link-specific parameters will be estimated from multiple triangular-shaped FDs, where each of the FDs is associated with a fixed speed limit assigned to the freeway link. The jam density $(\rho_{jam,i})$ is assumed to be independent of speed limits, yet it can be different for the various links. In the proposed model, the FDs are explicitly calibrated with the measured data. Thus, the shape and trends in parameters reflects actual impact of VSL on traffic flow.

Moreover, q_o in the control situation is modeled considering both the mainline demand, $D_{mainline}$, and the allowable input flow at the first link due to the current VSL values.

$$q_o(k) = min\left[D_{mainline}(k) + \frac{\omega_{mainline}(k)}{T}, q_{limit}(k) \right] \tag{2.11}$$

$$q_{limit}(k) = \begin{cases} \lambda_1 v_{free,1,V_{max}} \rho_{c,1,V_{max}} & If\,(min\,(u_1(k), v_1(k)) \geq V_{max}) \\ \lambda_1 v_{free,1,u_1} \rho_{c,1,u_1} & If\,(min(u_1(k), v_1(k)) < V_{max}) \end{cases}$$

$$\omega_{mainline}(k+1) = \omega_{mainline}(k) + T\left(D_{mainline}(k) - q_o(k)\right)$$

In Equation 2.11, V_{max} is the maximum allowable speed limit.

(2) The second modification is related to the convection term (the 3rd term) of Equation (2.6). This term indicates that, if the speed at upstream link i -1 in the k time step is greater than the speed of the current link (i) then the speed of link i will likely increase in $k+1$ time step; otherwise, it will decrease. This may be true

if the link i is not yet congested and the downstream link i +1 is in a free-flow condition. Lu et al. (2011) considered several other possible convection terms in the speed dynamics of METANET; however, in this research, it was found that taking a geometric mean of speed at link i and i -1 in order to lessen the influence of speed at link i -1 in the convection term as in Equation (2.12) results in the best speed prediction with the proposed model, DynaTAM-VSL.

$$\frac{T}{L_i} v_i(k)\left[\sqrt{0.5(v^2_{i-1}(k)+v_i^2(k))}-v_i(k)\right] \tag{2.12}$$

(3) A driver needs to accelerate or decelerate to follow the immediate downstream speed limit. In general, the reaction time in a deceleration situation is maintained as a minimum value that the driver can reach, while the reaction time in an acceleration situation is greater (Yeo 2008). Moreover, a driver could have a different reaction time based on the amount the speed limit is reduced or increased in the immediate downstream link i +1 compared with the current link i. Therefore, an extension is introduced in Equation 2.6 for capturing the reaction behavior of drivers when the downstream VSL sign shows a lower or higher speed limit than the current link in which the vehicle is travelling. In this situation, the reaction time parameter τ in Equation (2.6) is replaced by the speed limit-dependent parameter $\tau_i(k)$, according to Equation (2.13).

$$\tau_i(k) = \begin{cases} \tau_{low} & \text{if } \Delta u = \left[u_i(k) - u_{i+1}(k)\right] > 0 \\ \tau & \text{if } \Delta u = \left[u_i(k) - u_{i+1}(k)\right] = 0 \\ \tau_{high} & \text{if } \Delta u = \left[u_i(k) - u_{i+1}(k)\right] < 0 \end{cases} \tag{2.13}$$

It should be noted that τ in the basic METANET model is applicable to a homogenous speed limit; therefore, it has the same value for all the links and for all the time steps. For the VSL control situation, it is possible at any time step k

that the optimized speed limits in the consecutive links have the same value. The second constraint in Equation (2.13) models this phenomenon, whereas the first constraint in that equation indicates that drivers are more prompt to react if the downstream speed limit sign displays a lower speed than the current link in which the vehicles are travelling. The third constraint can be explained in the same fashion. On the contrary, Hegyi et al. (2005) split the anticipation parameter (υ) in the speed dynamics depending on whether the downstream density was higher or lower than the density in the current link. This modification influences only the anticipation term (the 4th term) in Equation (2.6). However, Lu et al. (2011) recognized that the anticipation term in speed dynamics is rather sluggish during simulation and thus has less influence on capturing speed dynamics under the VSL control. By contrast, introducing the proposed modification in τ could influence both the relaxation term and the anticipation term. It may also improve accuracy in speed estimation during VSL control.

(4) The traffic dynamics profile for individual link is used during the prediction by adding certain constraints to the model (Equation 2.14-2.19):

$$\rho_i(k+1) \in (0,......,\rho_{jam,i}) \tag{2.14}$$

$$v_i(k+1) \in (0,......,v_{free,i,u_i}) \tag{2.15}$$

$$\rho_i(k+1)v_i(k+1) \in (0,......,Q_{max,i,u_i}) \tag{2.16}$$

$$u_i(k) \in (V_{min},......,V_{max}) \tag{2.17}$$

$$|u_i(k) - u_i(k+1)| \le V_{max,diff} \tag{2.18}$$

$$|u_i(k) - u_{i+1}(k)| \le V_{max,diff} \tag{2.19}$$

In this research, V_{min}=20 kph and V_{max}=80 kph are considered to maintain minimum operating efficiency and safety on WMD, respectively. The constraint

$V_{max,diff}$ =10 kph is implemented in the temporal speed limit changes (Equation 2.18) on a particular VSL sign so that the driver should not encounter a decrease in the displayed speed limit larger than a certain amount. Moreover, the spatial changes in speed limits (Equation 2.19) among the VSL signs are essential in the event of multiple VSL signs. The last two constraints are necessary for safety.

In this way, this chapter proposes a new second-order traffic flow model, DynaTAM-VSL, using METANET as the base model; however, DynaTAM-VSL will replace Equation (2.2) with Equation (2.10), replace the FD with the VSL control variable (u) in the relaxation term of Equation (2.6), replace the convection term in Equation (2.6) with Equation (2.12), and introduce the speed-limit dependant reaction time parameter as in Equation (2.13) into Equation (2.6) together with the input flow at the first link as in Equation (2.11) and constraints as in Equation (2.14-2.19).

2.5 Model calibration in VSL control situation

2.5.1 *Traffic data*

To prepare the data for calibrating the DynaTAM-VSL, a base model for the 11-km WMD test site for the evening peak periods (t =4:00-6:30 PM) was coded within the microscopic traffic flow simulator VISSIM v5.3. The base model functions as a proxy for the real-world traffic system. The field data used as an input to calibrate the base model in the non-VSL situation were compiled from two separate sources: (1) dual loop detectors on the freeway mainline; and (2) the video data for on-ramps and off-ramps. To replicate the real-life bottleneck formation along the freeway section, several customized link behavior types were defined: namely, for the freeway merge section, the lane drop condition and the weaving section. The detail calibration of the base model is presented in Chapter 4. The base model was used to generate the calibration data in the VSL control situation. The test site was discretized into 13 links, where the link length is around 800 metres (m). The links are designated by the numbers L1, L2,………., L13, with the first link, L1, located in the most upstream. Note that, the two boundary links, i.e., L1 and L13 is immediate outside of the studied 11-km test side. The measured data from these two links will be considered as boundary conditions while validating macroscopic traffic flow models as presented in "Section 2.6". For each link in the WMD base model, one loop detector was placed on each lane. These detectors provided the mean speed and flow. Density was estimated from the fundamental relationship, i.e., $\rho_i = q_i / v_i$.

2.5.2 *Calibration method*

The calibration steps are illustrated in Figure 2.5. To calibrate all the parameters of the DynaTAM-VSL, the speed-limit-dependant link-specific parameters ($Q_{max}, v_{free}\ \rho_c, w$, ρ_{Jam}) must be estimated at the first step. In fact, the calibration of multiple triangular FDs with the field-implementable speed limits is performed to estimate those parameters for the discretized freeway links. The method to calibrate the FD for any speed limit can be found in Dervisoglu et al. (2009) that performs a least-squares fit and an approximate quantile regression to establish the left side and the right side of FD, respectively.

The global parameters related to the speed dynamics of DynaTAM-VSL are calibrated by including the link-specific parameters in the second step. To perform the calibration, a calibration dataset is required that includes VSL values assigned in the links over the time steps along with the traffic states $[q, v, \rho]$. This enables to calibrate the reaction time parameters $[\tau_{low}, \tau, \tau_{high}]$ along with the other global parameters $[\upsilon, \kappa]$. Thus, a calibration dataset must be generated in the VSL control situation. To prepare the data in the control situation, an appropriate speed limit using a flow-density-speed threshold-based VSL control algorithm was assigned to each link in the WMD base model. This candidate VSL control algorithm has been adopted from Allaby et al. (2007). Based on the real-time traffic data collected every 20-s from detector *i* (which corresponds to link *i*), the control algorithm determines the appropriate speed limit to be displayed at VSL sign *i* (which corresponds to link *i*).

With the above collected traffic data, this research finds the global parameters that are optimal with respect to an objective function. Specifically, this research minimizes Equation (2.20) using the multi-start (with fifty different starting points) Sequential Quadratic Programming (SQP) to minimize the function over a constrained parameter space. The multi-start SQP optimization method starts a local solver from multiple start points to increase the probability for finding the global solution. Similar to other gradient-based optimization method, the SQP involves two major tasks: (1) direction finding or where to go in the design space; and (2) step size selection or how far to go. This research employed a MATLAB optimization solver called "fmincon" based on multi-start SQP. The solver uses BFGS Method (approximates Hessian matrix) to compute the search direction. The step length parameter is determined to produce a sufficient decrease in merit function that was proposed by (Han 1977) and (Powell 1978). To confirm the optimality of the model parameters, this research ensures that none of the final parameter values passes its assigned lower boundary (LB) and upper boundary (UB) values.

$$f(\beta)=\sqrt{\sum_{i=1}^{M}\sum_{k=1}^{K}\left[\left(\rho_i^{m}(k)-\rho_i(k|\beta)\right)^2+\gamma\left(v_i^{m}(k)-v_i(k|\beta)\right)^2\right]} \tag{2.20}$$

In Equation (2.20), $\rho_i^m(k), v_i^m(k)$ are the measured density and speed from the WMD base model/real-world; $\rho_i(k)$, $v_i(k)$ are the simulated density and speed from the macroscopic traffic flow model, e.g., DynaTAM-VSL.

2.5.3 *Calibration results*

To estimate the speed-limit-dependant link-specific parameters, the WMD base model was run with different fixed speed limit values assigned to the links, and each time simulation was run for a period of 2.5 hours. Traffic data were collected every 20-s and were used to calibrate the FDs associated with different speed limits. In Figure 2.6, the positive slope associated with each FD, represents the free-flow speed for the speed limit. The figure shows the trend in the estimated critical density and capacity (the second and the third values within the bracket) of a typical link in the studied freeway section.

For all the links, the estimated link-specific parameters show that in general Q_{max} and v_{free} decreases, and ρ_c increases with lowering speed limits, which confirms the field observation by Papageorgiou et al. (2008). Also, similar to the above field research, beyond the ρ_c, there are cross points between the curves without and with VSL for some speed limits. Consequently, it is reasonable to adopt the above estimated link-specific parameters in the boundary constraints (Equation 2.10) and in the simplified constraints (Equation 2.14-2.19). If the experimentations are to be performed in the real-world, those parameters must be calibrated with the field loop detector data. Fortunately, in contrast to other METANET-based traffic flow models, the DynaTAM-VSL has the flexibility to adopt any other values of those link-specific parameters calibrated from the measured traffic data, thus can avoid mismatch with the traffic pattern in the VSL situation.

To investigate the accuracy of different VSL control modeling approaches, four METANET-based traffic flow models have been calibrated (see Table 2-1). M1 (Hegyi et al. 2005), M2 (Carlson et al. 2010a), M3 (Lu et al. 2011), and M4 (DynaTAM-VSL) adopt the VSL control modeling approaches as presented in Section 2.4.1.1, 2.4.1.2, 2.4.1.3, and 2.4.1.3, respectively. During the parameter optimization of each model, M =13; γ =0.8; K = (2.5 hours*3600 second /20 second) =450 were assigned in Equation (2.20). From the table, it can be seen that the optimal objective function value, $f(\beta^{optimal})$, is the minimum in case of M4, which demonstrates the accuracy of the model. The first three values of the calibrated global parameters for M4 satisfy the assumption made during the splitting of reaction time parameter τ as in Equation (2.13). The optimal parameters related to each of the models can be found in Table 2-1.

2.5.4 *Model sensitivity with respect to optimal parameter changes*

The optimal global parameters as calibrated above may vary in different situation by a small amount. Therefore, it is important to investigate the extent to which the performance of the DynaTAM-VSL model is degraded when small changes in the values of the above calibrated global parameters are considered. For this purpose, the performance criterion was evaluated using the nominal data for a perturbed parameter set $\beta = \beta^{optimal} + \Delta\beta$ as proposed in Cremer and Papageorgiou (1981). During this evaluation, the link-specific parameters were kept unchanged as obtained in the calibration stage (i.e., Step 1 in Figure 2.5). The sensitivity with respect to the parameter change $\Delta\beta$ was quantified by the following index:

$$\Omega(\Delta\beta) = \frac{f(\beta^{optimal} + \Delta\beta) - f(\beta^{optimal})}{f(\beta^{optimal})} x100 \tag{2.21}$$

From Table 2-2, it can be observed that the performance of the DynaTAM-VSL is not sensitive to small changes in the global parameters values. Furthermore, it can be observed that, out of the five global parameters, τ_{high} causes the highest degradation, which might require careful calibration and adaptation during the implementation of the model within the MPC.

2.6 Model's performance in control situation

This section compares the accuracy of the four chosen models. During the model's accuracy assessment, no measurement data from the WMD base model were used except the following setups for initial and boundary conditions.

(1) *Initial conditions*: at the first time step for all the links, the flow, density, and speed were assumed to be the measured values taken from the base model with the candidate VSL control algorithm, but after the first step, they were determined by the different traffic flow models individually.

(2) *Boundary conditions*: the flow, density, and speed at links 1 and 13 were assumed to be the measured value from the base model all the time. Therefore, only the 11 links between the two terminal links were simulated.

(3) *Known ramp flows*: the input flow from the on-ramp, i.e., r_i and the exit flow through the off-ramp, i.e., s_i, in Equation (2.1) were known. Specifically, the measured values obtained from the loop detectors placed on the ramps in the base model were known.

(4) *Known VSL values*: the 20-second VSL values for all the links were known and were calculated using the candidate VSL control algorithm (Allaby et al. 2007) implemented in the base model.

2.6.1 *Qualitative accuracy*

Figure 2.7 shows the qualitative accuracy in speed, flow, and density simulation according to different traffic flow models, i.e., M1, M2, and M3. Figure 2.7(a) proves that, with or without parameterization of the FD in the speed dynamics of METANET, significant errors appear close to the speed drops (transition from free-flow to congestion). By extension, to improve traffic mobility using predictive VSL control, accurate simulation of the speed drop phenomenon is important since traffic breakdown can occur in close proximity to this region or whenever a quick transition occurs between free-flow and congestion. The figure shows that, the speed simulation by M1 is comparable to that simulated by M3. This result could be because the FD has not been directly parameterized by the VSL control variable in M1. Instead, the desired speed is based on the lesser value of either the static FD or the control variable. Possibly, for the specific link, most of the times, M1 has taken u as the desired speed during the simulation. Moreover, as expected, the error in speed simulation by M2 is large since the desired speed in M2 has always been derived from the parameterized FD.

From Figure 2.7(b), it can be seen that none of the model has replicated the measured flow very well. Specifically, with M2, the simulated flow is sometimes unnecessarily higher than the measured values. Moreover, a significant mismatch in flow simulation is visible for M3. In M3, the link outflow is calculated based on the capacity and supply concept as in Equation (2.10); however, the link-specific parameters in the constraints were considered static and corresponded to a non-VSL situation. To safeguard against any unrealistic traffic flow evolution by the model simulation, the relevant speed-limit dependant link-specific parameters must be considered in calculating the link outflow. This has been properly realized in the model M4 (DynaTAM-VSL) through Equation (2.10) and the simplified constraints as in Equation (2.14-2.19). Model enhancement due to these modifications has been presented in Figure 2.8, Figure 2.9, and Figure 2.10. Moreover, as can be seen in Figure 2.7(c), the density simulations for the link are pretty much similar in all the models. In all the models, a density calculation is performed using the same equation (Equation 2.1), and in each case, the flow simulation errors for the different VSL control modeling approaches did not affect Equation (2.1) significantly.

Figure 2.8 shows the speed simulation accuracy of the DynaTAM-VSL (M4). The model with speed-limit-dependant parameters recovers from the speed drop without delays and returns to the free-flow speed in a similar fashion. It makes the model suitable for MPC-based VSL control design. Although both M3 and M4 adopt the same VSL control modeling approach as presented in Section 2.4.1.3, the proposed modifications in the convection term described in Equation (2.11) and in the τ of the speed dynamics described in Equation (2.12) ensure that Equation (2.6) can accurately simulate the traffic speeds in the VSL control situation. This is clear when comparing the simulation results for link 7 as presented in Figure 2.7 and Figure 2.8. However, the improvement in speed simulation is not due to the above two modifications only. The improvement also occurs partly due to Equation (2.10) where the link outflow is calculated in relation to the speed-limit-dependant link-specific parameters since the accuracy of the estimated link outflow affects the density simulation (as q is an input for Equation (2.1)) and therefore the traffic speed simulation (as ρ is an input for Equation (2.6)).

Moreover, as can be seen in Figure 2.9, the link outflow described in Equation (2.10) together with the simplified constraints described in Equation (2.14-2.19) has removed the fluctuations in the simulated flow values around the measured flow. Furthermore, due to the modifications, the proposed model also offers highly accurate density estimation (see Figure 2.10). It eliminates the accuracy issues that may arise from density simulation using the adopted VSL control modeling approach described by Lu et al. (2011).

2.6.2 *Quantitative accuracy*

To quantify the error between simulated and measured traffic states for the individual links and for the entire freeway section, two statistical measures as in Equation (2.22) and Equation (2.23) have been considered: namely, mean absolute error (MAE) and root mean relative square error (RMRSE), respectively.

$$\mathrm{MAE}_{i=1,2,......13} = \frac{\sum_{k=1}^{K=450} \left| \left(\mathrm{Simulated}\ (v, \rho, \mathrm{q})_k - \mathrm{Measured}\ (v, \rho, \mathrm{q})_k \right) \right|}{\sum_{k=1}^{K} \mathrm{Measured}\ (v, \rho, \mathrm{q})_k} \tag{2.22}$$

$$\mathrm{RMRSE} = \frac{1}{M} \sqrt{\frac{\sum_{i=1}^{M} \sum_{k=1}^{K} \left| \left(\mathrm{Simulated}\ (v, \rho, \mathrm{q})_{i,k} - \mathrm{Measured}\ (v, \rho, \mathrm{q})_{i,k} \right) \right|}{\sum_{i=1}^{M} \sum_{k=1}^{K} \mathrm{Measured}\ (v, \rho, \mathrm{q})_{i,k}}} \tag{2.23}$$

In Table 2-3, traffic flow simulation with M4 is for almost all the links more accurate than the other models considered in this research. However, in link 12, there were more errors in speed simulation with M4 than with M3. For the link, by contrast, flow and density simulation with M4 is more accurate than M3. Moreover, in this case, the error in speed simulation with M4 is lower than M1 by 17.5% and M2 by 45.7%. For link 2, the errors in speed simulation by all the models are very similar.

There are two recurrent bottlenecks on the 11-km the test site. Details on the bottleneck's characteristics will be presented in Chapter 4. For the current discretization of the test site, bottlenecks B1 (weaving) and B2 (virtual lane drop situation) are located in between L3-L4, and L7-L8, respectively as can be seen in Table 2-3. From the table it can be seen that, for the two recurrent bottlenecks, B1 and B2, noticeable improvements in simulation accuracy have been achieved due to the proposed modifications with the adopted VSL control modeling approach. Specifically, for B2, the amount of error in speed simulation with M4 is the lowest, and the error is lower by 68.4%, 81.3%, and 71.7% compared to M1, M2, and M3, respectively. It proves that the introduction of the proposed modified convection term and the speed-limit-dependant reaction time parameter in Equation (2.6) can capture the best speed dynamics when drivers face multiple VSL signs. This is obvious not only for the general freeway links, but also for the bottlenecks.

Moreover, for the entire freeway section, the RMRSE values for the speed simulation are 0.0420, 0.0502, 0.0430, and 0.0313 associated with M1, M2, M3, and M4, respectively (see Figure 2.11). Compared to M1, M2, and M3, the error in speed simulation by M4 is lower by 25.5%, 37.6%, and 27.2%, respectively. Similarly, the calculated RMRSE values in flow and density simulation are the smallest with M4 at 0.0407 and 0.0458, respectively. Compared to M1, M2, and M3, the improvements in flow simulation for the entire freeway section are 8.1%, 24.9%, and 17.6%, and the improvements in density simulation are 7.3%, 12.5%, and 10.2%, respectively. Indeed, the improvements in link outflow calculation and thus the density simulation have been achieved mostly due to the introduction of speed-limit-dependant link-specific parameters within Equation (2.10) as well as the use of constraints on traffic dynamics as described in Equation (2.14-2.19).

2.7 Sensitivity with respect to structural changes

This section further investigates the improvement in traffic flow simulation accuracy achieved through each of the proposed modifications in the base model ─ METANET for the VSL control situation. Table 2-4 shows that the DynaTAM-VSL can reproduce the traffic flow accurately over the 2.5 hour simulation (K =450). The errors between the measured and the DynaTAM-VSL simulated speed, flow, and density are 3.6%, 4.0%, and 4.9%, respectively. Note that, the values in RMRSE as presented in Table 2-4 is for a different demand profile compared to that in Figure 2.11. It confirms the proposed model's accuracy and robustness to simulate different traffic states as a result of assigned different demand levels. As expected, to accurately simulate the traffic flow with the DynaTAM-VSL, the boundary constraints (Equation 2.10) play the most important role. Dropping the boundary constraints from the model (by alternatively adopting Equation 2.2) results in a 28.7%, 35.0%, and 10.1% increase in RMRSE values in speed, flow, and density as compared to the respective values in the DynaTAM-VSL.

After that, the modified convection term contributes a higher accuracy in simulating the flow by the model. Keeping the convection term in the model as it appears in the METANET results in a 10.8% increase in error for speed estimation compared to the simulation with the modified convection term. Moreover, it can be found that traffic simulation errors occur both when the speed-limit-dependant τ is absent and if a modification in υ gets introduced. It can be seen that introducing the downstream density-dependent υ results in increasing error by 8.1%, 4.3%, and 4.1% for the speed, flow, and density estimation, respectively, compared to the DynaTAM-VSL. Therefore, this introduction is an unnecessary approach to evaluate the model performance considering both the speed-limit-dependant τ and the downstream density-dependant υ.

2.8 Summary and conclusions

It is essential to know how accurately the model adopted within the MPC framework can simulate the traffic flow in the VSL control situation. The METANET model provides a candidate model for VSL control design since it is coupled with both speed and density dynamics. Nevertheless, the model does not explicitly describe the impact of VSL control on traffic flow. Previously, several approaches were developed to modify the speed-density curve, i.e., the FD in speed dynamics of METANET. However, no analysis can be found that investigates whether the existing VSL control modeling approaches could represent traffic flow sufficiently in the control situation, specifically as concerned the congested equilibrium region of the FD. To this end, this research investigates the speed-density and flow-density curve resulting in different VSL control modeling approaches. There are six main findings from the above investigation:

(1) The direct parameterization of the FD with the affine functions of the VSL control variable can simulate cross points in the flow-density curves; however, traffic flow never completely stops. Nevertheless, density could reach a maximum value, i.e., jam density.

(2) Moreover, with this approach, there is a consistent decrease in flow capacity values with the reduction of speed limits. Whereas, several field studies found capacity improvements at least for some VSL.

(3) The desired speed was found to be unrealistic for all the possible density values. Under low densities, VSL results in traffic speeds that are considerably lower than the displayed VSL, and the speed that the driver would assume without VSL, which violates the equilibrium traffic state assumption. Moreover, in the moderate

to high densities, it shows that the densities are still affected that result in a no-VSL situation when speeds are already lower than the speed limit. This outcome exaggerates driver behaviour.

(4) In contrast to the above VSL modeling approach, which is an approach that takes the lesser value between the FD and VSL control variable, the desired speed in the control situation can better represent the driver speed choice behaviour. However, in high density regions, there would be inconsistency with the real-world control situation.

(5) Moreover, with the above approach, the flow-density curve with the VSL control was found to be more accurate and did not show (until the critical density associated with the no-VSL situation) a decrease in capacity due to speed limit reductions. Unfortunately, it cannot simulate cross points between the flow-density curves.

(6) On the contrary, replacing the FD in speed dynamics with linear VSL control variable can effectively circumvent the inaccuracy issue that arose from with or without parameterization of the FD. However, the speed-limit dependant link-specific parameters (i.e., capacity, free-flow speed, critical density, etc.) must be considered to avoid unrealistic traffic flow evolution in the VSL control situation.

Based on the above findings, this research proposes a new second-order traffic flow model, DynaTAM-VSL that drops the nonlinear parameterization of the speed limit control variable and instead uses the linear VSL control variable as the desired speed. Several modifications have been introduced using the VSL control modeling approach: (1) speed-limit-dependant link-specific parameters in the boundary constraints while calculating link outflow in which the link-specific parameters are estimated using multiple triangular-shaped fundamental diagrams (FDs); (2) a new convection term in the speed dynamics that considers whether the immediate downstream link is congested and/or the current link is saturated with the VSL control; (3) a speed-limit-dependant reaction time parameter considering whether a driver has a lower reaction time during the deceleration process when a lower speed limit is displayed in the downstream link and vice-versa; and (4) several simplified constraints to address system dynamics and traffic characteristics.

After that, a systematic calibration method of the traffic flow model, DynaTAM-VSL, in a control situation has been proposed. For which traffic data has been extracted from a field data-based microscopic simulation model. This chapter investigates the sensitivity of the calibrated macroscopic model with respect to small changes in the optimal global parameter values. The analysis showed that the proposed model is not sensitive to small changes in the optimal global parameter values. Out of the five global parameters, the parameter related to driver response is somewhat sensitive when the downstream VSL sign shows a higher speed limit than in the current link. For this parameter, 10.0% reductions of the optimal parameter value caused the model to degrade by 0.7%, which might require careful adaptation during the implementation of the model within the MPC. It was found that introducing the speed-limit-dependant link-specific parameters as boundary constraints while calculating link outflow can remove the inaccuracy in density simulation. Moreover, with the modified convection term and the speed-limit-dependant reaction time parameter, the speed dynamics of the model can recover from the speed drop without delays and will return to the free-flow speed in a similar fashion. It was found that, for almost all the links in the studied freeway section and when compared to the other METANET-based traffic flow models, the proposed model can simulate the traffic flow better. More importantly, the model performs better in simulating bottlenecks flow, which is critical. It was found that due to the speed-limit dependant parameters, accuracy in speed simulation for a lane drop bottleneck improved by 71.7% compared to the model M3 that does not consider speed-limit dependant parameters, yet adopts the same VSL control modeling approach. For a given demand inputs, the calculated root mean relative square error (RMRSE) values for the entire freeway section in speed, flow and density simulation were 0.0313, 0.0407, and 0.0458, respectively. Those values were found to be minimum compared to all other models considered in this research.

To determine the contributions of the proposed modifications in improving traffic flow simulation with the VSL modeling approach, this chapter investigates the sensitivity of the DynaTAM-VSL with respect to changes in the structure. It was estimated that without the speed-limit-dependant link-specific parameters, the DynaTAM-VSL results in a 28.7%, 35.0%, and 10.1% increase in RMRSE values respectively in speed, flow, and density simulations. After that, the modified convection term contributes a higher accuracy in simulating the flow by the model. Keeping the convection term in the model as it appears in the METANET results in a 10.8% increase in error for speed estimation. The simulation results show that splitting the anticipation parameter in the speed dynamics of DynaTAM-VSL does not work well. Specifically, introducing this modification results in increasing error by 8.1%, 4.3%, and 4.1% for the speed, flow, and density estimation, respectively. Basically, this parameter takes on one of the two values, υ_{high} or υ_{low}, based on the link density. This modification works well with the VSL control modeling approach in which a static FD exists for speed dynamics. Moreover, that FD depends on the link density. By replacing the FD with the VSL control variable, this coupling gets broken, which could be a reason for the above results.

2.9 References

Alessandri, A., Febbraro, A. D., Ferrara, A., and Punta, E. (1999). "Nonlinear optimization for freeway control using variable-speed signaling." *IEEE Transactions on Vehicular Technology*, 48(6), 2042-2052.

Allaby, P., Hellinga, B., and Bullock, M. (2007). "Variable speed limits: Safety and operational impacts of a candidate control strategy for freeway applications." *IEEE Transactions on Intelligent Transportation Systems*, 8(4), 671-680.

Carlson, R. C., Papamichail, I., Papageorgiou, M., and Messmer, A. (2010a). "Optimal mainstream traffic flow control of large-scale motorway networks." *Transportation Research Part C: Emerging Technologies*, 18(2), 193-212.

Carlson, R. C., Papamichail, I., Papageorgiou, M., and Messmer, A. (2010b). "Optimal motorway traffic flow control involving variable speed limits and ramp metering." *Transportation Science*, 44(2), 238-253.

Cremer, M., and Papageorgiou, M. (1981). "Parameter Identification for a Traffic Flow Model." *Automatica*, 17(6), 837-843.

Dervisoglu, G., Gomes, G., Kwan, J., Muralidharan, A., Horowitz, R., and Horowitz, R. (2009). "Automatic calibration of the fundamental diagram and empirical observations on capacity." *Transportation Research Board 88th Annual Meeting*.

Hadiuzzaman, M., Qiu, T. Z., and Lu, X. Y. (2013). "Variable Speed Limit Control Design for Relieving Congestion Caused by Active Bottleneck." *Journal of Transportation Engineering*, 139(4), 358-370.

Han, S. P. (1977). "A globally convergent method for nonlinear programming." *J. Optimization Theory and Applications*, 22 297.

Hegyi, A., Burger, M., Schutter, B. D., Hellendoorn, J., and Van den Boom, T. J. J. (2007). "Towards a Practical Application of Model Predictive Control to Suppress

Shockwaves on Freeways." *Proceedings of the European Control Conference 2007 (ECC'07), Kos, Greece,* 1764–1771.

Hegyi, A., De Schutter, B., and Hellendoorn, J. (2005). "Optimal coordination of variable speed limits to suppress shock waves." *IEEE Transactions on Intelligent Transportation Systems,* 6(1), 102-112.

Hellinga, B., and Mandelzys, M. (2011). "Impact of driver compliance on the safety and operational impacts of freeway variable speed limit systems." *J.Transp.Eng.,* 137(4), 260-268.

Kotsialos, A., Papageorgiou, M., Diakaki, C., Pavlis, Y., and Middelham, F. (2002). "Traffic Flow Modeling of Large-Scale Motorway Networks Using the Macroscopic Modeling Tool METANET." *IEEE Transactions on Intelligent Transportation Systems,* 3(4), 282-292.

Lee, C., Hellinga, B., and Saccomanno, F. (2006). "Evaluation of variable speed limits to improve traffic safety." *Transportation Research Part C: Emerging Technologies,* 14(3), 213-228.

Lenz, H., Sollacher, R., and Lang, M. (1999). "Nonlinear speed-control for a continuum theory of traffic flow." *In 14th World Congress of IFAC, Beijing, China,* Q 67–72.

Lu, X. -., Qiu, T. Z., Horowitz, R., Chow, A., and Shladover, S. (2011). "METANET model improvement for traffic control." *IEEE Conference on Intelligent Transportation Systems, Proceedings, ITSC,* 2148-2153.

Messmer, A., and Papageorgiou, M. (1990). "METANET: a macroscopic simulation program for motorway networks." *Traffic Engineering & Control,* 31(8-9), 466-470.

Papageorgiou, M., Blosseville, J. -., and Hadj-Salem, H. (1990). "Modelling and real-time control of traffic flow on the southern part of Boulevard Peripherique in Paris: Part I: Modelling." *Transportation Research Part A: General,* 24(5), 345-359.

Papageorgiou, M., Kosmatopoulos, E., and Papamichail, I. (2008). "Effects of variable speed limits on motorway traffic flow." *Transportation Research Record*, (2047), 37-48.

Payne,H.J.(1971)."Models of freeway traffic and control." *Math. Models Publ. Sys. Simul. Council Proc., 28,* 51-61.

Powell, M. J. D. (1978). "A fast algorithm for nonlinearly constrained optimization calculations." *Numerical Analysis, G.A.Watson Ed., Lecture Notes in Mathematics, Springer Verlag,* 630.

Sanwal, K. K., Petty, K., Walrand, J., and Fawaz, Y. (1996). "An extended macroscopic model for traffic flow." *Transportation Research Part B: Methodological*, 30(1), 1-9.

Yeo, H. (2008). "Asymmetric Microscopic Driving Behavior Theory." *University of California Transportation Center*.

Zackor, H. (1991). "Speed limitation on freeways: Traffic-responsive strategies." *M. Papageorgiou, Ed. Concise Encyclopedia of Traffic and Transportation Systems. Oxford, UK,* 507–511.

Table 2-1 Optimal values of parameters related to different METANET-based traffic flow models that are calibrated in the VSL control situation.

Different models	Model parameters	Parameter values ($\beta^{optimal}$)	$f(\beta^{optimal})$
M1	$\tau, \upsilon_{low}, \upsilon_{high}, \kappa$ $v_{free,i}, \alpha_i, \rho_{c,i}$	0.0057, 5.0, 71.4, 84.9, 84.7, 1.377, 50.0	2040
M2	$\tau, \upsilon, \kappa,$ $v_{free,i}, \alpha_i, \rho_{c,i}, A_i, E_i$	0.0043, 9.5, 10.4, 73.5, 2.356, 40.0, 1.46, 1.6	1834
M3	τ, υ, κ	0.0057, 5.0, 63.7	2067
M4	$\tau_{low}, \tau, \tau_{high}, \upsilon, \kappa$	0.008, 0.005, 0.012, 94.6, 98.9	1299

Table 2-2 $\Omega(\Delta\beta)$ for small changes in optimal parameter values.

Assumed values in parameter changes	$\beta_1 = \tau$	$\beta_2 = \tau_{low}$	$\beta_3 = \tau_{high}$	$\beta_4 = \upsilon$	$\beta_5 = \kappa$
$\Omega(\Delta\beta_J = +10\%)$	0.22	0.07	0.51	0.03	0.27
$\Omega(\Delta\beta_J = +20\%)$	0.11	0.50	0.34	0.23	0.46
$\Omega(\Delta\beta_J = -10\%)$	0.12	0.36	0.70	0.20	0.31
$\Omega(\Delta\beta_J = -20\%)$	0.48	0.50	0.33	0.11	0.25

Table 2-3 MAE between 20-s measured and METANET-based model simulated traffic parameters in WMD.

Link no.	Traffic parameters											
	v				q				ρ			
	M1	M2	M3	M4	M1	M2	M3	M4	M1	M2	M3	M4
L2	$\underline{0.094}$	$\underline{0.098}$	$\underline{0.095}$	0.104	$\underline{0.139}$	0.141	0.194	0.141	$\underline{0.356}$	0.370	$\underline{0.321}$	0.360
L3 (B1)	0.056	0.093	0.068	0.037	$\underline{0.173}$	0.175	0.204	0.175	0.290	0.353	$\underline{0.236}$	0.259
L4	0.076	0.110	0.084	0.073	$\underline{0.244}$	0.248	0.251	0.248	0.091	0.114	0.098	0.077
L5	0.166	0.241	0.243	0.046	0.303	0.509	0.446	0.270	0.052	0.046	0.045	0.033
L6	0.232	0.262	0.217	0.058	0.311	0.550	0.490	0.221	0.072	0.060	0.054	0.029
L7 (B2)	0.178	0.300	0.199	0.056	0.320	0.574	0.454	0.227	0.145	0.141	0.178	0.109
L8	0.135	0.223	0.114	0.063	0.269	0.476	0.351	0.207	0.124	0.120	0.127	0.111
L9	0.098	0.127	0.089	0.075	0.205	0.298	0.216	0.202	0.155	$\underline{0.140}$	0.172	0.152
L10	0.090	0.118	0.104	0.079	0.194	0.237	0.222	0.180	$\underline{0.216}$	0.246	0.327	0.218
L11	0.150	0.268	0.195	0.084	0.279	0.427	0.280	0.212	0.249	0.383	0.312	0.167
L12	0.113	0.140	$\underline{0.046}$	0.096	0.193	0.288	0.197	0.154	0.060	0.050	0.058	0.035

(*Note*: *In the table, the underline mark refers to a model that performs better compared to M4 in simulating the specific traffic parameter for the specific link. However, in those cases, the MAE values for M4 and the specific model are found to be almost same*.)

Table 2-4 Sensitivity of DynaTAM-VSL with respect to structural changes.

Change in model structure	Optimized global parameter values	RMRSE		
	$\tau_{low}, \tau, \tau_{high}, \upsilon, \kappa$	v	q	ρ
DynaTAM-VSL	0.008, 0.005, 0.012, 94.6, 98.9	0.0358 (n/a)	0.0400 (n/a)	0.0494 (n/a)
DynaTAM-VSL without boundary constraint (Equation 2.10)	0.0089, 0.013, 0 .028, 80.3, 109	0.0461 (-28.77%)	0.0540 (-35.00%)	0.0544 (-10.12%)
DynaTAM-VSL without modified convection term (Equation 2.12)	0.0037, 0.0093, 0.0090, 5.9, 81.3	0.0397 (-10.89%)	0.0430 (-7.50%)	0.0520 (-5.26%)
DynaTAM-VSL without speed-limit-dependant τ (Equation 2.13)	n/a, 0.00325, n/a, 56.8, 81.1	0.0368 (-2.79%)	0.0413 (-3.25%)	0.0508 (-2.83%)
DynaTAM-VSL with downstream density-dependant υ	n/a, 0.0028, n/a, υ_{high} =85.3, υ_{low} =9.9, 76.7	0.0387 (-8.10%)	0.0417 (-4.25%)	0.0514 (-4.05%)

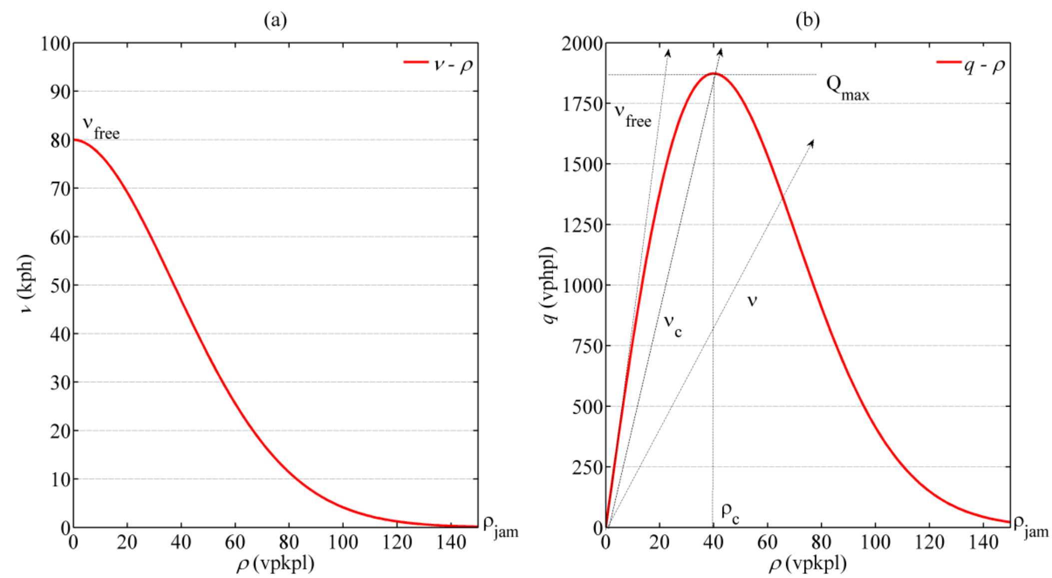

Figure 2.1 Parameter illustration in non-linear FDs: (a) v - ρ ; and (b) q - ρ .

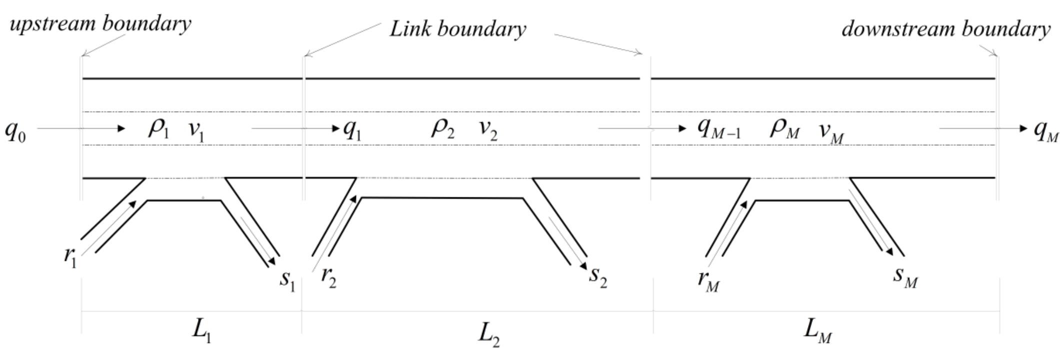

Figure 2.2 Freeway section divided into links. Each link has one on-ramp and off-ramp. While, ρ and v are segment-based parameters; q , r , S are point-based parameter.

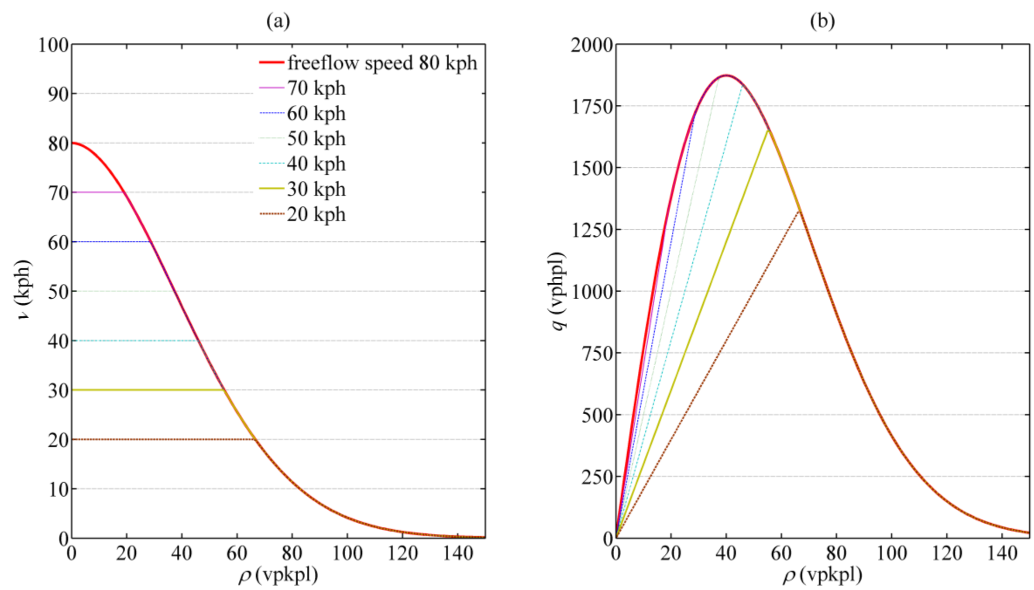

Figure 2.3 Curves without parameterization in FD: (a) v - ρ and (b) q - ρ. With, $v_{free,i}$ = 80 kph; u_i =70, 60, 50, 40, 30, 20 kph; $\rho_{c,i}$ =40 vpkpl; α_i =1.867.

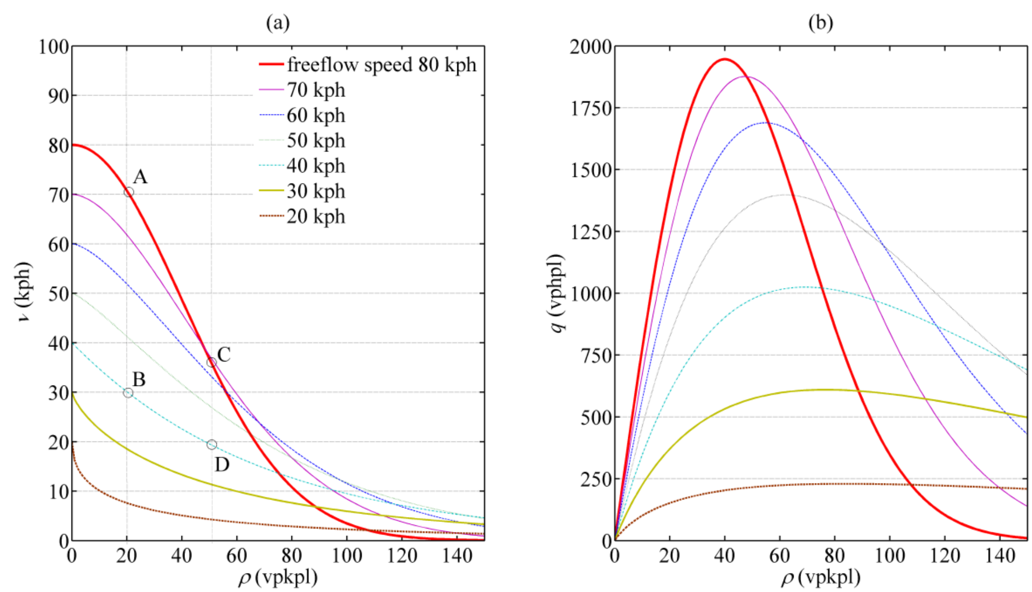

Figure 2.4 Curves due to parameterization in FD by affine functions: (a) v - ρ and (b) q - ρ. With, $v_{free,i}$ = 80 kph; u_i =70, 60, 50, 40, 30, 20; $\rho_{c,i}$ =40 vpkpl; α_i = 2.3568; A_i =1.4629; E_i =1.5504.

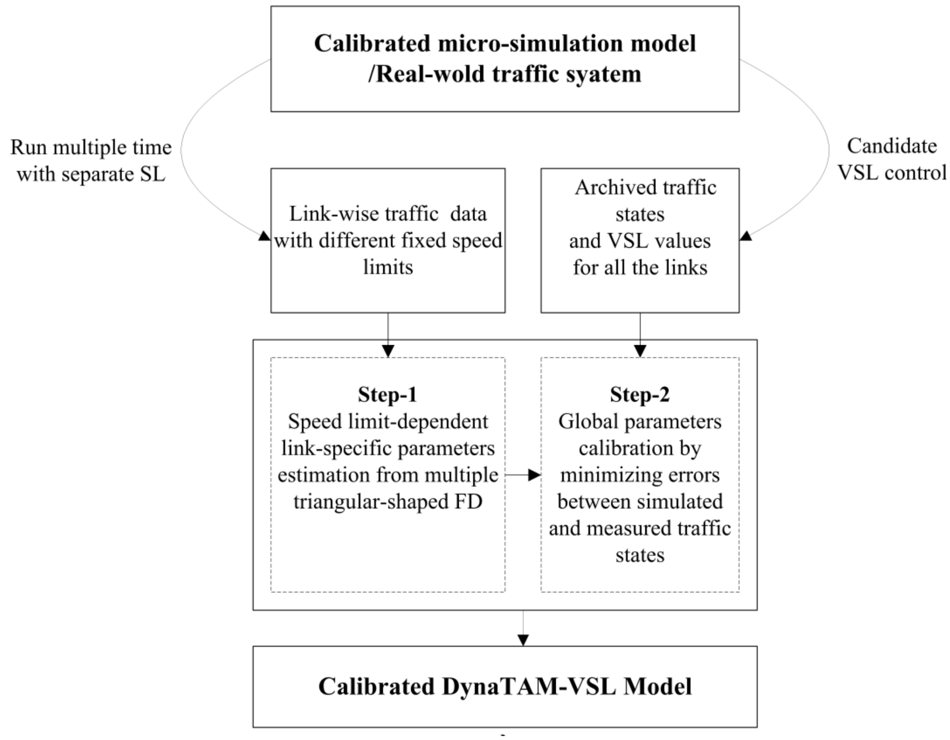

Figure 2.5 DynaTAM-VSL calibration method in control situation.

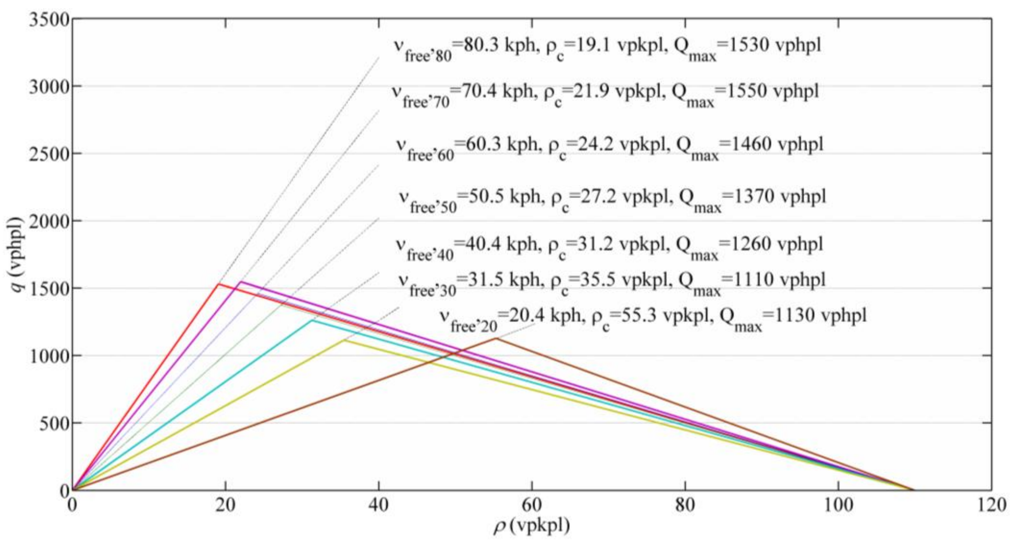

Figure 2.6 Estimating speed-limit-dependant link-specific parameters from multiple triangular-shaped FD. The left limb, apex, and vertical line from apex to *x*-axis respectively determine free-flow speed, capacity, and critical density for each SL.

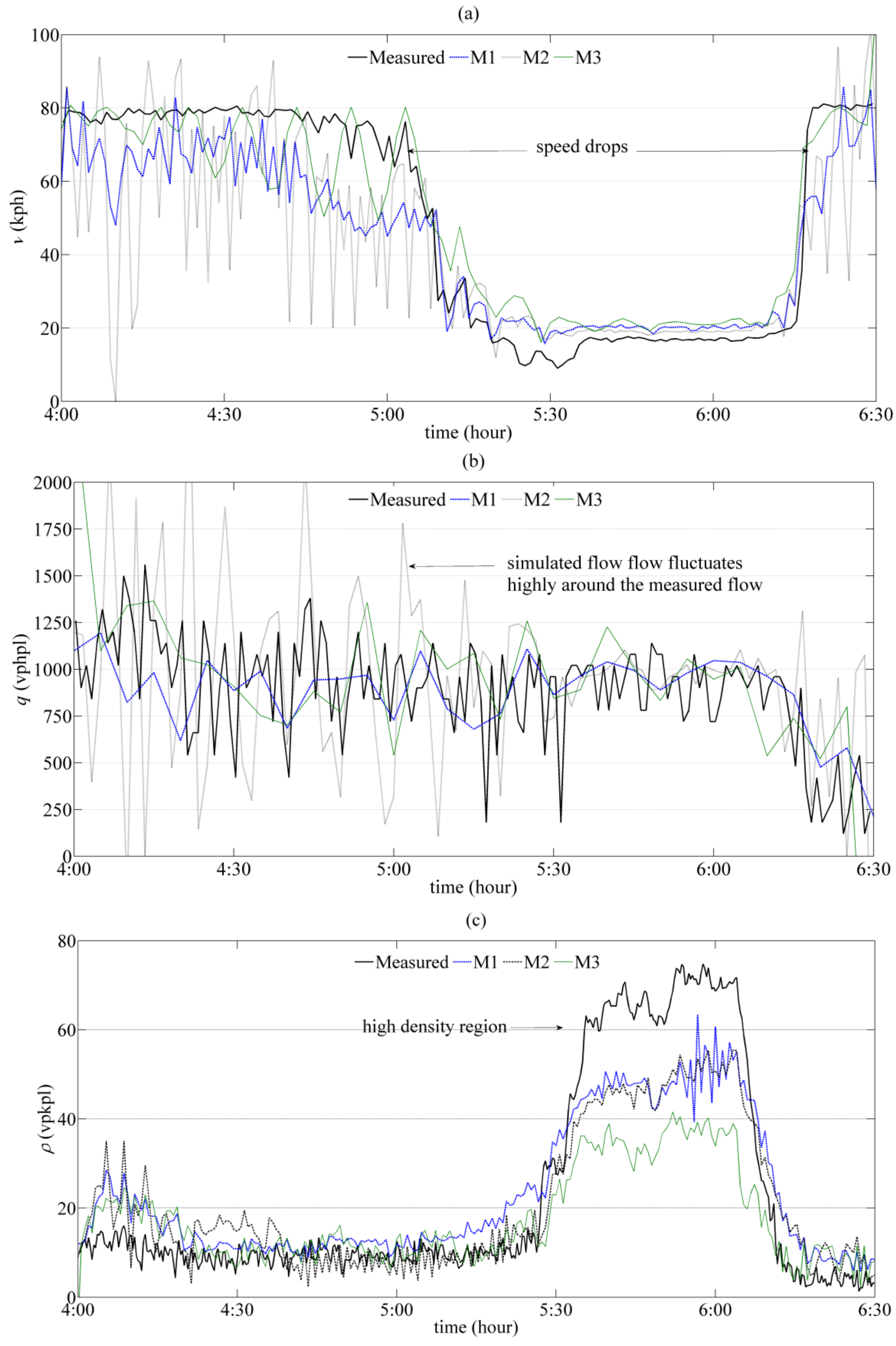

Figure 2.7 Comparison between measured and existing model simulated traffic states for a link with congested condition: (a) speed, (b) flow, and (c) density profile.

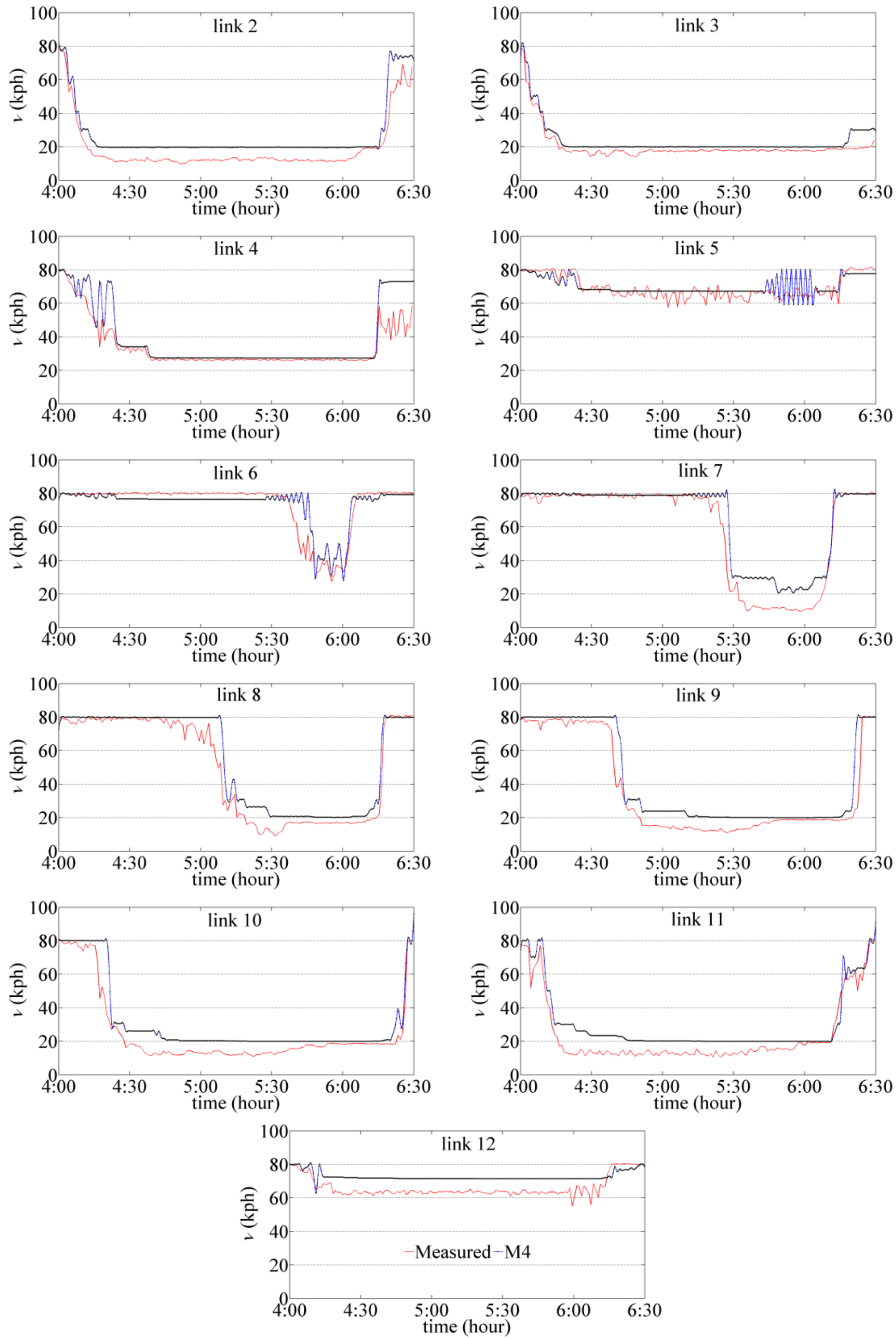

Figure 2.8 Comparison between measured and DynaTAM-VSL (M4) simulated speed profile.

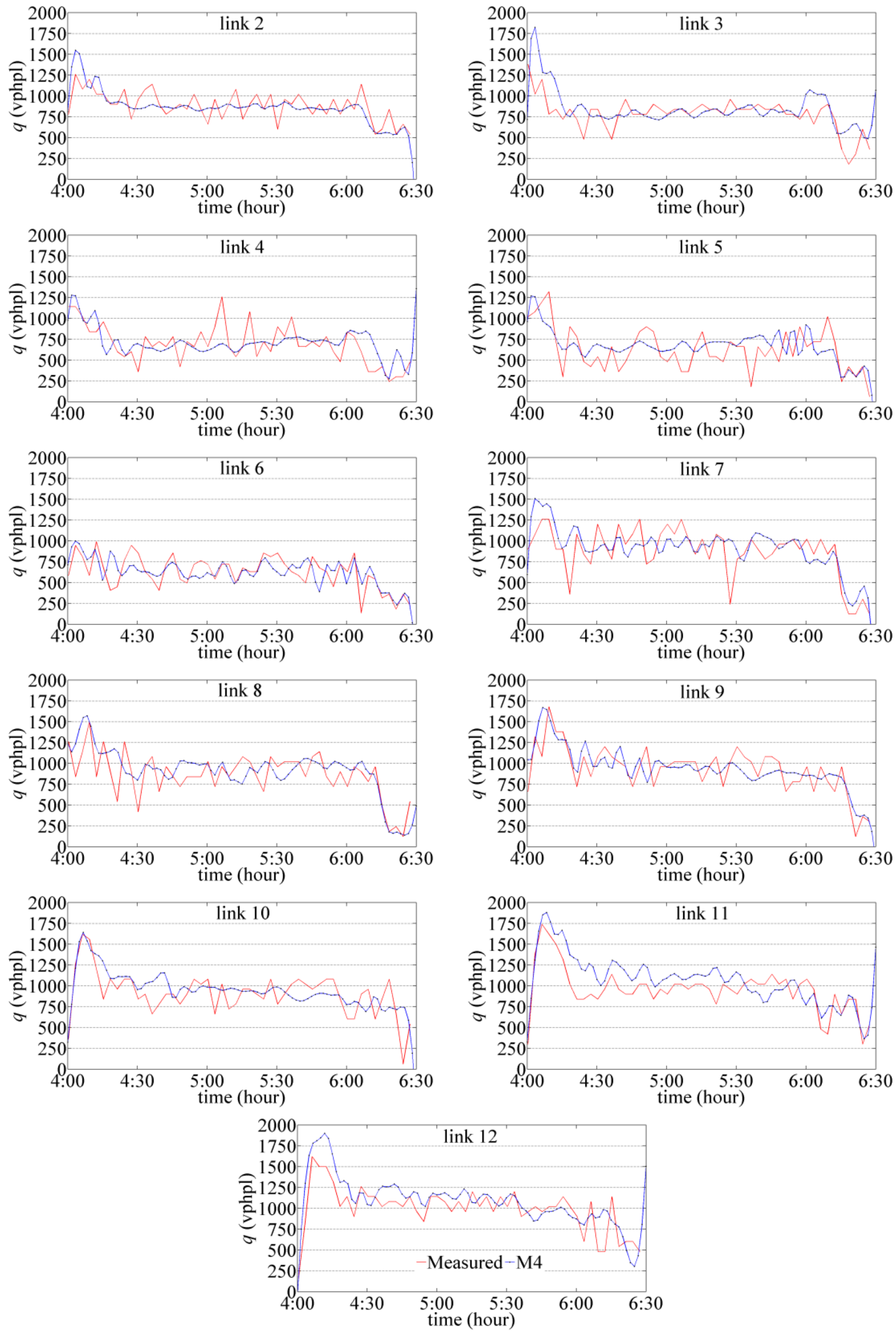

Figure 2.9 Comparison between measured and DynaTAM-VSL (M4) simulated flow profile.

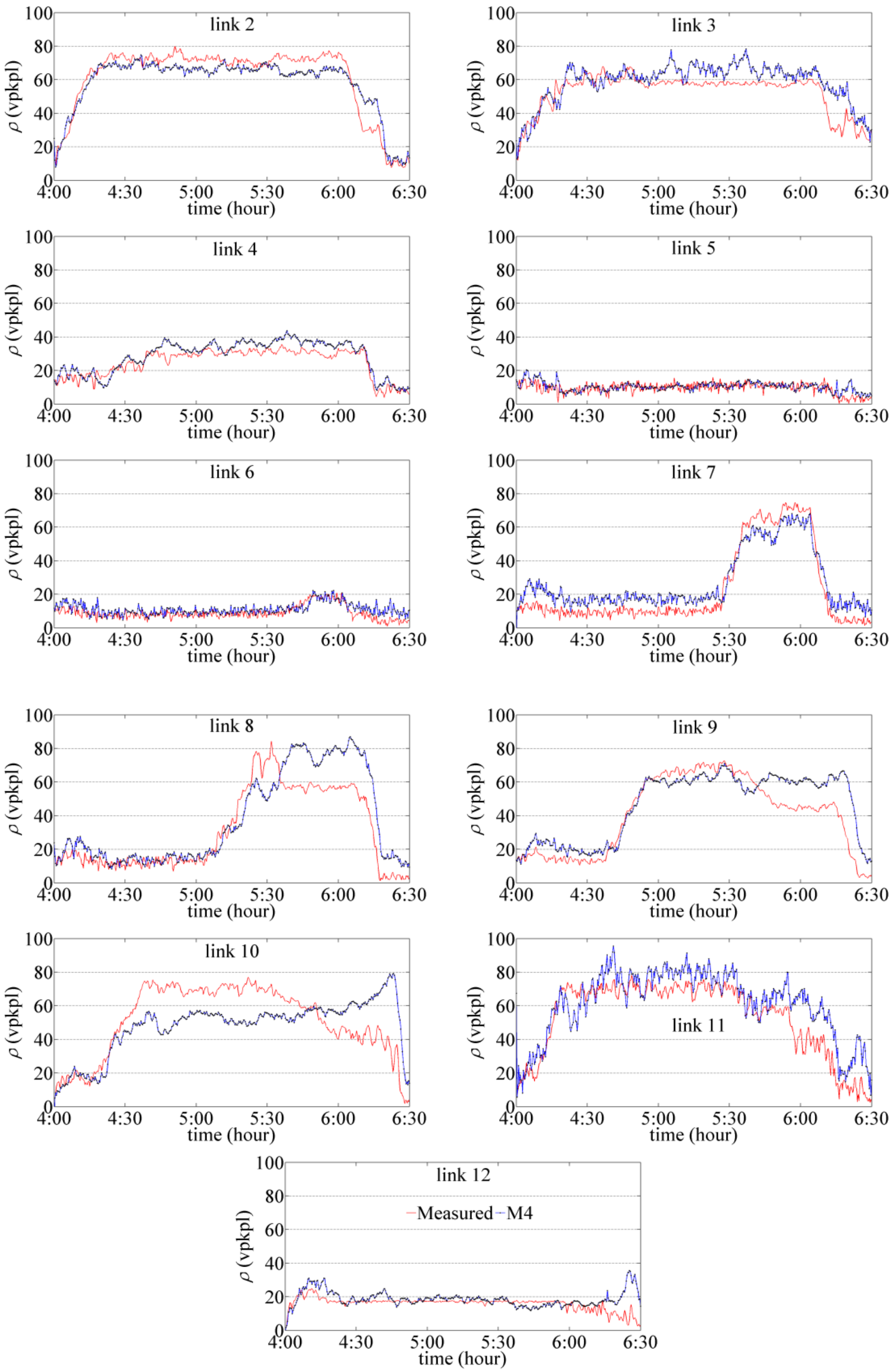

Figure 2.10 Comparison between measured and DynaTAM-VSL (M4) simulated density profile.

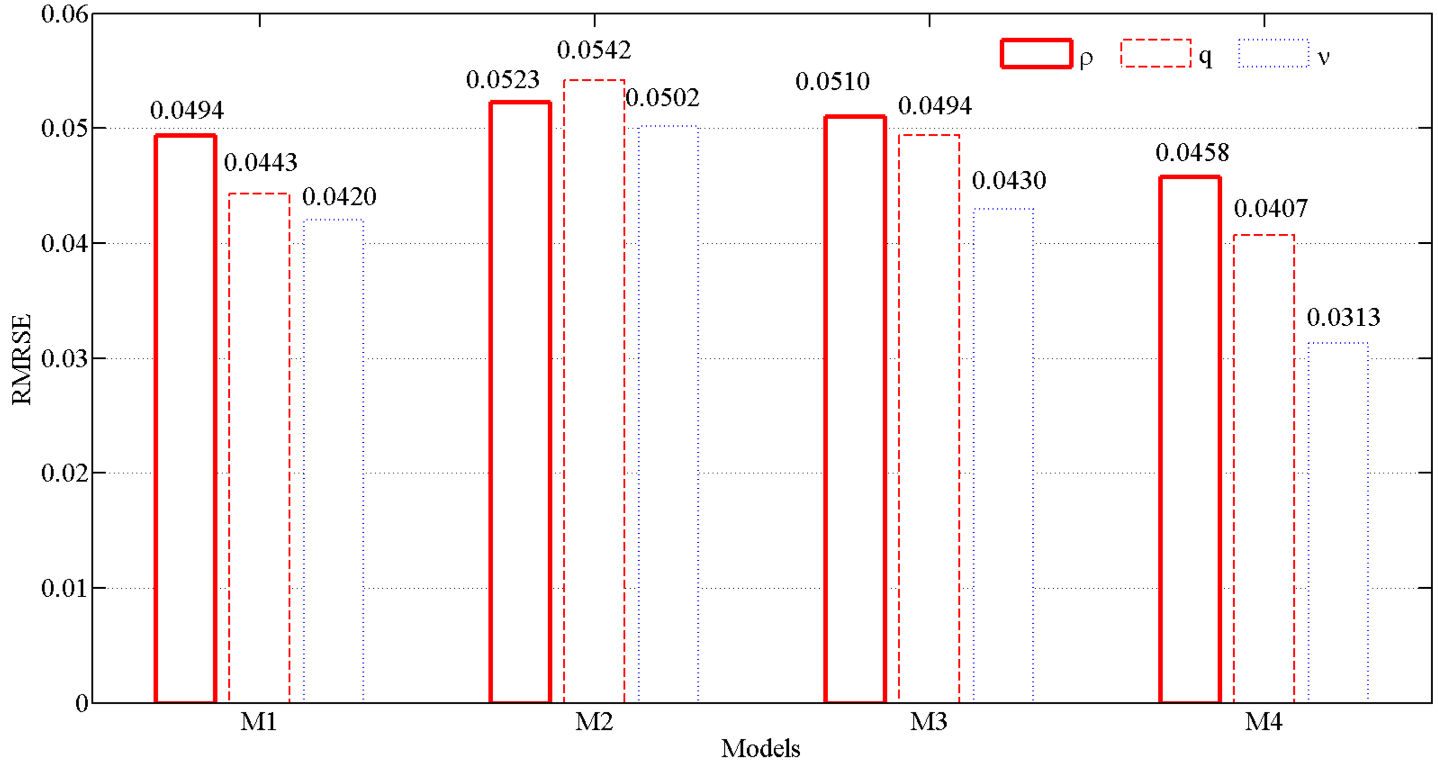

Figure 2.11 Network-wide errors in simulating traffic parameters in VSL control situation by different METANET-based traffic flow models.

Parameterization of FD with VSL control variable results in maximum error in traffic flow simulation.

Chapter 3

Impact of demand levels and MPC parameters on multi-objective optimization under coordinated VSL control*

3.1 Introduction

Variable Speed Limit (VSL) control is an Active Traffic Management (ATM) method that adjusts freeway speed limits based on real-time road, traffic, and weather conditions. It is perceived that when the VSL control is applied in a proactive manner, both the travel time and the link throughput can be improved in congestion periods. However, most simulation-based evaluations report that the proactive optimal VSL control strategy is capable of improving only the travel time. Due to the nature of the control, those VSL implementations could reduce input flow at the mainline upstream boundary, which consequently contributes to travel time reduction of the controlled freeway section. Yet, no established research could be found that proves that the VSL control can consistently improve both the travel time and the throughput during congestion periods, which is when efficient traffic control strategies are most needed.

* *This chapter is an extended version of an accepted article*. **Hadiuzzaman, M.,** Fang, J., Lan, C., and Qiu, T.Z**.** (2014). "Impact of Mainline Demand Levels and Control Parameters on Multi-Objective Optimization Involving Proactive Optimal VSL Control." *will be included on the 93rd Transportation Research Board (TRB) Annual Meeting Compendium of Papers*. (*peer-reviewed*)

This research finds that, in terms of improving the throughput, the VSL effectiveness largely depends on mainline demand levels. In general, during high demand periods, due to a capacity drop at fixed bottlenecks, throughput from the uncontrolled freeway section can decrease by 0–15.0% (Hegyi 2004). Thus, the VSL control can achieve throughput improvements within that range only by maintaining a flow that is higher than the dropped capacity (also known as congestion capacity), but less than the bottleneck free-flow capacity. By contrast, if the VSL control maintains a flow that is close to the free-flow capacity, travel time improvements could be minimal due to high traffic density and inhomogeneous flow. Consequently, to maintain a trade-off between travel time and throughput improvements, it is essential to develop a modeling framework that is accurate and that yields a correct solution when incorporated with the optimization method. This research designs the VSL control within the novel model predictive control (MPC) framework, which elicits maximum mobility benefits from the VSL control using an accurate macroscopic traffic flow model used for traffic state prediction and objective function evaluation during online control. Furthermore, the mobility benefits can be fine-tuned through three items related to the MPC: the prediction horizon, the control horizon, and the sub-objective weights.

In this research, a separate VSL sign is designed and implemented to control traffic flow in each link of the studied freeway test site, Whitemud Drive (WMD), where the link length is approximately 800 metres (m). The length of each link is longer than the free-flow travel distance to satisfy the *step size modeling constraint*. In simulation, deploying a separate VSL sign at each link yielded the most information regarding the MPC-based VSL control (under maximum flexibility) and potential impacts. Furthermore, to avoid any negative impacts to traffic flow in other locations, all the VSL control inputs were simultaneously optimized within the defined objective function. However, in real-life deployment, considering budget constraints and roadway geometry, the links could be aggregated into several clusters of links and each cluster could be operated with one VSL sign (e.g., link 1 and 2 have the same speed limit) also reducing the real-time computation time due to the reduced number of VSL control variables to be optimized.

For traffic state prediction on discretized freeway links with VSL control, this research implements the calibrated and validated DynaTAM-VSL model, which is presented in Chapter 2. With the model, this research assesses improvements in the mobility criteria considering typical values of control parameters and objective functions, and investigates what should be the optimal values of control parameters involving multi-objective optimization—reducing total travel time (TTT) and increasing total travel distance (TTD)—a measure of throughput from the freeway links. Finally, the VSL control is evaluated for a range of mainline demand levels. The objective is to determine when and how the VSL can provide maximum benefits without compromising any of the chosen mobility parameters.

This research uses the scatter search proposed in Ugray et al. (2007) to provide starting points for the gradient-based local solver, sequential quadratic programming (SQP), to find the global minimum of the objective function, and, thus, the optimal VSL values at each control horizon. The optimization method combines the superior accuracy- and feasibility-seeking behavior of gradient-based local nonlinear programming (NLP) solvers with the global optimization abilities of the scatter search. By contrast, the SQP that uses uniformly distributed start points with multi-start optimization was adopted in several macroscopic evaluation of MPC-based VSL control, including Hegyi et al. (2007); Hegyi et al. (2005); Long et al. (2008); and Zegeye et al. (2011). These applications increase the probability of reaching a global solution with an increased number of starting points; however, these applications are difficult to identify in real-time and in online control.

3.2 Literature review

This section reviews the typical objective functions adopted by the traditional optimal, and the MPC-based, VSL control strategy. Optimal control uses an objective function to optimize the traffic states. MPC is also an optimal control method which is applied in a rolling horizon concept, where the measured traffic data and the traffic demands are regularly fed back to the controller. Therefore, the controller can take demand prediction errors into account and correct for prediction errors resulting from model mismatch. Consequently, in some recent studies, MPC-based control framework has been adopted for different types of freeway traffic control design. It is important to summarize the outcome of this earlier research as it helped to design VSL control for this research.

3.2.1 *Objective function impacts on optimal VSL control*

Alessandri et al. (1999) performed a macro-simulation using link throughput as a cost function within an optimal control framework, and reported that VSL control was capable of preventing congestion and improving throughput, but that it had little impact on TTT.

Kang et al. (2004) proposed an optimal VSL control algorithm for freeway work zone operations based on the evolution of dynamic traffic states and macroscopic traffic characteristics using a CORSIM micro-simulation model. The evaluation showed that VSL control can increase the throughput over the work zone and reduce the average delay over upstream segments of the lane-closure location under only normal traffic conditions. The simulation results also indicated that, although the average speeds under the VSL control do not significantly vary from those under no VSL control, the resulting speed variance among vehicles traveling over the work zone is substantially lower.

Lin et al. (2004) proposed and implemented two online optimal VSL control algorithms in the CORSIM micro-simulation model, and adopted the work-zone maximum throughput, average delay and speed as the primary measures of effectiveness (MOEs). The simulation demonstrated that VSL can improve the throughput in a work zone and the average delay over upstream segments of the lane-closure location only under the normal traffic conditions. Later on, Kang and Chang (2006) presented an optimal time-of-day speed limit (TOD SL) control for freeway work-zone operations considering throughput as an objective function; and compared their control performance with optimal VSL control to Lin et al. (2004). To evaluate the effectiveness of the TOD SL model, this research employed the simulation program CORSIM. The work zone throughput was marginally improved compared to the no-VSL situation; however, it did not show better performance than the optimal VSL control during high demand periods.

Carlson et al. (2010a) evaluated VSL performance within the macroscopic AMOC (Advanced Motorway Optimal Control) software tool. The cost criterion was the travel time by all vehicles in the network. Simulation of the optimal VSL control in the Amsterdam ring-road A10, which is about 32 kilometres (km) in length, resulted in 47.0% travel time reduction. In another research, Carlson et al. (2010b) showed 15.3% travel time reduction using the optimal VSL control method as in Carlson et al. (2010a). However, neither research considers the throughput improvements of VSL implementation.

3.2.2 *Objective function impacts on MPC-based VSL control*

Hegyi et al. (2005) evaluated the MPC-based VSL control using TTT as the cost function, and reported a 21.0% network-wide travel time reduction. In another simulation research, Hegyi et al. (2007) implemented the MPC-based VSL control in PARAMICS software that resulted in a 32.0% TTT reduction. Interestingly, Long et al. (2008) performed another research on a hypothetical 5 km work zone using the same traffic flow model and optimization method to reduce TTT as used in Hegyi et al. (2005), but did not find any travel time improvements. However, the authors concluded that the VSL control can make traffic speed more homogeneous by mitigating dramatic changes within the traffic system.

Zegeye et al. (2011) proposed a MPC-based traffic control for the balanced reduction of travel times, emissions, and fuel consumption using a VSL control. To find the optimal values of the VSL control variable, four different objective functions were considered: (1) TTT; (2) Total Emissions (TE); (3) Total Maximum Dispersion Level (TMDL); and (4) a weighted sum of TTT, TE, and TMDL. To solve the MPC optimization problem, the authors used the SQP. However, the VSL control showed travel time improvement by 36.0% only when the objective of the controller was set to reduce the TTT. With all of the other objective functions, the VSL control increased the travel time by 10.0-20.0%.

Hadiuzzaman and Qiu (2013) proposed a cell transmission model (CTM)-based VSL control, and also used the MPC to dynamically change the speed limit in real-time considering the combined objectives: reducing TTT and increasing throughput. Their VISSIM simulation results with combined objectives showed 10.0-15.0% travel time reduction and 5.0-7.0% throughput improvement. In another research, Hadiuzzaman et al. (2013) proposed several modifications in the METANET model (Papageorgiou et al.

1990) for the MPC-based VSL control design for relieving congestion caused by recurrent bottlenecks. The proposed VSL control showed 39.0% travel time reduction and 6.0% flow improvement. MPC-based VSL control was also designed by Lu et al. (2011) within the AIMSUN microscopic simulator with similar combined objectives as above. The simulation results showed 45.0% travel time improvement. However, the authors did not present the benefits in terms of improving link throughput.

The following two conclusions can be drawn from the literature survey:

(1) Most of the previous studies have proved that the proactive optimal VSL control can improve travel time by keeping mainline traffic density at a low level compared to the no-VSL scenario; and

(2) Few studies have quantified throughput improvement, while many studies have concluded that throughput improvement is achievable under normal traffic conditions.

However, no research can be found that analyzes the MPC-based VSL performance with the combined objectives from the following three aspects:

(1) Impact of control parameters on the travel time and throughput;

(2) Impact of weights in sub-objectives; and how to choose the optimal weight values; and

(3) Impact of mainline demand levels and duration of high demand period. Thus, it remains to be determined whether VSL control can consistently improve both of the defined mobility parameters.

3.3 Methodology

3.3.1 *Simulation framework*

This research develops a macroscopic simulation tool within the MATLAB Toolbox Release 2012b to simulate and analyze the impact of control parameters and objective function on the MPC-based VSL control effectiveness. Note that, micro-simulation based evaluation is not suitable for such research, since the mobility parameters could also be impacted by lane-changing and driver behavior in addition to the above parameters. The simulation flowchart is presented in Figure 3.1. For the VSL control situation, this research used the DynaTAM-VSL as the prediction model, and SQP with the scatter search global optimization method, while for the no-VSL scenario, it used the basic METANET model (Papageorgiou et al. 1990) to simulate traffic flow with the same demand input, $\boldsymbol{D}$, as in the control scenario. Note that, in the control situation, the DynaTAM-VSL represents the traffic system, and the prediction model is same as traffic flow model.

Figure 3.1 shows the MPC framework adopts a rolling horizon approach, where the optimal VSL values, i.e., $\boldsymbol{u}*$, is calculated at each control sampling time index k_c. Based on the predicted demand $\hat{\boldsymbol{D}}$ and initial guessed values on the speed limits $\boldsymbol{u}$, the controller predicts future traffic states $\hat{\boldsymbol{z}}$ over a prediction horizon N_p. The objective is then to find the future trend of VSL values that result in optimal traffic states. The optimal VSL values correspond to the traffic states that result as the best performance with the chosen objective function over the entire N_P. The optimization problem is solved considering the constraints on speed limits and traffic dynamics. It was assumed that after the control horizon N_C (corresponds to control sampling index k_c) the same speed limits, i.e., $\boldsymbol{u}^*(k+N_c\text{-}1)$, remain effective until the N_P ($N_P \geq N_C$). However, only the control inputs $\boldsymbol{u}^*(k,k+1,.......k+N_c\text{-}1|k_c)$ are implemented on the MPC cycle over the control horizon N_C. After that, in a rolling horizon framework, the prediction and the control horizon are shifted one time index k_c forward, and the whole process starts all over again. For the next control sampling time k_c+1, the optimal speed limits $\boldsymbol{u}^*(k+N_c,.......k+N_P\text{-}1)$ that were calculated at k_c (but were not implemented) are used as initial guessed values for the speed limits in the optimization process.

3.3.2 *Traffic flow modeling*

To simulate traffic flow within the developed macroscopic simulation tool, the freeway is divided into several links i = (1, 2,…. …, M) of length L_i as shown in Figure 2.2 of Chapter 2. In regards to the discretization in time, a simulation time step of T = 20 s is used, where $t = k\ T$ for a time instant t and the corresponding time index k. The evolution of traffic flow $q_i(k)$ (vphpl), density $\rho_i(k)$ (vpkpl) and space-mean speed $v_i(k)$ (kph) for link i at time step k is described by the METANET model in the no-VSL situation and the DynaTAM-VSL model in the control situation. Both the models have been presented in Chapter 2. While simulating traffic flow within the developed simulation tool, the following parameters were adopted for METANET model that are obtained by minimizing Equation (2.20): $\beta^{optimal} = [\tau, \upsilon, \kappa, v_{free}, \alpha, \rho_C]$ =[0.0312, 63.5, 9.67, 82.3, 1.0051, 58.9] with $f(\beta^{optimal})$=1813. The detailed calibration method and the calibrated parameters for the DynaTAM-VSL have been presented in Chapter 2.

Since in this research, no-measurement data from the WMD base model is used, to perform the simulation with the above traffic flow models, the following initial and boundary conditions must be considered. It was assumed that demand on mainline upstream, $D_{mainline}$, and on-ramps, D_{ramp}, are known throughout the simulation. Moreover, to simulate traffic flow for first link, the mean speed v_o, which is to be known in Equation 2.6, was set equal to v_1 for the entire simulation. The density ρ_{M+1} that is needed in that equation for the last link M, was set equal to ρ_M. However, in cases when ρ_M becomes overcritical, this research set ρ_{M+1} to equal the critical density. When simulating speed for the link M, the reaction time parameter was set to τ at all times, as in the no-VSL scenario, assuming no VSL is implemented after the controlled section.

3.4 Optimization results

3.4.1 *Evaluation procedure*

To determine optimal MPC parameters and objective function that confirms the maximum mobility benefits from the VSL control, this research adopted three steps:

Step 1: Performing traffic flow optimization with the following objective functions with typical values of N_P and N_C: (1) Minimize TTT, (2) Simultaneously minimize TTT and maximize TTD, which is a measure of throughput from the freeway links, and (3) Maximize TTD.

Step 2: Simulate the calibrated and validated DynaTAM-VSL with different combinations of N_P and N_C with the objective function that provides the best performance as obtained in *Step 1*.

Step 3: Evaluate the MPC-based VSL performance for different mainline demand levels with the objective function and the control parameter values that provide the best performance, as analyzed in *Step 1* and *Step 2*.

3.4.2 *Objective function impacts on mobility parameters*

Minimizing TTT (Equation 3.1) as an objective function could keep mainline density at a low level by reducing inflow at upstream boundary. By contrast, maximizing TTD (Equation 3.2) may allow higher inflow than what the bottleneck can hold causing the travel time increment, possibly forcing the traffic state to the congested equilibrium region in FD. Therefore, vehicles might need to spend more time in the network. Thus, a combination of TTT and TTD could be appropriate (see Equation 3.3), where the first and second terms are TTT and TTD, respectively. For evaluating traffic performances with a different J, a simulation was run for a period of 2.5 hrs with each of the objective functions. The following typical MPC parameters are considered: N_P =5 min and N_C =1 min. T and T_C were 20 s and 1 min, respectively. VSL are allowed to change at every 1 min. The simulation results with J_3 for a different α_{TTT} are shown in Figure 3.5.

$$J_1(\mathrm{u})=T\sum_{j=1}^{N_p}\sum_{i=1}^{M}\lambda_i L_i \rho_i(k+j) \tag{3.1}$$

$$J_2(\mathrm{u})=T\sum_{j=1}^{N_p}\sum_{i=1}^{M}\lambda_i L_i q_i(k+j) \tag{3.2}$$

$$J_3(\mathrm{u})=T\sum_{j=1}^{N_p}\sum_{i=1}^{M}\lambda_i L_i\left[\alpha_{TTT}\rho_i(k+j)-\alpha_{TTD}q_i(k+j)\right] \tag{3.3}$$

For $D_{mainline}$ of 5500 vph (*t*=4:00 PM-6:00 PM) and 1000 vph (*t*=6:01 PM-6:30 PM); and D_{ramp} of 1500 vph (*t*=4:00 PM-4:30 PM) and 500 vph (*t*=4:31 PM-6:30 PM) (see, Figure 3.2), the TTT and throughput in the no-VSL scenario were 473 veh-hr and 15,931vphpl, respectively. The throughput is the summation of outflow from all 13 links of the test site as presented in Chapter 2. Specifically, the TTT and throughput were calculated by Equation (3.4) and Equation (3.5).

$$\mathrm{TTT}=T\sum_{k=1}^{K}\sum_{i=1}^{M}\lambda_1 L_i\rho_i(k) \tag{3.4}$$

$$\mathrm{throughput}=\sum_{i=1}^{M}\left(\frac{1}{K}\sum_{k=1}^{K}q_i(k)\right) \tag{3.5}$$

As expected, minimizing J_1 caused a 27.0% TTT improvement (with a TTT value of 348 veh-hr), which confirms the results published in several studies including Hegyi et al. (2007); Hegyi et al. (2005); Zegeye et al. (2011); Carlson et al. (2010a); Carlson et al. (2010b). However, the throughput was reduced by approximately 43.0% (with a throughput value of 9,080 vphpl) compared to the no-VSL scenario. Figure 3.3 shows that TTT minimization maintains low outflow from the upstream link of the controlled section, to keep downstream link density at a low level from the beginning of the simulation, which reduces travel time.

By contrast, maximizing J_2 results in the deterioration of all the mobility parameters: TTD maximization increases traffic flow without considering the impact of high traffic density evolution and, thus, the impact on mainline travel time. Also, for the same reason, while maximizing J_2, the VSL control allows higher inflow to the weaving section, which is located around 1.5 km downstream of the controlled test site, i.e., link 3, causing queue formation from the bottleneck. Due to the queue, the inflow at upstream boundary reduces after sometime of the simulation. As can be seen from Figure 3.4, downstream boundary flow was significantly decreased. Specifically, the downstream boundary flow is maintained at approximately 400 vphpl, but; slightly higher than that of the J_1 minimization. For the WMD test site, the throughput is reduced by 26.0% (with a throughput value of 11,788 vphpl). Also, travel time is increased by 33.0% (with a TTT value of 631 veh-hr). Thus, it can be concluded that J_2 is also not a candidate objective function for the MPC-based VSL control.

From the simulation, this research observed that minimizing J_3 can maintain higher outflow from all the links compared to the no-VSL scenario and when compared to optimizing J_1 and J_2 for most of the time during the simulation. Furthermore, with the current MPC parameters, it was found that the VSL control reduces by 12.0% the amount of vehicle entry from the on-ramp, which is located in the weaving section during *t*=4:00 PM-4:30 PM. Consequently, the VSL control avoids capacity drops at the bottleneck and maintains higher mainline flow. Later, this research presents the flow profile for minimizing J_3 with the best control parameters and weight in sub-objectives.

3.4.3 *Weight parameter impacts on multi-objective optimization*

As can be seen in Figure 3.5, minimizing J_3 with the different values of α_{TTT} could maintain a prudent relationship between both of the chosen mobility parameters: TTT and throughput. The objective function can take different values in the weighing coefficient, which is to be determined based on the control policy. If α_{TTD} is assumed to be 1, then α_{TTT} is the ratio between TTD and TTT, which equals the space-mean speed, i.e., v. This research uses the lowest value of α_{TTT}=20 to maintain the operating efficiency. Whereas, to guarantee travelers' safety, the highest value of α_{TTT}=80 is used, which is the static speed limit in the WMD.

Figure 3.5 shows that by giving lower weight to the TTT, the controller causes negative benefits in the mobility parameters. This result is similar to that of maximizing J_2. Specifically, the mainline travel time and the throughput were deteriorated by 27.0% and 16.2%, respectively at α_{TTT}=20. Whereas, by increasing the values in α_{TTT}, VSL can achieve positive benefits in the mobility parameters. In Figure 3.5, it can be observed that there is a point on the x-axis where the two curves related to the travel time and the throughput cross each other. Specifically, this point is obtained at α_{TTT}=43, which is about half of the maximum allowable speed limit on WMD. On the left of this point, the VSL control has (-ve) impact on all the mobility parameters with the combined objective functions. By contrast, both the mobility parameters improve on the right of the critical point. Furthermore, the rate of travel time improvement is higher than that for the throughput. However, close to α_{TTT}=80, the changes in both mobility parameters are imperceptible. Thus, α_{TTT}=80 is used for further analysis to find the optimal MPC parameters and the impact of mainline demand levels on traffic flow.

3.4.4 *Control parameter impacts on multi-objective optimization*

This research considered several combinations of the N_P (5, 7, 9, and 11 min) and the N_C (1, 3, and 5 min) while optimizing traffic flow with the combined objectives. Hegyi (2004) found that when the objective of the MPC is set to reduce only the TTT, the VSL performance depends strongly on the N_P with little influence by the N_C. However, a slightly different finding is obtained considering the combined objective functions, shown in Table 3-1. For example, for a prediction horizon of 9 min, improvements in the TTT and throughput are significantly different for N_C =1, 3, and 5 min. However, as in Hegyi (2004), for the same N_C, improvements strongly depend on N_P. In general, with the increasing N_P, the VSL performance decreases. Moreover, when a N_C of 5 min is chosen, travel time improvements drastically deteriorate for a little increase in N_P, which makes the control horizon non-preferable. A too-long control horizon could have negative influence, as the controller requires frequent calculation of the optimal VSL values to avoid flow breakdown during congestion periods.

However, a careful comparison is required between N_C =1 min and N_C =3 min. For both the N_C, TTT is set at the minimum of N_P =5 min, which is somewhat smaller than the maximum travel time for the test site (11 km / 80 kph = 0.11 hr = 8.2 min), because the MPC-based VSL control does not determine the optimal values of control variable based on only the predicted travel time. Moreover, the control aims at improving the throughput. The improvements in the TTT with N_C =1 min and N_P =5 min is 19.1% and that for N_C =3 min and N_P =5 min is 19.2%. However, for some N_P, the TTT and throughput improvements are very low for N_C =1 min. This is explained by the assumption that the VSL values are constant over $\{N_c, ..., N_P - 1\}$. If the difference between N_P and N_C is large, the VSL values for this period, which are represented by one optimized VSL value as illustrated in "Simulation Framework", will have a large influence on the chosen objective function. Thus, the optimization is focused more on this period than on the beginning of the control horizon, while in the MPC approach, only the optimized VSL values for $(k, k+1, ...k+N_c-1)$ are applied to the process. For this reason, a N_C =3 min is preferable. For the rest of the analysis, this research chooses the control parameters of N_C =3 min and N_P =5 min.

3.4.5 *Demand level impacts on multi-objective optimization*

Various traffic demand levels cause different traffic state evolutions. Accordingly, the above-determined VSL control with the optimal control parameters could give different levels of benefits. This research investigated at which demand level the VSL control could provide the maximum mobility benefits. The simulation experiment continued to increase the mainline demand until the VSL effectiveness is imperceptible. The duration of high demand period and the demand on on-ramps for each scenario were kept fixed.

Figure 3.6(a) shows that with the increase in mainline demand, $D_{mainline}$, the MPC-based VSL control shows consistent improvements in terms of travel time. The TTT improvement reaches to a maximum value of 25.0% at a demand level that is higher than the weaving bottleneck capacity, but; lower than the upstream link capacity, i.e., $Q_{max,1}$, which has three lanes. From the field loop detectors, the capacity at the weaving bottleneck (Q_b) was calibrated at 1620 vphpl (Hadiuzzaman et al. 2013). The VSL control provides lesser TTT improvements, when $D_{mainline}$ is very close to the $Q_{max,1}$, indicating that in addition to the bottleneck, other links are also getting congested at these high demand levels. Interestingly, the benefit is negative by a fixed amount of 8.3%, when $D_{mainline}$ exceeds the $Q_{max,1}$, because the amount of vehicles allowed by the VSL control in the freeway causes a negative impact on travel time.

However, as in Figure 3.6(b), throughput improvement is visible as $D_{mainline}$ exceeds a value of 1600 vphpl, which is slightly lower than the Q_b. Furthermore, throughput improvement reaches its maximum value of 12.0% at $D_{mainline}$ / Q_b =1.3, when $D_{mainline}$ reaches to the $Q_{max,1}$. Therefore, there is a small window of demand levels, i.e., $1.0 \leq D_{mainline} / Q_b \leq 1.3$, while improvements in both the mobility parameters are achievable, and uncompromising with each other, by the MPC-based VSL control. Furthermore, a fixed amount of throughput improvement is achievable even at higher demand levels by compromising travel time improvement, which is not desirable. Also, as the VSL will not allow more vehicles than the $Q_{max,1}$ as in Equation (2.11) of Chapter 2 when demand increases, by assigning higher mainline demand in the simulation increases the waiting time of the vehicles upstream of the test site.

In the simulation, high mainline demand persists over t =4:00-6:00 PM. The waiting time outside of the controlled section for several $D_{mainline}$ / $Q_{max,1}$>1.0 is shown in Figure 3.7, where it can be seen that after a time step of k=360 (corresponding t =6:00 PM), waiting time starts to decrease. From the above analysis, transportation practitioners can determine improvements in traffic operation achievable by the VSL control based on historical demand profile.

At this point, this research further investigated whether the duration of high demand period influences the VSL effectiveness. For this experiment, a fixed $D_{mainline} / Q_b$ of 1.1 is assumed, which represents typical traffic conditions on the test site. This research increased the duration from 30 min to 120 min at an interval of 15 min. Figure 3.8(a) shows that the curve for TTT with the VSL control always goes below that for no-VSL, showing a (+ve) benefits. By contrast, in Figure 3.8(b), the curve for throughput with VSL control always goes above that for no-VSL, showing a (+ve) benefits, regardless of high mainline demand duration. It was computed that for different high demand periods, the values of improvements in TTT and throughput vary between 13.0%-19.0% and 3.0%-6.0%, respectively.

The link outflow from the 12 links on WMD for minimizing combined objective functions with (α_{TTT} =80, N_C =3 min, and N_P =5 min) is shown in Figure 3.9. It can be seen that the MPC-based VSL control reduces the outflow from some links (e.g., Link 5, Link 6, and Link 7) around 4:30 PM, but on average its effects make a performance improvement when compared to entire test site and the simulation time periods. For example, the VSL control has maintained always higher flow in Link 9, Link 10, Link 11, and Link 12. Previously, several MPC-based VSL studies (Lu et al. 2010; Hadiuzzaman et al. 2013; Hadiuzzaman and Qiu 2013) also reported the similar findings. In fact, the flow reduction happens sometimes mainly due to high value in weight parameter (α_{TTT}), which tries to reduce input flow at a lane drop bottleneck (B2 in Table 2-3) to avoid queue formation, and thus to improve travel time, which clearly demonstrates the efficiency of the MPC–based VSL control and its reliability for future field deployment.

3.5 Improvement in control performances

In order to assess the improvements in the VSL control with the DynaTAM-VSL, this section recalls the three traffic flow models─M1, M2, and M3 from Chapter 2 that utilized the VSL modeling approaches as presented in Section 2.4.1.1, 2.4.1.2, and 2.4.1.3, respectively. Each of the traffic flow models was adopted separately within the MPC, and the optimized mobility parameters were compared in the control situation. Furthermore, during simulation, same demand on the mainline and on-ramps were assigned. This research minimizes combined objective functions (Equation 3.3) with (α_{TTT} =80, N_C =3 min, and N_P =5 min). The results are presented in Table 3-2.

From the table, it can be seen that the MPC-based VSL control performs the best when it considers M4 (DynaTAM-VSL) as a prediction model. Specifically, in terms of TTT and throughput, improvements are 19.2% and 4.2%, respectively compared to the no-VSL scenario. Moreover, M1 performs better than M2, which can be explained based on the arguments made in Section 2.4.1.1 and 2.4.1.2 and as a result of the model accuracy assessment results from Section 2.6. Moreover, in the absence of speed-limit-dependant parameters in calculating link outflow, M3 causes inaccurate prediction. Thus, compared to the no-VSL scenario, throughput decreases significantly (by 38.5%). Similarly, due to direct parameterization of FD parameters with VSL control variable, M2 also causes inaccurate prediction of flow. Specifically, the throughput is decreased by 31.2%. Certainly, the negative outcomes from these two models are not desirable as it does not satisfy the maximum utilization of freeway capacity. Indeed, due to the reduction of flow, it causes an increased travel time for the drivers upstream of the controlled section.

Model improvement due to the introduction of speed-limit-dependant parameters in the speed and density dynamics can be interpreted from Table 3-2. The controller has maintained a good trade-off between the two mobility parameters: TTT and throughput. The results are very consistent with the chosen objective function with the assigned weight parameter. The inflow profile at the first link due to adoption of different METANET-based traffic flow models have been presented in Figure 3.10.

3.6 Summary and conclusions

In recent years, proactive optimal VSL control has gained tremendous attention from transportation researchers and practitioners. The contents of this research were stimulated by an ongoing field operation test (FOT) in Edmonton, Canada, where a pioneer attempt has been made to deploy MPC-based VSL control in authentic traffic operation. To this end, it was investigated how the MPC parameters impact the VSL control goals – simultaneously improving freeway travel time and throughput. Also, the efficiency of the VSL control at various demand levels was analyzed. The ultimate objective is to see how and when MPC-based VSL control can give maximum mobility benefits. These analyses help the city transportation authority to consider important aspects for the MPC-based VSL FOT. The major findings from the simulation analysis are:

(1) It was proved that when the controller considers TTT as an objective function, it compromises throughput improvement. By contrast, maximizing TTD compromises both of the mobility parameters.

(2) It was observed that, during the congestion periods, the combined objectives with appropriate weight can facilitate throughput improvements without compromising TTT improvements.

(3) A heuristic method to tune the weight parameter in the combined objectives based on the control policy was proposed. It was observed that, by giving a weight of 20 (the lowest allowable speed limit on WMD) to TTT, traffic operation is similar to that of maximizing TTD.

(4) By increasing the values in α_{TTT}, positive benefits in both TTT and throughput were achieved. However, close to α_{TTT} =80 (the maximum allowable speed limit on WMD), both parameter changes are imperceptible.

(5) This research analyzed the sensitivity of the MPC-based VSL control on control parameters. It was revealed that with a longer control horizon, improvements in both of the tested parameters are imperceptible as prediction horizon increases.

(6) The TTT improvement is positively correlated with increasing mainline demand level. Moreover, the TTT improvement reaches to a maximum value at a demand level that is slightly higher than the downstream bottleneck capacity, but; lower than the upstream boundary link capacity.

(7) By contrast, throughput improvement is only possible when demand from the upstream is higher than the downstream bottleneck capacity, which is logical because a demand level less than the bottleneck capacity will not create capacity drops; therefore, vehicles can pass through efficiently without interruption. Therefore, there is no room for throughput improvement. This research determines that the range of the mainline demand / bottleneck capacity ratio is 1.0-1.3, where the lower and upper values of the range depend on the bottleneck capacity and capacity at the upstream boundary link of the controlled section, respectively, when VSL can improve both the mobility parameters.

(8) Moreover, within the above ratio, the MPC-based VSL control can provide maximum TTT and throughput improvements of 25.0% and 12.0%, respectively. However, the maximum benefits were not achieved at the same time, which prove that the mobility parameters are not independent of each other. Thus, the objective function within the MPC must include both of them, when the control goals are to simultaneously improving TTT and throughput during congestion periods.

(9) Regardless of the duration of the high demand period, the MPC-based VSL control can consistently maintain improved traffic flow operation provided that the demand / capacity ratio is in the range of 1.0-1.3. Furthermore, the improvements in the mobility parameters are positively correlated with the increased congestion duration considered in this research.

(10) It was proved that when the DynaTAM-VSL model is adopted as a prediction model within the MPC framework, the VSL control can provide consistent results with the chosen combined objective functions compared to the other METANET-based traffic flow models considered in this research. Furthermore, the prediction accuracy of the different models within the MPC was found to be very consistent with the results of the model's accuracy assessment with the 20-s loop detector data collected from the WMD base model as presented in Section 2.6.

3.7 References

Alessandri, A., Febbraro, A. D., Ferrara, A., and Punta, E. (1999). "Nonlinear optimization for freeway control using variable-speed signaling." *IEEE Transactions on Vehicular Technology*, 48(6), 2042-2052.

Carlson, R. C., Papamichail, I., Papageorgiou, M., and Messmer, A. (2010a). "Optimal mainstream traffic flow control of large-scale motorway networks." Transportation *Research Part C*, 18 193–212.

Carlson, R. C., Papamichail, I., Papageorgiou, M., and Messmer, A. (2010b). "Optimal motorway traffic flow control involving variable speed limits and ramp metering." *Transportation Science*, 44(2), 238-253.

Hadiuzzaman, M., Qiu, T. Z., and Lu, X. Y. (2013). "Variable Speed Limit Control Design for Relieving Congestion Caused by Active Bottleneck." *Journal of Transportation Engineering*, 139(4), 358-370.

Hadiuzzaman, M., and Qiu, T. Z. (2013). "Cell transmission model based variable speed limit control for freeways." *Canadian Journal of Civil Engineering*, 40(1), 46-56.

Hegyi,A.(2004)."*Model Predictive Control for Integrating Traffic Control Measures*." *PhD Thesis, Delft University of Technology, Delft, the Netherlands, TRAIL Thesis Series T2004/2*.

Hegyi, A., Burger, M., Schutter, B. D., Hellendoorn, J., and Van den Boom, T. J. J. (2007). "Towards a Practical Application of Model Predictive Control to Suppress Shockwaves on Freeways." *Proceedings of the European Control Conference 2007 (ECC'07), Kos, Greece,* 1764–1771.

Hegyi, A., De Schutter, B., and Hellendoorn, J. (2005). "Optimal coordination of variable speed limits to suppress shock waves." *IEEE Transactions on Intelligent Transportation Systems*, 6(1), 102-112.

Kang, K. -., and Chang, G. -. (2006). "A robust model for optimal time-of-day speed control at highway work zones." *IEEE Transactions on Intelligent Transportation Systems,* 7(1), 115-123.

Kang, K. -., Chang, G. -., and Zou, N. (2004). "Optimal dynamic speed-limit control for highway work zone operations." *Transportation Research Record,* (1877), 77-84.

Lin, P. W., Kang, K. P., and Chang, G. L. (2004). "Exploring the effectiveness of variable speed limit controls on highway work-zone operations." Journal of Intelligent *Transportation Systems: Technology, Planning, and Operations,* 8(3), 155-168.

Long, K., Yun, M., Zheng, J., and Yang, X. (2008). "Model predictive control for variable speed limit in freeway work zone." *Proceedings of the 27th Chinese Control Conference, CCC,* 488-493.

Lu, X. Y., Qiu, T. Z., Varaiya, P., Horowitz, R., and Shladover, S. E. (2010). "Combining Variable Speed Limits with Ramp Metering for freeway traffic control." *Proceedings of the 2010 American Control Conference, ACC 2010,* 2266-2271.

Lu, X. -., Qiu, T. Z., Horowitz, R., Chow, A., and Shladover, S. (2011). METANET model improvement for traffic control. *IEEE Conference on Intelligent Transportation Systems, Proceedings, ITSC,* 2148-2153.

Papageorgiou, M., Blosseville, J. -., and Hadj-Salem, H. (1990). "Modelling and real-time control of traffic flow on the southern part of Boulevard Peripherique in Paris: Part I: Modelling." *Transportation Research Part A: General,* 24(5), 345-359.

Ugray, Z., Lasdon, L., Plummer, J., Glover, F., Kelly, J., and Marti, R. (2007). "Scatter search and local NLP solvers: A multistart framework for global optimization." *INFORMS Journal on Computing,* 19(3), 328-340.

Zegeye, S. K., De Schutter, B., Hellendoorn, J., and Breunesse, E. A. (2011). "Variable speed limits for green mobility." *IEEE Conference on Intelligent Transportation Systems, Proceedings, ITSC,* 2174-2179.

Table 3-1 VSL performances due to different control parameters.

N_C, N_P	TTT (veh-hr)			Throughput (vphpl)		
	no-control	VSL Control	improvement (%)	no-control	VSL control	improvement (%)
1min, 5min	473.4	382.9	19.13	15931	16602	4.21
1min, 7min		387.1	18.23		16471	3.38
1min, 9min		421.4	10.99		16427	3.11
1min, 11min		394.9	16.59		16014	0.52
3min, 5min		382.5	19.21		16606	4.23
3min, 7min		390.0	17.63		16512	3.65
3min, 9min		390.0	17.63		16333	2.50
3min, 11min		381.7	19.37		16239	1.92
5min, 5min		382.5	19.21		16606	4.23
5min, 7min		388.1	18.02		16078	0.91
5min, 9min		460.8	2.67		16119	1.17
5min, 11min		460.8	2.67		16119	1.17

Table 3-2 MPC macroscopic simulation results with different traffic flow models.

Models	TTT (veh-hr)			Throughput[1] (vphpl)		
	no-VSL	VSL control	improvement (%)	no-VSL	VSL control	improvement (%)
M1	473.4	442	6.5	15931	16559	3.9
M2		421	11.1		10963	-31.2
M3		249	47.3		9795	-38.5
M4		382	19.2		16591	4.2

[1]*Summation of the flows over the discrete links. The flow at each link is taken as the average over the simulation periods (t =4:00-6:30 PM).*

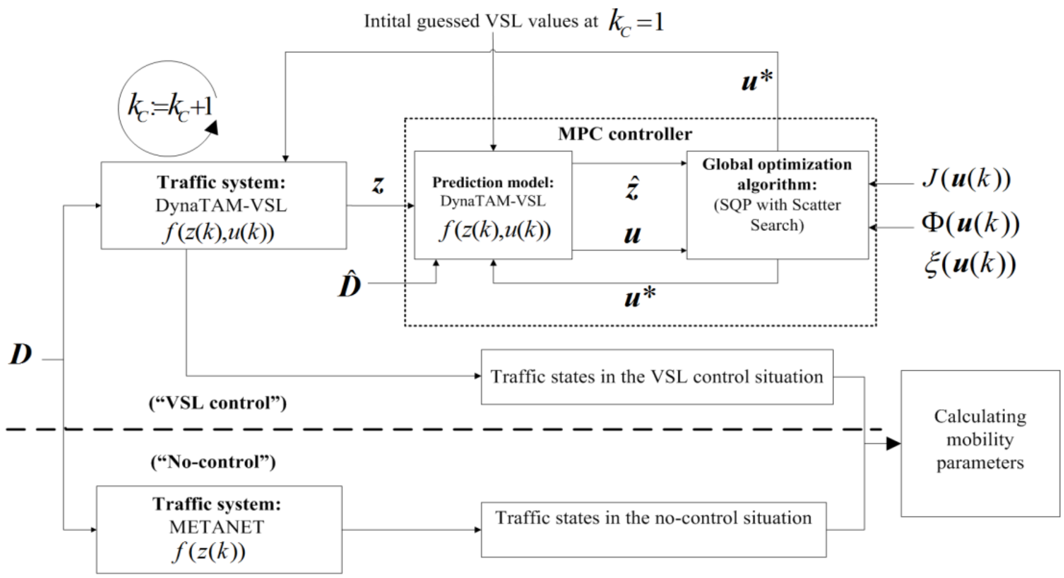

Figure 3.1 Architecture of developed macroscopic simulation tool to assess traffic performances for "no-VSL" and "VSL control" situation.

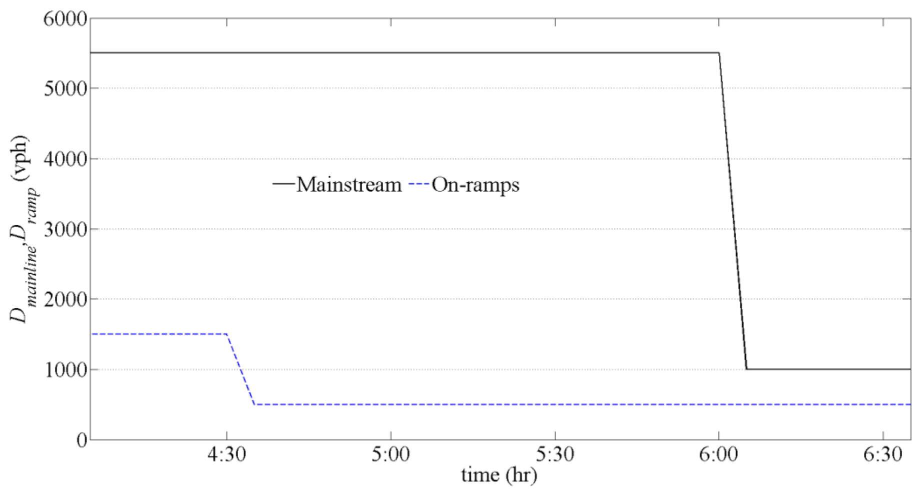

Figure 3.2 Demand profiles: high mainline traffic demand at the beginning of the simulation, and it drops after 2 hr. The demand on on-ramps remains constant to near capacity for 30 min, and decreases finally to a low value.

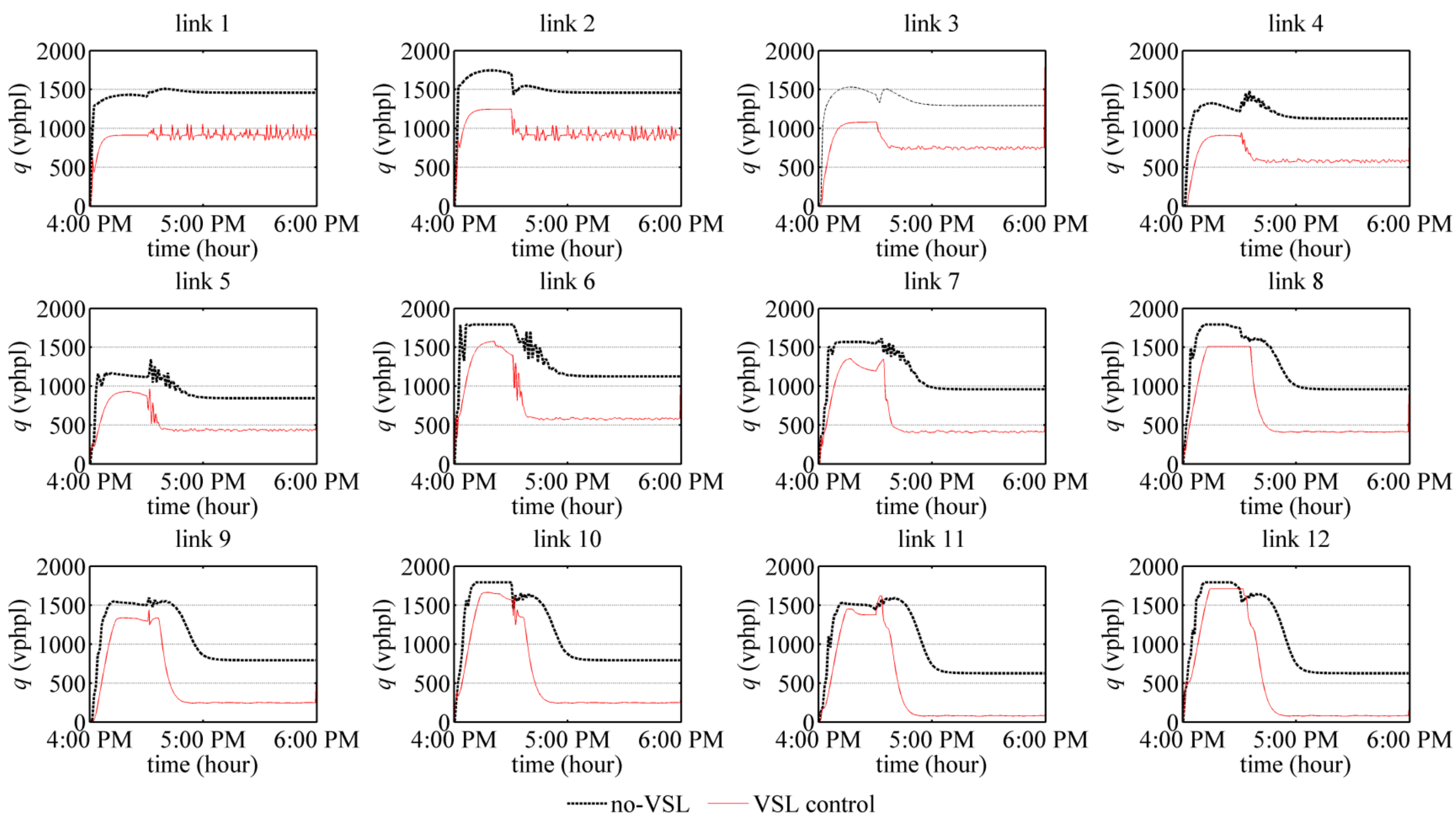

Figure 3.3 Comparison between outflow from the WMD freeway links for no-VSL and for minimizing TTT during congestion periods. At all the time, the MPC-based VSL control maintained less flow than the no-VSL situation.

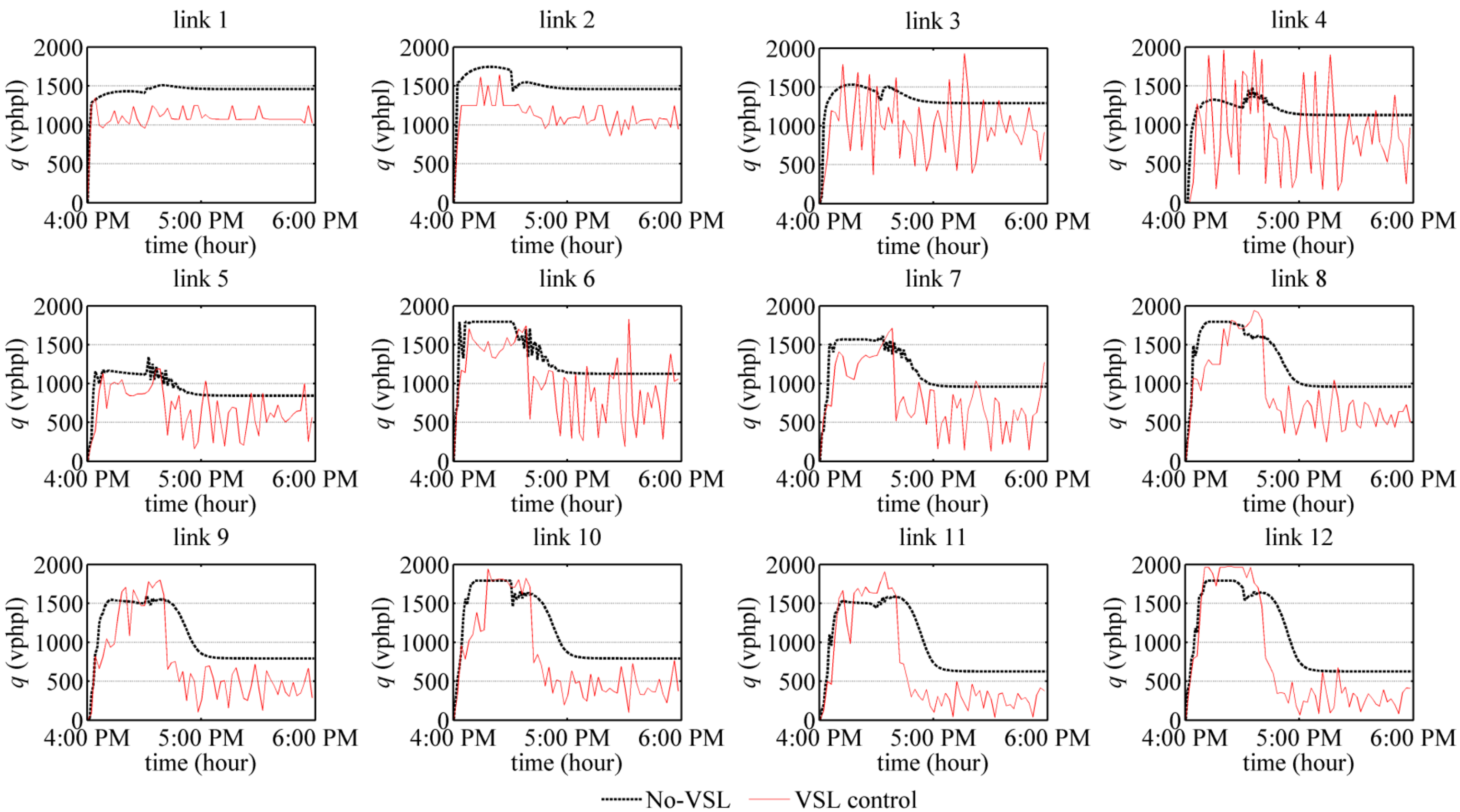

Figure 3.4 Comparison between outflow from the WMD freeway links for no-VSL and maximizing TTD during congestion periods. Most of the times, MPC-based VSL control maintained less flow than the no-VSL situation.

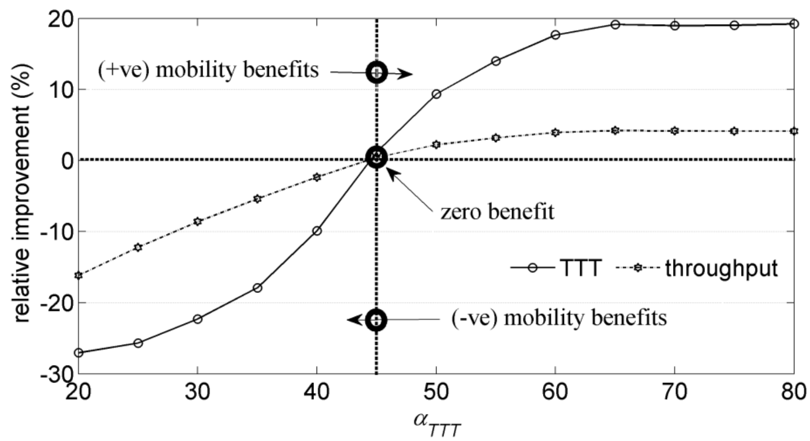

Figure 3.5 Weight parameter effects on multi-objective optimization. At lower values of α_{TTT}, both the chosen mobility parameters are negatively impacted.

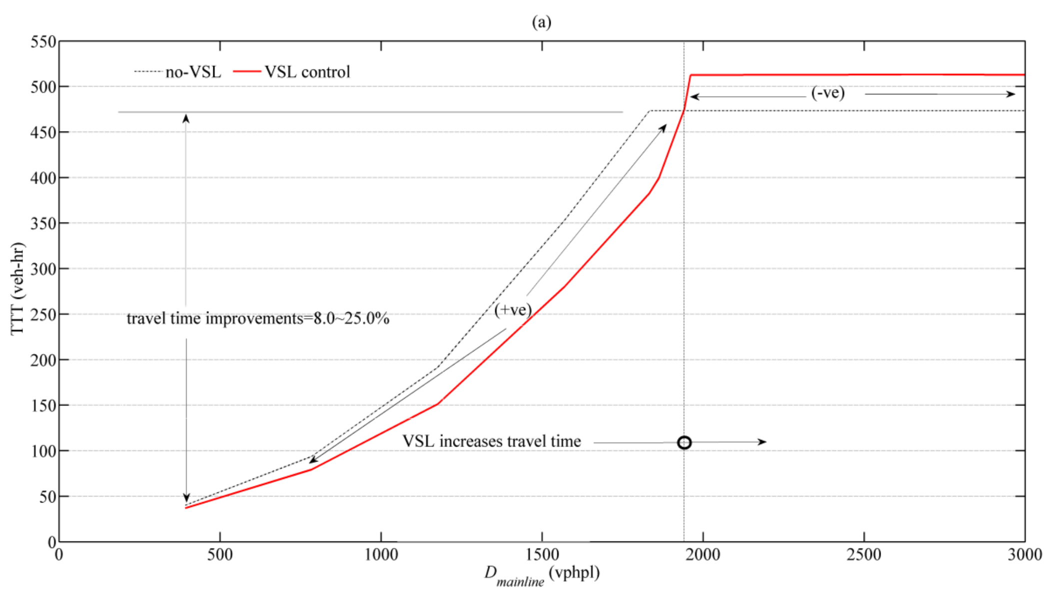

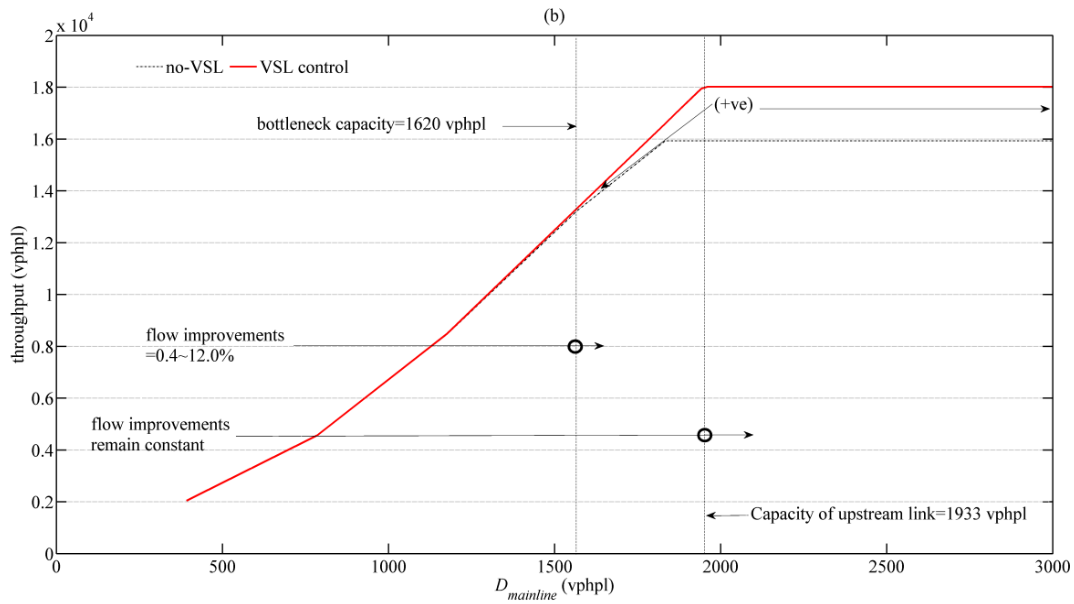

Figure 3.6 Impact of mainline demand on mobility: (a) TTT; (b) throughput.

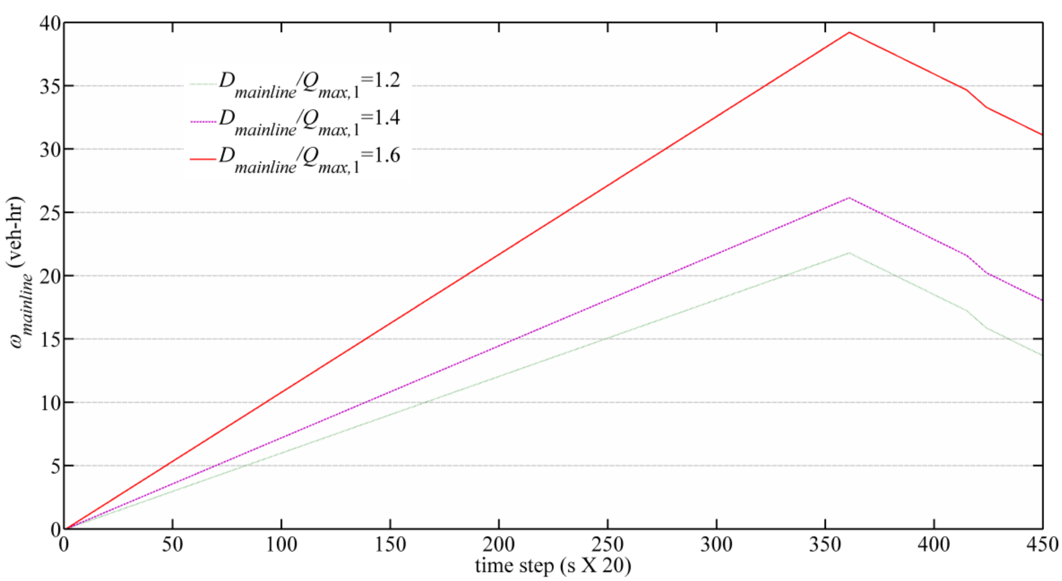

Figure 3.7 Waiting time on mainline due to $D_{mainline} \,/\, Q_{max,1}$>1.0.

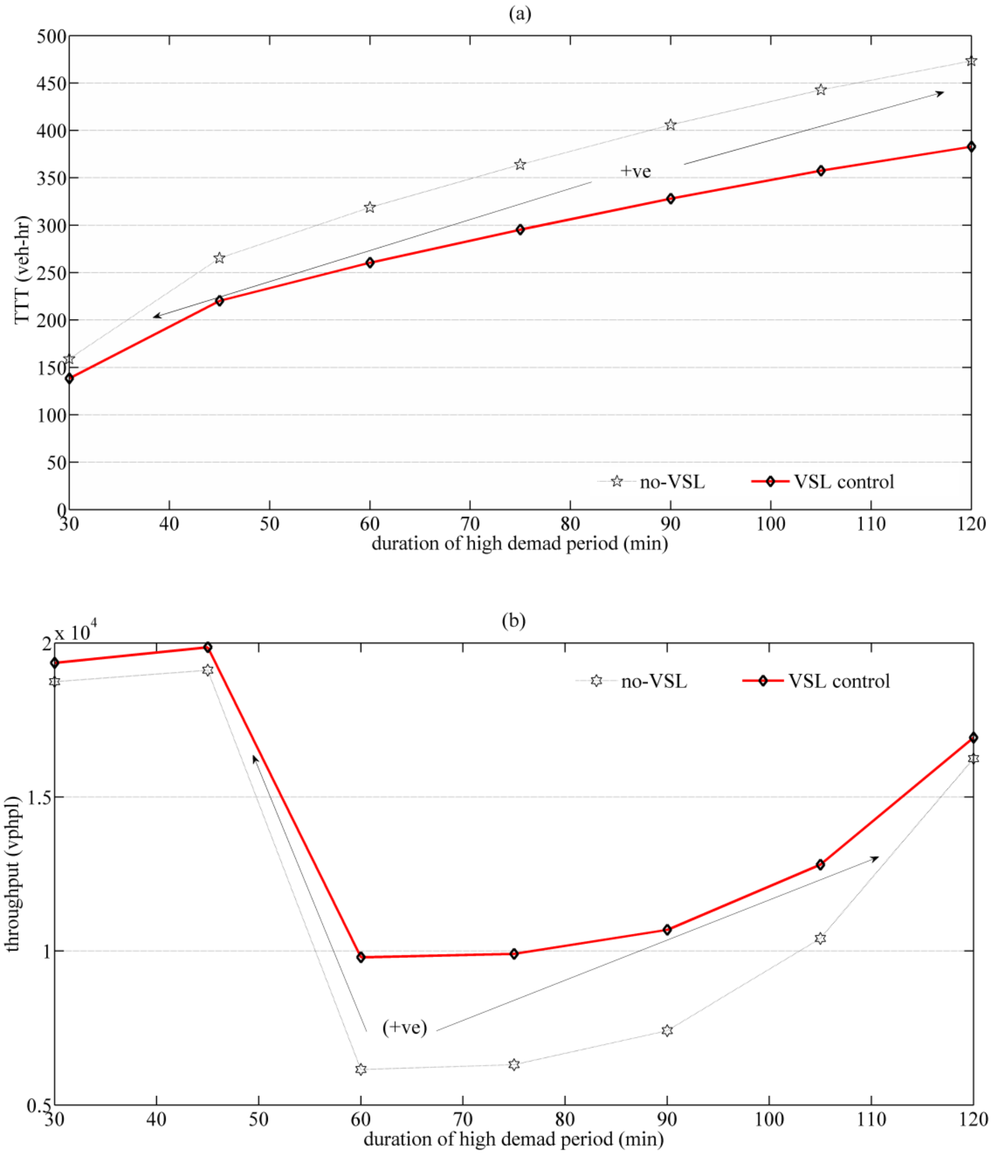

Figure 3.8 Sensitivity of VSL effectiveness on duration of high demand period: (a) TTT; (b) throughput.

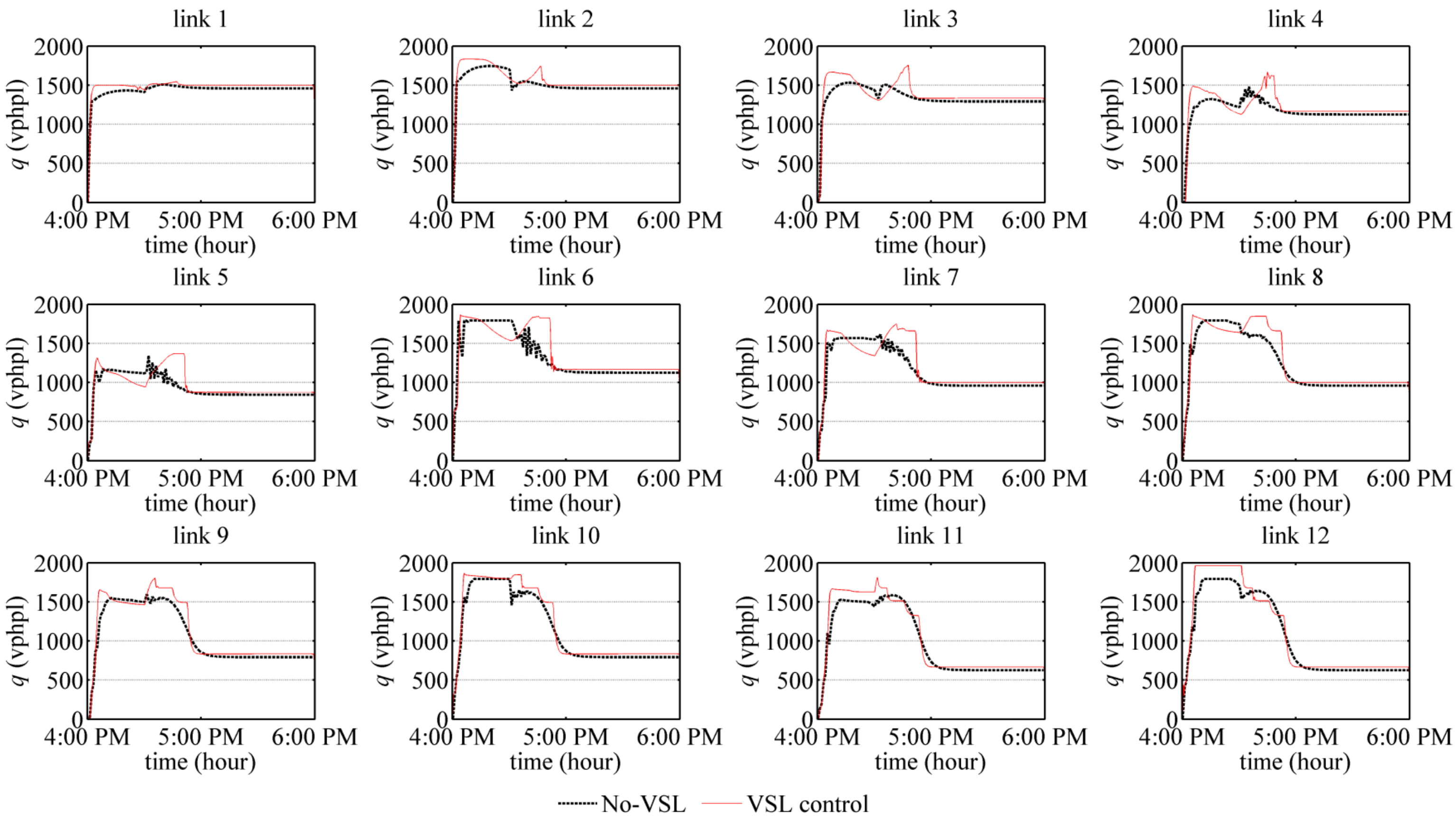

Figure 3.9 Outflow from the freeway links for no-VSL and minimizing combined objective functions. Most of the times, VSL maintained higher flow than the no-VSL scenario.

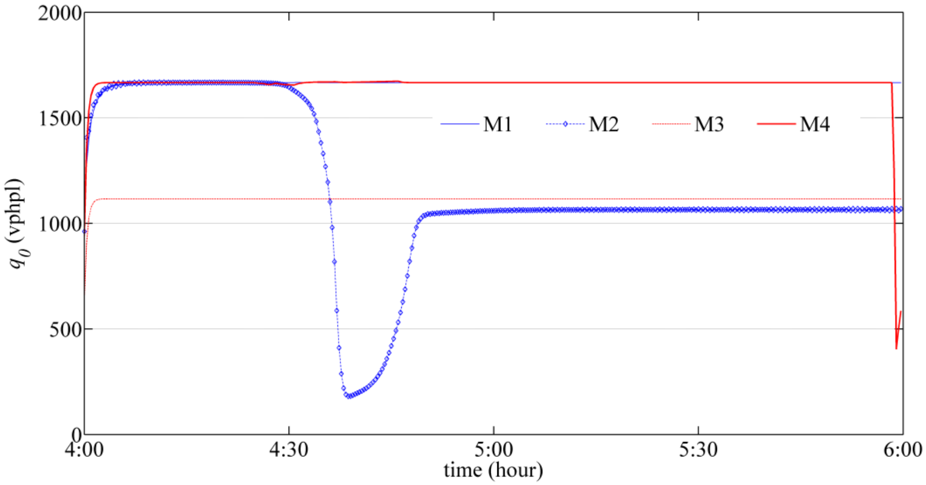

Figure 3.10 Inflow into the first link of the WMD test site due to adopting different prediction models within MPC.

Chapter 4

Designing isolated VSL control with DynaTAM-VSL for improving congestion capacity at recurrent bottlenecks[*]

4.1 Introduction

Recurrent bottlenecks limit traffic flow on freeway sections. During peak periods, these bottlenecks are often activated by high traffic demand from mainline upstream and onramps, causing capacity drops. Due to this capacity drop, overall throughput from the uncontrolled freeway section can be decreased by 0–15.0% (Hegyi 2004). Any improvements in traffic operation that result in the maximum utilization of bottleneck capacity could increase freeway throughput as well as reduce travel time.

In the literature, two general views evolved on the use of speed limits. The first emphasizes the homogenization effect (Zackor 1979; Smulders 1992; Harbord 1995), whereas the second is more focused on avoiding or mitigating flow breakdown (Chien et al. 1997; Lenz et al. 1999). The theoretical research by Kohler (1974) showed that when the headways in a chain of vehicles are below a certain bound, the chain is unstable. Inhomogeneity in the traffic stream leads to congestion. Inhomogeneity can arise from

[*] *A version of this chapter has been published.* **Hadiuzzaman, M.**, Qiu, T. Z., and Lu, X. Y. (2013). "Variable Speed Limit Control Design for Relieving Congestion Caused by Active Bottleneck." *Journal of Transportation Engineering*, 139(4), 358-370.

speed differences between consecutive vehicles in one lane, speed differences among the lanes and (or) flow differences among the lanes. Through VSL control, traffic planners may achieve a more uniform distribution of traffic density over freeway links, thereby preventing the high traffic density that leads to flow breakdown. Although the safety benefits from homogenization effects are proven in real-world applications (Smulders 1992; Ulfarsson et al. 2005; Kwon et al. 2007; McMurtry et al. 2008; Robinson 2000; Bertini et al. 2006) and in the simulation studies (Abdel-Aty et al. 2006b; Abdel-Aty et al. 2006a; Lee and Abdel-Aty 2008; Hellinga and Mandelzys 2011; Lee et al. 2006; Lee et al. 2003), homogenization has failed to improve bottleneck flow efficiency:

(1) Most of the existing VSL control strategies work in a reactive manner, and they lack the benefits that can be achieved through traffic state prediction;

(2) The existing strategies are too simple, and are not tightly coupled with mobility factors (e.g., capacity drops and shockwave formations).

This research proposes a VSL control strategy that maximizes bottleneck capacity and can be implemented in a real-world traffic system. The control strategy explicitly considers the traffic characteristics at recurrent bottlenecks, and their upstream-downstream segments. The proposed control strategy is modeled within the model predictive control (MPC) framework. Within the MPC, a customized DynaTAM-VSL model is used for predicting traffic flow on freeway segments that operate with VSL control, which, with the control strategy, accurately presents dynamic traffic state changes. Specifically, to model recurrent bottlenecks, this research introduces the capacity drop concept in the FD (flow-density relation) of the density dynamics. Also, as the control strategy aims at improving flow through a bottleneck under an isolated VSL strategy, the spatial constraints among two VSL signs (Equation 2.19) as presented in Chapter 2 are dropped. However, in the customized model, speed dynamics follow a similar modeling approach to what was presented in Chapter 2 where the basic METANET model is used for traffic state prediction for links that uncontrolled by VSL. The major assumption in the proposed VSL modeling approach is that the posted speed limit can be achieved by the driver. In the no-VSL scenario, a driver's desired speed will be determined based on the surrounding traffic conditions, as in METANET. Therefore, for the links without VSL, this research utilizes METANET as the prediction model.

Microscopic traffic simulation was found to be the most suitable and cost-effective tool to perform the experiments mimicking real-world traffic conditions. Thus, the proposed VSL strategy was tested in the WMD base model using a special purpose software module developed in Visual C++ using the Component Object Model (COM) interface. The base model works as a proxy for real-world traffic conditions and was calibrated with field data to mimic prevailing recurrent bottlenecks conditions. Then, the analysis was carried out to see when and how VSL control can simultaneously improve the mobility parameters—total travel time (TTT) and throughput—of multiple recurrent bottlenecks. The optimal objective function (as obtained in Chapter 3), safety constraint (limiting the maximum speed difference between two successive time steps) for a particular VSL sign, was introduced in the proposed VSL control strategy to ensure traffic safety. A comparison of the performances was made for various VSL update frequencies and for different values of the safety constraint to obtain the best control scenario.

In the above experiments, to find the optimal VSL values, an efficient optimization method was proposed that does not require computing gradient of the objective function.

The optimization method could be suitable for real-world applications. A traditional gradient-based optimization method could be difficult for real-world applications in terms of computation time requirements (it is difficult to obtain a global solution). For example, with a control horizon (N_C) of 1 min, the MPC framework performs an optimization to find the optimal set of VSL values at every 1 min interval. However, to finish one optimization process may require more than 1 min (based on the network size and number of VSL signs), and could vary between different N_C . In addition, online traffic data collected from field sensors needs to be corrected to remove unreasonable values, and then fed into the MPC framework, which will also consume time before the optimization process starts. Therefore, this research focuses on designing an MPC-based VSL control that is easily implementable in the real-world.

4.2 Literature review

This section presents the previous VSL field implementation results, which could help this research to design an efficient VSL control strategy to improve mobility. A number of empirical studies have been conducted in the U.S. since the 1960s in several states, considering demand responsive control strategies. New Jersey uses enforced VSL system with approximately 120 signs to provide early warning to motorists of slow traffic, hazardous road conditions, and accidents. The posted speed limit was reduced from the normal speed limit in 5-mph decrements to 30 mph. The New Jersey Turnpike Authority has concluded that the VSL signs are effective to improve safety (Smulders 1992).

Ulfarsson et al. (2005) studied the effects of VSL control on mean speed and speed variance on the I-90 in Washington. The objective of the VSL system was to address the variations in speed due to the vehicle mix, inclement weather, and road geometry.

Although the authors did not quantify the mobility benefits, it was concluded that VSL entailed benefits when used for adverse conditions due to speed homogenization.

A two-stage speed reduction scheme was developed and implemented at one of the I-494 work zone bottlenecks in the Twin Cities, Minnesota, for a 3-week period in 2006. Despite the advisory driving speed, data collected from the field indicated a 25.0% to 35.0% reduction of the average 1-min maximum speed difference along the work zone area during the 6:00 to 8:00 AM morning peak periods. The reduction in speed difference also resulted in an approximate 7.0% increase of the total throughput volume measured at the downstream work zone boundary during the 6:00 to 7:00 AM periods (Kwon et al. 2007). The volume increase during the 7:00 to 8:00 AM periods was not significant.

A six-mile test site with a long-distance work zone on I-80 north of Wanship, Utah, was used to test the response of drivers to VSL signs. Five speed detectors and two VSL signs were placed and vehicle speeds were monitored for about 3 months. Though the average speeds between static speed limit signs and VSL signs were not statistically different at a 95% confidence level, variation in speeds was reduced (McMurtry et al. 2008). However, that research did not mention anything about travel time or capacity improvement at work zone bottlenecks. Recently, field deployment of VSL in Seattle has resulted in reducing the numbers of congestion-related collisions significantly (WSDOT 2011).

VSL has also been widely implemented and tested in European countries. The key difference in European and U.S. VSL deployments is the enforcement. Most European deployments have had automated speed enforcement, and have high compliance rates. In 1995, the UK Highways Agency introduced mandatory VSL signs between Junctions 11 and 15 at one mile intervals on the M25 motorway. The UK Highways Agency (2004) reported a 9.0% reduction in the amount of flow breakdown (speeds less than 25 mph) and a 6.0% reduction in start-stop driving conditions. VSL implementation resulted in traffic headways becoming more uniformly distributed within the narrow range of 0.8-1.5 seconds. Noted that, to mimic real-world situation, during microscopic VSL simulation, this kind of driver behavior should be reflected. Rämä (1999) investigated the effects of weather-controlled speed limits and signs for slippery road conditions on the 14-km-long Finnish E18 test site. The author observed that the VSL served to reduce the mean speed and variance of speed, and increased the extent of speed reduction. The Dutch experiment examined homogenization of the traffic flow along a stretch of highway using enforced VSL (Hoogen and Smulders 1994). Only two speed limits, 70 and 90 kph, were used, with updates at 1 min increments. Test results showed that speed control was effective in reducing speed and speed variation, as well as the number of shock waves.

VSL has also been used in Germany (Robinson 2000; Bertini et al. 2006). In these studies, an empirical approach was adopted to investigate the impact of VSL control on congestion reduction. To improve driver safety, feedback was given to the driver using advisory variable message sign about the speed limit and road conditions. An analysis of the data showed that safety levels improved by 20.0%-30.0%. Improvements in terms of safety were more significant than improvements in terms of mobility.

An empirical evaluation of the implemented VSL control strategies on M42 in the UK was conducted by Papageorgiou et al. (2008). That research concluded that there was no clear evidence of a positive impact of VSL on traffic flow. However, the authors also observed that their research was limited due to the demand responsive (reactive) VSL control strategy. The authors suggested that a more robust VSL control strategy could be developed and implemented to investigate the mobility benefits.

In 2009, a field trial was held in the Netherlands over a six-month period on the A12 freeway (between Gouda and Utrecht), a freeway stretch of 16.5 km. Two algorithms were evaluated: (1) a rain algorithm; and (2) a shockwave algorithm (SPECIALIST). The implementation results of these two algorithms have been summarized by Jonkers et al. (2011). It was reported that traffic safety had been improved substantially and was asserted that it is indeed possible to resolve shockwaves by applying VSL control. It was also suggested that not all shockwaves can be resolved by applying a lower speed limit.

The following four conclusions can be drawn from the literature survey:

(1) Several inconsistent results can be found in terms of VSL mobility benefits. Although, few studies quantified freeway throughput and travel time improvements, those were achieved separately.

(2) While observing corridor wide performance measures is necessary to assess overall mobility benefits of the VSL control, almost all those VSL evaluation studies focused on a few segments in the corridor.

(3) It remains to be determined whether or not it is possible to improve bottleneck capacity through VSL implementation during the congestion periods.

(4) Most of the VSL studies showed safety benefits due to speed homogenization effect. However, one cannot conclude that VSL is not capable of improving mobility since the implemented VSL control strategies were demand responsive and they were not tightly coupled with the mobility factors.

To this end, it is important to design a control strategy that explicitly considers the mobility factors. Moreover, it is essential to develop a modeling framework that provides optimal solution when incorporated with the optimization framework. In order to effectively manage and control traffic flow through bottlenecks, traffic state variables need to be accurately predicted with dynamic capacity. This research have chosen the DynaTAM-VSL as the prediction model, which, with the proposed VSL control strategy, could accurately present dynamic traffic state change. To ensure safety and driver acceptance, appropriate constraints on the VSL control variable have been imposed during the online optimization. The experiments will give the answer in which situations VSL control can simultaneously improve the mobility as well as safety parameters.

4.3 Studied test site traffic condition

The test site consisted of the westbound 11-km section (between east of 122 St. and west 159 St.) of the Whitemud Drive (WMD), Edmonton, Canada (Figure 1.1). However, in contrast to the previous chapters, the test site in this research includes a long-distance construction zone (approximately 5.0 km) in the middle section of the test site with a reduced posted speed limit of 50 kph. Specifically, the speed limit is implemented from 1.5 km downstream of 122 St. on-ramp to upstream of 149 St. on-ramp. Because of construction activities, several lanes were dropped. Consequently, the test site experiences recurrent heavy congestion, and it gives more challenges in the VSL control.

4.4 Recurrent bottleneck characteristics

Since this research aims at improving bottleneck capacity through VSL control, understanding of their characteristics is crucial to the development of an efficient VSL control strategy. A bottleneck is defined as a location for which queues exist on the upstream and unrestricted traffic flows continue on downstream segments (Daganzo

1999). During high demand periods, bottlenecks may be activated due to work-zone lane closures, the geometric design of the roadway, or freeway splits, as vehicles are forced to slow down upstream of the bottleneck's geometric starting point (Figure 4.1).

Typically, lane changing and weaving maneuvers lead to a speed reduction just upstream of the bottleneck, in which case the passing vehicles have to accelerate from lower speeds (within the formed congestion) to higher speeds (downstream of the bottleneck); this, in turn, leads to a capacity drop (Carlson et al. 2010), i.e., an active bottleneck outflow $q_b^{(d)}$ = Q_b' that may be 5–20% lower than the free-flow capacity, Q_b. Several studies (Cassidy and Bertini 1999; Hall and Agyemang-Duah 1991; Banks 1991a; Banks 1991b), in carefully examining traffic data from prior to and following breakdown at active bottlenecks, have found that maximum flow rates diminish after queues from upstream. The capacity drop causes serious degradation of the freeway operation. Avoiding the capacity drop at recurrent bottlenecks could increase the throughput.

Figure 4.2 shows examples of capacity drop due to the weaving and lane reduction on the studied freeway corridor. A least-square fit and an approximate quantile regression were performed to establish the left side and the right side of FD, respectively. After that, a vertical line from the tip of the FD was drawn. The intersection between the vertical line and the right side of FD determines the capacity drop (CD). Further details on how to calibrate other parameters related to FD can be found in Dervisoglu et al. (2009). Following this calibration procedure, it was estimated that the free-flow capacity (FC) and the congestion capacity (CC) at the immediate upstream of weaving section on WMD as 1620 vphpl and 1452 vphpl, respectively. Thus, the estimated CD was 10.3%.

Whereas, the estimated FC and CC at the immediate upstream of lane drops were 1750 vphpl and 1465 vphpl, respectively. Thus, the estimated CD was 16.2%.

4.5 Methodology

4.5.1 *Control strategy*

The proposed VSL control strategy is to maximize utilization of bottleneck's free-flow capacity. The following control strategy is used for the following situation based on the given traffic characteristics. If the demand is too high from both upstream and on-ramp, and congestion is unavoidable without control, it is necessary to create a discharge section (L_{dis}) with adequate length (500~700 m) immediately upstream of the bottleneck, L_b. To this end, a critical VSL must be defined as shown in Figure 4.3. The objective is to maintain a feeding flow to the bottleneck that is close to the capacity flow of the bottleneck. In order to maximize bottleneck flow, the discharge flow of three lanes is maintained at a level close to bottleneck capacity flow, i.e., in Figure 4.3(a) $q = 3q_{b'}^{(d)} = 3q_b^{(u)} \approx 3Q_b$ and in Figure 4.3(b) $q = 3q_{b'}^{(d)} = 2q_b^{(u)} \approx 2Q_b$. Here, Q_b defines the bottleneck capacity, $q_{b'}^{(d)}$ and $q_b^{(u)}$ are the transition flows at the boundaries $(L_{crit} \rightarrow L_{dis})$ and $(L_{dis} \rightarrow L_b)$, respectively. As can be seen, control of upstream traffic can improve bottleneck flow. The critical VSL is required in order to manipulate the speed limit to control the flow into the discharge section, and to make sure that the bottleneck reaches capacity flow. The critical link (L_{crit}) is a very short section, usually 200-250 m. in length. The L_{crit} is determined assuming vehicle might decelerate from the free-flow speed to zero speed (the worst case). In this research, the designed L_{crit} assumed the driver's perception-reaction time (PRT) of 2.5 sec and the normal deceleration value of 1.5 m/s^2, so that drivers need not experience uncomfortable and unsafe deceleration. Moreover, the L_{crit} depends on the speed limit of the location. However, the L_{crit} must be long enough based on the roadway geometry where the VSL is implemented and the average deceleration rate of drivers when they perceive each critical VSL sign.

4.5.2 *Traffic flow model*

To predict traffic flow within the MPC, a freeway section is divided into several links as in Figure 2.2 of Chapter 2, and time is segmented into discrete time steps of duration T. The evolution of traffic flow $q_i(k)$ (vphpl), density $\rho_i(k)$ (vpkpl) and space-mean speed $v_i(k)$ (kph) for link *i* at time step k are as follows.

4.5.2.1 Density dynamics

The density of each link (for both no-VSL and VSL control situation) can be predicted by Equation 4.1, which is essentially the law of flow conservation. Under the assumption of a triangular fundamental diagram (FD) (flow vs. density curve), this research adopted the following constraints (Equation 4.2 and Equation 4.3) to estimate the link outflow (q). The link-specific parameters in the equation are (with some variation) as follows: Q_{max} =1700 vphpl, w =11.5 kph, ρ_c = 40 vpkpl, ρ_{jam} = 110 vpkpl, and θ =15%, which have been computed from calibrated FDs with the traffic data collected from the microscopic WMD based model. In Equation 4.2, at any time index k, transition flow from i to $i+1$, depends on the average link flow at i, the capacity of the downstream link $i+1$, and the supply from the link $i+1$. The basic METANET model includes only the first constraint of Equation 4.2, assuming the link outflow are equivalent to average link flow.

$$\rho_i(k+1)=\rho_i(k)+\frac{T}{L_i\lambda_i}\left[\lambda_{i-1}q_{i-1}(k)-\lambda_i q_i(k)+r_i(k)-s_i(k)\right] \tag{4.1}$$

$$q_i(k)= min\left\{v_i(k)\rho_i(k)+r_{i+1}(k)-s_{i+1}(k), Q_{max,i+1}, w_{i+1}\left(\rho_{Jam,i+1}-\rho_{i+1}(k)\right)\right\} \tag{4.2}$$

Equation 4.2 is applicable when the links have a static capacity. However, once the density at bottleneck exceeds its critical value, ($\rho_{bottleneck}(k)>\rho_{c,bottleneck}$), the discharge flow from the bottleneck is reduced by θ fraction to $Q'_b=(1-\theta)Q_b$. This phenomenon is known as capacity drop. Assuming the FD as in Figure 4.4, the transition flow from the immediate upstream link to the downstream of a bottleneck can be calculated using Equation 4.3:

$$q_{i-1}(k)=min\left\{v_{i-1}(k)\rho_{i-1}(k)+r_i(k)-s_i(k), Q'_b, w_{bottleneck}\left(\rho_{Jam,bottleneck}-\rho_{bottleneck}(k)\right)\right\} \tag{4.3}$$

4.5.2.2 Speed dynamics

The customized dynamic model used the same VSL modeling approach as in Chapter 2. It was derived from the original METANET model (Equation 4.4). The FD (speed-density relation) as it appears in the relaxation term (2nd term) was replaced with the VSL control variable u. Thus, mean speed at each freeway link without and with VSL control was predicted using Equation 4.4 and Equation 4.5, respectively. The following global parameter values for the speed dynamics are adopted: τ =0.03 hr, υ =50 km^2/hr and κ =47 vpkpl, by minimizing error between model simulated and measured traffic data.

$$v_i(k+1)=v_i(k)+\frac{T}{\tau}\left[V[\rho_i(k)]-v_i(k)\right]+\frac{T}{L_i}v_i(k)\left[v_{i-1}(k)-v_i(k)\right]-\frac{1}{\tau}\left[\frac{T\upsilon}{L_i}\frac{\rho_{i+1}(k)-\rho_i(k)}{\rho_i(k)+\kappa}\right] \tag{4.4}$$

Where, $V[\rho_i(k)]=v_{free,i}\exp\left[-\frac{1}{\alpha_i}\left(\frac{\rho_i(k)}{\rho_{c,i}}\right)^{\alpha_i}\right]$

$$v_i(k+1)=v_i(k)+\frac{T}{\tau}\left[u_i(k)-v_i(k)\right]+\frac{T}{L_i}v_i(k)\left[v_{i-1}(k)-v_i(k)\right]-\frac{1}{\tau}\left[\frac{T\upsilon}{L_i}\frac{\rho_{i+1}(k)-\rho_i(k)}{\rho_i(k)+\kappa}\right] \tag{4.5}$$

4.5.3 *Objective function*

As shown in Chapter 3, if only total travel time (TTT) is used in the objective function, minimization of TTT would result in lower density. In other words, it would result in a lower flow on the mainline, which is in conflict with the proposed VSL control's objective of improving throughput. On the other hand, if only total travel distance (TTD) is used as an objective function, the maximization of TTD would increase flow to nearly the capacity level that would create flow instability. Thus, the objective function in this research is selected as the weighted summation of TTT and TTD as shown in Equation (4.6). Here, the intent is to minimize TTT and at the same time maximize TTD.

$$J(\mathrm{u}) = T\sum_{j=1}^{N_p}\sum_{i=1}^{M}\lambda_i L_i\left[\alpha_{TTT}\rho_i(k+j) - \alpha_{TTD}q_i(k+j)\right] \qquad (4.6)$$

The first term in Equation (4.6) is TTT and the second term is TTD. Different values of the parameters α_{TTT} and α_{TTD} can be selected to reflect the preference of the control policy. If α_{TTD} is assumed to be one, then α_{TTT} is equivalent to speed (v). In this research, α_{TTD} was assumed to be 1 and α_{TTT} was set as the free-flow speed of the link. The justification of the chosen values in the weight parameters can be found in Chapter 3.

4.5.4 *Constraints*

Based on a consideration of safety and traffic flow characteristics in real-world, the following constraints on the VSL control variable were adopted:

C1: To guarantee the drivers' safety, the optimal speed limit of VSL operated link must be kept equal or lower than the maximum value V_{max}, i.e., $u_i(k) \le V_{max}$

C2: To maintain the operating efficiency on the freeway, the optimal speed of the VSL operated link is to be higher than the minimum speed V_{min}, i.e., $u_i(k) \geq V_{min}$

C3: For the safe operation of VSL control, the change of speed between two successive time steps should satisfy the following constraints: $\left|u_i(k) - u_i(k+1)\right| \leq V_{max,diff}$

The VSL using the proposed model considers only discrete values. This is expressed by a constraint set, $u_i(k) \in (V_{min}$ =10, 20, 30, 40, 50, 60, 70, V_{max} =80 kph). In this research, a sensitivity of the $V_{max,diff}$ is performed with the values of 5, 10, 15, and 20 kph. The VSL update frequency might have an impact on mobility. Thus, a sensitivity of the VSL update frequency is performed to investigate these impacts. VSL update frequencies of 1, 2, 3 and 5 minutes are considered for sensitivity analysis. Mobility performances in a total of 16 VSL control scenarios (four different $V_{max,diff}$, each with four different VSL update frequency) are compared to identify the best combination of "VSL update frequency" and "maximum speed difference between two successive time steps".

4.6 Building WMD base model

Multiple days of traffic data was used to calibrate and validate the WMD base model and was compiled from two sources: (1) dual loop detectors on the mainline; and (2) video data from on-ramps and off-ramps. To replicate the real-life work-zone traffic operation, calibration was conducted from both a system and an operational point of view. The calibration and validation procedure[3] of the freeway work-zone can be viewed in Figure

[3] *The calibration and validation results have been taken from a journal paper:* **Hadiuzzaman, M.**, Zhang, Y., Lu, M., Qiu, T.Z., and AbouRizk, S.M. "Modeling the Impact of Traffic Flows upon Concrete Construction: An HLA Based Simulation Framework." (*under-review*)

4.5. First, detailed network geometry data (following a detailed corridor survey and the roadway geometric map, which were both provided by the traffic operation group in the City of Edmonton), including construction zone lane, the exact location of on-ramps and off-ramps, auxiliary lane and tapers length, configuration of weaving sections, and exact location of speed limit signs, was coded through the VISSIM graphical user interface (GUI). After the network coding, the base model was run with certain mainline and on-ramp demand and default driver behavior parameters; and traffic operation was observed at on-ramps, merge sections and work-zone bottlenecks. Second, this research adjusted the origin-destination (OD) matrix, as well as several operational parameters (as follows), so that the model replicates real-world traffic operations on WMD.

4.6.1 *WMD base model calibration*

4.6.1.1 System calibration

This research have used a TFlowFuzzy Procedure in VISUM (Appendix A) that produces a revised OD matrix based on a given seed matrix. The base demand or trip matrices for the present WMD model came from matrices imported from the City of Edmonton 2005 WMD VISSIM model. To estimate a synthetic trip matrix, link traffic count data recorded in the test site were used. TFlowFuzzy performs a synthetic OD estimation based on an extended application of the Willumsen method (Willumsen 1984). Estimation of OD matrices using TFlowFuzzy is an iterative process repeated until the resulting assignment of the refined OD matrices meets the calibration criteria. When the estimated OD (see Appendix A) was assigned to the network, simulated link volumes for more than 85% of cases were within 5% for measured volumes <500 vph; within 10% for measured volumes between 500~1500 vph; and within 15% for measured volumes >1500 vph. The summation of the simulated link volumes was kept within 5% of the total measured flow. Four vehicle types were created to replicate traffic composition in the test site: (1) WMD car (90.0%); (2) WMD truck (6.0%); (3) WMD heavy truck (3.0%); and (4) WMD bus (1.0%). The simulation warm-up period was set to 30 minutes.

4.6.1.2 Operational calibration

To replicate the bottleneck formation along the test site, three customized link behavior types were defined: (1) the freeway merge section; (2) the lane drop condition; and (3) the construction zone along the freeway. In VISSIM, the Safety Distance Reduction Factor (SDRF) values for the freeway lane drop, merge section, and construction zone were changed to 0.1, 0.2, and 0.05, respectively, from the default value of 0.6. The driving behaviour parameter sets for the customized freeway links were adjusted to alter the aggressiveness of the drivers near the merge areas. Specifically, by lowering the SDRF values, it was possible to make the merging drivers more aggressive to generate realistic merge behavior on the freeway. Moreover, the headway time (CC1) was set to 1.30, 1.20, and 1.40 for freeway lane drop, merge section, and construction zone, respectively, from the default value of 0.9 seconds. Those parameters were adjusted with the trial-and-error method and numerous iterations until the simulated capacities are within 10% of estimated capacities conforming to the macroscopic fundamental diagram (FD) as calibrated from the field traffic data. Visibility parameters (emergency stop and lane change) were also adjusted at each link connector of the WMD base model to represent the local conditions. Note that, CC1, which controls the safety distance in the car-following logic of VISSIM, has the strongest influence on freeway capacity adjustment. As a guideline, when all other operational parameters in VISSIM are kept in their default values, increasing the CC1 results in consistent reduction of freeway capacity. However, as several operational parameters were altered in addition to the CC1, the trend was found to be slightly different. By calibrating the freeway capacities as above, it was also possible to keep the simulated average travel time within 10% for the measured mainline segments. The WMD base model is being presented in Figure 4.6.

4.6.2 *WMD base model validation*

The calibrated WMD base model was further validated against field data independent of the calibration dataset. This research adopts the Geoffrey E. Heavers (GEH) statistic to compare field loop detector volumes with those obtained from the WMD base model. As a general guideline for model validation, GEH values less than 5 indicate good fit; values between 5-10 require further investigation, while values above 10 indicate a poor fit (Holm et al. 2007). This research obtained an average GEH value of 3.47. Another five simulation runs with different random seeds were performed to confirm the GEH value.

$$GEH = \sqrt{\frac{(simulated - observed)^2}{0.5(simulated + observed)}} \qquad (4.7)$$

4.7 Application results

4.7.1 *MPC design in WMD base model*

The calibrated microscopic WMD base model is used as a platform for the evaluating the MPC-based VSL control. Therefore, following the proposed VSL control strategy and identified bottleneck locations, the base model was divided into 11 links. In addition, two VSL signs were implemented upstream of the identified bottleneck locations (see Figure 4.7). The proposed VSL control strategy was implemented in the simulation using a special-purpose software module developed in C++ using the COM interface.

In the simulation, one loop detector was put on each lane of the mainline links and ramps (see, Figure 4.7) in order to obtain the initial measurements of traffic variables, $v_i(k)$ and $Q_i(k)$. The spacing of the loop detector stations is approximately 700 m. Density, $\rho_i(k)$, is estimated from the fundamental relation among the traffic variables. Alternatively, VISSIM has the function of providing link-specific density directly. However, considering field implementation and data availability, this research circumvented the use of the VISSIM built-in function for density measurement. Traffic density is usually not measured in reality. In order to predict mean speed for the time steps ($k+1$, $k+2$, ………..) in the freeway links, the mean speed values, v_0, in Equation 4.4 and Equation 4.5 was set for the most upstream link equal to v_1. The density, ρ_{M+1}, needed in that equations for the last link, M, is set equal to ρ_M. However, in cases ρ_M becomes overcritical, ρ_{M+1} was set equal to the critical density. In other words, traffic conditions downstream of the considered freeway section are assumed to be non-congested.

For the density prediction using Equation (4.1), the outflow, q_0, for the most upstream link was set as the measurement for the current time step. It is obtained from the loop detector placed at the link boundary. In the successive time steps (over the prediction horizon), these flows as well as ramp flows are predicted by generating random numbers, assuming a truncated normal distribution. The generated flows for the next prediction step varied within 10% of the previous step. It also confirms the field observations. However, if the density ρ_1 is overcritical, mainstream flow q_0 is limited to $Q(\rho_1)$, i.e., to the value of the fundamental diagram corresponding to ρ_1. Furthermore, it is assumed that the exit flow from the last link is equal to the average flow of that link. This assumption is valid when a free-flow condition exists in the downstream.

This research used an online optimization method based on the measurement of the current and future predicted traffic states. Using the proposed traffic flow model and numerical optimization, the sequence of speed limit inputs that optimize (minimize) the performance criterion (J) over a given future time horizon (N_P=5 min) was determined. In this research, a 5-min prediction horizon is equivalent to 5 steps prediction. The length of simulation time step (T) is 1 min. Figure 4.8 shows an example of a generated speed limit sequence, and the highlighted arrows show a complete branch. At each time step, these speed limit values were generated using a C++ program (see Appendix B) based on previous speed limit values along with the constraints (*C1*-*C3*).

For each time step, the total number of decision tree branches is $C^{prediction\ steps}$; where C is the choice number, which could be 2 or 3. For the lower and upper bound speed limits, the choice number for the immediate next time step is 2. The optimal speed limits for successive prediction steps correspond to a branch that results minimum value of (J). However, the control horizon (N_C) in this research is 1 min. So, the VSL controller uses only the first VSL input for the system as in the moving horizon concept. At each control time step, only the first sample of the optimal control input is applied; afterward, the time axis shifts to one control sample time step. Then, based on the new traffic states and control inputs of the system, a new sequence of optimal control inputs is generated. Once again the first control input is applied. At every time step, this process is repeated until the end of the simulation. In this research, a Visual C++ application program was developed that controls the WMD base model through the COM interface. In the base model, the desired speed decision point is used to alter the vehicles' initially-assigned desired speed distributions. They represent speed limit signs or VSL signs in real life.

4.7.2 *Simulation results for no-VSL scenario*

The simulation in this research has been run over a period from 4:00-6:30 PM. First 2-hr corresponds to an afternoon rush hour. Moreover, demand is very high for the first hour of the simulation. In this first hour, about 5300 vehicles were assigned at the mainline origin (see, q_0 in Figure 4.7). In addition, out of four on-ramps in Figure 4.7, r_2 and r_3 contribute relatively higher input flow on the test site. The demand on these ramps increases to near 700 vph, remains constant for 2 hrs, and decreases finally to a low value of 305 vph. For the given demand inputs, two bottlenecks were identified on WMD. Bottleneck B1 is activated due to intense weaving maneuver between mainline vehicles with those coming from ramp r_1. Around 30% of the vehicles coming from on-ramp, r_1, take off-ramp, S_1, at the last moment. Bottleneck B2 represents a virtual lane drop. At this point, around 95% of all the vehicles coming from upstream take the route via B2.

Figure 4.9(a) and Figure 4.9(b) show the shockwave propagation from the two bottlenecks. At B1, the speed begins to drop at $t = 4{:}08$. Within a very short time it drops from 80 kph to 40 kph and then 20 kph. A shockwave propagates in the upstream direction. In order to satisfy the definition of active bottlenecks, vehicles downstream of link 4 (corresponding to B1) must maintain free-flow speed. Free-flow on link 5 continues until $t = 4{:}40$, when the link is hit by another shockwave caused by downstream bottleneck, B2. At $t = 4{:}11$, speed begins to drop in bottleneck link 10 (corresponding to B2). It decreases to below 30 kph rapidly and maintains this level for the entire simulation period. However, downstream (L11) of this bottleneck, flow is always at the free-flow condition. From Figure 4.9(a) and Figure 4.9(b), it can be observed that the immediate upstream links (L3 and L9) of recurrent bottlenecks are highly affected by the speed drop, eventually much higher than the bottlenecks themselves. Figure 4.9(c) presents density profiles for all the links. Time dependant shockwaves propagation can be clearly observed in this figure.

4.7.3 *Simulation results for VSL-control scenario*

Two VSL signs are implemented at approximately 500 m. upstream of the identified recurrent bottlenecks. Specifically, VSL-1 and VSL-2 are operated in L2 and L8 (see Figure 4.7), respectively. Those two VSL signs are optimized separately within the objective function, since they are operated in an isolated mode. During the optimization, the value of α_{TTT} in the objective function, (J), were set equal to 80 and 50 for L1-L4 and L5-L11, respectively. The parameter α_{TTD} was set to 1. Due to the ongoing construction activities on the WMD, link L5-L11 have speed limit of 50 kph. Whereas, link L1-L4 have speed limit of 80 kph. As the simulation is conducted during the peak period, higher weight to TTT was given, and the motivation is to maintain free-flow speed at the discharge segment (L_{dis}). In the evaluation of the proposed VSL control strategy, it was assumed that 90% drivers comply within 5 kph of the posted speed limit.

Figure 4.10 shows traffic state improvement for the proposed VSL control strategy. Implementation of the proposed VSL control has kept traffic speed above 30 kph, and density below or close to critical density (40 vpkpl) for all the links. In Figure 4.10(a) and (b), the notations A and B define lower speed and free-flow speed regions at the bottlenecks. Although the proposed VSL control has not completely eliminated speed drop, the shockwaves have been suppressed to a great extent, as can be seen in Figure 4.10 (a). Now, L5 is operating with the free-flow speed for the entire simulation period.

It can be observed from Figure 4.11, compared to the no-VSL scenario, flow has been improved in the bottleneck significantly during the high demand period. More interestingly, moving further downstream, higher improvement in flow over the links can be observed. This is due to more uniform distribution of traffic over the links as a result of the VSL implementation. However, during the time period $t =$ 5:20-6:00, during which demand is comparatively low (around 65% of the first hour of simulation), implementation of the VSL control has no significant impact in terms of bottleneck flow improvement. Eventually, in the time horizon $t =$ 5:20-5:40, flow has been decreased at some points. It is no wonder that the implementation of VSL control has reduced the flow during comparatively low traffic demand, and several empirical and simulation studies (Papageorgiou et al. 2008; Lu et al. 2010) confirm this result. This clearly indicates that, in terms of traffic mobility improvement, VSL is effective during the congestion period. This leads to the comparison of mobility parameters: TTT and throughout with and without VSL control in the congestion period.

Figure 4.12 shows changes in optimal speed limit values over the simulation time horizon. The speed limit for the VSL-1 was reduced to 70 kph at $t =$ 4:06, and then the controller further lowered the speed limit values in order to avoid a capacity drop at bottleneck B1. From $t =$ 4:40, the values of the VSL control variables began to increase. During the last 30 min of the simulation, speeds were maintained at 80 kph. Similarly, for the VSL-2, the speed limit value decreased from 50 kph to 40 kph, and then was further reduced to 30 kph at $t =$ 4:08. However, during the last 20 min, it maintained at 50 kph.

Table 4-1 presents the numerical values of TTT and throughput before and after VSL implementation. In order to estimate the MOEs, the data have been averaged over several simulation runs (random seeds were 43, 25, 20, 27, 30, 35, 65, 55, 80, and 42). It is calculated that the proposed VSL control strategy has decreased TTT significantly (around 39%). It was estimated that for the bottleneck B1, the congestion capacities are 1393 vphpl and 1445 vphpl for the “no-VSL” and “VSL-control”, respectively. Thus, the VSL control has improved the capacity at B1 by 3.7%. Whereas, for the bottleneck B2, the congestion capacities are 1907 vphpl and 2103 vphpl for the “no-VSL” and “VSL-control”, respectively. Thus, the capacity at B2 is improved by 10.2%. These amount of capacity improvements in the bottlenecks resulted in 5.4% increase in throughput for the entire test site in the congestion periods (see, Table 4-1). Obviously this level of improvement is valid for the simulation scenario and for the time period considered in the evaluation of the isolated VSL control strategy.

4.7.4 *Impact of sub-optimal solution on control performance*

Successful field implementation of the proposed VSL control requires a computationally simple optimization method without compromising desired accuracy level. Although the sophisticated gradient-based optimization method ─ SQP as presented in Chapter 3 can provide global optimal solution, the continuous solution from the SQP cannot be implemented in the real-world considering different factors: computational efficiency, driver compliance, safety, etc. In other word, heuristic rule is required to find discrete speed limit values from the continuous values. However, it makes the optimal solution as sub-optimal, which may compromise performance improvements.

By contrast, this research has proposed the non-gradient-based optimization method ─ decision tree that does not need above conversion and find directly the discrete speed limit values by minimizing a user-defined objective function. To compare the VSL control performance with the discrete VSL values as obtained by the two optimization method, a comparison on mobility benefits under the same demand levels is made. Specifically, it was found that the TTT improvements due to implementing decision tree solution and post-processed SQP solution (to the nearest 10 kph) are 38.8% and 28.0%, respectively. Thus, the post-processed SQP solutions result in 10.8% lower improvement than the decision tree. Interestingly, Hegyi (2004) found that due to rounding the continuous VSL values from SQP to the nearest 10 kph can result in performance loss in terms of travel time as much as 21.5% (see Table 6.2 of the above referred thesis manuscript). Furthermore, the throughput improvements in this research were 5.4% and 3.71%, respectively. Thus the performance loss due to implementing post-processed SQP solutions in the network is 1.7%. In addition, the computation time and objective function values (Equation 4.6) at each control sampling time for optimizing the VSL control variables with the SQP and decision tree methods are presented in Figure 4.13, which clearly demonstrates the efficiency of the decision tree-based optimization method. Based on the above discussion, it can be concluded that the decision tree-based optimization method is suitable for the real-world isolated VSL application.

4.8 Sensitivity of VSL update frequencies and safety constraint

With the efficient decision tree-based optimization methods, in this section[4], a total of 16 VSL control scenarios are evaluated and compared with the base scenario (no-VSL). To confirm the robustness of the VSL control strategy, peak demand in the WMD base model was slightly changed compared to that considered in the previous section. Table 4-2 presents the summary of the percentage improvement of TTT and throughput under various scenarios for the peak 2-hour simulation period for the test site. Clearly, the VSL controls always improve the mobility parameters. More than 30.0% improvement in TTT was obtained by implementing MPC-based VSL control in the studied freeway section. A

---

[4] *Results included in this section have been taken from:* Islam, T., **Hadiuzzaman, M.,** Fang, J., Qiu, T.Z., and El-Basyouny, K. "Assessing Mobility and Safety Impacts of a Variable Speed Limit Control Strategy." *Transportation Research Record*, (2364), 1-11.

2-3% improvement in throughput was obtained. Interestingly, no substantial differences in these aggregated mobility performances were found across the various VSL scenarios.

As shown in Table 4-3, average collision probabilities for all the VSL control scenarios are lower than that of the “no-VSL”. This implies that the proposed VSL control strategy has the potential to improve freeway safety. The table arranges the VSL scenarios based on the percentage improvement of collision probabilities (CP). The top five scenarios are shown in italic letters. It shows that VSL control can reduce collision probability as much as 50.0%. There is a noticeable difference in collision probabilities for the various combinations of VSL update frequency and maximum speed difference constraint. In general, CPs are considerably lower for a VSL update frequency of 5 minutes as compared to 1-minute, 2-minute and 3-minute VSL update frequencies. This result implies that frequent changes in VSL may create a disturbance in the traffic stream; hence, safety benefit diminishes. It can also be concluded that the VSL update frequency has a higher influence on safety than the maximum speed difference constraint.

Figure 4.14 presents the collision probability[5] for VSL control scenarios and the no-VSL scenario for all the links. For each link, an average of the 2-hour collision probability was calculated. When the collision probabilities at different links are compared, it shows that collision probabilities are reduced from the “no-VSL” scenario in most of the cases. Certain VSL scenarios cause higher collision probabilities for links 2 and 8 when compared to the “no-VSL” scenario. Note that these two are the links where the VSL signs were placed. The figure shows that high collision probabilities occur for links 2 and 8 for those scenarios having a frequent VSL update (i.e., 1 min, 2 min). This result

[5] Collision probability is computed with a Logistic Regression Model, where the model parameters were calibrated with the real data collected from WMD (see Islam et al. 2013).

indicates that the speed disturbance occurs at the VSL installed links when the speed limit changes too frequently. The top five scenarios in terms of safety improvements are shown by dotted lines. These five scenarios have lower collision probabilities than that of the "no-VSL" scenario for all the links. This figure also shows that there is no potential migration of collision risk from the VSL-operated links to adjacent links.

Figure 4.15(a) shows the average of link collision probabilities over the simulation time period for "no-VSL" and the top-five VSL scenarios. It was found that the VSL controls yield a high reduction in collision probabilities for most of the simulation period. Improvement in collision probabilities diminishes towards the end of the simulation period. For the first and last few minutes of simulation, it is found that the VSL controls and the "no-VSL" scenarios yield almost the same collision probabilities. This result has important implications in terms of the implementation of VSL control. In the research area, traffic congestion starts a few minutes past 4:00 PM (i.e., the beginning of the simulation) and reduces towards the end of the simulation period (6:00 PM) until the free flow condition appears approximately in the last 15 minutes of the simulation. The result from this research suggests that the VSL can improve safety under non-free flow traffic conditions. The highest safety improvement occurs when the freeway is highly congested, and the improvement diminishes with lower levels of congestion. This finding complies with the results obtained by several previous studies.

TTT for every one minute for all the links is shown in Figure 4.15(b). It was found that the VSL controls reduce the TTT for most of the simulation period, except for the first and last few minutes. One notable observation is that Figures 4.15(a) and Figure 4.15(b) have similar profiles. This indicates that the proposed VSL control strategy can improve the safety and travel time saving simultaneously for the non-free flow traffic situation.

Based on results mentioned above, it was found that the VSL control scenario with a 5-minute speed limit update frequency and 10 kph as the maximum speed difference between two successive time steps produces the best performances. A 49.9 % reduction in collision probability and 33.3 % reduction in total travel time can be obtained for this scenario based on this research. Lee et al. (2004) found that, for the congested traffic situation, VSL reduced collision potential by 20.0% to 45.0% when operated according to the 5 to 10 minute speed limit update frequencies. The safety improvement was realized at the cost of increased system travel time. However, due to heuristic VSL control strategy, the reported negative impact on mobility parameters might not be accurate. By contrast, Abdel-Aty et al. (2006a) suggested changing the speed limit by 5 mph (8 kph) every 10 minutes to improve safety as well as travel time in uncongested situations. The findings from the current research comply with both previous studies to a certain extent.

4.9 Summary and conclusions

This research proposes a VSL control strategy that aims at maximizing the bottleneck flows and can be easily implemented in the authentic traffic operation. The control strategy explicitly considers the traffic characteristics at recurrent bottleneck, and its upstream-downstream segments. This VSL control strategy was designed within the MPC framework. To deeply understand the effectiveness of VSL control to improve bottleneck capacity, an analytical model was developed to represent drivers' response to updated speed limits and macroscopic speed dynamical change with respect to changeable speed limits. To model traffic flow at active bottleneck, capacity drop concept was introduced in the FD of the density dynamics. This modification allows analyzing in which situations VSL control can markedly improve bottleneck capacity.

Furthermore, considering the real-world applicability, this research proposes an optimization method which searches the optimal set of control variable values based on a generated decision tree at each control sampling time. It was found that, in terms of mobility, VSL is mostly effective during congestion periods. Specifically, for the 11-km studied test site improvements to TTT and throughput were around 39.0% and 5.4%, respectively with the proposed decision tree-based optimization method. In addition, it was found that due to rounding the continuous VSL values obtained from the SQP and sending them in the VSL signs cause 10.8% and 1.7% losses in TTT and throughput improvements, respectively. In addition, the CPU time and objective function values at most of the control sampling indices were at the minimum values with the decision tree method compared to the post-processed SQP solution. Thus, it was concluded that the proposed decision tree-based optimization method is suitable for the real-world application.

With the decision tree-based optimization method, it was estimated that out of two identified recurrent bottlenecks, for the weaving bottleneck, the proposed VSL control strategy has improved the capacity by 3.7%. Whereas, for the lane drop bottleneck, the amount of improvement is 10.2%. The preceding results clearly demonstrate the robustness of the proposed VSL control strategy and the benefits of its implementation. The research findings also prove that the proposed VSL control strategy could result in uniform traffic distribution over the freeway links, thereby mitigating the high traffic density that leads to traffic breakdown. This research proves that the VSL control has the capability to delay the onset of congestion and recover the speed early.

The VSL sensitivity analysis on safety constraints and VSL update frequencies are promising in terms of supporting the implementation of the VSL control strategy for improving freeway safety and mobility. It provides important insight for selecting VSL control parameters for the field implementation of VSL. It also demonstrates the traffic situations in which VSL control can be beneficial as follows.

(1) The proposed VSL control strategy improves both safety and mobility simultaneously under non-free flow traffic situation.

(2) No noticeable changes in collision probability and travel time were found under free-flow traffic situation due to same flow pattern for VSL and no-VSL situation.

(3) VSL update frequency has a high influence on traffic collision, but no substantial influence on mobility performances.

(4) More frequent speed limit changes with high speed difference between two successive time steps diminishes the safety benefit of VSL.

(5) Based on both the safety and travel time savings, VSL control with a 5-minute speed limit update frequency and 10 kph maximum speed difference between two successive time steps yielded the best results.

(6) A 50.0% reduction in collision probability and a 33.0% reduction in total time were obtained for the above-mentioned VSL control scenario.

4.10 References

Abdel-Aty, M., Dilmore, J., and Dhindsa, A. (2006a). "Evaluation of variable speed limits for real-time freeway safety improvement." *Accident Analysis and Prevention,* 38(2), 335-345.

Abdel-Aty, M., Dilmore, J., and Hsia, L. (2006b). "Applying variable speed limits and the potential for crash migration." *Transportation Research Record,* (1953), 21-30.

Banks, J. H. (1991b). "Two-capacity phenomenon at freeway bottlenecks: a basis for ramp metering?" *Transportation Research Record,* 1320 pp. 83-90.

Banks, J. H. (1991a). "The two-capacity phenomenon: some theoretical issues." *Transportation Research Record,* 1320 234–241.

Bertini, R. L., Boice, S., and Bogenberger, K. (2006). " Dynamics of a variable speed limit system surrounding a bottleneck on a German autobahn. " *85th TRB Annual Meeting, Washington D. C., Jan. 22-26.*

Carlson, R. C., Papamichail, I., Papageorgiou, M., and Messmer, A. (2010). "Optimal mainstream traffic flow control of large-scale motorway networks." *Transportation Research Part C,* 18 193–212.

Cassidy, M. J., and Bertini, R. L. (1999). "Some traffic features at freeway bottlenecks." *Transportation Research Part B: Methodological,* 33B(1), 25-42.

Chien, C. -., Zhang, Y., and Ioannou, P. A. (1997). "Traffic Density Control for Automated Highway Systems." *Automatica,* 33(7), 1273-1285.

Daganzo, C. F. (1999). "Remarks on traffic flow modeling and its applications in traffic and mobility." *Proceedings of the Traffic and Mobility Simulation, Economics and Environment Conference,* 105-115.

Dervisoglu, G., Gomes, G., Kwan, J., Muralidharan, A., Horowitz, R., and Horowitz, R. (2009). "Automatic calibration of the fundamental diagram and empirical observations on capacity." *Transportation Research Board 88th Annual Meeting*.

Hall, F., and Agyemang-Duah, K. (1991). "Freeway capacity drop and the definition of capacity." *Transportation Research Record*, 1320 91-98.

Harbord, B. (1995). "Application of SISTM to dynamic control on the M25." *IEE Colloquium (Digest),* 5/1-5/5.

Hegyi, A. (2004). "Model Predictive Control for Integrating Traffic Control Measures." *PhD Thesis, Delft University of Technology, Delft, the Netherlands, TRAILThesis Series T2004/2*.

Hellinga, B., and Mandelzys, M. (2011). "Impact of driver compliance on the safety and operational impacts of freeway variable speed limit systems." *J.Transp.Eng.*, 137(4), 260-268.

Holm, P., Tomich, D., Sloboden, J., and Lowranc, C. (2007). "Traffic Analysis Toolbox Volume IV: Guidelines for Applying CORSIM Microsimulation Modeling Software." Federal Highway Administration, Report No. FHWA-HOP-07-079, Washington D.C.

Hoogen, V. E., and Smulders, S. (1994). "Control by variable speed sign: results of the Dutch experiment " *In Proc. of 7th Int.. Conference on Traffic Monitoring and Control, London, England, April 26-28, no. 391,* 145-149.

Islam, M., Hadiuzzaman, M., Fang, J., Qiu, T. Z., and El-Basyouny, K. (2013). "Assessing Mobility and Safety Impacts of a Variable Speed Limit Control Strategy." *Transportation Research Record*, (2364), 1-11.

Jonkers, E., Wilmink, I. R., Stoelhorst, H., Schreuder, M., and Polderdijk, S. (2011). "Results of field trials with dynamic speed limits in the Netherlands: improving throughput and safety on the A12 freeway." *14th International IEEE Conference on Intelligent Transportation Systems Washington, DC, USA. October 5-7*.

Kohler, U. (1974). "Stability of vehicle platoons." *In D. J. Buckley Proceedings of Rhe Sixth Infernational Symposium on Transportation and Traffic Theory. Elsevier, New York*.

Kwon, E., Brannan, D., Shouman, K., Isackson, C., and Arseneau, B. (2007). "Development and field evaluation of variable advisory speed limit system for work zones." *Transportation Research Record,* (2015), 12-18.

Lee, C., and Abdel-Aty, M. (2008). "Testing effects of warning messages and variable speed limits on driver behavior using driving simulator." *Transportation Research Record,* (2069), 55-64.

Lee, C., Hellinga, B., and Saccomanno, F. (2006). "Evaluation of variable speed limits to improve traffic safety." *Transportation Research Part C: Emerging Technologies,* 14(3), 213-228.

Lee, C., Hellinga, B., and Saccomanno, F. (2004). "Assessing safety benefits of variable speed limits." *Transportation Research Record*, (1897), 183-190.

Lee, C., Hellinga, B., and Saccomanno, F. (2003). "Proactive freeway crash prevention using real-time traffic control." *Canadian Journal of Civil Engineering*, 30(6), 1034-1041.

Lenz, H., Sollacher, R., and Lang, M. (1999). "Nonlinear speed-control for a continuum theory of traffic flow." *In 14th World Congress of IFAC, Beijing, China*, Q 67–72.

Lu, X. Y., Qiu, T. Z., Varaiya, P., Horowitz, R., and Shladover, S. E. (2010). "Combining Variable Speed Limits with Ramp Metering for freeway traffic control." *Proceedings of the 2010 American Control Conference, ACC 2010,* 2266-2271.

McMurtry, T., Saito, M., Riffkin, M., and Heath, S. (2008). "Variable Speed Limit Signs: Effects on Speed and Speed Variation in Work Zones." *85th TRB Annual Meeting, Washington D. C.,Jan. 11-15*.

Papageorgiou, M., Kosmatopoulos, E., and Papamichail, I. (2008). "Effects of variable speed limits on motorway traffic flow." *Transportation Research Record,* (2047), 37-48.

Rämä, P. (1999). "Effects of weather-controlled variable speed limits and warning signs on driver behavior." *Transp.Res.Rec.,* (1689), 53-59.

Robinson, M. D. (2000). "Examples of variable speed limit applications." *Speed Management Workshop. 79th TRB Annual Meeting, Jan. 9-13*.

Smulders, S. (1992). "Control by variable speed signs - the dutch experiment." *IEE Conference Publication,* 99-103.

UK Highways Agency. (2004). "M25 Controlled Motorways: Summary Report." (1).

Ulfarsson, G. F., Shankar, V. N., and Vu, P. (2005). "The effect of variable message and speed limit signs on mean speeds and speed deviations." *International Journal of Vehicle Information and Communication Systems*, 1(1/2), 69-87.

Willumsen, L. G. (1984). "Estimating Time-Dependent Trip Matrices from Traffic Counts." *9th International Symposium on Transportation and Traffic Theory, VNU Science Press*, 397-411.

WSDOT.(2011). "**http://www.wsdot.wa.gov/projects/lkwamgt/lkwaatm/** Accessed December 04, 2011."

Zackor, H. (1979). "Self-sufficient control of speed on freeways." *In Proceedings of the International Symposium on Traffic Control Systems, Berkeley, California: California University, Aug.6–9*, 2A 226–249.

Table 4-1 MPC-based VSL performance with DynaTAM-VSL during congestion period.

MOE	Without VSL control	With VSL control	(%) Improvement
TTT (veh-h)	701	429	38.8
throughput (vphpl)	14019[a]	14776[a]	5.4
Objective Function Value	36,230	12,879	—

[a] *Summation of the flows (in unit of vphpl) over the discretized links; and the flow at each link is taken as the average over the congestion period*.

Table 4-2 Mobility performances under various scenarios.

Scenario*	TTT improvement (%)	Throughput improvement (%)
No VSL	—	—
1min-5kph	31.93	3.13
2min-5kph	32.01	3.18
3min-5kph	32.31	3.10
5min-5kph	31.94	3.18
1min-10kph	31.59	2.00
2min-10kph	32.53	2.06
3min-10kph	33.16	2.05
5min-10kph	33.34	2.01
1min-15kph	31.47	3.15
2min-15kph	31.59	3.17
3min-15kph	31.71	3.16
5min-15kph	31.53	3.07
1min-20kph	30.93	3.17
2min-20kph	28.64	3.16
3min-20kph	28.92	3.20
5min-20kph	30.91	3.27

* *1min-5kph means the VSL update frequency is 1 min and the maximum difference between two successive time steps is 5kph*.

Table 4-3 Safety performances under various scenarios.

Scenario*	Average CP	CP improvement (%)
No VSL	0.5230	—
5min-15kph	*0.2607*	*50.1*
5min-10kph	*0.2619*	*49.9*
5min-5kph	*0.2688*	*48.6*
3min-10kph	*0.2752*	*47.4*
5min-20kph	*0.2797*	*46.5*
2min-15kph	0.3036	41.9
3min-15kph	0.3088	41.0
2min-10kph	0.3092	40.9
2min-5kph	0.3113	40.5
1min-5kph	0.3245	37.9
3min-5kph	0.3260	37.7
1min-15kph	0.3306	36.8
3min-20kph	0.3379	35.4
1min-10kph	0.3517	32.8
1min-20kph	0.3590	31.4
2min-20kph	0.3598	31.2

* *1min-5kph means the VSL update frequency is 1 min and the maximum difference between two successive time steps is 5kph*.

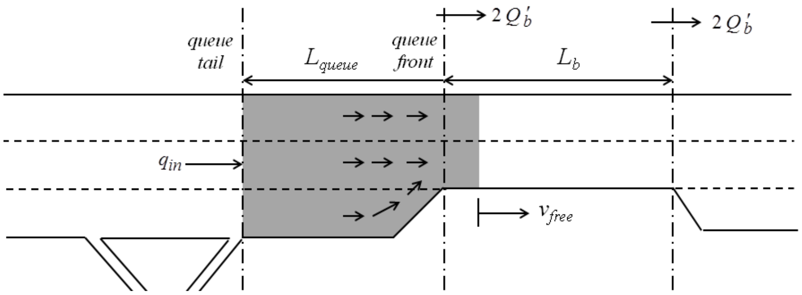

Figure 4.1 Recurrent bottleneck formation mechanism. Due to intense merging at upstream of lane drop bottleneck, shockwave forms. The discharge capacity from queue formed could be 0-20% lower than free-flow condition.

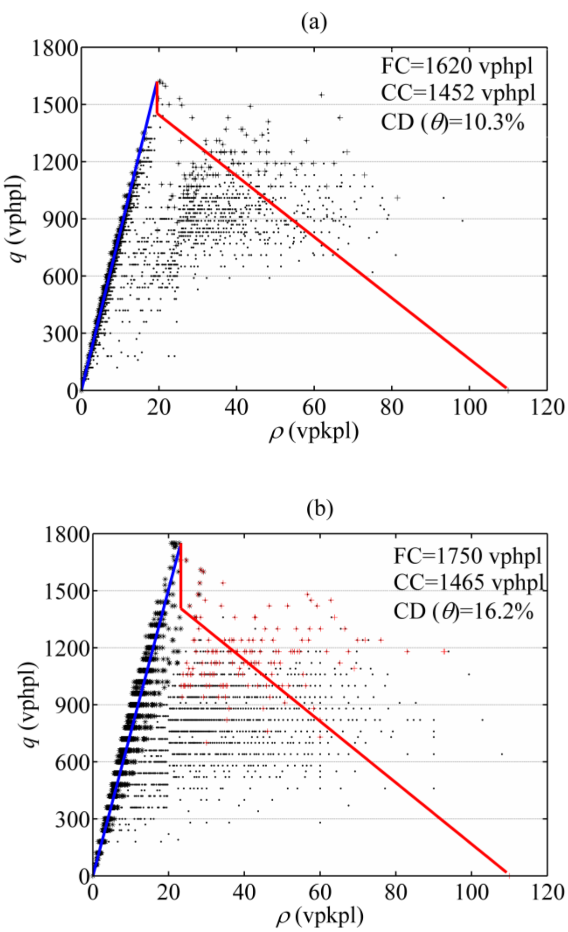

Figure 4.2 FDs of the links immediate upstream of: (a) weaving section; and (b) lane drop. '*' and '+' show the data used to establish left- and right-side of FDs, respectively.

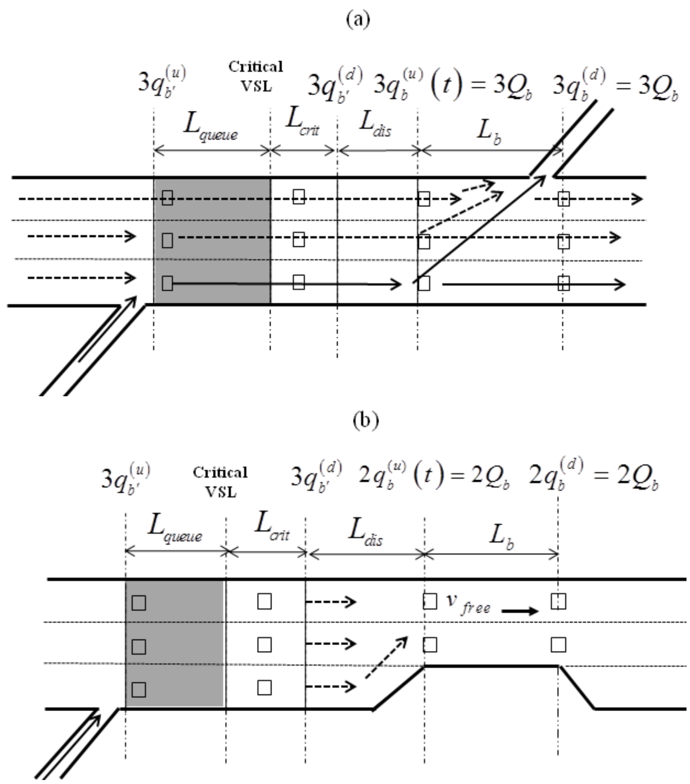

Figure 4.3 Maintaining flow close to nominal capacity at: (a) weaving section; and (b) lane drop.

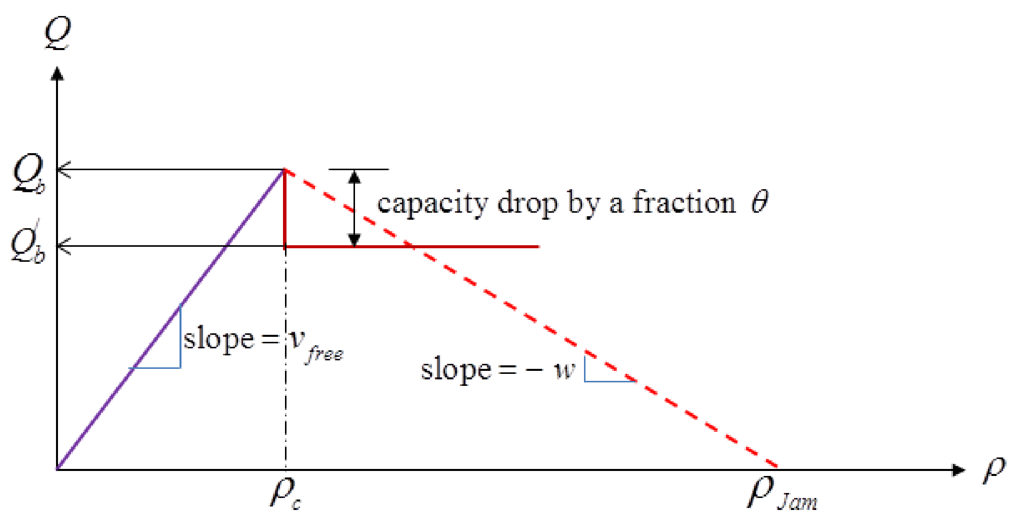

Figure 4.4 Proposed FD to model active bottleneck.

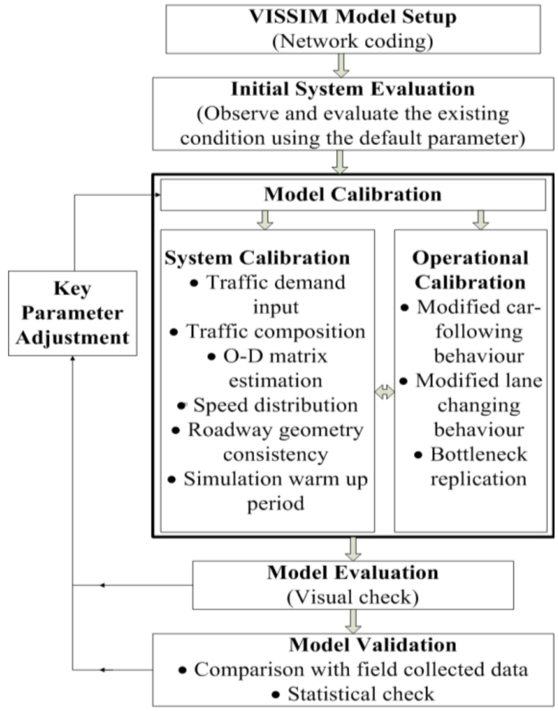

Figure 4.5 Microscopic WMD base model calibration and validation flow chart.

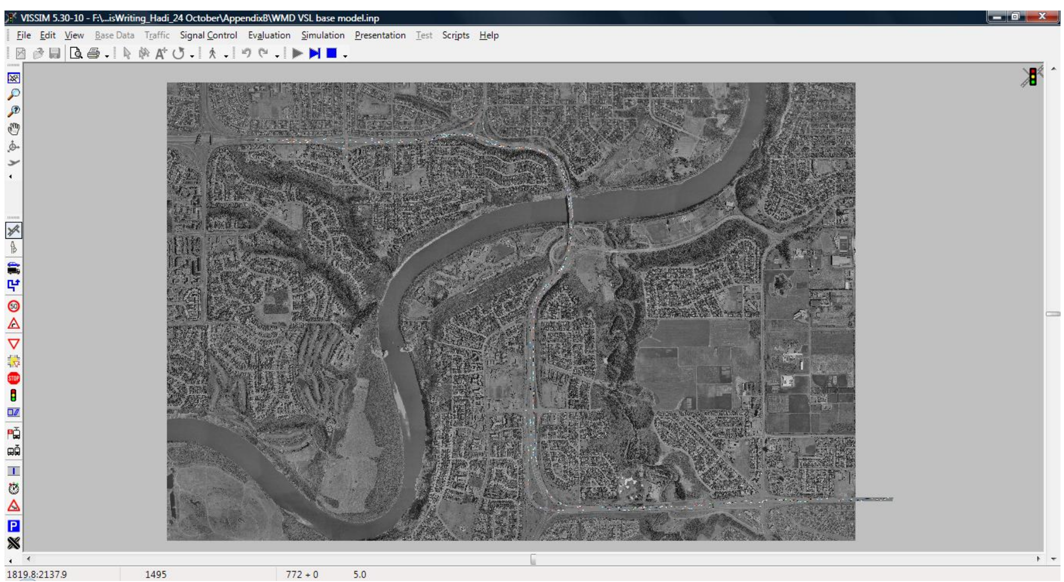

Figure 4.6 Calibrated WMD base model with background map. Vehicles presence in the network can be realized.

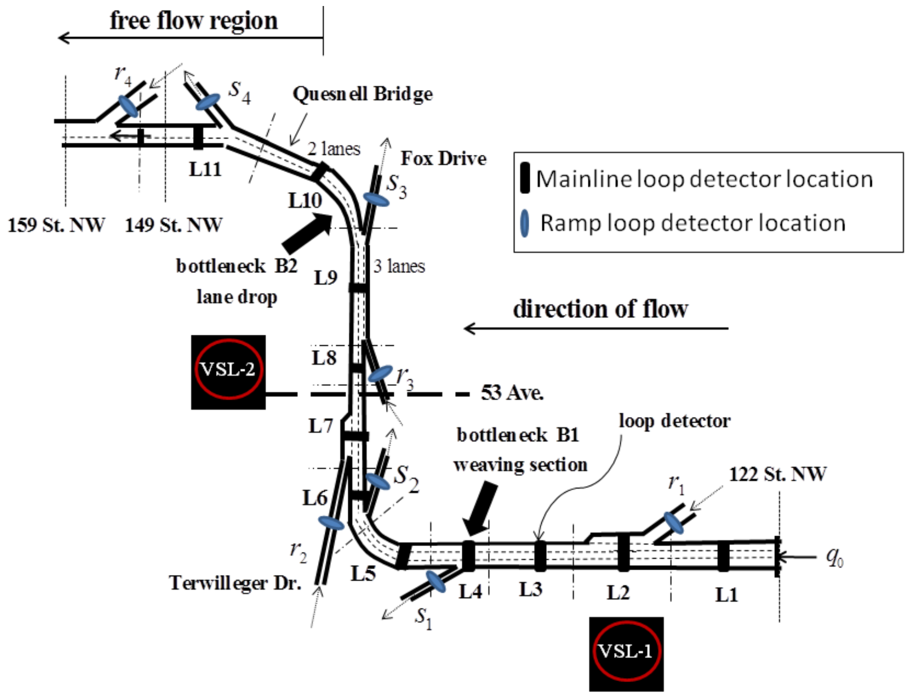

Figure 4.7 The test site is discretized into 11 links following the proposed VSL control strategy. Links are around 800 m. in length except L2 and L8. Static speed limit for L5-L11 is 50 kph and for the other links is 80 kph.

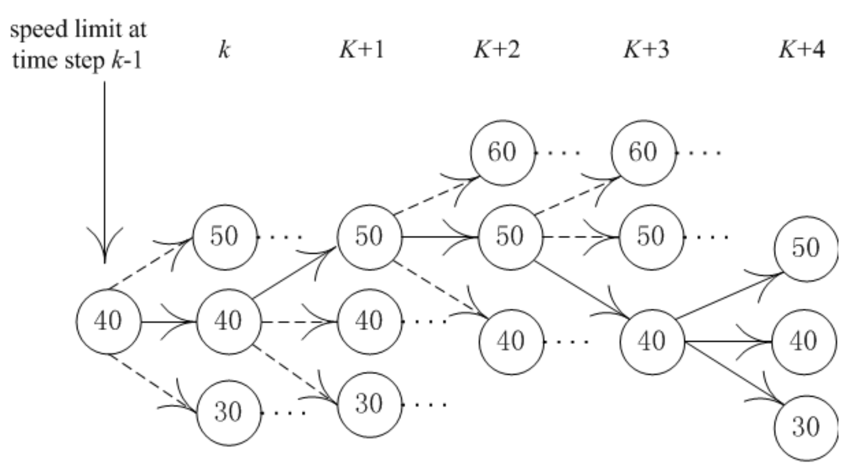

Figure 4.8. Sequence of speed limit values for different decision tree branches due to implementing temporal constraints on VSL values. Solid arrows show a complete branch.

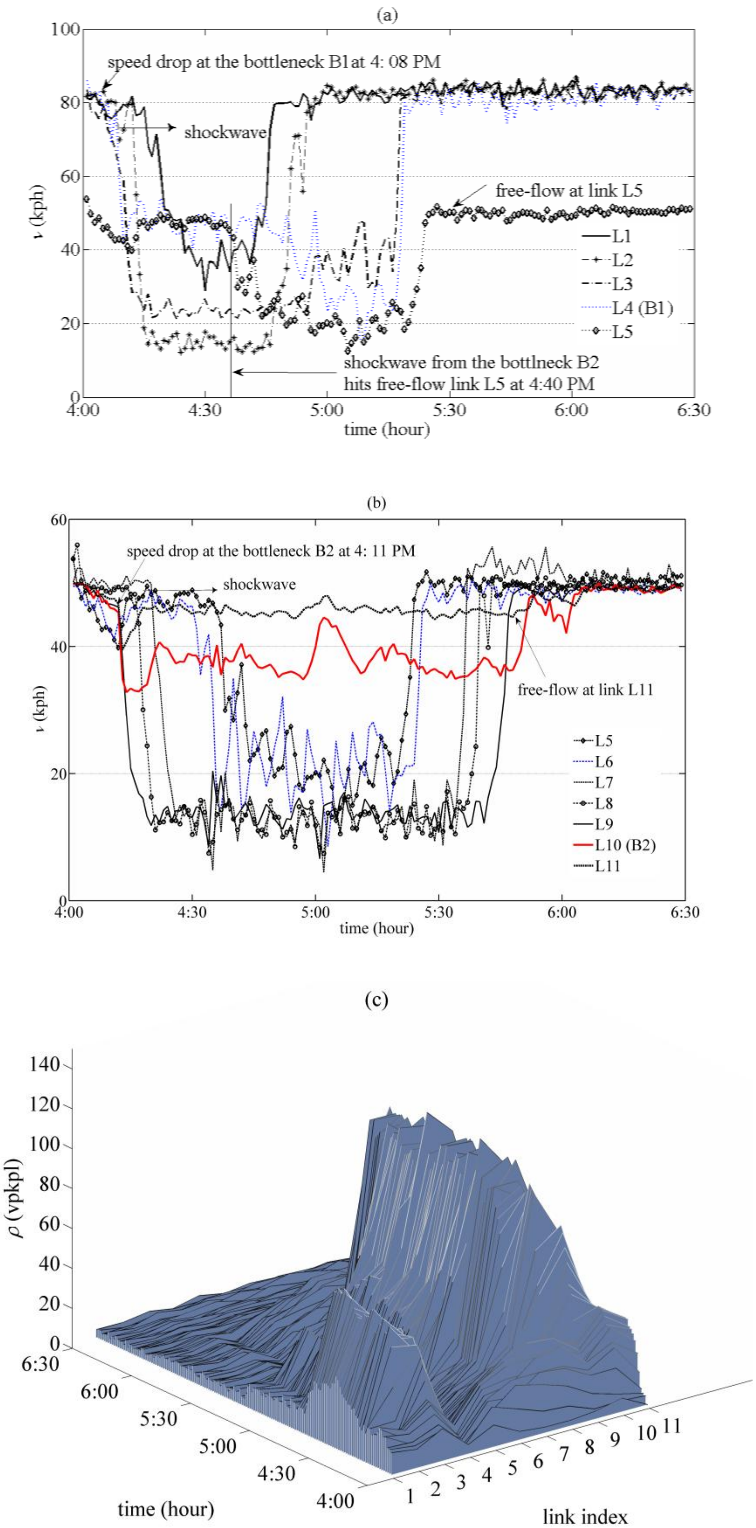

Figure 4.9 No-VSL scenario: (a) speed drop at the bottleneck B1; (b) speed drop at the bottleneck B2; and (c) density profile for the discretized links.

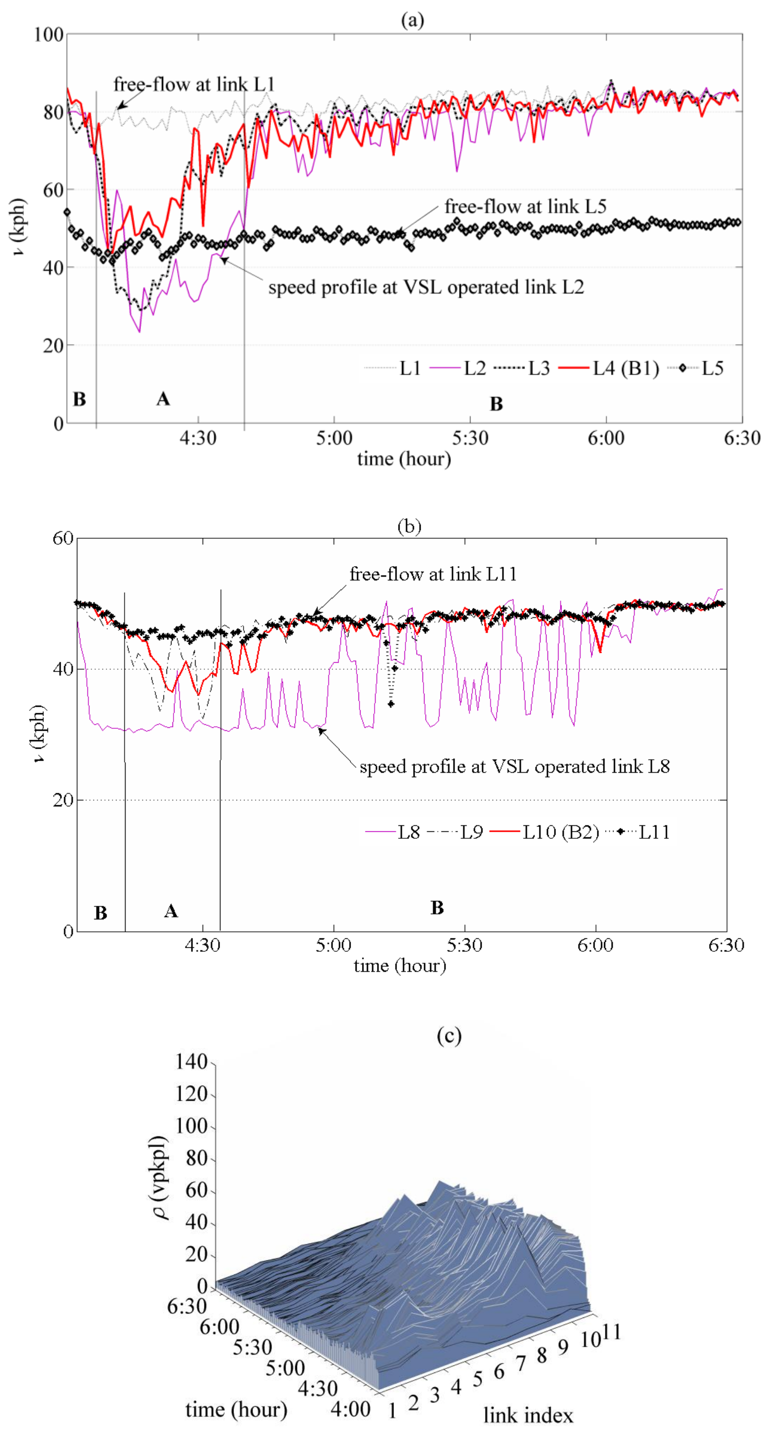

Figure 4.10 VSL-control scenario: (a) speed profile at the links close to the bottleneck B1; (b) speed profile at the links close to the bottleneck B2; (c) density profile.

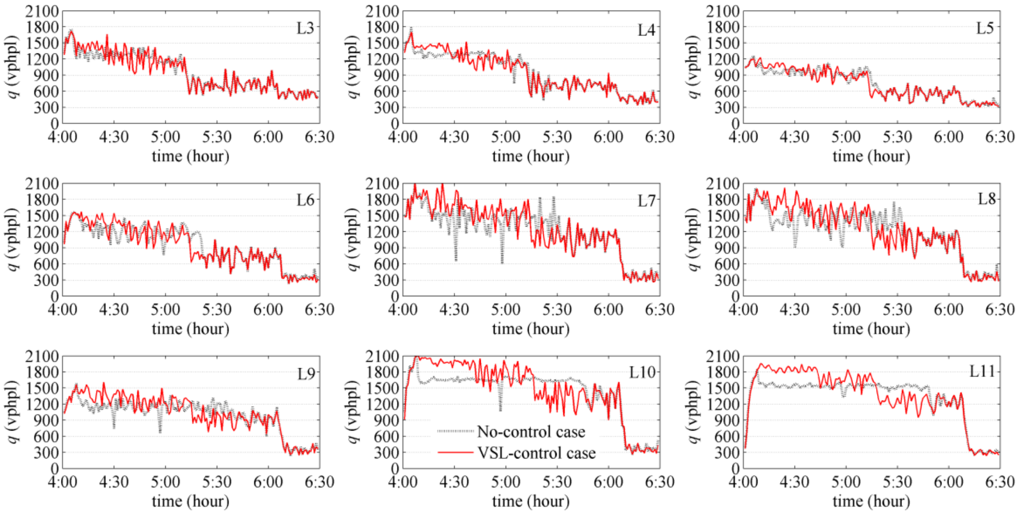

Figure 4.11 Flow profile before-after VSL control.

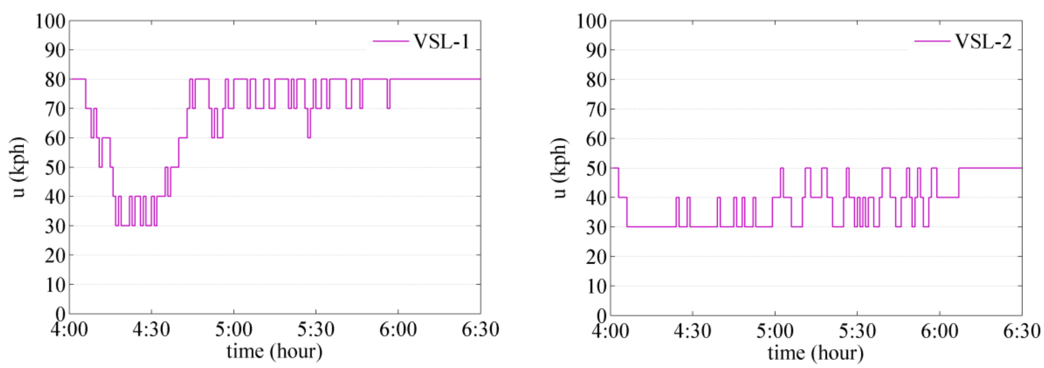

Figure 4.12 VSL trajectory over the 2.5-hr simulation.

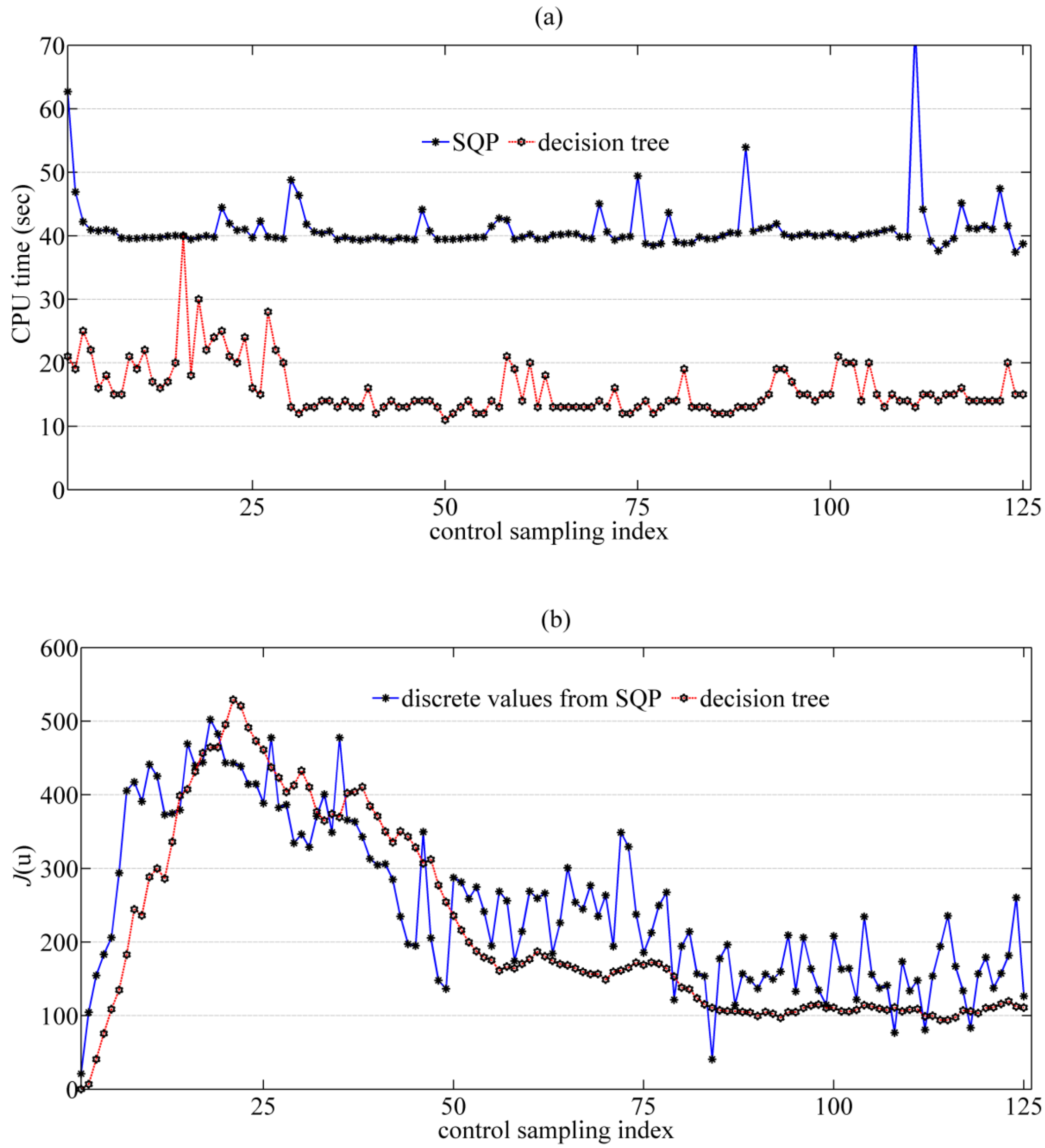

Figure 4.13 VSL performance at each control sampling time with discretized values from SQP and decision tree: (a) CPU time; (b) combined objective functions $J(\mathrm{u})$ values.

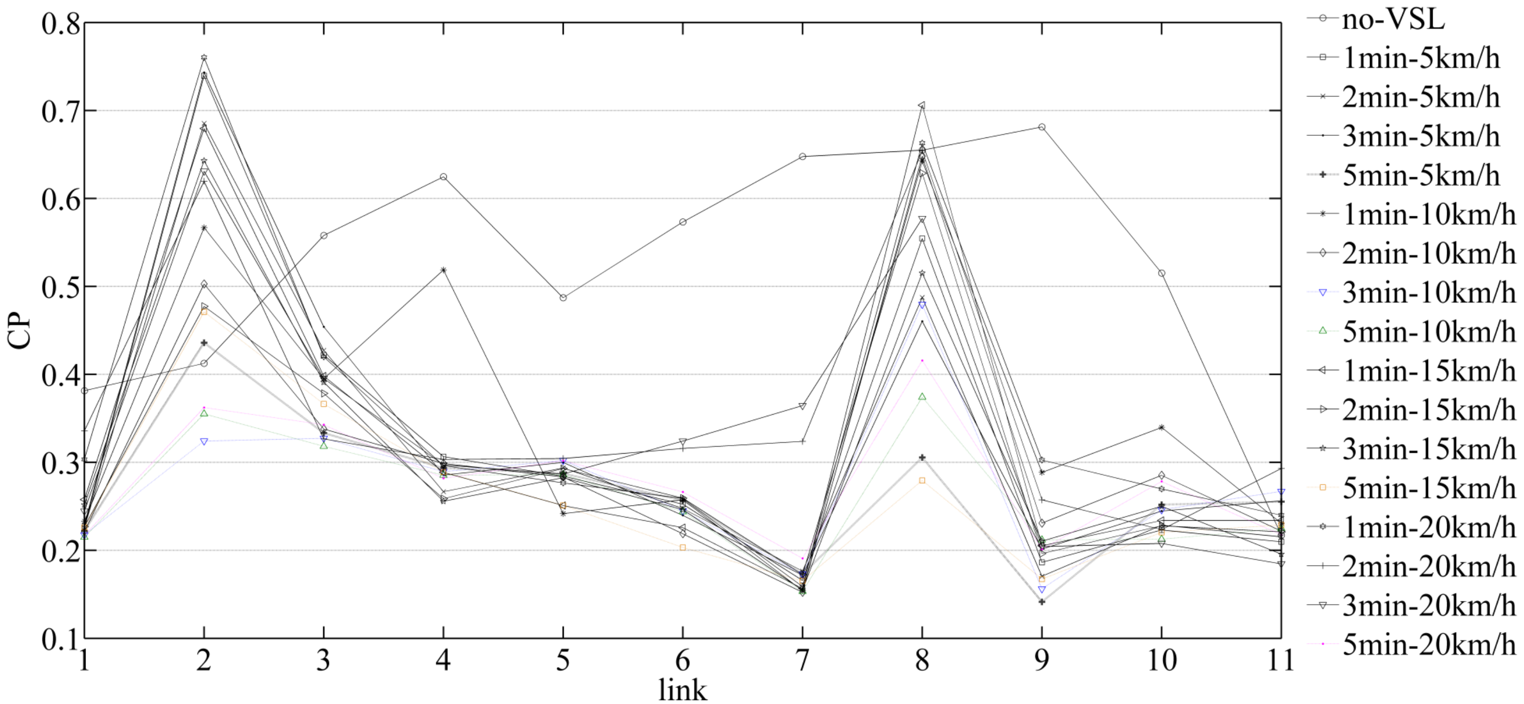

Figure 4.14 Average collision probabilities (CP) under different control scenarios.

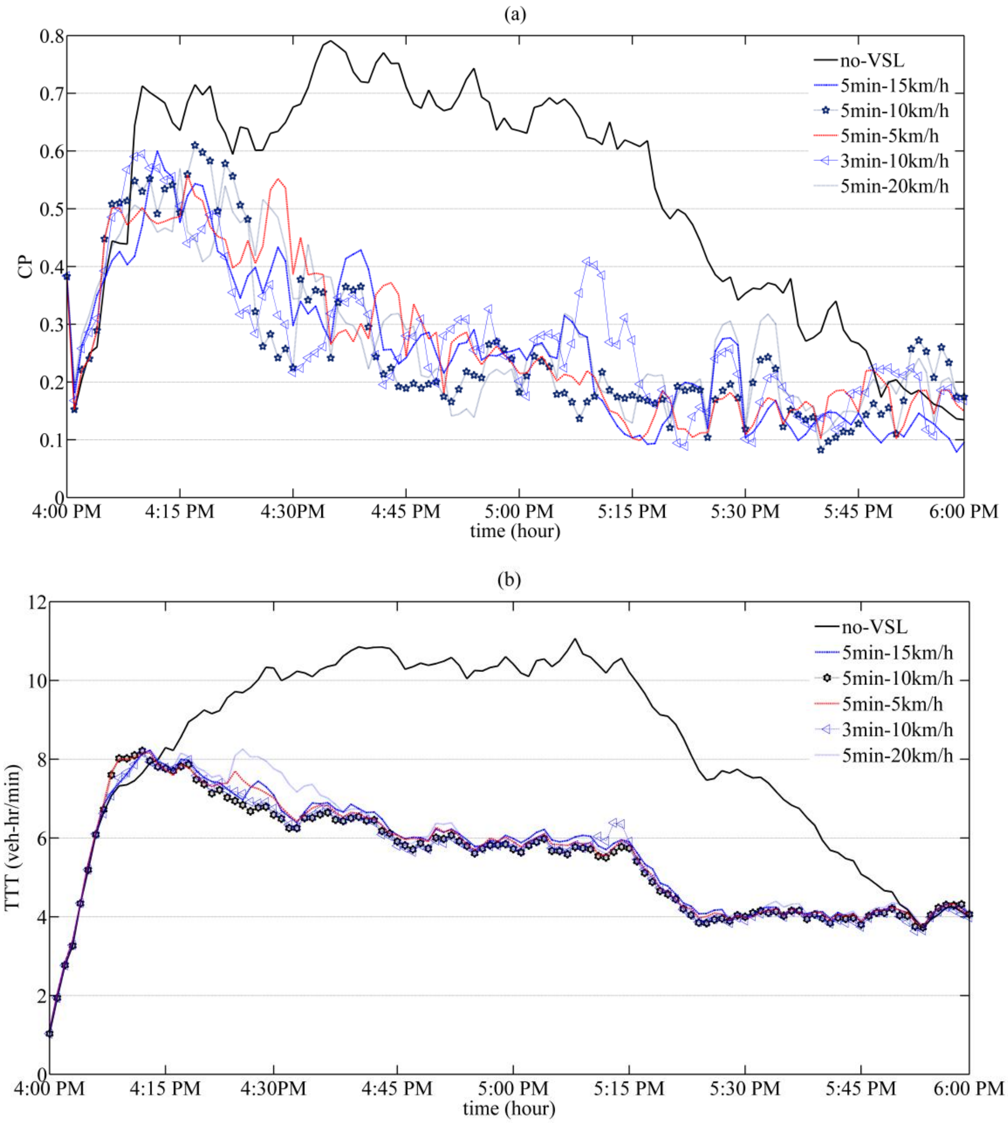

Figure 4.15 Performances over the simulation period: a) average link collision probabilities; b) average link travel time.

Chapter 5

Designing isolated VSL control with CTM-VSL for improving congestion and mitigating shockwaves*

5.1 Introduction

Over the past decade, several studies (Hegyi et al. 2005; Carlson et al. 2010; Chen et al. 2013) derived macroscopic traffic flow models with the VSL control variable considering the second-order METANET (Papageorgiou et al. 1990) as the base dynamic model. Although the models with predictive VSL control have proven beneficial in terms of travel time, they are more expensive to execute online (in terms of computational demand) and require more advanced calibration methods. Until now, the METANET-based traffic flow model parameters for the network were determined from validation of the simulated network traffic flow model against real field data/micro-simulation data without VSL control. However, with VSL control, the influence of those parameters could be different. As a consequence, those models would have low predictive power. Furthermore, with the change of road and weather conditions, those parameters msut be re-calibrated online to improve traffic state prediction, which requires great effort and may restrict field deployment.

---

* *A version of this chapter has been published.* **Hadiuzzaman, M.** and Qiu, T. Z. (2013). "Cell Transmission Model Based Variable Speed Limit Control for Freeway." *Canadian Journal of Civil Engineering*, 40(1), 46-56.

Another class of macroscopic model that has received remarkable attention in traffic flow modeling and analysis is the first-order Cell Transmission Model (CTM) (Daganzo 1994), which is essentially a density dynamics model. In addition to having the strength inherited from LWR, the CTM has four distinctive features:

(1) The model is trusted because it is founded on sound traffic flow theory;

(2) It is parsimonious, only including parameters that can be estimated in both an online and offline basis;

(3) Model parameters can be calibrated using routinely available point detector data; and

(4) To predict the traffic variables in real-time requires very low computational requirements (Gomes et al. 2008).

CTM is used for both freeway and arterial traffic control purposes: arterial traffic signal control (Lo 2001; Almasri and and Friedrich 2005); and freeways with ramp metering control (Gomes et al. 2008; Zhang and Levinson 2010; Gomes and Horowitz 2006). However, in this research, to understand the effectiveness of the VSL control, an analytical model based on the CTM is developed. Specifically, this research proposes several modifications in CTM to model traffic flow in the VSL control situation and can be adopted within the model predictive control (MPC) framework to improve recurrent bottleneck flows. Implementation of the proposed CTM-VSL model requires only the calibration of the fundamental diagram (FD), which is possible for both offline and online estimations (Dervisoglu et al. 2009). Although the original CTM uses cell occupancy[6] as

[6] In the CTM, occupancy is defined as the number of vehicles present in any cell at any time step.

the state variable, the CTM-VSL uses cell density as the state variable. The benefit of using cell density is two-fold (Munoz 2004):

(1) Using cell densities instead of cell occupancies permits the CTM to include uneven cell lengths, which leads to greater flexibility in partitioning the freeway;

(2) Non-uniform cell lengths enable the use of a smaller number of cells to describe a freeway section, thus reducing the size of the state vector $[\rho_1, \rho_1, ..., \rho_M]^T$ that needs to be optimized, where ρ_i is the density of the i^{th} cell.

To implement the CTM-VSL, the freeway is partitioned into small segments (cells[7] of length L_i), as shown in Figure 5.1, and into discrete time steps (of duration T). In each cell i at time index k the density is approximated by a constant value $\rho_i(k)$ and its exit flow $q_i(k)$ can be expressed as the minimum between the upstream demand and the downstream supply by applying the Godunov scheme (Godunov 1959).

From a practical standpoint, this research also discusses the principle of choosing VSL sign location and proposes a discrete formulation of a queue estimation model to update the mainline storage capacity in real-time. Most of the previous research has assumed that, with VSL control, shockwave speed is expected to be diminished or even avoided. Therefore, the speed of the congestion tail propagation is expected to be smaller than the

[7] This thesis manuscript uses the term cell and link for explaining the parameters related to CTM-VSL and DynaTAM-VSL, respectively. Basically, cell/link represents small segment of freeway. Without any loss of generosity, these two terms can be used interchangeably.

shockwave speed without control. In reality, though, this depends on many factors, such as the upstream mainline flow, input flow from on-ramp and mainline storage capacity. So, it is possible that the tail of any formed congestion at VSL sign propagates upstream and covers nearby on-ramps and off-ramps leading to an additional reduction of the freeway throughput. Thus, in addition to reducing input flow at bottlenecks with the isolated VSL control strategy (as presented in Chapter 4), the VSL control strategy in this research also incorporates real-time updates of the freeway storage capacity by utilizing the developed queue estimation model. From a mobility standpoint, a separate VSL sign for the storage segment is designed to avoid blockage of upstream ramps.

5.2 Background concept

5.2.1 *The Godunov's demand- supply approach*

As indicated in Godlewski and Raviart (1996), the best numerical method to solve the partial differential equations along roads is a Godunov scheme (Godunov 1959), as it is first-order, correctly predicts shock propagations and has a physical interpretation. Specifically, the scheme applies a time-space dicretization for solving partial differential equations in macroscopic models by converting them into approximate finite difference equations. In Godunov scheme, boundary flow between cells is computed based on the local demand-supply concept. The local demand function computes the maximum possible flow the upstream can send to downstream. Similarly, the local supply function computes the maximum possible flow the downstream can consume. The boundary flow is then computed by taking the minimum between the local demand and the local supply.

5.2.2 *The CTM model*

The CTM is a time-space discrete Godunov approximation to the LWR model (Lighthill and Whitham 1955.; Richards 1956). To simulate traffic flow by the CTM, a freeway is divided into i = (1, 2,………, M) homogeneous and interconnected cells of length L . Assume vehicles are moving from left to right, and cell i is upstream of cell $i+1$. There are two boundary conditions. Free flow prevails downstream of cell M; upstream of the freeway is a source with infinite capacity. Under light traffic condition, in between two time steps all the vehicles in a cell are assumed to advance to the next cell as follows.

$$n_{i+1}(k+1) = n_i(k) \tag{5.1}$$

Where, n_i is the number of vehicles in cell i . If the flow exceeds the downstream capacity, Equation (5.1) becomes irrational. Consequently, a more robust vehicle advancement equation (5.2) was proposed by Daganzo. During high demand period, vehicle advancement equation can be written as follows: the cell occupancy at time index $k+1$ equals its occupancy at time index k, plus the inflow and minus the outflow number of vehicles.

$$n_i(k+1) = n_i(k) + y_{i-1}(k) + r_i(k) - y_i(k) - s_i(k) \tag{5.2}$$

Where, y_i (veh/period) is the outflow from cell i to i +1. Equation (5.2) is so called vehicle conservation law. In the above equation the flows are related to current condition at time index k as indicated below:

$$y_i(k) = min\ \{v_{free,i} n_i(k), F_{i+1}, w_{i+1}[\bar{n}_{i+1}(k) - n_{i+1}(k)]\} \tag{5.3}$$

Where, F (veh/period) is the cell capacity, v_{free} (cell/period) is the free-flow speed and w (cell/period) is the congestion speed. In the above equations, the length of all cells is normalized to 1 by absorbing differences in length in the speeds v_{free} , w_i . To satisfy the *step size modeling constraint*: $v_{free} \in [0,1]$ and $w_i \in [0,1]$. The parameters in Equation

(5.3) correspond to the triangular FD of Figure 5.2. With, $n^{C}{}_{i}$ and $\overline{n_i}$ are critical occupancy and jam occupancy, respectively.

Off-ramp flows are modeled as a portion $\phi_i(k)$ of the total flow leaving the cell.

$$s_i(k) = \frac{\phi_i(k)}{1-\phi_i(k)} y_i(k) \tag{5.4}$$

5.3 Methodology

5.3.1 *Control strategy*

This research adopts a similar control strategy as in Chapter 4 that aims at maximizing the bottleneck flow. It explicitly considers the FDs at active bottleneck, and its upstream-downstream cells (Figure 5.3). The control strategy can be illustrated as follows. During high demand period $(q_{in} > Q_b)$ as density increases on the freeway segments, small disturbances caused by merging and weaving maneuver before the bottleneck readily causes speed drop $(v_{free} \rightarrow v_c)$. It results in flow breakdown, and reduces discharge flow from the segment immediately upstream of the bottleneck. Queue (highlighted area) will build up from the active bottleneck geometric starting point. Due to the flow conservation, the discharge flow from the bottleneck will be limited to Q'_b. Here, Q_b and Q'_b define the bottleneck capacity and the dropped capacity, respectively. In Figure 5.3, blue and red dots show traffic state at different cells during low and high demand periods, respectively. F and C stands for free-flow and congestion regions, respectively.

The following control strategy is used for the following situation based on the given traffic characteristics and can be adopted to avoid capacity drop at any type of recurrent bottlenecks (lane drops, weaving, merging, etc). If the demand is too high from both upstream and on-ramp, and congestion is unavoidable without control, it is necessary to create a discharge section (L_{dis}) with adequate length (500~700 m) immediately upstream of the bottleneck. To this end, a critical VSL must be defined as shown in Figure 5.4. The objective is to limit feeding flow to the bottleneck. In order to maximize bottleneck flow, the discharge flow of three lanes is maintained at a level close to the bottleneck capacity flow: $q = 3q_{b'}^{(d)} = 2q_b^{(u)} \approx 2Q_b$. Here, $q_{b'}^{(d)}$ and $q_b^{(u)}$ are the transition flows at the boundaries $(L_{crit} \to L_{dis})$ and $(L_{dis} \to L_b)$, respectively. As can be seen, controlling of upstream traffic can improve bottleneck flow. The critical VSL manipulates the speed limit to control the flow into the discharge section, and to make sure that the bottleneck reaches capacity flow. The critical VSL cell (L_{crit}) is a very short section, usually, 200-250 m in length, which is designed based on common driver acceleration/deceleration characteristics. Further details can be found in Chapter 4.

However, if q_{in} is significantly higher than Q_b, due to flow reduction at critical VSL, after certain time period shockwave may be created. Queue will grow up from the critical VSL location. The critical VSL creates two different traffic flow regions (upstream of this section has low density). It might cause the tail of the congestion to move upstream and cover nearby ramps. So, for an effective VSL control strategy, it is necessary to ensure adequate storage capacity of the controlled congestion cell (highlighted area in Figure 5.4). It is possible by adding further upstream cell to current storage cell (L_{st}) and designing a separate VSL for the updated storage cell in the real-time control.

5.3.2 *The CTM-VSL model*

To implement the CTM-VSL, it is required to partition the freeway into variable segments (cells of length L_i) as in Figure 5.1 and time into discrete time steps (of duration T). The length of the each cell must be longer than or equal to the free-flow travel distance, i.e., $v_{free}T \le L_i$ (*step size modeling constraint*). This constraint is necessary for the convergence of CTM solutions to LWR solutions as mentioned in Daganzo (1995), so that vehicles travelling at the maximum speed may not cross multiple cells in one time step. In the figure, vehicles move from left to right. In each cell i at time step k , the density is approximated by a constant value $\rho_i(k)$ and its exit flow $q_i(k)$ can be expressed as the minimum between the upstream demand $\sigma(\rho)$ and the downstream supply $\delta(\rho)$ by applying the Godunov scheme (Godunov 1959).

In order to design bottleneck flow control following the proposed VSL control strategy, two modifications in the FD are proposed. The first permits one to model recurrent bottleneck in which there is a capacity drop once the bottleneck is activated. The second modification permits variable free-flow speeds. The CTM-VSL parameters are depicted in Figure 5.5. The triangular-shaped FD is convenient because the slopes of its two sides and its apex are explicit parameters in the CTM-VSL. They can be valid for all cells or allowed to vary for each cell. Figure 5.5 (b) shows FD of the cell considering they are operated with VSL control; and Figure 5.5(c) shows FD of the bottleneck having capacity drop. The underlying assumption for the demand function (dark line) in Figure 5.5(c) is that flow at the bottleneck will not reach to jam density. Surely, this assumption is valid as in the real-world vehicles always accelerate from bottleneck geometric starting point toward downstream. The high vehicle concentration is to be observed in the immediate upstream of active bottleneck (see, Figure 5.3).

5.3.2.1 Density dynamics

Let assume each cell i is characterized by its triangular shape FD, of which the left limb represents demand function $\sigma_i(k)$ and the right limb represents supply function $\delta_i(k)$, both are functions of their density values. The interpretation of demand and supply function can be illustrated as follows. If cell density is $\rho_i(k)$, cell i demands space from its downstream cell $(i+1)$ for a flow of $\sigma_i(k) = \sigma_i(\rho_i(k))$ vphpl; and it supplies space to upstream cell $(i-1)$ for a flow of $\delta_i(k) = \delta_i(\rho_i(k))$ vphpl.

The supply and demand functions for those cells operated with VSL control can be written as follows:

$$\sigma_{i,VSL}(k) = \min\left\{v_{free,i}, u_i\right\}\rho_i(k) \tag{5.5}$$

$$\begin{aligned} \delta_{i,VSL}(k) &= Q_{max} & & if\ \rho_i(k) \le \rho_c \\ \delta_{i,VSL}(k) &= w_i\left(\rho_{jam,i} - \rho_i(k)\right) & & if\ \rho_i(k) > \rho_c \end{aligned} \tag{5.6}$$

The interpretation of Equation (5.5) is that when the control variable u is less than free-flow speed $\left(u < v_{free}\right)$, the critical cell demands for a flow of $u\rho(k)$ vphpl; otherwise demand would be limited to $v_{free}\rho(k)$ vphpl. This is the role of VSL in the CTM-VSL and it could avoid flow breakdown reducing the input flow to the bottleneck.

In case of high density at the immediate upstream of the bottleneck, discharge flow from L_{dis} will be reduced, and thereby this research proposes the following model that needs to be implemented during VSL control. For this case, the demand function for the bottleneck is different but its supply function is same as the VSL operated cells. The underlying assumption for the demand function (solid line) in Figure 5.5(c) is that flow within the bottleneck (L_b) will not reach to jam density. The jam density is to be observed in the immediate upstream of bottleneck.

$$\sigma_{i,bottleneck}(k) = \begin{cases} v_{free,i}\rho_i(k) & \text{if } \rho_i(k) \le \rho_c \\ Q'_b & \text{if } \rho_i(k) > \rho_c \end{cases} \tag{5.7}$$

$$\begin{aligned} \delta_{i,bottleneck}(k) &= Q_b && \text{if } \rho_i(k) \le \rho_c \\ \delta_{i,bottleneck}(k) &= w_i\left(\rho_{jam,i} - \rho_i(k)\right) && \text{if } \rho_i(k) > \rho_c \end{aligned} \tag{5.8}$$

If the density $\rho_i(k)$ in bottleneck is below its critical density, vehicles can leave this cell at a rate of $v_{free}\rho(k)$ vphpl and speed of v_{free} kph. So, the maximum flow is limited to $v_{free}\rho_c(k)$. However, once the density exceeds its critical value $\left(\rho(k)>\rho_c\right)$, the flow is reduced by θ fraction to $Q'_b = (1-\theta)Q_b$. The demand function $\sigma(\rho)$ models the phenomenon that when bottleneck becomes congested $(\rho > \rho_c)$, the vehicle discharge rate drops to Q'_b. So, the cell's demand is limited to Q'_b. Supply of bottleneck is determined using Equation (5.8). Once the demand and supply functions are determined, the outflow from each cell could be determined as follows:

$$q_i(k) = \min\{\sigma_i(k), \delta_{i+1}(k)\} \tag{5.9}$$

In Equation (5.9), capacity constraint does not appear. It has been considered explicitly by introducing piecewise linear FD. It can be viewed from Equations (5.5)-(5.8). Now density evolution in the cells could be predicted using Equation (5.10), knowing current density and outflow values from Equation (5.9). The proposed VSL control model can be implemented for any number of cells in the same manner as explained above.

$$\rho_i(k+1)=\rho_i(k)+\frac{T}{L_i\lambda_i}\left(q_{i-1}(k)\lambda_{i-1}-q_i(k)\lambda_i+r_i(k)-s_i(k)\right) \tag{5.10}$$

5.3.2.2 Speed estimation

This section introduces a formula for estimating mean speed at different cells that is derived from piecewise linear triangular-shaped FD. It is applicable for the cells other than those operated with VSL control. Equation (5.11) shows the relationship between average flow and density. Considering the steady-state traffic, Equation (5.12) can be derived. Now, knowing the predicted density in different cells from Equation (5.10), mean speed for the corresponding cells can be predicted using Equation (5.12). It is worthy to mention here that all the parameters in Equation (5.12) can be estimated both online and offline which make it suitable in real-world implementation.

$$Q_i\left(\rho_i(k+1)\right)=\begin{cases} v_{free}\rho_i(k+1) & \text{if } \rho_i(k+1)\le\rho_c \\ Q_{\max}\left(1-\dfrac{\rho_i(k+1)-\rho_{c,i}}{\rho_{Jam}-\rho_{c,i}}\right) & \text{if } \rho_{c,i}\le\rho_i(k+1)\le\rho_{Jam} \end{cases} \tag{5.11}$$

$$v_i(\rho_i(k+1))=\begin{cases} v_{free} & \text{if } \rho_i(k+1)\le\rho_c \\ \dfrac{v_{free}\left(\dfrac{\rho_{Jam}}{\rho_i(k+1)}-1\right)}{\left(\dfrac{\rho_{Jam}}{\rho_{c,i}}-1\right)} & \text{if } \rho_{c,i}\le\rho_i(k+1)\le\rho_{Jam} \end{cases} \tag{5.12}$$

For those cells operated with VSL control, mean speed can be predicted as follows:

$$v_i(k+1)=u_i(k) \tag{5.13}$$

As can be seen in Equation (5.13), the model is valid only for the condition of perfect obedience by drivers to VSL control, since it shares same property of the CTM model.

5.3.3 *Objective function*

As in Chapter 4, this chapter also uses the weighted summation of TTT and TTD (Equation 5.14) as an objective function within MPC. Furthermore, the impact of variable weighing coefficient to α_{TTT} (Equation 5.15) that could capture different operating traffic flow regions during online VSL simulation has been analyzed. As MPC has a modular structure, it is possible to update the parameter even in each control sampling time.

$$J_1 = T \sum_{j=1}^{N_p} \sum_{i=1}^{M} \lambda_i L_i \left[\alpha_{TTT,STATIC} \rho_i(k+j) - \alpha_{TTD} q_i(k+j) \right] \tag{5.14}$$

$$J_2 = T \sum_{j=1}^{N_p} \sum_{i=1}^{M} \lambda_i L_i \left[\alpha_{TTT,VARIABLE} \rho_i(k+j) - \alpha_{TTD} q_i(k+j) \right] \tag{5.15}$$

The first term of the objective functions is TTT and the second term is TTD. The parameters $(\alpha_{TTT}$ and $\alpha_{TTD})$ were selected in the simulation stage.

5.3.4 *Constraints*

Based on consideration of safety, driver acceptance and traffic flow characteristics, the following constraints on the VSL control variable are imposed:

C1: To guarantee the drivers' safety, the optimal speed limit of VSL operated cell must be kept lower than the maximum value V_{max}, i.e. $u_i(k) \leq V_{max}$

C2: To maintain the operating efficiency on freeway, the optimal speed of VSL operated cell is to be higher than the minimum speed V_{min}, i.e. $u_i(k) \geq V_{min}$

C3: For the safe operation of VSL control, the change of speed between two consecutive time steps should satisfy the following constraints $\left|u_i(k) - u_i(k+1)\right| \le V_{max,diff}$

In practice, variable speed limit signs display speed limits in increment/decrement of, e.g., 10 or 20 kph. This research uses $V_{max,diff} = 10\ kph$. The updated VSL using the CTM-VSL considers only discrete values. This is expressed by a constraint set. For this research, the set is= (V_{min} =10; 20; 30; 40; 50; 60; 70; V_{max} =80).

5.4 Validation of the CTM-VSL

This section presents the accuracy of the derived CTM-VSL model to simulate traffic flow. During the model's accuracy assessment, no measurement data from the WMD base model were used except the setups for initial and boundary conditions as in Chapter 2. Moreover, to prepare 20-s traffic data from the WMD base model, the test site was disctretized into 13 segments as in Chapter 2. To satisfy the basic assumption of the CTM, in the microscopic simulation model, it was assumed that drivers strictly follow the VSL. Furthermore, to quantify the error between CTM-VSL simulated and measured traffic states, mean absolute error (MAE) and root mean relative square error (RMRSE) are respectively used for the individual cells and for the entire freeway section.

Table 5-1 presents the cell-wise error in simulation by the proposed model. It can be seen that for the general cells as well as bottleneck, the CTM-VSL can simulate traffic speed pretty well. However, the errors can be found higher than that with the DynaTAM-VSL as presented in Chapter 2. In addition, the calculated RMRSE values using Equation (2.23) for the speed, flow, and density for the entire test site were 0.0457, 0.0389, and 0.0479, respectively. Among these three values, error in speed simulation by the CTM-VSL is comparatively higher than the DynaTAM-VSL. However, accuracy in simulating other two parameters with the CTM-VSL and the DynaTAM-VSL are comparable. In particular, RMRSE values for speed, flow, and density simulation with the DynaTAM-VSL were 0.0313, 0.0407,0 .0458, respectively.

5.5 Real-time queue estimation models

5.5.1*Model formulation*

Estimating real-time queue lengths is a challenge for traffic operation and control. Although, the characteristics of queue formation and onset time are represented by the field traffic data observed before and after congestion, this data cannot be used to estimate queue length; rather, the input-output model and shockwave analyses are the two most common methods for estimating queue length. However, input-output models cannot provide the spatial distribution of queue lengths in time (Michalopoulos et al. 1981) because the models only provide the number of vehicles in the queue but little detailed information about how the queue forms and dissipates. So, this section develops discrete models to detect time dependant queue tail with and without VSL control based on shockwave analysis. This type of analysis was first conducted by R.M Oliver (Oliver 1964) in case of recurrent bottleneck without any control and capacity drop.

In Figure 5.4, it is assumed that for the no-VSL scenario, queue tail begins to propagate from the bottleneck geometric starting point at $x = x_2$. Bottleneck exit flow restricts to Q_b'. With VSL control, queue tail propagates from the critical VSL location. For both scenarios, it is required to have a loop detector in each travel lane at the upstream of the bottleneck at $x = x_1$ (see Figure 5.4) to measure time varying input demand from upstream. In the figure, traffic stream moves from left to right. The time dependant flow rate at the upstream loop detector location at $x = x_1$ is $q(x_1, t) = q(t)$. To detect time dependant queue tail location with VSL control, another loop detector is required at $x = x_2'$ at the critical VSL cell, since flow will change based on the different speed limits.

At the instant t_0 when the input flow $q(t_0)$ at $x = x_1$ first exceeds the capacity flow of the bottleneck [$q(t_0) > Q_b$], the queue will form at $x = x_2$ at t_0' [$t_0' = t_0 + \frac{(x_2 - x_1)}{v_{free}}$] (*Coordinate translation*), and will move backward over the time until the flow into the queue less than the bottleneck capacity. It is assumed that each vehicle occupies a space in the queue equal to the inverse of jam density (ρ_{jam}) and that outside the queue the traffic speed is free-flow speed, v_{free}. Also, vehicles can decelerate instantaneously upon joining the queue. The flow rate and density at a point x before the bottleneck is:

$$q(x,t) = \begin{cases} q(x_1, t - \frac{(x - x_1)}{v_{free}}) & \text{(left of shockwave boundary)} \\ Q_b' & \text{(right of shockwave boundary)} \end{cases} \tag{5.16}$$

$$\rho(x,t) = \begin{cases} \frac{q(x,t)}{v_{free}} & \text{(left of shockwave boundary)} \\ \rho_{jam} & \text{(right of shockwave boundary)} \end{cases} \tag{5.17}$$

Now from LWR model, the position of the shockwave separating the high- and low-density region satisfies the following first-order non-linear differential equation:

$$v_{shockwave} = \frac{dx}{dt} = \frac{q(x,t)_{\text{(left of shockwave boundary)}} - q(x,t)_{\text{(right of shockwave boundary)}}}{\rho(x,t)_{\text{(left of shockwave boundary)}} - \rho(x,t)_{\text{(right of shockwave boundary)}}} \tag{5.18}$$

From Equation (5.16), (5.17), and (5.18) the following equation is obtained:

$$\frac{dx}{dt} = (q(x_1, t - \frac{(x - x_1)}{v_{free}}) - Q_b') / (\frac{q(x_1, t - \frac{(x - x_1)}{v_{free}})}{v_{free}} - \rho_{jam}) \tag{5.19}$$

The numerator of Equation (5.19) is simply the difference in flow rates into and out of shockwave; the denominator is the difference between left-hand and right-hand densities at the shock front. Now expanding the right-side of Equation (5.19) using Taylor series about t and neglecting the terms of the order of $\frac{1}{(v_{free})^2}$, the following first order ordinary differential equation (ODE) can be obtained:

$$\frac{dx}{dt} + a(x_1,t)x(t) = b(x_1,t) \tag{5.20}$$

Where, $a(x_1,t) = \dfrac{\frac{dq}{dt}}{q(x_1,t) - v_{free}\rho_{jam}}$; and $b(x_1,t) = \dfrac{v_{free}\ (Q_b' - q(x_1,\ t))}{v_{free}\rho_{jam} - q(x_1,\ t)}$

By selecting appropriate integrating factor and imposing condition that shockwave can be located at $x = x_2$ at the time t_0' (thus, equation 5.20 turns into initial value problem [IVP]) when the traffic flow at the bottleneck first exceeds Q_b is:

$$x(t) = \frac{N_b'(t - t_0') - [N(x_1,t) - N(x_1,t_0')]}{\rho_{jam} - \rho(x_1,t)} + \frac{\rho_{jam} - \rho(x_1,t_0')}{\rho_{jam} - \rho(x_1,t)}(x_2 - x_1) \tag{5.21}$$

With, $\rho(x_1,t) = \dfrac{q(x_1,t)}{v_{free}}$ and $N(x_1,t) = \int_0^t q(x_1,t)dt$ is the cumulative vehicle number.

In the discrete form, the above Equation (5.21) can be written as follows:

$$x(k=K) = \frac{\sum_{k=n}^{K} Q_b'T - (\sum_{k=1}^{K} q_{x_1}(k)T - \sum_{k=1}^{n} q_{x_1}(k)T)}{\rho_{jam} - \rho_{x_1}(K)} + \frac{\rho_{jam} - \rho_{x_1}(n)}{\rho_{jam} - \rho_{x_1}(K)}(x_2 - x_1) \tag{5.22}$$

Where, k is the time index, n and K are the time indices when the shockwave first forms, and the end of analysis time period, respectively.

With VSL control, Equation (5.22) could be written as follows:

$$x(k=K)=\frac{\sum_{k=n}^{K}\rho_{crit}(k)u(k)T - (\sum_{k=1}^{K}q_{x_1}(k)T - \sum_{k=1}^{n}q_{x_1}(k)T)}{\rho_{crit}(K) - \rho_{x_1}(K)} + \frac{\rho_{crit}(K) - \rho_{x_1}(n)}{\rho_{crit}(K) - \rho_{x_1}(K)}(x_2' - x_1) \tag{5.23}$$

Where, ρ_{crit} is the density in the critical cell of Figure 5.4. The queue length from the geometric starting of the bottleneck at time index k can be written as: $L_{queue}(k) = L' - x(k)$. Where, L' denotes the length between x=0 and the queue starting location at $x = x_2$. Implementation of Equation (5.22) in the real-world requires only one loop detector in each travel lane to measure the time dependant input demand. Whereas, for the implementation of Equation (5.23) requires one loop detector at the upstream (similar to model 5.22) and one loop detector at the critical VSL cell as shown in Figure 5.4 to measure the traffic variables, namely flow and speed.

5.5.2 *Validation of queue estimation model*

It is important to investigate whether the developed queue estimation models can accurately simulate the queue lengths before they can be adopted to track queue location with the control strategy. Since the VSL performance is evaluated within microscopic simulator, a comparison of queue length (that grows from a bottleneck starting point) simulated by the Equation (5.22) and measured by the microscopic simulator is made. During simulation, queue location is updated at a time interval of T=20 sec and T =60 sec separately. From Figure 5.6 (a, b), it can be observed that the proposed model has a good agreement with the ground truth (measured) except the time period between 4:22 to 4:27. This discrepancy could be due to the internal queue definition used by the simulator. Specifically, four parameters were defined as to record a vehicle in queue in the WMD base model. A snapshot of queue measurement configuration file is shown in Figure 5.7.

(1) If speed is less than the "*Begin*" speed (30 kph), and has not exceeded the "*End*" speed (30 kph);

(2) "*Maximum Headway*" of 20 m. (which defines the maximum distance between two vehicles so that the queue is not disrupted);

(3) "*Maximum Length*" of 3000 m. (which defines the maximum length of the queue, even if the actual queue is longer).

The last parameter is helpful if longer queues are detected in a network. From Figure 5.6, it can be concluded that with a T =20 sec time step, the queue estimation model (Equation 5.22) performs better. Specifically, for the no-VSL scenario, the mean absolute error (MAE) between measured and simulated queue location considering T =20 sec and T =60 sec were 13.7% and 33.2%, respectively. Thus, this research will also consider T =20 for estimating queue location that propagates from a critical VSL sign (Figure 5.6c).

5.6 Application results

5.6.1 *MPC design in WMD base model*

This research uses the same calibrated microscopic model as in Chapter 4 to simulate traffic flow with and without MPC-based VSL control. The MPC parameters and optimization method are also same as Chapter 4. However, this research adopts the CTM-VSL as prediction model within the MPC framework. In addition, to keep consistency with the basic CTM model presentation, the discretized freeway segments will be represented by the notation "C" instead of "L" as in Chapter 4, where C and L stand for Cell and Link, respectively. To verify the CTM-VSL's performance within MPC, at first, the input demand on the mainline (q_0) was reduced compared to Chapter 4 to simulate a single recurrent bottleneck case on the test site. Specifically, that demand was reduced from 5300 vehicles to 3600 vehicles in the peak hour, which avoids formation of bottleneck B1 (weaving bottleneck). However, very high demand from both Terwilleger on-ramp (r_2) and 53 Avenue on-ramp (r_3) activates the downstream bottleneck B2. Note that, due to reduced mainline demand, the TTT and throughput values should be different, as can be seen in Table 4-1 and Table 5-3. However, later in this research, a comparison of MPC performance with the CTM-VSL and the DynaTAM-VSL models is conducted, where the same traffic conditions prevail in the WMD base model as in Chapter 4.

5.6.2 *Simulation results for no-VSL scenario*

Firstly, this research simulates a single bottleneck. The simulation has been run over a period from 4:00-6:00 PM, which corresponds to an afternoon rush hour. To compute the mobility parameters with and without VSL control, the test site was discretized into 11 cells (as in Figure 4.7). The cell 10 is the lane drop bottleneck. With the given demand inputs, heavy congestion appears and large queues are built from the bottleneck. Around 95% of all the vehicles coming from upstream take the route via the bottleneck. Remaining vehicles take the off-ramp S_3. The observed congestion is due to the capacity drop at the bottleneck. In the first hour of the simulation, about 4800 vehicles need to pass the bottleneck. As the flow from C9 is about to exceed 1200 vphpl as in Figure 5.8(a), demand from this cell rises to 3600 vph (having three lanes). The maximum flow that could be absorbed by the bottleneck is 3440 vph (having two lanes). The calibrated capacity of this bottleneck in the WMD base model is 1720 vphpl. As the demand from C9 is higher than the bottleneck capacity, additional vehicles are spilled back. This causes congestion shortly after the beginning of the simulation time horizon. Sooner the flow at C9 is reduced due to flow breakdown. It causes bottleneck exit flow lower than its capacity (θ=9.5%). The simulated capacity drop at the bottleneck is slightly different than that of Chapter 4 to verify the robustness of the MPC-based VSL control as the amount of capacity drop could vary from day-to- day (Dervisoglu et al. 2009).

For the no-VSL scenario, congestion originates at the downstream of C9 (near the diversion point), and propagates upstream, disturbing the cell 9, 8, 7, and 6, successively. The bottleneck C10 is also influenced to some extent. The speed profiles of the influenced cells are shown in Figure 5.8(b). When flow exceeds the bottleneck capacity, initially speed drops at the cell C9. Speed drops from 50 kph to 15 kph. It creates shockwave. Shockwave tail propagates backward at a speed of 10.8 kph. Sooner it causes speed drop at the other cells. The static speed limit on the test site for C1-C4 was 80 kph and the rest of the cells were operating at 50 kph due to construction activity. Figure 5.8(c) shows the density profile at the different cells over the peak 2-hr simulation periods. Very high density is observed during time period $t=$4:20-5:40.

5.6.3 *Simulation results for VSL-control scenario*

The following parameter values are adopted in the CTM-VSL model (with some variation over the cells): Q_{max} =1700 vphpl, w =11.5 kph, ρ_C = 40 vpkpl, ρ_{jam} = 110 vpkpl, θ=9.5%. The model was adopted within the MPC to improve traffic flow at the simulated lane drop bottleneck on the test site.

Four control scenarios are simulated. Table 5-2 summarizes the difference among the scenarios in terms of input parameters and number of implemented VSL signs. For scenario-1 and 2, one critical VSL (the authors call it VSL-1) is operated in C8. For scenario-3 and 4, C6 and C8 are operated with two different VSL signs. VSL-1 (*critical VSL*) is for the flow control into the bottleneck. VSL-2 is for keeping the queue length smaller that might grow from the critical VSL. The purpose is to avoid blocking of upstream on-ramp r_2 (see Figure 4.7). VSL values for C6 are obtained by dividing bottleneck capacity flow by the expected density in C7 (storage cell). Specifically, this research keeps the expected density close to critical density (ρ_c) of C7.

For scenario-2 and 4, the objective function takes different values in the α_{TTT}, which are to be determined based on the control policy. Since the VSL signs in this research are operated in cells having speed limit of 50 kph, a α_{TTT} values higher than 50 will not have much impact on flow optimization as shown in Chapter 3. However, the objective function within MPC also includes traffic states for the cells having speed limit of 80 kph. Thus slightly higher α_{TTT} values are assigned for the first 30 min of simulation when demand is very high compared to rest of the simulation period, and the motivation is to maintain free-flow speed at the discharge cell. The remaining 90 min of simulation a trade-off between TTT and TTD is maintained by giving lower weight to TTT. Indeed, by assigning lower weight to TTT (alternatively higher weight to TTD), the controller tries to release the vehicles that were held by the critical VSL sign for the first 30 min. Furthermore, it could reduce the queue length that might be created from the VSL sign during the first 30 min. However, such a lower value in α_{TTT} should not be assigned during very high demand period. Otherwise, the control performance would be equivalent to minimize TTD only (instead of minimizing combined objective functions) that will compromise the mobility benefits. Thus, for the real-life implementation, tuning the parameter values based on historical demand profile and operators' judgment is required.

From Figure 5.9 (a), it can be observed that compared to the no-VSL scenario, flow has been improved in the bottleneck significantly during the high demand period for all the scenarios. Unfortunately, scenario-1 keeps bottleneck flow close to the no-VSL scenario for the time horizon $t =$ 4:30-4:40. This could be due to the higher value of the parameter α_{TTT}. Interestingly, during the last 40 min of the simulation, during which demand is comparatively low (around 65% of highest demand period), implementation of VSL has no significant impact in terms of bottleneck flow improvement. Eventually, in the time horizon $t =$ 5:20-6:00, flow has been decreased at some points. It is no wonder that the implementation of VSL has reduced the flow, and several empirical and simulation studies (Papageorgiou et al. 2008; Lu et al. 2010) confirm this result. It seems that without control, vehicles those formed the queue at the bottleneck are now discharging at a higher rate due to lower network demand at the end of the simulation.

Figure 5.9 (b) and (c) show speed and density profile for the immediate upstream cell of the bottleneck, i.e., C9. Without VSL control this cell operates at near jam density and speed drops to 15 kph. Implementation of the VSL control for all the scenarios has kept density below critical density (40 vpkpl), and speed above 30 kph. However, scenario-2 and scenario-4 can recover free-flow speed earlier than scenario-1 and 3. The values of the weight parameter α_{TTT} play a significant role in this matter.

Figure 5.9(d) shows a comparison of time dependant queue tail location. Implementation of the proposed VSL control has built the queue earlier than the no-VSL scenario. But the queue has disappeared earlier. All the scenarios have kept the queue length smaller than that in the no-VSL scenario. However, both scenario-1 and 2 hit the upstream on-ramp r_2. As expected earlier that queue might grow from the critical VSL. Due to queue control by implementing VSL-2, queue length is kept close to 300 m. Figure 5.10 shows the change of VSL over the simulation time horizon.

Table 5-3 shows the numerical values of MOEs for the above different control scenarios. To compute the MOEs, the data have been averaged over several simulation runs (random seeds: 43, 25, 20, 30, 35, 65, 80, 83 and 42). From the table, it can be observed that compared to scenario-1, sceneario-2 performs better. The estimated link throughput for scenario-1 and scenario-2 are 9935 vphpl and 10068 vphpl, respectively. Compared to the no-VSL scenario, VSL control has around 5.9% and 7.3% improvement for the test site. Scenario-1 and Scenario-2 reduce TTT by 9.1 % and 15.1%, respectively.

Interestingly due to the queue control, both scenario-3 and 4 have very similar outcome (see, Figure 5.9). The computed throughput for scenario-3 and scenario-4 are 10025 vphpl and 10059 vphpl, which is around 6.9% and 7.2% improvement, respectively. Scnerio-3 and scnerio-4 have reduced TTT by 12.3% and 14.6%, respectively.

Furthermore, it can be evaluated that scenario-2 and scenario-4 performs pretty close. The percent improvements in all the MOEs are comparable for these two control scenarios. However, as explained earlier, scenario-4 can avoid blockage of upstream on-ramp, which in turn could reduce waiting time for the upstream on-ramp vehicles. Also, queue control has improved scenario-1. Now, scenario-3 and scenario-4 are very close in MOEs except the TTT. Considering these facts, scenario-4 could provide the best performance compared to the other scenarios considered in this research.

5.7 MPC with 1st and 2nd order models

This section evaluates the VSL performance when the CTM-VSL and the DynaTAM-VSL are used separately as a prediction model within MPC framework. For this evaluation, same demand levels (both on mainline and on-ramps) in the WMD base model are used as in Chapter 4, which activates two bottlenecks─B1 and B2 without VSL control situation (see, Figure 4.7). However, to avoid impact of random values in the predicted mainline and on-ramp flows (that can drive control performances differently for the two models), it was assumed that the predicted demand are same for both the control scenarios. To estimate the mobility parameters: TTT and throughput with and without VSL control, the data have been averaged over 10-simulation runs (with the following random seeds: 42, 43, 44, 45, 46, 47, 48, 49, 50, and 51) and the following statistics are obtained for the no-VSL and MPC-based VSL control situation as in Table 5-4.

The mean TTT for no-VSL situation, VSL with the CTM-VSL as prediction model, and VSL with the DynaTAM-VSL as prediction model are 711 veh-hr, 441 veh-hr, and 446 veh-hr, respectively. The MPC-based VSL implementation results in 38.0% and 37.3% TTT improvement respectively for adopting the CTM-VSL and the DynaTAM-VSL. The computed throughput values for the above three situations are 13753 vphpl, 14699 vphpl, and 14715 vphpl, respectively. Thus, the MPC-based VSL implementation results in 6.9% and 7.0% improvements, respectively. Figure 5.11(a) shows the time consumed by CPU at each control sampling time to find the optimal VSL trajectories over the 5-minutes prediction horizon. It is observed that due to simple structure of the CTM-VSL, the online optimization time is lower for most of the times compared to the DynaTAM-

VSL. In addition, it can be seen from Figure 5.11(b), the objective function values at each control sampling time are comparable when the above models are adopted within MPC.

5.8 Summary and conclusions

This research proposes a new first-order traffic flow model ─ CTM-VSL for the VSL control situation. Unlike second-order models, it is flexible to use in macroscopic simulation and requires calibration of piece-wise linear fundamental diagram (FD) of discretized freeway cells only. The following two modifications of FD are proposed.

(1) The first permits one to model recurrent bottleneck in which there is a capacity drop once feeding flow exceeds its capacity; and

(2) The second modification permits variable free-flow speed for the cells operated with a VSL control.

To verify the accurateness of the CTM-VSL, a comparison of the model simulation and 20-s loop detector data from the WMD base model was made. It was found that although the model could simulate the flow and the density pretty well, the cell-wise and network-wide speed simulation error are higher compared to the DynaTAM-VSL model.

The CTM-VSL model was adopted within the MPC to reduce input flow at a lane drop bottleneck following the proposed VSL control strategy. To update freeway storage capacity of upstream segment of a recurrent bottleneck, a real-time queue estimation model is proposed, which takes only upstream mainline demand (free from bottleneck influence) as input for computing real-time queue locations. The validation of the queue estimation model showed that with the frequent update of queue location (60 s verses 20

s), the model performs pretty well. The micro-simulation of MPC-based VSL evaluation results indicated the potential benefit of implementing active traffic management (ATM) to avoid or mitigate congestion and save travel time. Specifically, for the test site WMD, with a given demand level, improvements to TTT and throughput were in the range of 9.0%-15.0% and 6.0%-7.5%, respectively for different control scenarios. It was observed that queue control is necessary when very high demand approaches to the bottleneck. Through the VSL implementation, the start point of the idling (very low speed) was delayed, and free-flow speed was regained earlier compared to no-VSL. Results showed that the MPC-based VSL control can avoid the dramatic change in the traffic system.
Despite the simple structure of the CTM-VSL, the isolated MPC-based VSL control showed comparable results to that of the DynaTAM-VSL. The values in the mobility parameters were not statistically different at 95% confidence level. It was found that considering multiple recurrent bottlenecks in the test site WMD, the CTM-VSL and the DynaTAM-VSL results in TTT improvement by 38.0% and 37.3%, respectively. The values of throughput improvements with those models were 6.9% and 7.0%, respectively.

Interestingly, it was computed that within MPC, due to simple structure, the online simulation time for the CTM-VSL is lower for most of the times compared to the DynaTAM-VSL. However, the CTM-VSL model is valid only for the condition of perfect compliance by the drivers to VSL control, since it shares same property of the CTM model. It can be argued that conditions where some drivers obey the VSL and others do not result in significantly variance among mean driving speed and be even more unsafe than without VSL control situation. Thus, if the CTM-VSL model is adopted within MPC framework in the real-world application to improve recurrent bottleneck flows, the implementation of the VSL control should be coupled with strict speed limit enforcement, for example, reason of lowering the speed limit together with speed enforcement cameras, and strong promotion of drivers' education, to encourage familiarity with the VSL control measures as well as improved compliance.

5.9 References

Almasri, E., and and Friedrich, B. (2005). "Online offset optimisation in urban networks based on cell transmission model." *ITS Hanover*.

Carlson, R. C., Papamichail, I., Papageorgiou, M., and Messmer, A. (2010). "Optimal motorway traffic flow control involving variable speed limits and ramp metering." *Transportation Science,* 44(2), 238-253.

Chen, D., Zhang, Y., and Xia, L. (2013). "Sensitivity simulation analysis of urban expressway under speed guidance control." *Journal of Theoretical and Applied Information Technology*, 48(1), 288-292.

Daganzo, C. F. (1995). "A finite difference approximation of the kinematic wave model of traffic flow." *Transportation Research Part B*, 29(4), 261-276.

Daganzo, C. F. (1994). "The cell transmission model: A dynamic representation of highway traffic consistent with the hydrodynamic theory." Transportation *Research Part B*, 28(4), 269-287.

Dervisoglu, G., Gomes, G., Kwan, J., Muralidharan, A., Horowitz, R., and Horowitz, R. (2009). "Automatic calibration of the fundamental diagram and empirical observations on capacity." *Transportation Research Board 88th Annual Meeting*.

Godlewski, E., and Raviart, P. -. (1996). "Numerical Approximation of Hyperbolic Systems of Conservation Laws." *Springer-Verlag, Berlin, Germany*.

Godunov, S. K. (1959). "A difference scheme for numerical computation of discontinuous solutions of equations of fluid dynamics." *Matematicheskii Sbornik, 47, 271–306, Translated by the US Publication Research Service, JPRS 7226, 1969*.

Gomes, G., and Horowitz, R. (2006). "Optimal freeway ramp metering using the asymmetric cell transmission model." *Transportation Research Part C: Emerging Technologies*, 14(4), 244-262.

Gomes, G., Horowitz, R., Kurzhanskiy, A. A., Varaiya, P., and Kwon, J. (2008). "Behavior of the cell transmission model and effectiveness of ramp metering." *Transportation Research Part C: Emerging Technologies*, 16(4), 485-513.

Hegyi, A., Burger, M., Schutter, B. D., Hellendoorn, J., and Van den Boom, T. J. J. (2007). "Towards a Practical Application of Model Predictive Control to Suppress Shockwaves on Freeways." *Proceedings of the European Control Conference 2007 (ECC'07), Kos, Greece,* 1764–1771.

Hegyi, A., De Schutter, B., and Hellendoorn, J. (2005). "Optimal coordination of variable speed limits to suppress shock waves." *IEEE Transactions on Intelligent Transportation Systems*, 6(1), 102-112.

Lighthill, M. J., and Whitham, J. B. (1955.). "On kinematic waves. I. Flow movement in long rivers. II. A theory of traffic flow on long crowded roads." *In Proc. R. Soc. London: Ser. A*, 229(1178), 281-345.

Lo, H. K. (2001). "A cell-based traffic control formulation: Strategies and benefits of dynamic timing plans." *Transportation Science*, 35(2), 148-164.

Lu, X. Y., Qiu, T. Z., Varaiya, P., Horowitz, R., and Shladover, S. E. (2010). "Combining Variable Speed Limits with Ramp Metering for freeway traffic control." *Proceedings of the 2010 American Control Conference, ACC 2010*, 2266-2271.

Michalopoulos, P. G., Stephanopoulos, G. and Stephanopoulos, G. (1981). "An Application of Shock Wave Theory to Traffic Signal Control." *Transportation Research Part B: Methodological*, 15(1), 35-51.

Munoz, L. R. (2004). "Macroscopic Modeling and Identification of Freeway Traffic Flow." *PhD Thesis, University of California, Berkeley*.

Oliver, R. M. (1964). "Travel times through shock waves." *Operations Research*, 15(2), 139–144.

Papageorgiou, M., Blosseville, J. -., and Hadj-Salem, H. (1990). "Modelling and real-time control of traffic flow on the southern part of Boulevard Peripherique in Paris: Part I: Modelling." *Transportation Research Part A: General*, 24(5), 345-359.

Papageorgiou, M., Kosmatopoulos, E., and Papamichail, I. (2008). "Effects of variable speed limits on motorway traffic flow." *Transportation Research Record*, (2047), 37-48.

Richards, P. I. (1956). "Shockwaves on the highway." *Operation Research*, 4(1), 42-51.

Zhang, L., and Levinson, D. (2010). "Ramp metering and freeway bottleneck capacity." *Transportation Research Part A: Policy and Practice*, 44(4), 218-235.

Table 5-1 MAE between 20-s measured and CTM-VSL simulated traffic parameters in WMD.

Cell number*	Traffic parameters v	q	ρ
C2	0.228	0.138	0.3443
C3 (B1)	0.159	0.186	0.2075
C4	0.135	0.242	0.1126
C5	0.147	0.232	0.0587
C6	0.038	0.201	0.0421
C7 (B2)	0.091	0.194	0.1102
C8	0.114	0.182	0.107
C9	0.155	0.186	0.1626
C10	0.183	0.168	0.3093
C11	0.203	0.183	0.1743
C12	0.189	0.137	0.0733

*The above 13 cells are consistent with the discretized segments of the 11-km test site for validating the DynaTAM-VSL model as presented in Chapter 2.

Table 5-2 Summary of different control scenarios when CTM-VSL is used as prediction model within MPC.

Scenarios	Objective function considered	Weighing coefficient related to J: α_{TTT}	α_{TTD}	No. of VSL signs	Cells operated with VSL control
1	J_1	55	1	1	C8
2	J_2	(55,20)*	1	1	C8
3	J_1	55	1	2	C6 and C8
4	J_2	(55,20)*	1	2	C6 and C8

* *The 1st and 2nd values within the bracket indicate the coefficient values for the objective function chosen for the first 30 min and last 90 min of 2-hr simulation, respectively*.

Table 5-3 VSL performance considering CTM-VSL during congestion period.

Scenarios	Objective function values	TTT (veh-hr)		Throughput (vphpl)	
		values	% improvement	values*	% improvement
no-VSL	-	405	-	9378	-
1	6040	368	9.1	9935	5.9
2	4520	344	15.1	10068	7.3
3	5213	355	12.3	10025	6.9
4	4645	346	14.6	10059	7.2

**Summation of the flow (in unit of vphpl) of the discretized cells and the flow at each cell is taken as the average over the congestion period*.

Table 5-4 Comparing MPC-based VSL control performance when CTM-VSL and DynaTAM-VSL are separately used as prediction models.

	no-VSL		MPC-based VSL control using CTM-VSL as prediction model[a]				MPC-based VSL control using DynaTAM-VSL as prediction model[a]			
experiment* no	TTT (veh-hr)	Throu-ghput (vphpl)	TTT (veh-hr)	*Imp*[b] (%)	Throu-ghput (vphpl)	*Imp*[b] (%)	TTT (veh-hr)	*Imp*[b] (%)	Throu-ghput vphpl)	*Imp*[b] (%)
1	712	13723	435		14616		432		14637	
2	722	13716	431		14784		427		14760	
3	671	13832	432		14770		442		14792	
4	671	13832	428		14692		427		14680	
5	712	13874	443		14751		447		14746	
6	753	13675	439	38.0	14645	6.9	447	37.3	14666	7.0
7	674	13704	420		14565		413		14567	
8	708	13653	463		14622		478		14674	
9	750	13705	465		14748		457		14785	
10	733	13819	454		14794		486		14838	
mean	711	13753	441		14699		446		14715	

**Experiments are performed within base model for different seed numbers*.

[a] *t-stat for TTT (-0.52), t-stat for throughput (-0.389), t-critical (1.73).*

[b] *Imp stands for improvement*.

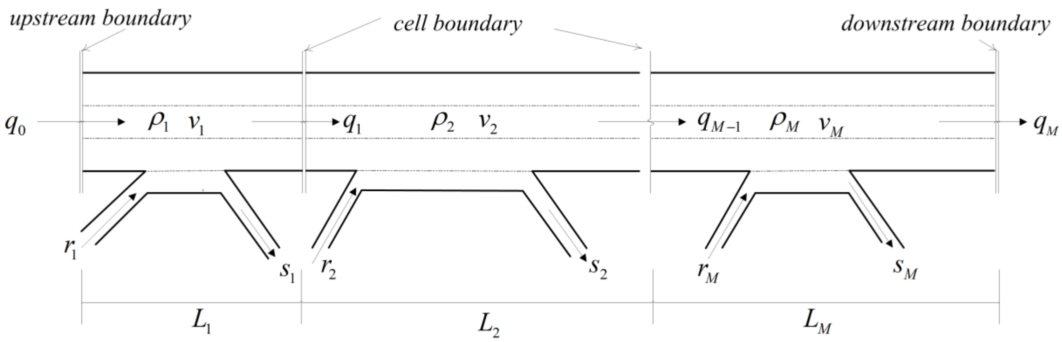

Figure 5.1 Freeway section divided into M cells. Each cell has one on-ramp and off-ramp. Cell boundaries are located at upstream of successive on-ramps.

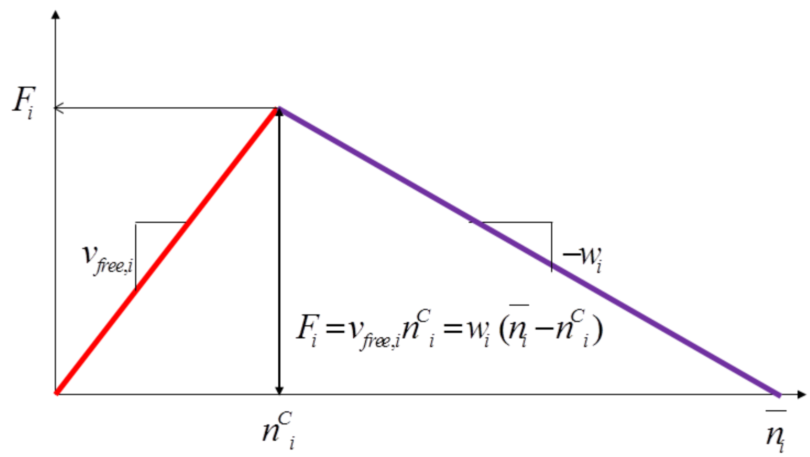

Figure 5.2 CTM parameters illustration in triangular-shaped FD. Traffic states on left-side and right-side of $n^C{}_i$ correspond to free-flow and congestion.

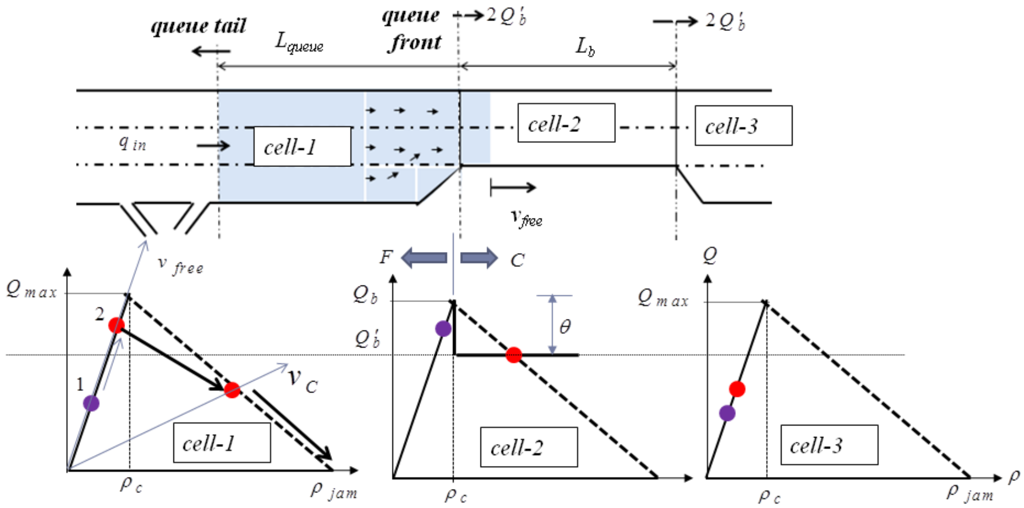

Figure 5.3 Traffic states on FD due to different demand levels. Bottleneck will be activated when demand is higher than the downstream bottleneck capacity. At this high demand situation, outflow from bottleneck will be lower than its capacity.

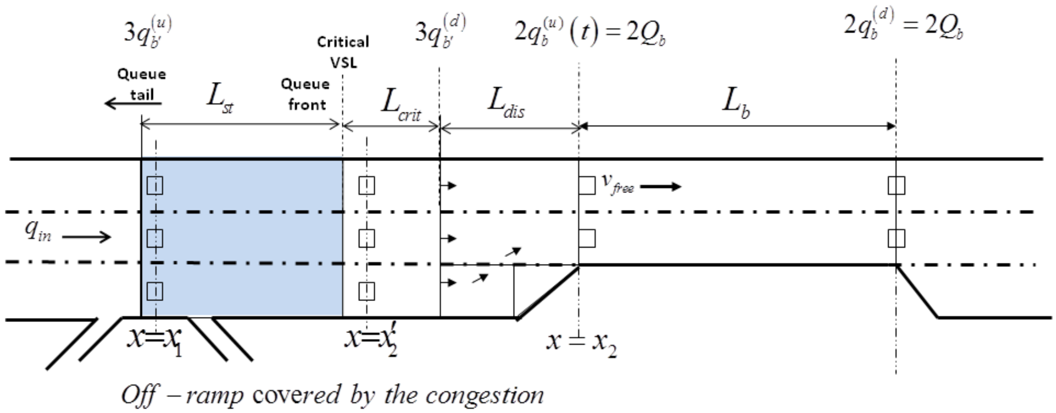

Figure 5.4 Control strategies: (1) maintaining bottleneck flow close to its capacity; and (2) avoiding blocking of upstream ramps to maximize throughput.

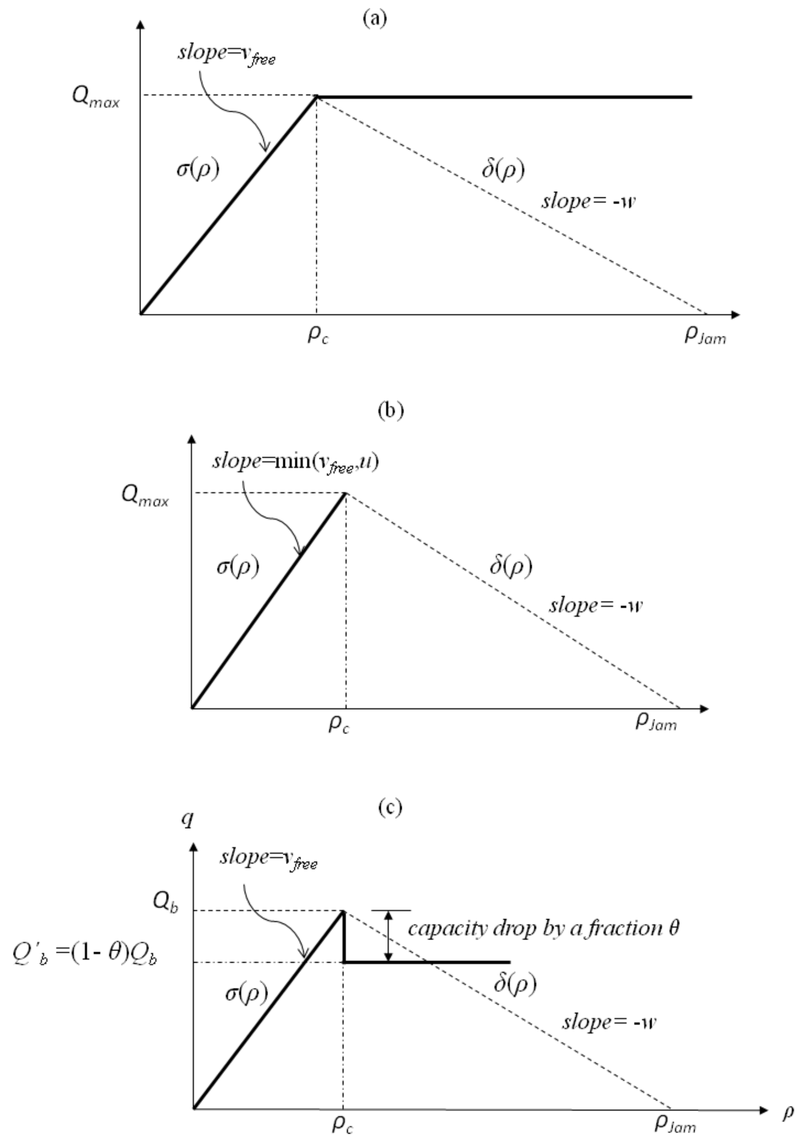

Figure 5.5 Proposed FDs in the CTM-VSL model for a cell: (a) with no-VSL; (b) with VSL control; and (c) bottleneck with capacity drops. In all FDs, dark line and dotted line represent demand and supply function, respectively.

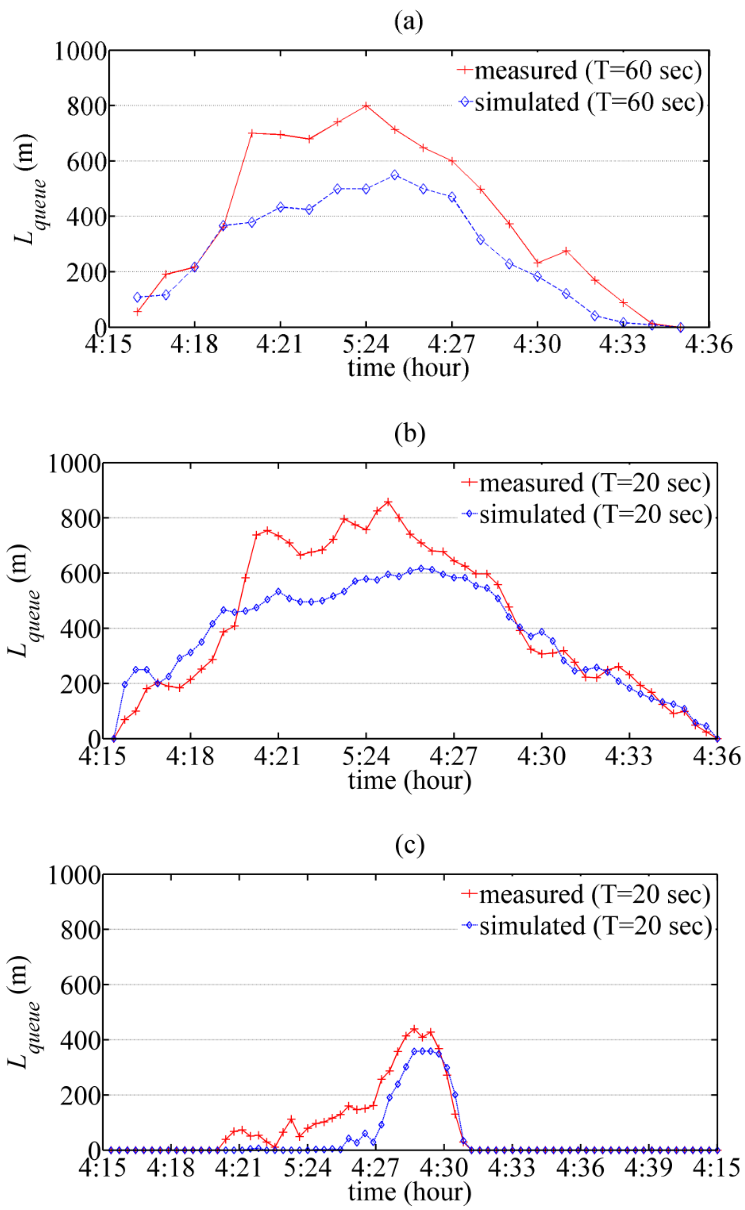

Figure 5.6 Comparison between simulated and measured queue length: (a-b) without VSL control; and (c) with VSL control. The models have accurately captured queue start and end time. However, peak has been slightly underestimated.

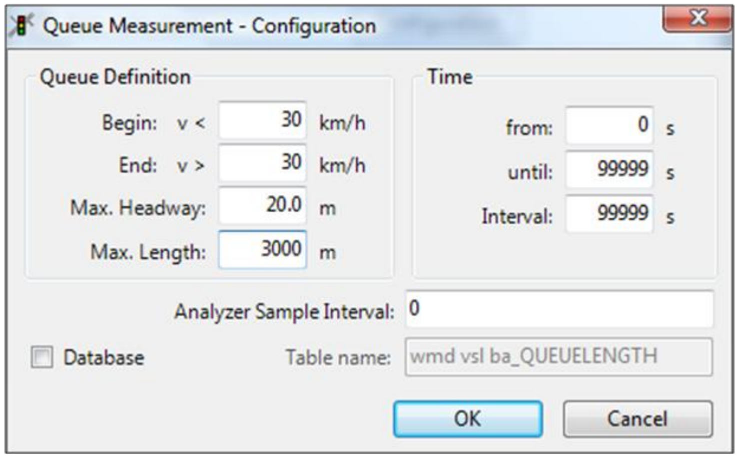

Figure 5.7 Configuring queue measurement parameters.

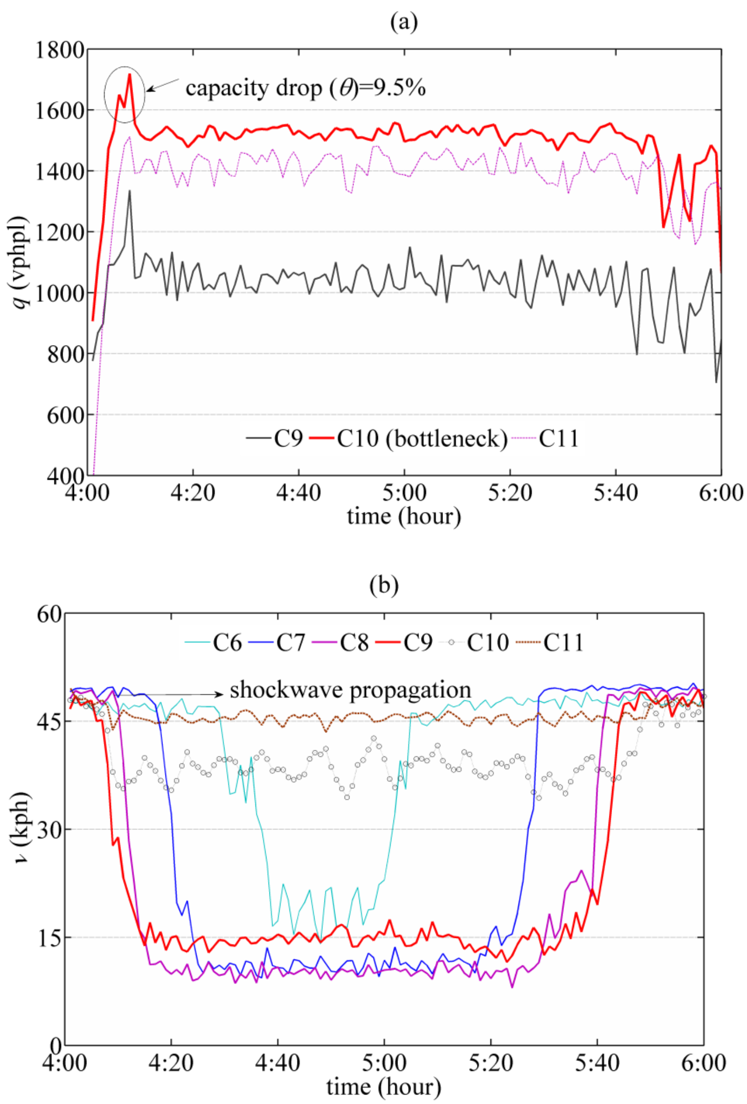

(c)

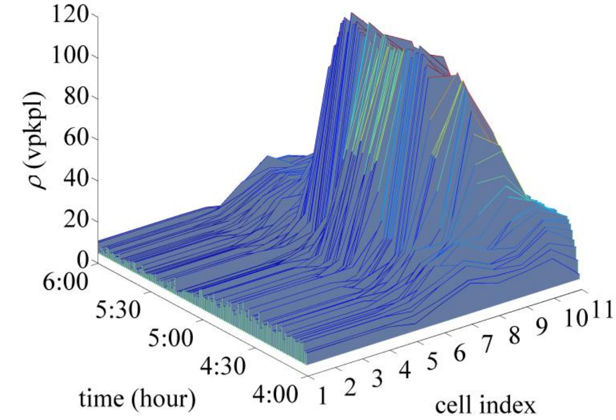

(d)

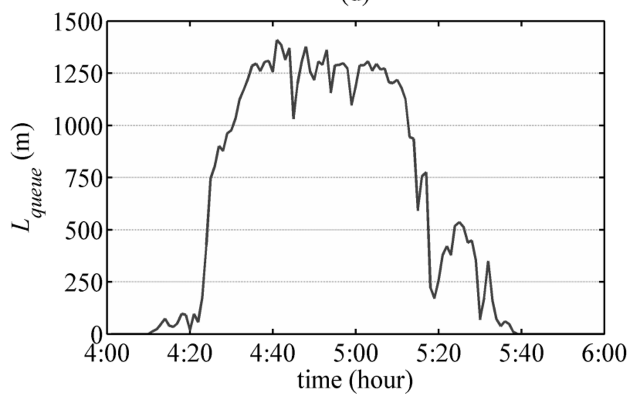

Figure 5.8 No-VSL scenario: (a) flow profile with capacity drop at lane drop bottleneck; (b) speed profile demonstrating shockwave propagation; (c) density profile; (d) computed queue length from the bottleneck starting point.

(a)

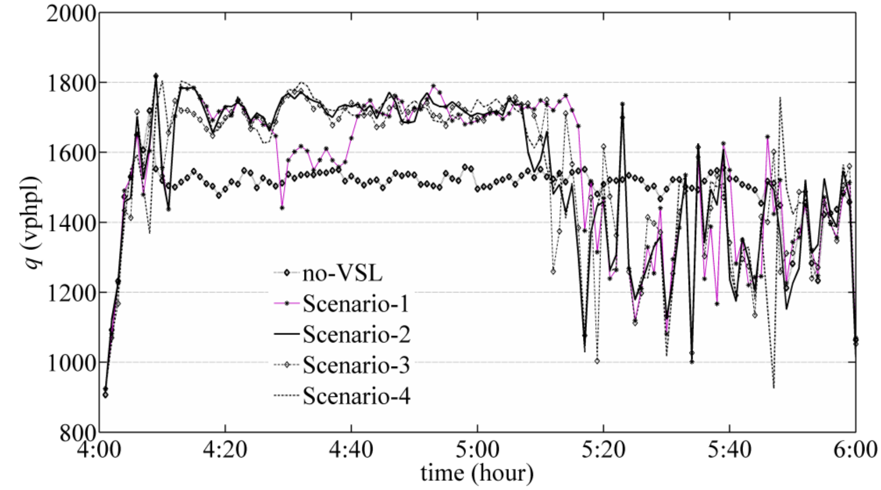

2000
1800
1600
1400
1200
1000
800
q (vphpl)
no-VSL
Scenario-1
Scenario-2
Scenario-3
Scenario-4
4:00
4:20
4:40
5:00
5:20
5:40
6:00
time (hour)

(b)

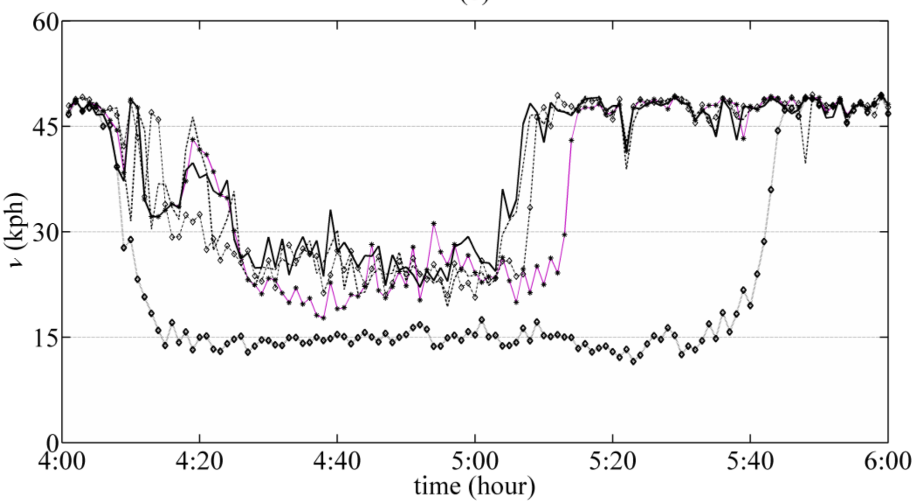

60
45
30
15
0
v (kph)
4:00
4:20
4:40
5:00
5:20
5:40
6:00
time (hour)

(c)

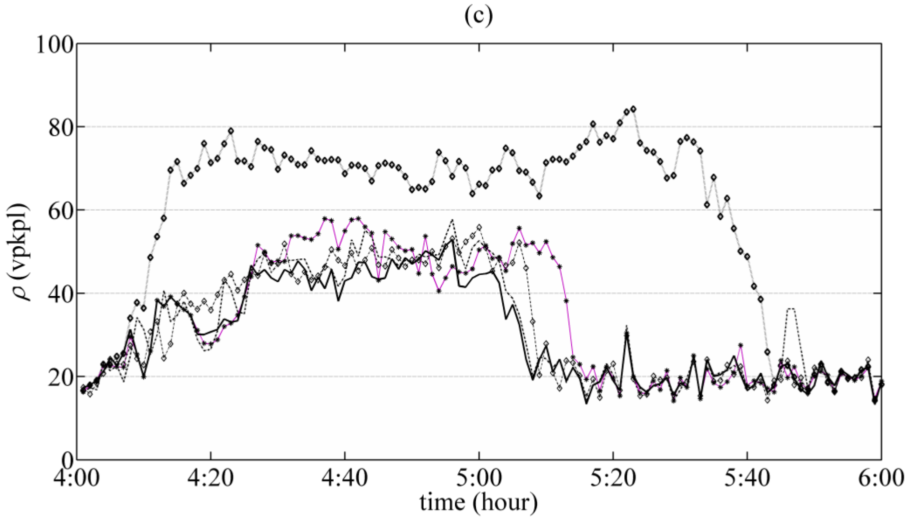

100
80
60
40
20
0
ρ (vpkpl)
4:00
4:20
4:40
5:00
5:20
5:40
6:00
time (hour)

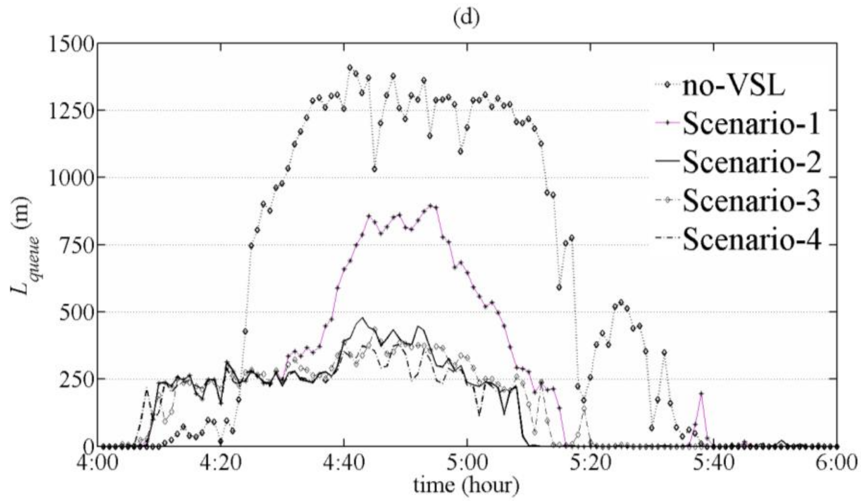

Figure 5.9 VSL-control scenario: (a) flow profile; (b) speed profile; (c) density profile; and (d) time dependant queue tail location.

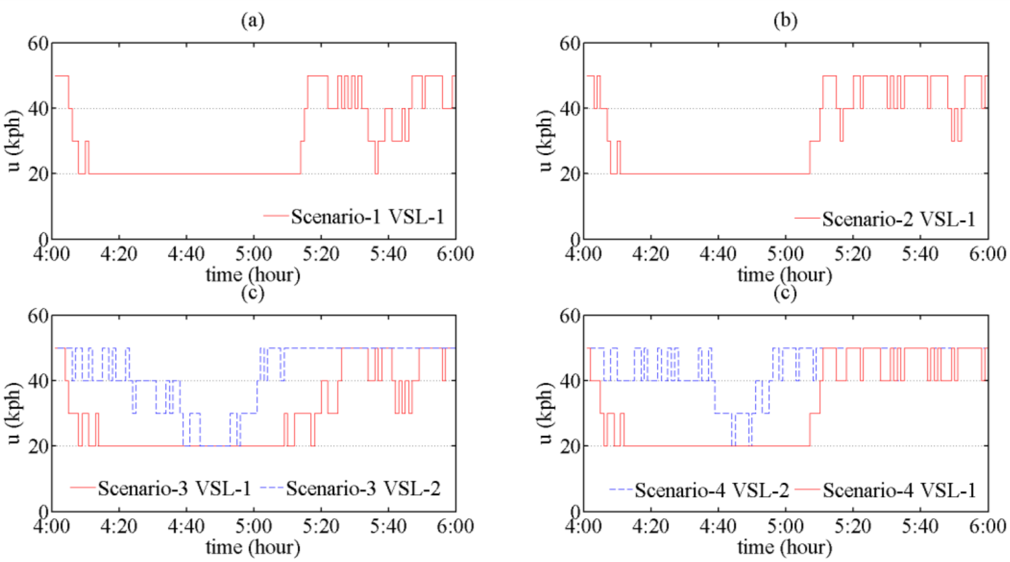

Figure 5.10 VSL trajectory for different control scenarios.

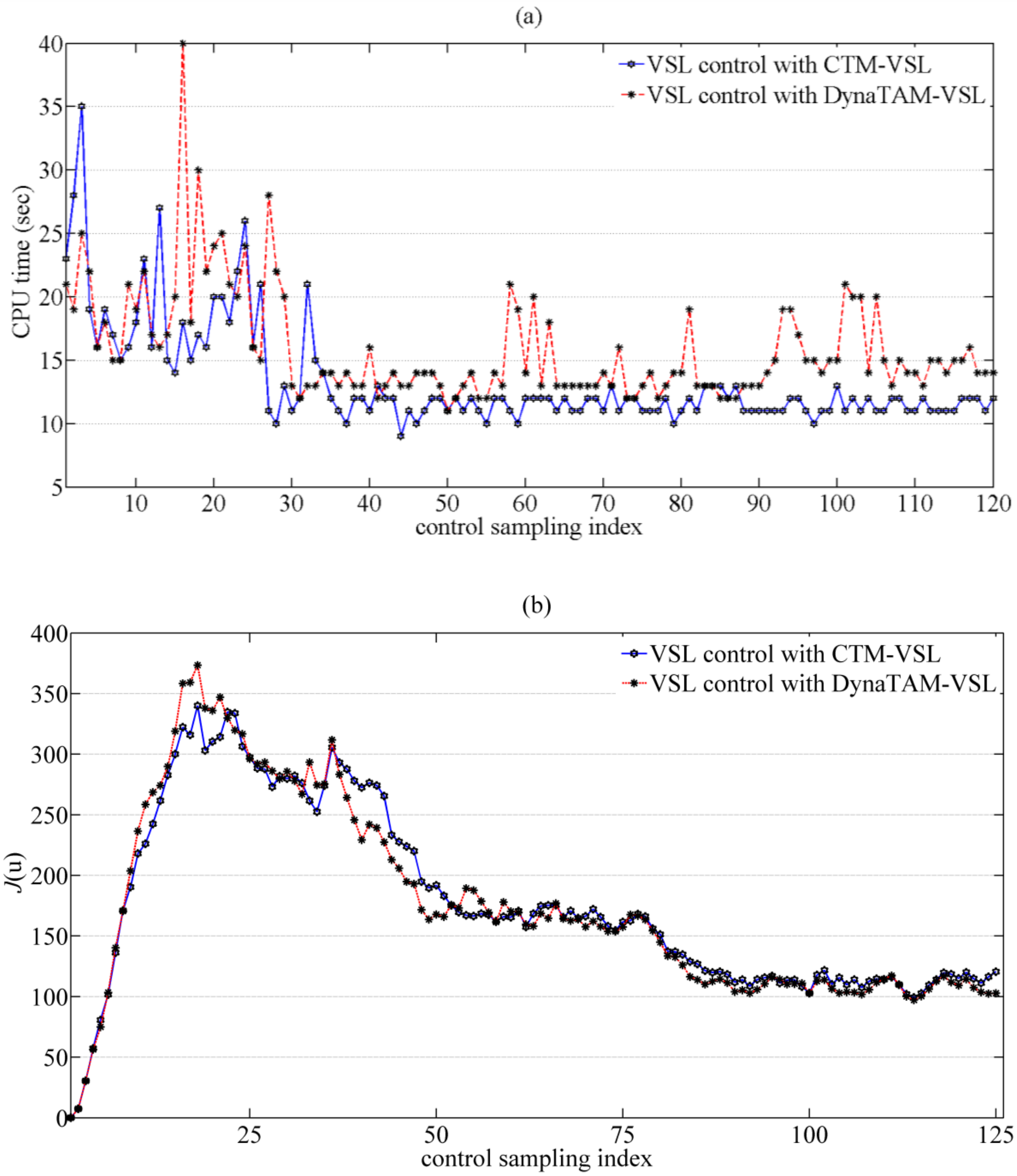

Figure 5.11 Comparison of VSL performance due to using the CTM-VSL and the DynaTAM-VSL as prediction models: (a) CPU time; (b) objective function values.

Chapter 6

Modeling driver compliance to VSL and quantifying relative impacts of VSL with CLs to mitigate congestion*

6.1 Introduction

Although it is well understood that motorist compliance with the speed limit (SL) and the variable speed limit (VSL) is paramount to traffic mobility and safety, during real-world VSL control design and implementation, limited attention has been given to the impact of driver response. While field implemented VSL control strategies provide consistent improvements in traffic safety (20-30%), the speed homogenization effect has rendered inconsistent results in terms of mobility benefits. It is not clear whether the inconsistent VSL mobility performance is caused by an inappropriate control strategy design or the driver compliance level (CL). Indeed, one cannot conclude that VSL is incapable of improving freeway mobility, since field-implemented VSL control strategies are demand-responsive and heuristic in nature without considering traffic dynamics. However, in several recent simulation studies, it has been shown that to improve freeway mobility, the VSL control must proactively consider particular mobility parameters: capacity drops and

* *This chapter is an extended version of an accepted article*. **Hadiuzzaman, M.,** Fang, J., Luo, A., Karim, A., and Qiu, T.Z**.** (2014). "Modeling Driver Compliance to VSL and Quantifying Impacts of Compliance Levels and Control Strategy in Mobility and Safety." *will be included on the 93rd Transportation Research Board (TRB) Annual Meeting Compendium of Papers*. (peer-reviewed)

shockwave arrival. However, due to insufficient evidence in reliably predicting driver response to VSL, those studies typically assumed that 100% of drivers follow the SL. Consequently, the mobility benefits were overestimated.

The primary objective of this research is to distinguish the relative contributions of not only CLs exclusively, but also a proactive optimal VSL control with different CLs, to improve freeway mobility and safety. Improving the latter could also reduce non-recurrent congestion. The secondary objective is to investigate whether the VSL mobility benefits are at the expense of increased collision probability. For such a research, the analysis of before-and-after field observations is hindered by the presence of confounding effects, including other policies undertaken during SL changes (e.g. intensive speed enforcement) and other factors that may affect safety (e.g. changes in traffic volume) (TRB 1998). So, performing experiments within a traffic flow simulator is more suitable. Furthermore, to mimic realistic driver response to changes in SL, microscopic simulation is preferable over macroscopic simulation. Thus, this research has modeled several CLs within the microscopic WMD base model, testing real-world driver behaviour. The CLs include speed distributions for aggressive, compliant, and defensive drivers.

Furthermore, compared to most of the microscopic simulation studies, where the VSL control rules are based on a flow-density-speed threshold (Allaby et al. 2007; Hellinga and Mandelzys 2011); an estimated collision potential (Lee et al. 2006; Abdel-Aty et al. 2006; Abdel-Aty et al. 2008); and predefined traffic scenarios (Lin et al. 2004; Kang and Chang 2006; Kang et al. 2004), this research computes the optimal VSL values within a model predictive control (MPC) framework. For the MPC short-term traffic state prediction, this research uses the calibrated and validated macroscopic traffic flow model, DynaTAM-VSL (as presented in Chapter 2). The MPC-based VSL control can drive the traffic system to its optimal state based on the chosen objective function, satisfying the constraints on traffic states and SL changes. This research uses the scatter search proposed in Ugray et al. (2007) to provide starting points for the gradient-based local solver—sequential quadratic programming (SQP)—to find the global minimum of the objective function, and, thus, the optimal VSL values. The optimization method was made to combine the superior accuracy- and feasibility-seeking behaviour of gradient-based local nonlinear programming (NLP) solvers with the global optimization abilities of scatter search. To quantify the impact of CLs on VSL performance, the optimal VSL values were implemented in the microscopic simulator. This research chose three performance parameters: (1) total travel time (TTT); (2) throughput; and (3) relative safety benefit (RSB).

6.2 Literature review

This section presents the common assumptions on driver compliance to VSL, as well as the impacts of driver response to VSL performance. In general, there is little evidence in literature that shows the impact of driver-VSL compliance on mobility and safety parameters.

6.2.1 *Driver compliance assumptions*

6.2.1.1 In macroscopic simulation studies

Hegyi et al. (2005) evaluated the MPC-based VSL control assuming a VSL compliance rate (CR) of 100%. The research concluded that VSL could reduce travel time by 21%. However, that research did not quantify the safety benefit of the VSL. In another research assuming a CR of 100%, Long et al. (2008) showed that the MPC-based VSL control could make traffic speed more homogeneous, which improves safety. Carlson et al. (2010) evaluated VSL performance in the Amsterdam ring road, A10, which resulted in a

47% reduction of TTT. The simulation research did not present the assumption for driver response to VSL.

6.2.1.2 In microscopic simulation studies

Park and Yadlepati (2003) tested VSL control at work zones using VISSIM under a varying CR, of 70%, 80%, and 100% and two demand conditions (under-saturated and over-saturated). The simulation results showed increased travel time in the bottleneck merge and activity area with increasing CRs.

Hellinga and Mandelzys (2011) evaluated the sensitivity of the safety and operational impacts of VSL on driver compliance. For each of the CLs, an expected mean speed was assumed with each of the VSLs. The speed variance was calculated based on a fixed coefficient of variation (COV), as observed with the static SL on the studied corridor, Queen Elizabeth Way (QEW), near Toronto. The simulation evaluation within the PARAMICS traffic simulator showed that safety is positively correlated with CLs. In contrast, travel time is negatively correlated. However, due to the heuristic nature of the VSL control strategy, the reported mobility and safety impacts might not be exact. Furthermore, in PARAMICS, rather than speed distribution, the degree of compliance is expressed as a numerical value (the higher the value, the more aggressive the driver) and it is assumed to follow a normal distribution.

In a recent research, Habtemichael and Santos (accepted) evaluated VSL benefits under different CLs using simulated data from VISSIM. The research found that VSL has the highest safety benefits during congested traffic conditions. By contrast, VSL has no mobility benefit during congested conditions. However, the research was limited by implementing a simple heuristic VSL control strategy. Moreover, the research assumed that non-compliant vehicles completely ignore the VSL, and retain the speed of 120 kilometres per hour (kph) assigned by the static SL. Thus, during their simulation, if a VSL of 60 kph was posted, many non-compliant drivers remained at speeds around 120 kph. The preceding assumption is unreasonable during congestion periods. Due to high traffic density, drivers are forced to decrease speed. Furthermore, the research did not mention how to model speed distributions with each of the VSLs from critical aspects: (1) the mean speed; (2) lower and upper ranges of speed; (3) the distribution of aggressive and defensive drivers within the non-compliance category.

Lu et al. (2011) evaluated an MPC-based VSL control within the AIMSUN traffic simulator. That research found similar mobility benefits with CR at 100% and 30%. However, no description was provided for the distribution of speed of a given VSL. Furthermore, in AIMSUN, a vehicle parameter measuring the driver degree of compliance with the SL is used, rather than speed distribution.

Hadiuzzaman et al. (2013) evaluated in VISSIM an MPC-based VSL control for relieving congestion caused by recurrent bottlenecks. The VSL control showed 39% travel time reduction and 5.4% throughput improvements with a CR of 90%. In another research, Hadiuzzaman and Qiu (2013) proposed the Cell Transmission Model-based VSL control, and also used the MPC to dynamically change the SL in real-time. The VISSIM simulation with a CR of 90% showed 10-15% travel time reduction and 5-7% throughput improvement for different control scenarios. Later, Islam et al. (2013) evaluated the MPC-based VSL control using the same macroscopic traffic flow model as in Hadiuzzaman et al. (2013). The research showed safety and mobility benefits of 50% and 30%, respectively. However, that research also assumed a CR of 90%, and concluded that the benefits of the VSL could be quite different under reduced CR.

6.2.2 *Impact of driver compliance in the real-world*

A two-stage speed reduction scheme was implemented at one of the I-494 work zone bottlenecks in the Twin Cities, Minnesota. Despite the advisory SL, data collected from the field operation test (FOT) indicated 25-35% reduction of the average 1-min maximum speed difference (Kwon et al. 2007). Moreover, it was observed that drivers are less likely to comply with the VSL if the posted speed is significantly different from the speed they would otherwise choose. A six-mile test site with a long-distance work zone on I-80 north of Wanship, Utah, was used to test drivers' response to VSL signs. Though the average speeds between static SL signs and VSL signs were not statistically different at a 95% confidence level, variation in speeds was reduced (McMurtry et al. 2008). Ulfarsson et al. (2005) studied the effects of VSL control on mean speed and speed variance on the I-90 in Washington, U.S. Distributions of speed were generated; however, those distributions included congested and uncongested conditions. Consequently, the distributions do not solely reflect drivers' response to the posted SL.

VSL has also been widely implemented and tested in European countries. The key difference between Europe and U.S. is that in Europe VSL deployments are enforced. Most European deployments have automated speed enforcement, and have high CR. The UK Highways Agency (2004) reported a 9% reduction in the amount of flow breakdown, and a 6% reduction in start-stop driving conditions. An empirical research was performed along an 18-km section of Autobahn 9 near Munich, Germany to investigate how the VSL affects driver behaviour and bottleneck formation (Bertini et al. 2006). The VSL sign was augmented by traveler information systems and speed enforcement cameras to promote higher CL. It was found that VSL can control dense, but still flowing traffic, and traffic continued to flow during congested periods at speeds between 30-40 kph. Weikl et al. (2013) reported that the VSL could not improve freeway capacity; however, the authors also recommended analyzing further features, including speed compliance.

The following three conclusions can be drawn from the literature survey:

(1) A few studies have analyzed the impacts of CLs on VSL benefits with heuristic control strategies. There is no evidence that shows sensitivity of the proactive optimal VSL effectiveness on CLs.

(2) Drivers are less likely to comply with SL, if the real-time posted speed is not appropriate, which could diminish VSL benefits. Thus, it is important to advise appropriate VSL values to find the true effects of the VSL control.

(3) None of the previous studies quantified the relative contribution of the VSL control strategy combined with the CLs to improving mobility and safety.

6.3 Modeling driver compliance with VSL

6.3.1 *Compliance with static speed limit*

Analyzing driver response to the static SL on WMD is required to model driver compliance to VSL, as there is a lack of evidence in the latter. The traffic data was obtained from the traffic operation group within the City of Edmonton, and gathered over 2 months. The off-peak time period was selected to ensure that traffic was free flowing. Speed measures were computed by using a commercial software TOPS (sample size, n=89578): (1) mean =82 kph, (2) standard deviation (σ) =7.34 kph, and (3) coefficient of variation (COV)=0.09. Typically, the percentage of drivers operating below the mean speed is considered compliant. By contrast, this research considered a driver to be compliant if his or her speed falls ±5 kph of the advised SL. This consideration allows the modeling and analyzing of the impact of aggressive as well as defensive drivers. From the cumulative speed distribution curve, it was obtained that the CR for a static SL of 80 kph on WMD is approximately 45%. Furthermore, following the above definition, it was also obtained that 20% of drivers are defensive and 35% driver are aggressive.

6.3.2 *Experimental setup for compliance levels*

This research modeled several CLs using the desired speed distribution curve in VISSIM. During the simulation, if the surrounding traffic conditions allowed, then the vehicle attempted to travel at the desired speed. Furthermore, each vehicle was assigned a fixed fractile value for speed distributions when entering the network. For example, if the fractile value is 50%, the vehicle will always get the 50 percentile of the desired speed distribution curve related to the SL. This research models a CR of 20% (low CL), 45% (moderate CL as observed in WMD), 80% (high CL), and 100% (ideal CL). Furthermore, to replicate a real-world scenario, it is assumed that not many compliant drivers travel at the speed exactly equal to the SL. By contrast, they are assumed to travel within ±5 kph of SL. The above intermediate CRs are used to analyze real-world scenarios; however, the assumed CRs could vary based on the corridor's traffic condition.

6.3.3 *Non-compliance rate distribution*

For each CL, it is also assumed that a certain percentage of non-compliant drivers will drive below the SL; those are defined as 'defensive drivers'. By contrast, a certain percentage will exceed the SL; those are defined as 'aggressive drivers'. The rest of the drivers are assumed to comply at ±5 kph of the SL. This assumption is made to induce the realistic speed variance following the evidence from WMD. The non-compliance rate distribution for the field implementable SLs are presented in Table 6-1. The table shows that, as the posted SL decreased, the percent of aggressive drivers increased. This is validated by the real-world observation presented in Giles (2004). The research found that as the SL rises, the proportion of vehicles traveling above the limit falls from 55.7% with an SL of 60 kph, to 27.4% with an SL of 110 kph. As shown in Table 6-1, for a 'low' CL and an SL of 80 kph, out of 80% non-compliant, 40% driver will tend to drive below the SL, while the other 40% driver will exceed the SL. Whereas, for the same CL and an SL of 20 kph, the percentages of defensive and aggressive drivers are 30% and 50%, respectively. The rest of the values in the table can be explained in a similar fashion. The resulted cumulative speed distribution curves with the field implemented VSL as functions of CLs are shown in Figure 6.1.

In Figure 6.1, the horizontal axis represents the desired speed in kph, and the vertical axis represents the percentage of drivers traveling at or below given speed. The lower, middle, and upper diagonal lines associated with each CL accounts for the defensive, compliant, and aggressive drivers, respectively. The difference in the cumulative percentage between the two extreme points of the middle diagonal represents the CR. Note that, for computing the impacts of CLs exclusively on freeway mobility and safety, only a speed distribution of 80 kph related to different CLs is implemented during the simulation. In Figure 6.1, the lower and upper values of the speed are bounded by $\pm 2\sigma$ of the mean speed related to SL, where σ = mean speed*COV. With a fixed COV, the formula results in decreasing σ as the SL decreases. This conjecture can also be validated from the real-world observation shown in Giles (2004). Specifically, the research found that two thirds of drivers travel within 10–14 kph of the posted SL. This range increases for progressively higher SLs. For example, the σ for an SL of 60 kph and 110 kph are 10.71 and 14.26, respectively. Thus, to mimic a real-world scenario, this research assumes a fixed COV of 0.09, and mean speed is 1.025 times higher than the posted SL.

6.4 Methodology

6.4.1 *Integrated simulation platform for MPC-based VSL control*

The proposed integrated simulation platform for VSL control can be divided into four modules, as in Figure 6.2:

Module-1: performs short-term traffic state prediction and determines the optimal VSL values over the prediction horizon with the chosen objective functions;

Module-2: acts as an interface between the microscopic traffic simulator and the traffic state prediction module;

Module-3: simulates the traffic flow with the modeled CLs and analyzes the VSL effectiveness due to different CLs; and

Module-4: archives the measured and predicted traffic states along with the SL posted to the VSL signs.

To change the speed limits assigned in the freeway links during the simulation run time, the VISSIM COM application programming interface (API) is used. Moreover, the Visual C++ program is used to load the traffic network through the VISSIM API, and to start the simulation process. The communication between MATLAB and C++ is established through MATLAB COM API.

Following the analysis results as obtained in Chapter 3, within the MPC framework, the calibrated DynaTAM-VSL model (as presented in Chapter 2) considers a simulation time step of T =20 second (sec). The optimal VSL values are calculated for every N_C=3 min, i.e., the control horizon. This research uses the SQP with scatter search global optimization method to find the VSL values. Every 3 minute (min), the measured traffic states obtained from *Module-3* are fed back into *Module-1* for traffic state prediction. In this research, the traffic states are predicted for a horizon of N_P=5 min. Once the prediction horizon exceeds the 3 min interval, it is assumed that the SLs remain fixed. Typically, the prediction horizon should be larger than the control horizon. At the same time, the difference between these two horizons should not be very large. Otherwise, one optimized VSL value that represents the time interval between N_C and N_P will have a very large influence on the chosen objective function.

6.4.2 *Evaluation procedure*

To obtain traffic data for different CLs with the no-VSL scenario, the WMD base model was run with a static SL of 80 kph in standalone mode with the field demand, where 5500 vph are needed to pass the weaving bottleneck during the congestion period (*t*=4:00 PM-6:00 PM), and 1000 vph during *t*=6:01 PM-6:30 PM. Furthermore, an additional 30 min demand, which is considered the warm-up period, was assigned before the beginning of the 2.5 hr simulation. To obtain traffic data in the VSL control scenario with different CLs, simulation was performed within the integrated simulation platform. The optimal VSL values within *Module-1* were calculated by minimizing the weighted summation of TTT (1st term) and total travel distance (TTD) (2nd term)—a surrogate measure of throughput as in Equation (6.1). To eliminate the random effect of the results, ten simulations, each with a different random number seed were conducted for each CL, and the average mobility and safety performance parameters were computed from these simulation runs. In this analysis, traffic speed and volume were imported from loop detectors coded in the WMD base model every 20 s throughout the simulation.

$$J(u) = T \sum_{j=1}^{N_p} \sum_{i=1}^{M} \lambda_i L_i \left[\alpha_{TTT} \rho_i (k+j) - \alpha_{TTD} q_i (k+j) \right] \tag{6.1}$$

With, α_{TTT} =80 and α_{TTD} =1 are considered for optimizing the mobility parameters.

The impact of exclusive CL is quantified by comparing performance parameters among no-VSL scenarios with different CLs, assuming low CL as the base. The effect of the combined impact, i.e., MPC-based VSL and CL, is quantified by comparing performance parameters for no-VSL and VSL scenarios at the low and the particular CL, respectively. The contribution from CL and VSL control are shown in Table 6-2 and Table 6-3.

6.4.3 *Results and discussion*

6.4.3.1 Impact of compliance levels and VSL on mobility

From Table 6-2, it can be seen that the TTT consistently decreased by a small amount as the compliance rate (CR) increased with static speed limit (SL). The improvement is statistically significant. A paired t-test for two sample means in SPSS 14.0 was performed. A detailed examination of the simulation results showed that the increased CRs resulted in a slightly improved average speed on some links that are not close to the bottleneck. Specifically, with a CR of 100%, the TTT on WMD is improved by 4.8% compared to a CR of 20%.

It can be seen that with a CR of 100%, the MPC-based VSL control reduces the TTT on WMD by 14.8%. The improvements are much higher than that for SL with the same compliance level (CL), which demonstrates the effectiveness of the MPC-based VSL control. Furthermore, for the VSL scenario, the travel time is at minimum with the ideal CL. As can be seen from Figure 6.3, the MPC-based VSL control can maintain lower density in most of the freeway links, including the weaving segment (link 3), which is a recurrent bottleneck and main source of congestion on the WMD when demand is high. Furthermore, in that figure, both the link 6 and link 7 are very close to a virtual lane drop bottleneck, where densities for no-VSL and VSL control are pretty similar. The reason is that the presented figure is for a compliance rate of 45%. However, for a compliance rate of 100%, this research observed significant density reduction for those links, which can be verified by observing the TTT values presented in Table 6-2. This implies that CL has significant impact in and around the bottlenecks to avoid flow breakdown.

By contrast, this research finds that the throughput improvement is not sensitive to the CRs with the static SL, which shows that just improving average speed cannot itself improve traffic volume. In theory, the improvement in average speed can increase the time to breakdown, but cannot avoid capacity drops. The preceding phenomenon was also observed in previous FOT (van den Hoogen and Smulders 1994; Jonkers et al. 2011). Moreover, this research proves that regardless of the CLs, the MPC-based VSL control can provide similar throughput improvements. Figure 6.4 presents the WMD link outflows during the simulation periods (*t*=4:00 PM-6:30 PM) with a CR of 45%. It can be seen that for most of the times, the VSL control can maintain higher flow than the no-VSL scenario, which increases freeway throughput by 7.4%.

6.4.3.2 Impact of compliance levels and VSL on safety

To quantify the safety impact of the MPC-based VSL control and CLs only, this research adopts a previously developed precursor-based collision prediction model (CPM) for WMD (Islam et al. 2013). For each simulation run, in each loop detector, a value of collision probability (CP) is calculated at 20-s intervals using Equation 6.2:

$$\mathrm{CP}(\psi) = \frac{\exp^{-3.694-1.207 SV2+3.149 LogAD1+4.028 LogSS2}}{1+\exp^{-3.694-1.207 SV2+3.149 LogAD1+4.028 LogSS2}} \tag{6.2}$$

In Equation 6.2, the dependent variable ψ is a collision, and the explanatory variables *SV2*, *AD1*, and *SS2* are the standard deviation of volume 5-10 min prior to collision, average density 0-5 min prior to collision, and standard deviation of speed 5-10 min prior to collision, respectively. The model was developed using collision data and field loop detector data collected from the test site WMD. The overall model goodness-of-fit and the significance of the model parameters can be found in the above referred literature.

Table 6-3 shows that due to improved CLs with the static SL, the CP is reduced; however, the improvements are not statistically significant. Moreover, the reduction in CP is the maximum with a CR of 100%; while the RSB is around 8%.

Furthermore, Table 6-3 shows that the RSB due to the VSL implementation is the highest (60.3%) with a CR of 100%. By contrast, the RSB is the lowest (51.3%) with a CR of 20%. In the table, RSB for the VSL control is computed by Equation 6.3. Similar trends can also be found in the mobility parameters. Thus, it can be concluded that the MPC-based VSL mobility benefits are not at the expense of increased collision probability and vice-versa. In Equation 6.2, the *SV2*, which is taken across the lanes, is negatively related to CP, indicating that with a lower value of *SV2*, the likelihood of conflict increases due to uniform traffic in all lanes. The positive coefficient for the *AD1* indicates that CP increases with congestion 0-5 min prior to a collision. Again, this is expected since the CP is likely to increase with exposure. The *SS2* is also positively related to CP. In summary, high speed variability with less traffic volume variability followed by congestion is found to increase CP. It can be seen from Figure 6.5 that the VSL contributed to RSB by reducing *AD1* and increasing *SV2*. By contrast, speed variance does not decrease while the VSL control is applied, since the optimal VSL values are obtained by minimizing link density and increasing outflow, as shown in Equation (6.1).

$$\text{Relative safety benefit (RSB)} = \frac{\mathrm{CP}_{\text{no-VSL}} - \mathrm{CP}_{\text{MPC-based VSL}}}{\mathrm{CP}_{\text{no-VSL}}} \tag{6.3}$$

This research further quantifies the amount of achievable safety benefit by reducing *SS2*, while the objective function within the MPC is set to minimize summation of speed variance within the links and among two successive links over the entire simulation time as in Equation 6.4. Unfortunately, for this case, the VSL reduces the *SS2* by comprising *AD1*, as shown in Figure 6.6(b, c). It is computed that for a CR of 45%, the CP on WMD is 0.2182 and 0.2139 due to minimizing Equation 6.1 and Equation 6.4, respectively. The VSL provides an RSB of 58.3% and 58.7%, respectively. Similar outcomes were also found for other CRs considered in this research. Figure 6.6(c) proves that by minimizing speed variance only, it is not possible to improve TTT. The VSL will increase the travel time due to increased density. Thus, it can be concluded that the speed variance is not a candidate objective function for the VSL control strategy design when the control goals are to improve traffic mobility and safety concurrently during congestion periods.

$$J(u) = T \sum_{j=1}^{N_p-1} \sum_{i=1}^{M} \left\{ [v_i(k+j) - v_i(k+j+1)]^2 + [v_i(k+j+1) - v_{i+1}(k+j+1)]^2 \right\} \tag{6.4}$$

At this point[8], this research further investigates whether MPC-based VSL control can improve safety without compromising mobility when CPM (Equation 6.2) is used within the rolling horizon system instead of speed variance as mentioned above. The optimization process can be seen as a problem of minimizing the objective function *J*:

[8] *Results in this section have been taken from a journal paper*: Fang, J., **Hadiuzzaman, M.**, Luo, A., Karim, A., and Qiu, T.Z. “A Novel VSL Control Strategy with Traffic State Prediction based Collision Probability Assessments.” (*under-review*)

$$J(u) = \sum_{j=1}^{N_p} \sum_{i=1}^{M} \mathrm{CP}_{i,j}(\psi) \tag{6.5}$$

As shown in Equation (6.5), the objective function measures the summation of collision probability over all the *i* analyzed links, as well as the entire prediction horizon. The collision probabilities were evaluated at every link and at all time steps within the prediction horizon $CP_{i,j}(\psi)$, separately for each feasible control input. The averaged overall collision probability was then used to determine the optimal VSL control input.

It was found that considering Equation (6.5), the VSL control algorithm has significantly lowered the collision probability. For the two identified bottleneck locations where the network has the highest safety risks, the collision probability was significantly reduced from 36 to 23, which is a 35% relative reduction. This is achieved by quantitatively analyzing the impact of the VSL control on traffic flow dynamics. Another interesting fact is that under the proposed control, improving network safety performance does not lead to compromises in mobility performance. The comparisons of TTT show that the proposed control algorithm has decreased the TTT by approximately 6%. According to Equation (6.2), the control algorithm managed to restrain the traffic flow density as an effect of lowering the collision probability. This also contributes to mobility improvements, as the experienced delay has been reduced (indicated by the reduced TTT). There is also a slight increase observed in the throughput calculation (0.9%). However, comparing the MPC-based VSL performance with Equation 6.1 and 6.5, it is pretty much clear that Equation 6.1 could offer higher mobility and safety benefits.

6.5 Summary and conclusions

This research quantified the mobility benefits of different CLs with static SL and the MPC-based VSL control. As a secondary objective, it also quantified the safety benefits, in order to assess whether the VSL mobility benefit is at the expenses of increased collision probability. For the short-term traffic state prediction within the MPC, it used a calibrated and validated macroscopic model ─ DynaTAM-VSL having several attractive features as presented in Chapter 2. The SQP with a scatter search method was implemented to find the optimal VSL values based on the predicted traffic states by the above model. The optimal VSL values were pushed back into the microscopic WMD base model, where several CLs were modeled. The research generated compelling findings:

(1) Both the VSL mobility and safety benefits are positively correlated with increasing CLs. The optimal VSL values within the MPC are computed with a CR of 100%; thus, the higher the percentage of drivers who follow the optimal speed limit in the microscopic WMD base model, the greater the benefits. These results proved that VSL mobility benefit is not at the expense of increased collision probability and vice-versa.

(2) The TTT and the throughput improvements due to the MPC-based VSL control with the different CLs are always significantly higher than that of static SL with the same CL.

(3) Specifically for the test site WMD, the TTT improvement due to the VSL control is the maximum (14.8%) for a CR of 100%. Whereas, the improvement is only

4.8% for a static SL with the same CR. Therefore, the travel time benefits of VSL are more than three times the benefits obtained under no-VSL.

(4) The throughput improvement for the static SL and the VSL control are 1.2% and 7.9%, respectively, with a CR of 100%. In addition, the throughput improvement is not sensitive to CRs when considered for either VSL or no-VSL scenario.

(5) During the congestion periods, increased CRs with static SL results in reducing CP, but the amount was found to be statistically insignificant. The RSB reaches a maximum value of 7.7% with a CR of 100%.

(6) For a CR of 20~100%, the MPC-based VSL control provides RSB in the range of 50-60%. Similar to the mobility improvements, the maximum RSB is obtained for a CR of 100%.

(7) With the prevailing CL to the SL on WMD, the VSL can provide improvements in TTT, throughput, and CP by 11.1%, 7.4%, and 58.3%, respectively.

(8) When the objective function within the MPC is set to reduce TTT and increase throughput, the VSL contributes to RSB by minimizing *AD1* and by increasing *SV2*.

(9) Minimizing speed variance gives a safety benefit only by reducing *SS2*. However, it increases *AD1* significantly, which could increase travel time. Thus, it can be concluded that the speed variance is not a candidate objective function for the MPC-based VSL control when the control goals are to improve both traffic mobility and safety concurrently during the congestion periods. By setting the above objective function within the MPC framework, it was computed that the RSB is similar for that of minimizing the combined objective functions.

(10) Lastly, this research investigates whether MPC-based VSL control can improve safety without compromising mobility when CPM is used as an objective function within the rolling horizon system instead of speed variance as mentioned above. It was found that with the current objective function, MPC-based VSL performs better. However, it did not offer better results compared to adopting combined objective functions that includes mobility parameters.

6.6 References

Abdel-Aty, M., Cunningham, R. J., Gayah, V. V., and Hsia, L. (2008). "Dynamic variable speed limit strategies for real-time crash risk reduction on freeways." *Transportation Research Record,* (2078), 108-116.

Abdel-Aty, M., Dilmore, J., and Dhindsa, A. (2006). "Evaluation of variable speed limits for real-time freeway safety improvement." *Accident Analysis and Prevention,* 38(2), 335-345.

Allaby, P., Hellinga, B., and Bullock, M. (2007). "Variable speed limits: Safety and operational impacts of a candidate control strategy for freeway applications." *IEEE Transactions on Intelligent Transportation Systems,* 8(4), 671-680.

Bertini, R. L., Boice, S., and Bogenberger, K. (2006). "Dynamics of variable speed limit system surrounding bottleneck on German autobahn." *Transportation Research Record,* (1978), 149-159.

Carlson, R. C., Papamichail, I., Papageorgiou, M., and Messmer, A. (2010). "Optimal mainstream traffic flow control of large-scale motorway networks." *Transportation Research Part C,* 18 193–212.

Giles, M. J. (2004). "Driver speed compliance in Western Australia: A multivariate analysis." *Transp.Policy,* 11(3), 227-235.

Habtemichael, F. G., and Santos, L. D. P. "Safety and Operational Benefits of VSL Under Different Traffic Conditions and Driver Compliance Levels." *Transportation Research Record, Accepted*.

Hadiuzzaman, M., Qiu, T. Z., and Lu, X. Y. (2013). "Variable Speed Limit Control Design for Relieving Congestion Caused by Active Bottleneck." *Journal of Transportation Engineering,* 139(4), 358-370.

Hadiuzzaman, M., and Qiu, T. Z. (2013). "Cell transmission model based variable speed limit control for freeways." *Canadian Journal of Civil Engineering*, 40(1), 46-56.

Hegyi, A., De Schutter, B., and Hellendoorn, J. (2005). "Optimal coordination of variable speed limits to suppress shock waves." *IEEE Transactions on Intelligent Transportation Systems*, 6(1), 102-112.

Hellinga, B., and Mandelzys, M. (2011). "Impact of driver compliance on the safety and operational impacts of freeway variable speed limit systems." *J.Transp.Eng.*, 137(4), 260-268.

Islam, M., Hadiuzzaman, M., Fang, J., Qiu, T. Z., and El-Basyouny, K. (2013). "Assessing Mobility and Safety Impacts of a Variable Speed Limit Control Strategy." *Transportation Research Record*, (2364), 1-11.

Jonkers, E., Wilmink, I. R., Stoelhorst, H., Schreuder, M., and Polderdijk, S. (2011). "Results of field trials with dynamic speed limits in the Netherlands: improving throughput and safety on the A12 freeway." *14th International IEEE Conference on Intelligent Transportation Systems Washington, DC, USA. October 5-7*.

Kang, K. -., and Chang, G. -. (2006). "A robust model for optimal time-of-day speed control at highway work zones." *IEEE Transactions on Intelligent Transportation Systems*, 7(1), 115-123.

Kang, K. -., Chang, G. -., and Zou, N. (2004). "Optimal dynamic speed-limit control for highway work zone operations." *Transportation Research Record*, (1877), 77-84.

Kwon, E., Brannan, D., Shouman, K., Isackson, C., and Arseneau, B. (2007). "Development and field evaluation of variable advisory speed limit system for work zones." *Transportation Research Record*, (2015), 12-18.

Lee, C., Hellinga, B., and Saccomanno, F. (2006). "Evaluation of variable speed limits to improve traffic safety." *Transportation Research Part C: Emerging Technologies*, 14(3), 213-228.

Lin, P. W., Kang, K. P., and Chang, G. L. (2004). "Exploring the effectiveness of variable speed limit controls on highway work-zone operations." Journal of *Intelligent Transportation Systems: Technology, Planning, and Operations*, 8(3), 155-168.

Long, K., Yun, M., Zheng, J., and Yang, X. (2008). "Model predictive control for variable speed limit in freeway work zone." *Proceedings of the 27th Chinese Control Conference, CCC*, 488-493.

McMurtry, T., Saito, M., Riffkin, M., and Heath, S. (2008). "Variable Speed Limit Signs: Effects on Speed and Speed Variation in Work Zones." *85th TRB Annual Meeting, Washington D. C.,Jan. 11-15*.

Park, B. K., and Yadlepati, S. S. (2003). "Development and testing of variable speed limit logics at work zones using simulation." *In Proc. 82nd Annu. Meeting Transportation Research Board (TRB), Washington, D.C., National Research Council, CD-ROM*.

Lu, X. Y., Varaiya, P., Horowitz, R., Su, D., and Shladover, S. E. (2011). " Novel Freeway Traffic Control with Variable Speed Limit and Coordinated Ramp Metering." *Transportation Research Record*, (2229), 55-65.

Transportation Research Board (1998). "Managing Speed: Review of Current Practices for Setting and Enforcing Speed Limits." *TRB Special Report*, 254.

Ugray, Z., Lasdon, L., Plummer, J., Glover, F., Kelly, J., and Marti, R. (2007). "Scatter search and local NLP solvers: A multistart framework for global optimization." *INFORMS Journal on Computing*, 19(3), 328-340.

UK Highways Agency. (2004). "M25 Controlled Motorways: Summary Report." (1).

Ulfarsson, G. F., Shankar, V. N., and Vu, P. (2005). "The effect of variable message and speed limit signs on mean speeds and speed deviations." *International Journal of Vehicle Information and Communication Systems*, 1(1/2), 69-87.

van den Hoogen, E., and Smulders, S. (1994). "Control by variable speed signs. Results of the Dutch experiment." *IEE Conference Publication*, 145-149.

Weikl, S., Bogenberger, K., and Bertini, R. L. (2013). "Empirical Assessment of Traffic Management Effects of a Variable Speed Limit System on a German Autobahn: Before and After." *Transportation Research Board 92nd Annual Meeting, Washington D.C., January 13-17*.

Table 6-1 Distribution of non-compliance drivers as function of compliance levels.

posted speed limit (kph)	driver compliance levels							
	low (CR=20%)[a]		moderate (CR=45%)[a]		high (CR=80%)[a]		ideal (CR=100%)[a]	
	defensive	aggressive	defensive	aggressive	defensive	aggressive	defensive	aggressive
V_{min} =20	30%	50%	15%	40%	5%	15%	0%	0%
u =30	30%	50%	15%	40%	5%	15%	0%	0%
u =40	30%	50%	15%	40%	5%	15%	0%	0%
u =50	30%	50%	15%	40%	5%	15%	0%	0%
u =60	40%	40%	20%	35%	10%	10%	0%	0%
u =70	40%	40%	20%	35%	10%	10%	0%	0%
V_{max} =80	40%	40%	20% [b]	35% [b]	10%	10%	0%	0%

[a]*compliance within ± 5 kph of advised*

[b]*observed non-compliance rate with the static speed limit of 80 kph in WMD*

Table 6-2 Mobility benefits under various compliance levels.

cases	control scenarios	average TTT (veh-hr)	percent improvement in TTT, (t-stat)[a]	average throughput[b] (vphpl)	percent improvement in throughput, (t-stat)[a]
base case	no-VSL, CR=20%	555.8	n.a.	18039	n.a.
alternative cases	VSL, CR=20%	526.7	5.2, (**4.73**)	19172	6.3, (**-15.91**)
	no-VSL, CR=45%	546.4	1.7, (**4.88**)	18100	0.3, (**-2.33**)
	VSL, CR=45%	494.2	11.1, (**12.72**)	19368	7.4, (**-26.89**)
	no-VSL, CR=80%	541.0	2.7, (**6.38**)	18188	0.8, (**-7.43**)
	VSL, CR=80%	492.5	11.4, (**10.82**)	19396	7.5, (**-25.93**)
	no-VSL, CR=100%	529.1	4.8, (**10.03**)	18252	1.2, (**-5.37**)
	VSL, CR=100%	473.5	14.8, (**11.58**)	19470	7.9, (**-20.18**)

Table 6-3 Relative safety benefits under various compliance levels.

cases	control scenarios	average collision probability[c]	percent improvement in RSB, (t-stat)[a]
base case	no-VSL, CR=20%	0.5230	n.a.
alternative cases	VSL, CR=20%	0.2546	51.3, (**24.19**)
	no-VSL, CR=45%	0.5188	0.8, (-0.53)
	VSL, CR=45%	0.2182	58.3, (**24.95**)
	no-VSL, CR=80%	0.5119	2.1, (-0.77)
	VSL, CR=80%	0.2151	58.9, (**21.07**)
	no-VSL, CR=100%	0.4827	7.7, (1.57)
	VSL, CR=100%	0.2076	60.3, (**27.35**)

n.a., *not applicable*

[a]*degree of freedom=9; level of confidence=95%; t-critical=1.83; the values in boldface indicate that the related improvement is statistically significant*

[b]*the throughput is the summation of outflow from all the 13 links of the test sites*

[c]*shows the average 2.5-hours collision probability*

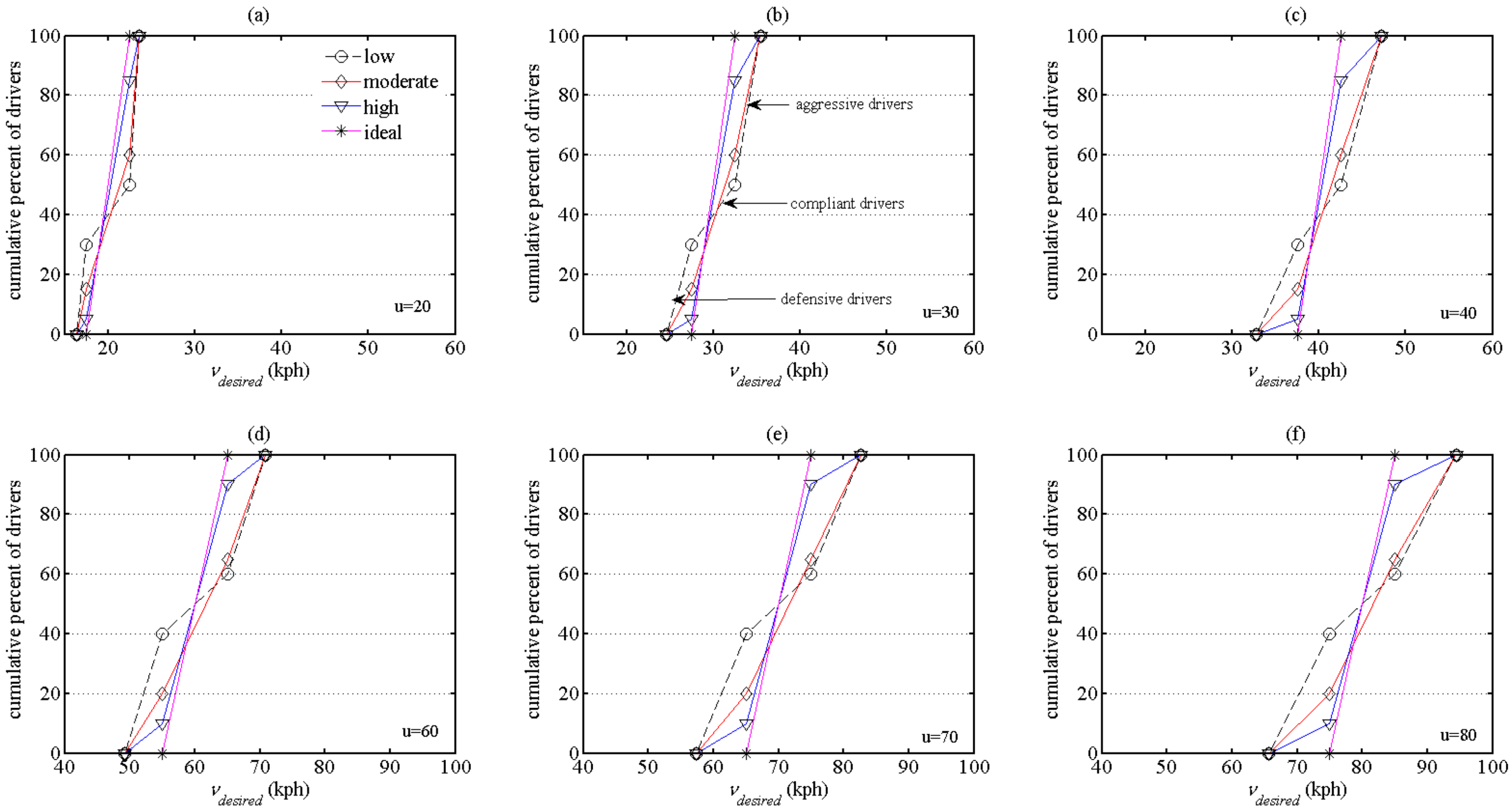

Figure 6.1 Modeling speed distribution as a function of compliance levels for different VSL. Boundary values of VSL are bounded by ±2σ of mean speed.

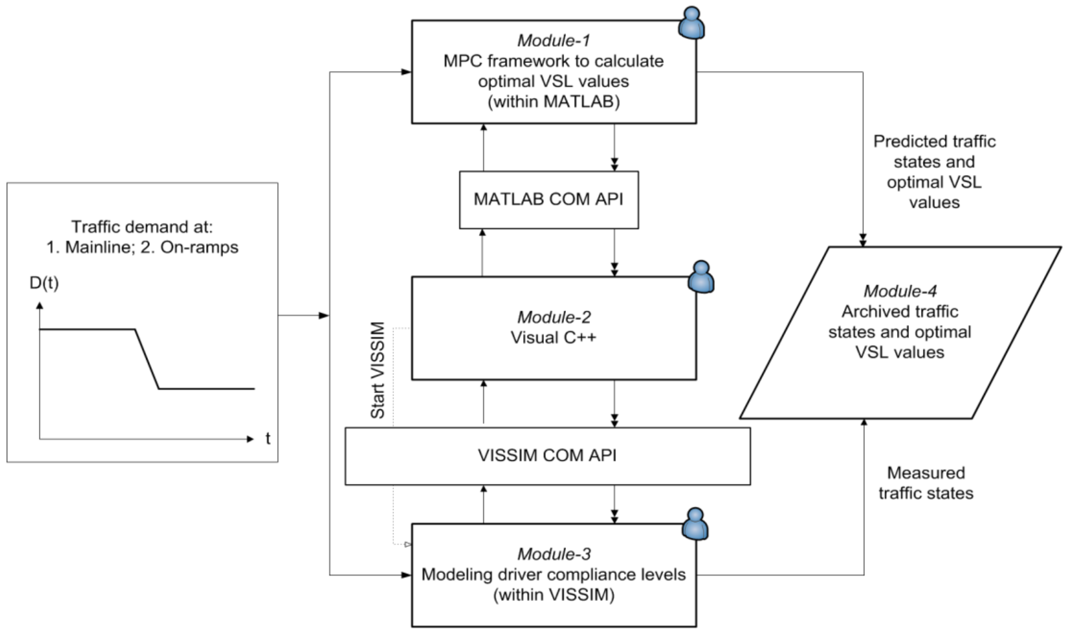

Figure 6.2 Relation between different modules in integrated simulation platform.

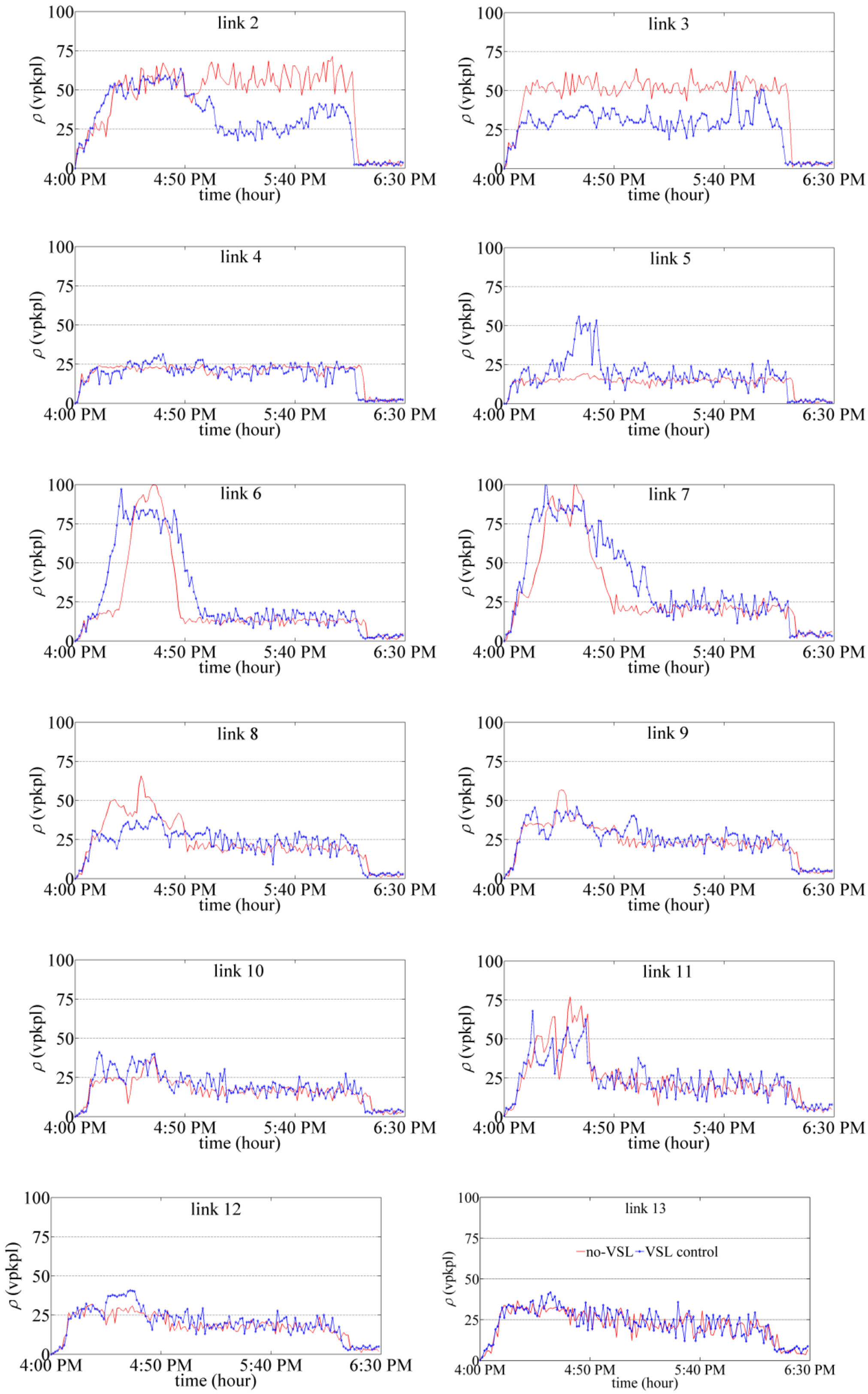

Figure 6.3 Contributing factor in improving TTT (Seed 20, CR=45%).

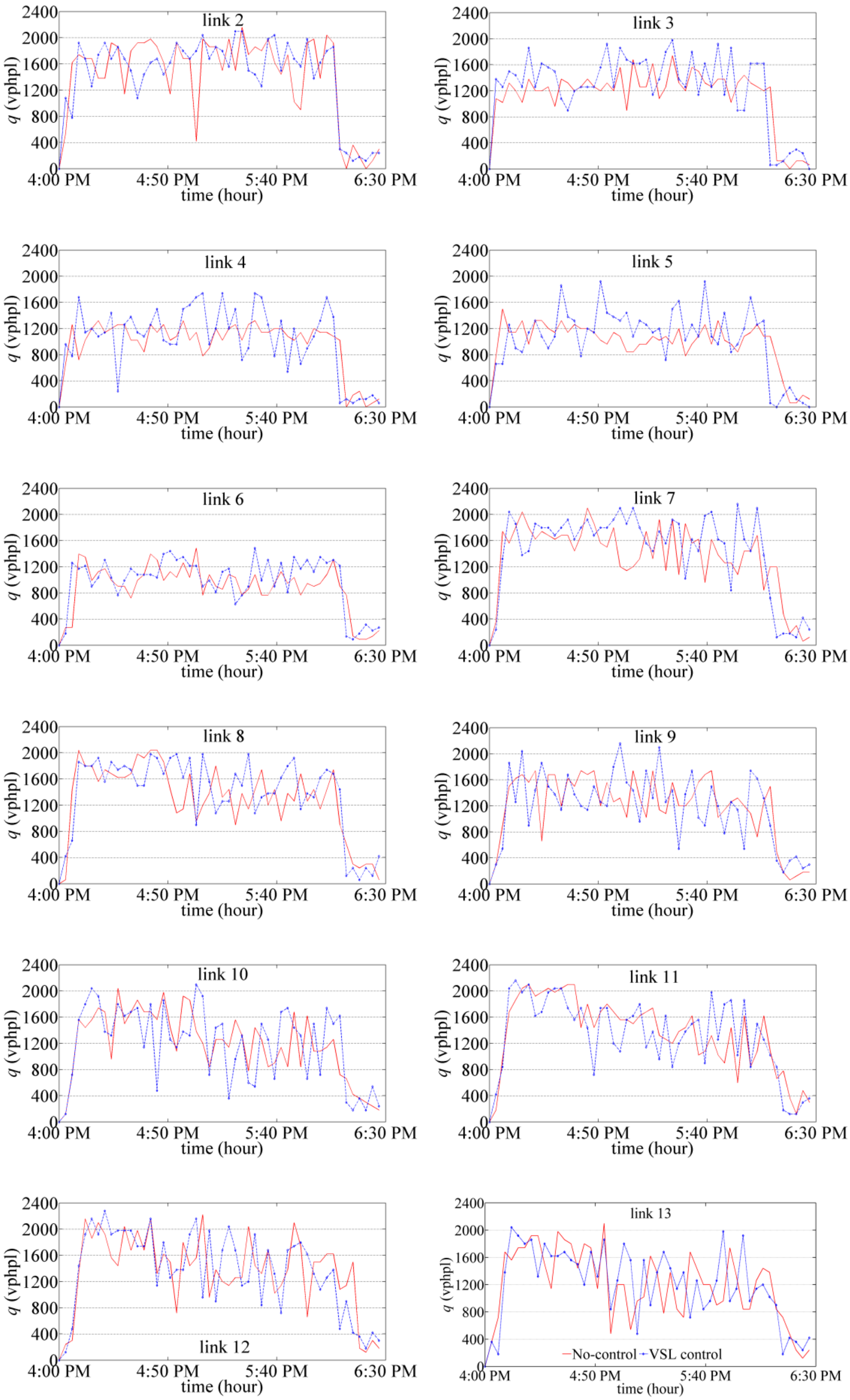

Figure 6.4 Contributing factor in improving throughput (Seed 20, CR=45%).

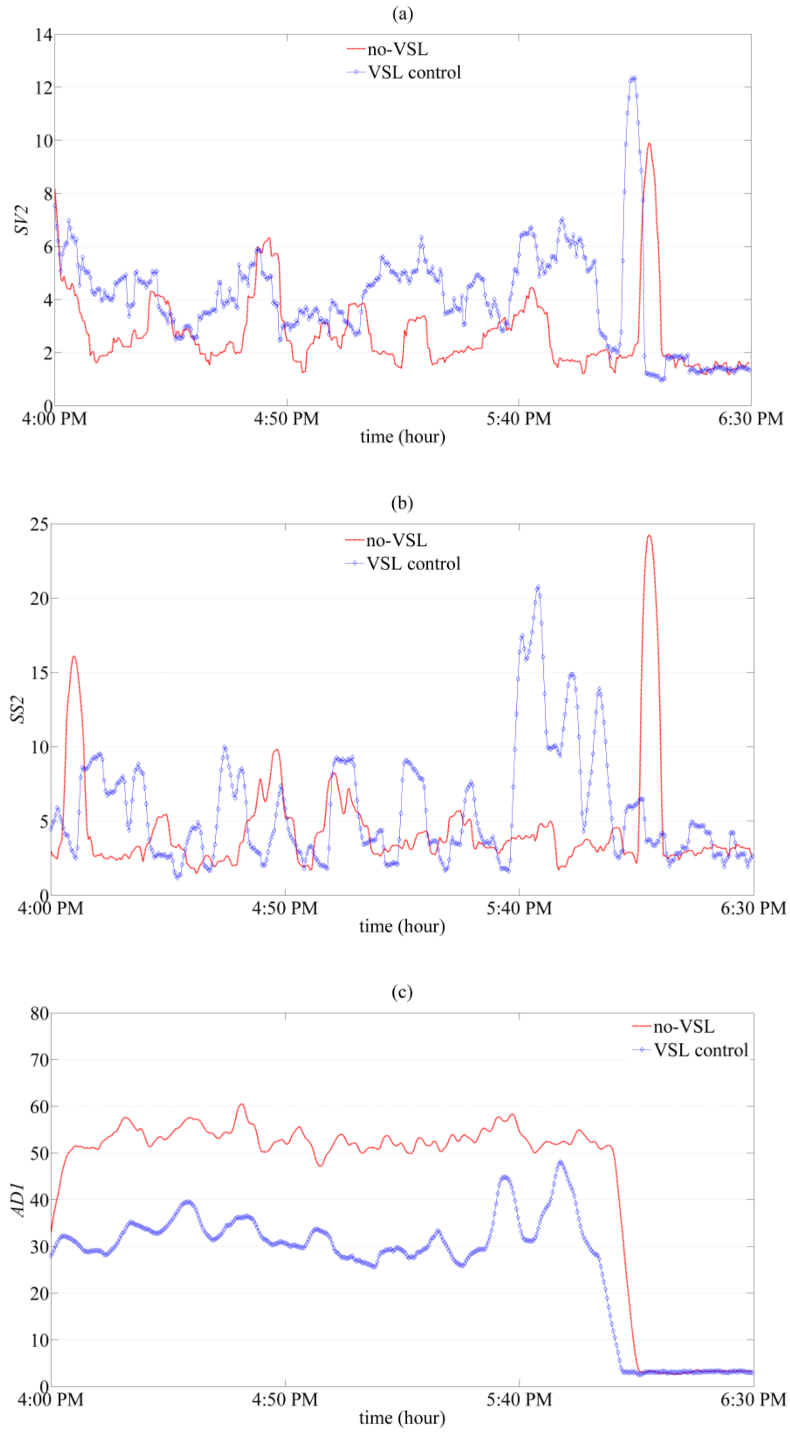

Figure 6.5 Contributing factors in RSB due to optimizing combined mobility parameters: TTT and throughput (Seed 20, CR=45%).

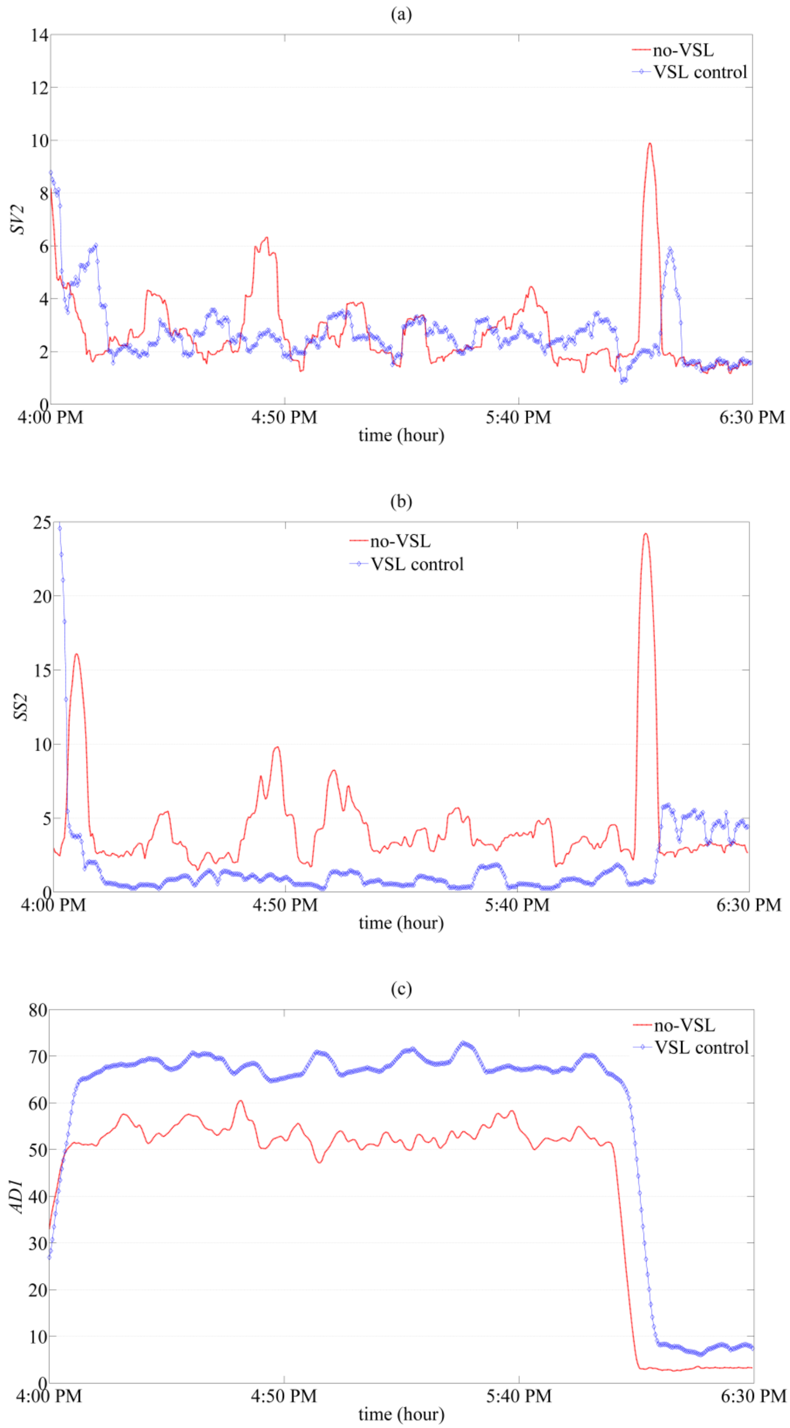

Figure 6.6 Contributing factors in RSB due to minimizing summation of speed variance within each link and between successive links (Seed 20, CR=45%).

Chapter 7

Conclusions and recommendations

7.1 General conclusions

This paper-based thesis is primarily concerned with investigating the impact of VSL control on traffic flow, and developing a proactive optimal VSL control strategy to improve freeway mobility. There are several general conclusions:

- Chapter 2 investigated the flow-density and speed-density curves that resulted in different METANET-based VSL modeling approaches. It was found that all of the previous VSL modeling approaches violated the equilibrium traffic state assumption. Specifically, under low densities, the direct parameterization of the FD in METANET's speed dynamics with the affine functions results in traffic speeds that are considerably lower than both the displayed VSL and the speed that the driver would assume without VSL. Another approach that takes the lesser value between the FD and VSL control variable shows inconsistency with the real-world control situation in high density regions. Specifically, the speed-density curve shows that rather than following speed limits, drivers adopt speeds based on their judgment. This finding questions the effectiveness of VSL control, since the displayed VSL and the adopted driver speed could be significantly different. On the contrary, replacing FD with linear VSL control variable avoids violation of the equilibrium traffic state assumption. However, the speed-limit-dependant link-specific parameters must be considered to avoid unrealistic traffic flow evolution in the control situation. Furthermore, to improve prediction accuracy within MPC, models' parameters must be calibrated in the VSL control situation. To investigate the simulation accuracy of different VSL control modeling approaches, four METANET-based traffic flow models were considered. It was found that for a lane drop bottleneck, the DynaTAM-VSL (M4) improved speed prediction by 71.7% compared to model (M3), which does not consider speed-limit dependant parameters, but adopts the same VSL control modeling approach. Furthermore, the calculated RMRSE values for the 11-km test site (WMD) in speed, flow and density simulation were 0.0313, 0.0407, and 0.0458, respectively, which were the lowest values compared to all of the other METANET-based models considered in this research. In the order of magnitude of network-wide traffic flow prediction accuracy, M4>M1>M3>M2. M1 and M2 adopted the VSL modeling approaches of without parameterization and with parameterization, respectively. The sensitivity of the DynaTAM-VSL with respect to changes in the structure showed that in the order of magnitude, the speed-limit-dependant link-specific parameters, the modified convection term, and the speed-limit-dependant reaction time parameters have the greatest contribution on improving flow prediction.

- Chapter 3 investigated the impact of MPC parameters on multi-objective optimization: reducing travel time and increasing link throughput under the coordinated VSL control. The efficiency of the MPC-based VSL control at various demand levels was also investigated. The ultimate objective was to see how and when the VSL control gives maximum mobility benefits. The MPC with gradient-based SQP optimization method proved that when the controller considers TTT as an objective function, it compromises throughput improvement. By contrast, maximizing TTD compromises both of the mobility parameters. It was observed that, during the congestion periods, the combined objectives with appropriate weight can facilitate throughput improvements without compromising TTT improvements, which resolves several existing paradoxical results. Furthermore, a method to tune the weight parameter in the combined objectives based on the control policy was proposed. It was observed that when close to the maximal allowable speed limit on the test site, the VSL control provides maximum mobility benefits. Interestingly, it was found that with a longer control horizon, improvements in both of the tested parameters are imperceptible as the prediction horizon increases. This research determines that the range of the mainline demand / bottleneck capacity ratio is 1.0-1.3, where the lower and upper values of the range depend on the bottleneck capacity and capacity at the upstream boundary link of the controlled section, respectively, when VSL can improve both the defined mobility parameters. Moreover, in the order of magnitude of improvements in the mobility parameters, M4>M1>M3>M2.

- Chapter 4 proposed an isolated VSL control strategy aimed at maximizing bottleneck flows. The control strategy explicitly considers the FD at a recurrent bottleneck, and its upstream-downstream segments. This VSL control strategy was designed within the MPC approach. A customized version of the DynaTAM-VSL was used for traffic prediction within MPC. To evaluate the effectiveness of the proposed control strategy, a base model of the test site was calibrated to reproduce the existing traffic conditions and the proposed control strategy was implemented to evaluate their impact. Considering real-world applicability, this research proposes an optimization method that not only does not require the evaluation of the gradient of the dynamic objective function, but also searches the optimal set of control variable values based on a generated decision tree at each control sampling time. The microscopic simulation-based evaluation showed that, in terms of mobility, VSL is mostly effective during congestion periods. Specifically, for the studied test site, improvements to TTT and throughput were around 39.0% and 5.4%, respectively. Furthermore, it was estimated that for the weaving and lane drop bottlenecks, the proposed control strategy improved the capacity by 3.7% and 10.2%, respectively, which shows the robustness of the VSL control strategy. The VSL sensitivity analysis on safety constraints and VSL update frequencies are promising in terms of supporting the implementation of a VSL control strategy for improving freeway safety and mobility. Based on both safety and travel-time savings, the VSL control with a 5-minute speed limit update frequency and a 10 kph maximum speed difference between two successive time steps yields the best results. In addition, it was found that, due to rounding the continuous VSL values (to the nearest 10 kph) obtained from the SQP optimization, the loss in TTT and throughput improvements are 10.8% and 1.7%, respectively, compared to the optimization with the discrete values obtained from the decision tree-based optimization. In addition, the CPU time and objective function values at most of the control sampling times over the 2.5 hr simulation were at the minimum values with the proposed optimization method. Consequently, it was concluded that the proposed decision tree-based optimization method is suitable for real-world application.

- Chapter 5 proposed a new first-order traffic flow model: CTM-VSL, which is flexible for use in macroscopic simulation and requires calibrating piece-wise linear FDs. Two modifications of FD of the basic CTM are proposed: (1) the first modification permits the modeling of recurrent bottlenecks in which there is a capacity drop once feeding flow exceeds its capacity; and (2) the second modification permits variable free-flow speed for the cells operated with VSL control. A comparison of the CTM-VSL (1^{st} order) with the DynaTAM-VSL (2^{nd} order) revealed that errors in speed simulation for an individual link as well as for the entire test site are higher in the 1^{st} order model.

Specifically, the calculated RMRSE values for the speed simulation in CTM-VSL and DynaTAM-VSL are 0.0457 and 0.0313, respectively. To assess the effectiveness of the MPC-based VSL control with a 1st order model, the CTM-VSL was adopted within the MPC to reduce input flow at a lane drop bottleneck following the VSL control strategy with strict speed compliance. To update the freeway storage capacity of an upstream segment of a VSL sign, a real-time queue estimation model was proposed. It was found that smaller time steps (60 s verses 20 s) in the queue estimation models results in better simulation. The micro-simulation of the MPC-based VSL implementation indicated the potential mobility benefits of ATM. Specifically, for the test site WMD, improvements to TTT and throughput were in the range of 9.0%-15.0% and 6.0%-7.5%, respectively, for different control scenarios. It was observed that queue control is necessary when very high demand approaches the bottleneck. Despite the simple structure of the CTM-VSL, the designed isolated MPC-based VSL control showed comparable results to that of the DynaTAM-VSL. Although the CTM-VSL showed slightly higher error in speed prediction compared to the DynaTAM-VSL due to regular feedback into the control framework with the measured traffic data derived from the above findings. However, the model is valid only for absolute driver compliance to the VSL control.

- Chapter 6 quantified the mobility and safety benefits of different CLs with static SL and the MPC-based VSL control. The secondary objective was to assess whether VSL mobility benefits are at the expense of increased CP and vice-versa. Improving safety on the test site can avoid collision-related congestion. Thus, several CL-to-VSL strategies were modeled with a fixed COV of speeds obtained from the static speed limit. The assumption accurately mimics real-world traffic behavior reported in the literature. The CLs included speed distributions for aggressive, compliant, and defensive drivers. The SQP optimization results were pushed back into the base microscopic simulation model, where several CLs were modeled. The research found that the VSL mobility and safety benefits are positively correlated with increasing CLs, disproving previous conclusions that the VSL safety benefit is at the cost of increased travel time. Specifically, for the test site WMD, the travel time, throughput, and collision probability are improved in the range of 5-15%, 6-8%, and 50-60%, respectively. This chapter also showed the impact of the objective function on both mobility and safety. It was found that when the objective function within the MPC is set to reduce TTT and increase throughput, the VSL contributes to RSB by minimizing *AD1* and by increasing *SV2*. However, minimizing speed variance gives a safety benefit only by reducing *SS2*. However, the controller increases *AD1* significantly, which could increase travel time. Thus, it was concluded that the speed variance is not a candidate objective function for the MPC-based VSL control design when the control goals are to simultaneously improve both traffic mobility and safety during congestion periods. Furthermore, it was revealed that by considering CPM in the objective function, it is possible to simultaneously improve both the mobility and safety parameters; however, the control performance is not better than that of considering combined mobility parameters in the MPC objective function. The above results also provide important implications for MPC-based VSL implementation in freeways with varying collision and traffic characteristics.

7.2 Recommendations for future research

Research on active traffic management (ATM) in Canada as well as in other North American countries is extremely scarce and challenging. The contents of this thesis were stimulated by an ongoing Field Operation Test in Edmonton, Canada, where a pioneer attempt has been made to deploy an MPC-based VSL control in authentic traffic operation. Future research in this area can be classified into three categories:

7.2.1 *Topics related to traffic flow modeling*

- **Validation of VSL modeling approach**. This research has made several modifications, improvements and extensions of the METANET model to improve traffic state prediction accuracy with the adopted VSL modeling approach. Although the model has been validated with traffic data collected from the field-data-based microscopic simulation model, in the future, it will be validated with real field data. To do so, both the speed-limit-dependant link-specific parameters and speed-limit-dependant driver behaviour parameters must be re-calibrated. Further validation of the DynaTAM-VSL model can be conducted with 20-s field loop detector data.

- **Relaxing the assumption in speed dynamics.** While deriving the speed dynamics in the VSL control situation, it was assumed that the advised speed limits are achievable. This assumption can be relaxed by introducing a non-compliance rate, i.e., (1+€). Specifically, by multiplying the linear VSL control variable in the relaxation term of METANET with a term (1+€). The parameter € represents the level of driver compliance to the advised VSL. If €>0, it indicates that more drivers tend to achieve a higher speed than the advised VSL and the desired speed is € percent higher than the advised VSL. If €=0, the desired speed is same as the advised VSL. If €<0, the desired speed is € percent lower than the advised VSL. In this research, the authors planned to calibrate the drivers' non-compliance rate with field data and quantify the proposed model's accuracy to reproduce prevailing traffic conditions. Unfortunately, the necessary data was not available to conduct such research. In future studies, this type of data and research will be meaningful and will enhance field VSL control performance by introducing the non-compliance rate in traffic dynamics.

- **Comparison among different METANET-based models.** The prediction accuracy by different METANET-based traffic flow models should be independent of implemented VSL control strategies, as these models include several parameters to capture driver response to traffic conditions and link-specific parameters. Therefore, once field data in the control situation is available, the authors plan to evaluate prediction accuracy of different METANET-based traffic flow models with the field loop detector data. All the models considered in this research will be re-calibrated.

- **Combined impact of VSL and RM control variables.** In this research, the METANET's speed dynamic has been extended to incorporate the impact of VSL control variables on traffic flow. In the future, the combined impact of VSL and RM control variables (through METANET's density dynamics) can be modeled and the effectiveness of active traffic control strategies can be further explored.

- **Modeling congestion side of FD for different speed limits.** In this research, the base model of the test site WMD was coded within VISSIM to reproduce existing traffic conditions in the non-VSL situation. FDs for different links with different speed limits were calibrated with the traffic data collected from the base model by applying a VSL control strategy. By contrast, once field data in the VSL control situation is available, the FDs could be re-calibrated using this field data and could be replicated in microscopic simulation. To do so, the VISSIM parameters (e.g., CC0, CC1) must be changed during the simulation run-time. Also, it will be interesting to see how the VSL control impacts the congestion side of the FD in a real-world traffic situation. After that, research can target at modeling cloud distribution (one density corresponds to several values of flow) in the congestion side with multiple lines.

7.2.2 *Topics related to traffic flow optimization*

- **Objective function with combined safety and mobility parameters.** In the test site WMD, traffic congestions are also observed due to collisions. A number of previous studies mentioned that freeway efficiency can be improved, taking into account the interaction between safety and efficiency. It is believed that if traffic is safer, then there are fewer collisions, and, consequently, the traffic flow is higher. Conversely, an improved traffic flow is usually achieved through more stable flow by avoiding flow breakdowns, which can be expected to result in fewer collisions. However, due to inadequate evidence on how to choose the weight parameters and find a trade-off between safety and mobility, it is challenging to include both the mobility and safety parameters in one objective function and optimize the parameters simultaneously.

- **Objective function that includes predicted queue length.** A number of heuristic VSL strategies have been proposed and evaluated in the literature; however, queue dynamics as a critical parameter for traffic management strategies were overlooked. To this end, an MPC-based VSL control can explicitly consider queue dynamics. Specifically, the optimal VSL values can be calculated by optimizing a combined objective function, which is a weighted summation of the predicted queue length (by using a model as proposed in Chapter 5), total travel time (TTT) and total travel distance (TTD).

7.2.3 *Topics related to investigating VSL effectiveness*

- **Generating dynamic O-D for control situation**. Over time, more vehicles enter the network, modifying the dynamics of the system operation. An operational model cannot predict this demand. Traffic demand prediction is particularly important to improve control performance. As demand prediction was out of the scope of this research, it was assumed that the demand on mainline and ramps were absolutely known. In reality, only historical demand data is known from the City's transportation planning model. Furthermore, due to dynamic control implementation, the O-D matrix can be affected differently than in the uncontrolled situation. Future research topics can include estimating the dynamic O-D matrix from loop detector data and probe counts in real-time. For VSL control, this demand could be the input for macro traffic flow models.

- **Investigating the impact of inaccurate traffic data.** In the traffic control and management community, there is a growing interest in the relationship between traffic data quality and the efficiency of ATM. Therefore, future research can quantify the impact on ATM performances of inaccurate measurements from loop detectors. Specifically, the relationship between different accuracy levels of flow and speed measurements as inputs at each control sampling time can be investigated both in microscopic simulation and the field.

- **Investigating control strategy performance for non-recurrent congestion.** Further studies could be conducted to assess the robustness of the VSL control strategy to improve bottleneck capacity caused by non-recurrent events (e.g. collision). Evaluation experiments could be designed from two practical perspectives: (1) the control effectiveness of when a queue encounters the VSL sign; and (2) the impact of system detection delay in VSL control.

- **Assessing real-life benefits from MPC-based VSL control.** Although the MPC-based VSL control is a promising solution to improve freeway congestion, the real-life benefits of such a control application are not yet available. This may be attributable to several factors: (1) inaccuracy of traffic data obtained from the available traffic sensors and failure to transmit real-time and online data to the Traffic Management

Centre (TMC); (2) inaccurate traffic dynamics for real-time traffic prediction; and (3) unreliable field application software in ATM. In this research, DynaTAM, a field application tool, was being developed (see Appendix C). It can be used to analyze, simulate, and optimize the traffic network in offline or online mode. The software has adopted the DynaTAM-VSL and the CTM-VSL models that were presented in this thesis. In the future, using this newly developed software, the authors will present the benefits that can be achieved in the real-world with different factors: driver response to the VSL, accuracy of measured traffic data, data timeliness due to sending measured traffic data from field loop detectors to the TMC, and more.

Appendix A

Peak hour traversal matrix in VISSIM model

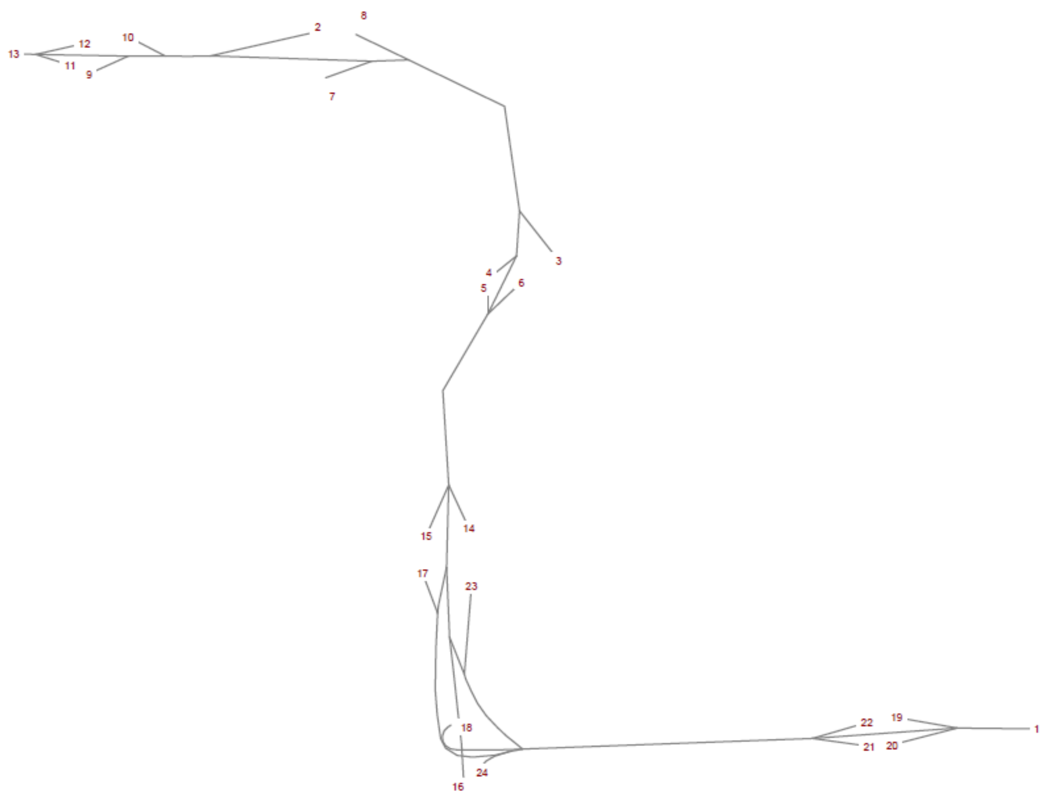

Figure A.1 Routing decision numbers in VISUM model.

Table A-1 Assigned O-D matrix into the WMD base model.

Zones	1	2	3	4	5	6	7	8	9	10	11	12	13	14	15	16	17	18	19	20	21	22	23	24
1	0	0	0	0	0	2	0	15	0	2	0	0	44	0	0	0	0	20	8	0	0	0	9	0
2	0	0	0	0	0	0	0	0	0	5	0	0	95	0	0	0	0	0	0	0	0	0	0	0
3	0	0	0	0	0	0	0	0	0	0	0	0	0	0	0	0	0	0	0	0	0	0	0	0
4	0	0	0	0	0	0	0	0	0	0	0	0	0	0	0	0	0	0	0	0	0	0	0	0
5	45	0	0	0	0	0	0	0	0	0	0	0	0	0	7	41	0	0	0	0	8	0	0	0
6	0	0	0	0	0	0	0	0	0	0	0	0	0	0	0	0	0	0	0	0	0	0	0	0
7	37	0	0	18	0	0	0	0	0	0	0	0	0	0	5	34	0	0	0	0	6	0	0	0
8	0	0	0	0	0	0	0	0	0	0	0	0	0	0	0	0	0	0	0	0	0	0	0	0
9	37	0	0	18	0	0	0	0	0	0	0	0	0	0	5	34	0	0	0	0	6	0	0	0
10	0	0	0	0	0	0	0	0	0	0	0	0	0	0	0	0	0	0	0	0	0	0	0	0
11	0	0	0	0	0	0	0	0	0	0	0	0	0	0	0	0	0	0	0	0	0	0	0	0
12	0	0	0	0	0	0	0	0	0	0	0	0	100	0	0	0	0	0	0	0	0	0	0	0
13	32	0	0	15	0	0	0	0	0	0	13	0	0	0	5	29	0	0	0	0	6	0	0	0
14	0	0	0	0	0	3	0	24	0	3	0	0	69	0	0	0	0	0	0	0	0	0	0	0
15	0	0	0	0	0	0	0	0	0	0	0	0	0	0	0	0	0	0	0	0	0	0	0	0
16	0	0	0	0	0	3	0	24	0	3	0	0	69	0	0	0	0	0	0	0	0	0	0	0
17	85	0	0	0	0	0	0	0	0	0	0	0	0	0	0	0	0	0	0	0	15	0	0	0
18	0	0	0	0	0	0	0	0	0	0	0	0	0	0	0	0	0	0	0	0	0	0	0	0
19	0	0	0	0	0	0	0	0	0	0	0	0	0	0	0	0	0	0	0	0	0	0	0	0
20	100	0	0	0	0	0	0	0	0	0	0	0	0	0	0	0	0	0	0	0	0	0	0	0
21	0	0	0	0	0	0	0	0	0	0	0	0	0	0	0	0	0	0	0	0	0	0	0	0
22	0	0	0	0	0	2	0	16	0	2	0	0	48	0	0	0	0	22	0	0	0	0	10	0
23	0	0	0	0	0	0	0	0	0	0	0	0	0	0	0	0	0	0	0	0	0	0	0	0
24	85	0	0	0	0	0	0	0	0	0	0	0	0	0	0	0	0	0	0	0	15	0	0	0

Appendix B

C++ code for generating decision tree-based optimal VSL

```
#include "StdAfx.h"
#include <vector>
#include <stack>
#include <map>
#include <set>
#include <math.h>
#include <algorithm>
#include <fstream>

using namespace std;


/*-----------------------------------------------------------------------------------------------------------
    The following constants should be set according to concrete application situation
  -----------------------------------------------------------------------------------------------------------*/
const int PredictStepNo = 5;            // the number of prediction steps with METANET model
const int ChoiceNumForCurSpeedLim = 3;   // choice number of current speed limit, such as: -1,
0, 1
const int MinSpeedChangeAmp = 20;        // minimum speed change amplitude for each step,
usually set to 10 km/h
const int UpLimForSpeedLim = 80;
const int DownLimForSpeedLim = 20;
/*-----------------------------------------------------------------------------------------------------------*/



long generateDecisionTree(int curSpeedLim)
// "curSpeedLim" is the speed limit for current time step
{
        if (numOfDecisionBranches > 0) // the decision tree exists, do not need to generate it
again
                return numOfDecisionBranches;

        int choiceNum;
        int scope;
        long i, j;
        vector <CString> strList, strList2;
        vector <vector <CString> > strLists;
        vector <vector <CString> >::iterator strListIter;
        set <vector <int> > tmpDTree;
        set <vector <int> >::iterator treeIter;
```

```
CString str;
short delta, speedLim;

if (curSpeedLim == DownLimForSpeedLim || curSpeedLim == UpLimForSpeedLim)
        choiceNum = 2;
else
        choiceNum = ChoiceNumForCurSpeedLim;

if(choiceNum=3)
numOfDecisionBranches = long(pow(choiceNum, PredictStepNo));
else
numOfDecisionBranches =2* long(pow(3, PredictStepNo-1) );

decisisonTreeBranches.clear();
decisisonTreeBranches.resize(numOfDecisionBranches);

// set dimension for the decision tree branches
for (i = 0; i < numOfDecisionBranches; i ++)
{
        decisisonTreeBranches[i].resize(PredictStepNo);
}

if (choiceNum == ChoiceNumForCurSpeedLim)
{
        scope = (ChoiceNumForCurSpeedLim - 1) / 2;
        for (i = -scope; i <= scope; i ++)
        {
                str.Format("%d", i);
                strList.push_back(str);
        }
}
else if (curSpeedLim == DownLimForSpeedLim)
{
        for (i = 0; i <= 1; i ++)
        {
                str.Format("%d", i);
                strList.push_back(str);
        }
}
else if (curSpeedLim == UpLimForSpeedLim)
{
        for (i = 0; i >= -1; i --)
        {
                str.Format("%d", i);
                strList.push_back(str);
        }
}
else;

for (i = 0; i < PredictStepNo; i ++)
{
        strLists.push_back(strList);
}
descartTotalProduct(strLists, strList);
for (i = 0; i < long(strList.size() ); i ++)
{
```

```
			str = strList[i];
			extractString(str, ",", strList2);
			speedLim = curSpeedLim;
			for (j = 0; j < PredictStepNo; j ++)
			{
				delta = atoi(strList2[j] );
				speedLim += MinSpeedChangeAmp * delta;
				speedLim = __min(speedLim, UpLimForSpeedLim);
				speedLim = __max(speedLim, DownLimForSpeedLim);
				decisisonTreeBranches[i][j] = speedLim;
			}
		}
		if (!decisisonTreeBranches.empty() )
		{
			tmpDTree.clear();
			for (i = 0; i < long(decisisonTreeBranches.size() ); i ++)
			{
				tmpDTree.insert(decisisonTreeBranches[i]);
			}

			decisisonTreeBranches.clear();
			for (treeIter = tmpDTree.begin(); treeIter != tmpDTree.end(); treeIter ++)
			{
				decisisonTreeBranches.push_back(*treeIter);
			}
			numOfDecisionBranches = decisisonTreeBranches.size();
		}

		return numOfDecisionBranches;

	}
```

Appendix C

DynaTAM: an on-line field application software tool for computing optimal VSL values within MPC

Over the last decade, there has been an increase in the interest surrounding proactive optimal VSL control strategy design; unfortunately the real life benefits of the strategy are not available. This may be attributable to (1) inaccuracy of traffic data obtained from the available traffic sensors and failure to transmit real-time and online data to the Traffic Management Centre (TMC); (2) inaccurate traffic dynamics for real-time traffic prediction; and (3) unreliable field application software in ATM.

To bridge these gaps, DynaTAM, a field application software tool of ATDM is being developed by the authors. This tool stemmed from the authors' participation in the project "Variable Speed Limit Control Algorithm Design and Development for Whitemud Drive in Edmonton". The software tool can be used to analyze, simulate, and optimize the traffic network in both offline and online mode. This appendix presents the software design and implementation and its communication protocol with the outer system, i.e. traffic control devices and field sensors. In the data management module, DynaTAM realized a practical data conditioning method, which makes it suitable for field application. As a Realistic and fast Traffic Simulator (Ref-TS), DynaTAM has adopted the METANET-based and CTM-based traffic flow models as presented in the chapter 4 and Chapter 5. A snapshot of the software interface is presented in Figure C.1.

DynaTAM is a complicated software system based on object-oriented design coded with C++. To reduce the use of pointers and structured text files to store data, DynaTAM uses the STL template library to organize its data structure and it uses MS Access 2007 and SQL server to store data. It is composed of several models and algorithms to achieve broad functionalities: (1) estimation of the current state of a traffic network using both historical and real-time data; and (2) generation of prediction-based information for a given time horizon with the control variable. The two functions interact in a rolling horizon concept. Figure C.2 illustrates the framework of DynaTAM implementation. It was 4:00 pm: DynaTAM starts an execution cycle, and performs a state estimation using data collected during the previous 5 minutes (user can choose different intervals). When the state of the network at 4:00 pm is available, DynaTAM starts predicting for a given horizon, say fifteen minutes, and computes an optimal set of VSL control variable values that minimizes the user-defined objective function. When DynaTAM finishes its computation, it is ready to implement the control variable on the real network. This control variable will be in effect until a new set of control variable values are generated. Immediately following that, the software starts a new execution cycle. Now, the state estimation is performed for the next 5 minutes. While DynaTAM was busy computing and implementing the new control variable, the surveillance system continued to collect real-time information, and DynaTAM will update its knowledge of the current network conditions using that information. The new estimation is used as a basis for a new prediction.

Occasionally failures can occur at the sensors or real-time measured traffic data transmission to the TMC. So, it is important to perform data conditioning before the data is used by DyanTAM for traffic state prediction and for finding the optimal VSL control variable. This software tool realized practical ways to remove the outlier in the real-time traffic operation: (1) if the data obtained from any loop detector (outfitted on a lane) is found to be unintuitive (e.g. negative flow or negative speed), the average of the data from the adjacent loops placed on the same segment is considered; (2) if data from all of the loop detectors at any segment is found unintuitive, values from the same set of loop detectors during the preceding time steps are used for traffic state prediction; and (3) data beyond the threshold value is discarded (e.g. any flow data more than the capacity is not be considered). Figure C.3 summarizes the data conditioning process.

DynaTAM has two main components: (1) the master module for finding optimal VSL control variable values, and (2) the graphical user interface (GUI) for control variable display for operators. Interfaces between DynaTAM and Outer Systems are shown in Figure C.4. The connection protocol between the real-time database and DynaTAM is ADO (ActiveX Data Object) based on OLE DB, which works with any language that supports component object model (COM) or ActiveX objects. ADO provides consistent and high-performance access to data. The master module of the software comprises the traffic simulator. The CTM-based and METANET-based models have been implemented in DynaTAM for traffic state prediction with the control variable. The software requires human intervention for sending the updated control variable values to the VSL signs. Any action taken by the operators will be stored in the historical database for future reference. DynaTAM has the function to exchange traffic data with the on-shelf micro-simulation software for the offline evaluation of the VSL strategy (See, Figure C.4).

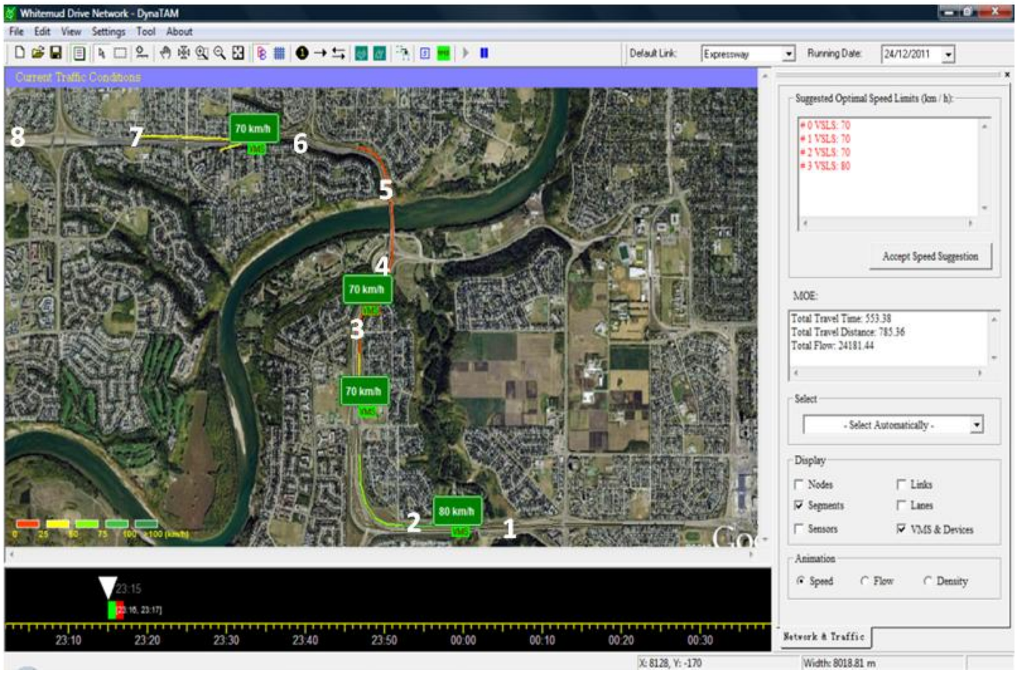

Figure C.1 DynaTAM UI with the background map of WMD. The numeric numbers on the figure shows mainline field loop detectors locations.

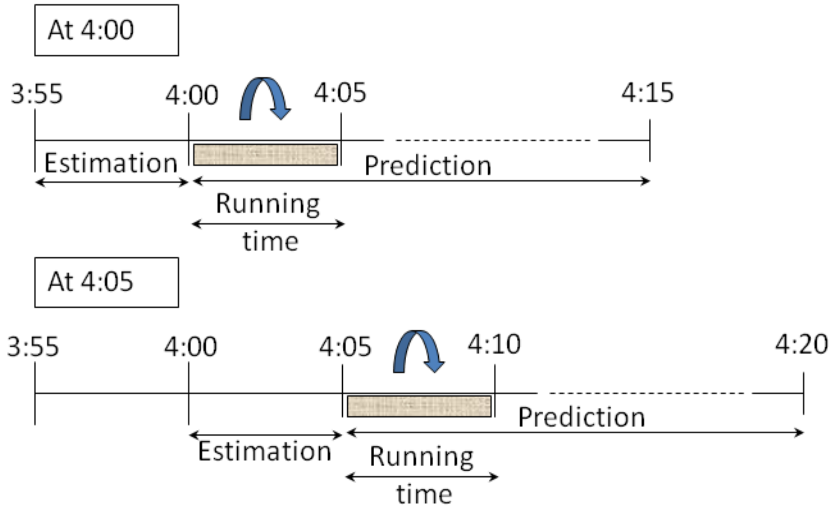

Figure C.2 Rolling horizon concept adopted by DynaTAM.

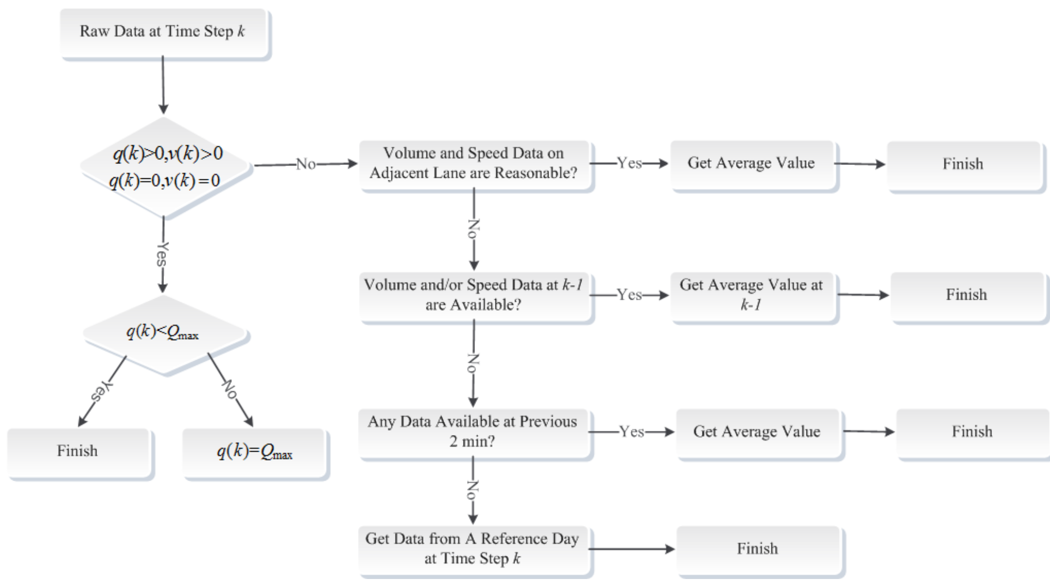

Figure C.3 Real-time data conditioning procedure in DynaTAM.

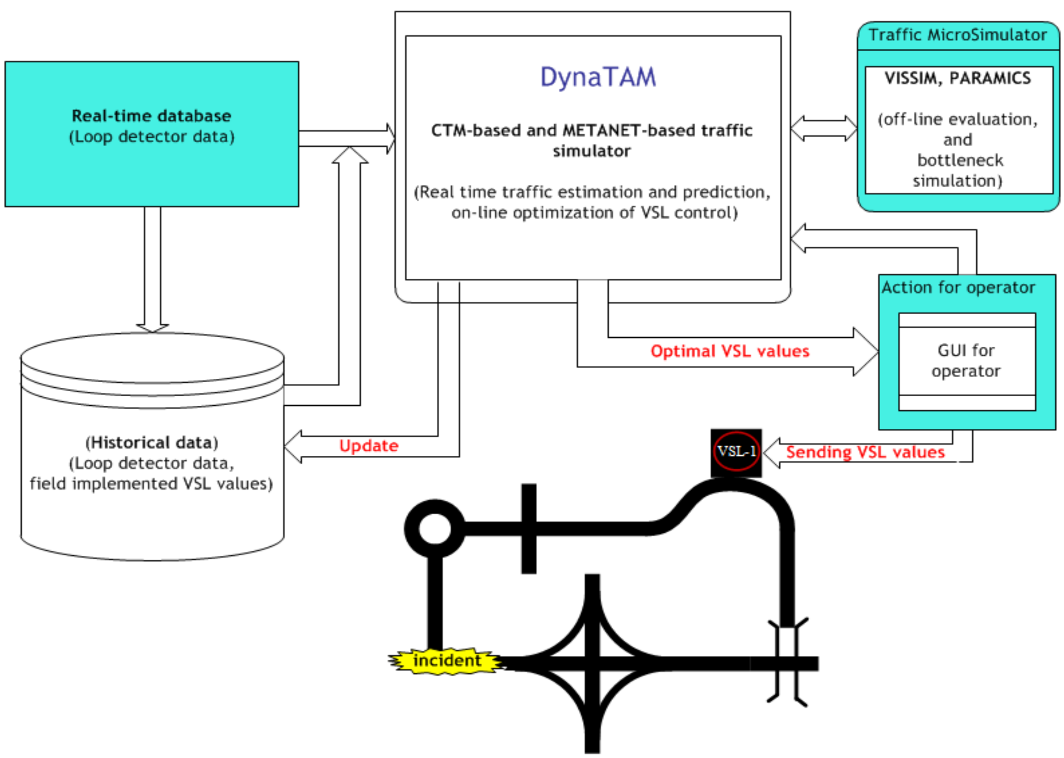

Figure C.4 DynaTAM interaction with the outer systems.